UNIVERSITY OF CALGARY

Improving Vacuum Gas Oil Hydrotreating Operation

via

a Lumped Parameter Dynamic Simulation Modeling Approach

by

Darius Remesat

A THESIS

SUBMITTED TO THE FACULTY OF GRADUATE STUDIES

IN PARTIAL FULFILMENT OF THE REQUIREMENTS FOR THE

DEGREE OF DOCTOR OF PHILOSOPHY

DEPARTMENT OF CHEMICAL AND PETROLEUM ENGINEERING

CALGARY, ALBERTA

JULY, 2007

Abstract

Hydrotreating, a process that uses hydrogen and catalyst to remove sulfur from crude oil streams, has become a larger part of refining operations due to transportation regulations and the necessary processing of heavier, more sour crudes. Refiners/Upgraders rarely achieve their run lengths and crude through-put objectives for vacuum gas oil (VGO) hydrotreaters. The performance shortfall is due to the occurrence of disturbances, in the form of crude flow changes, feed compositional changes, sulfur and metals changes, or hydrogen partial pressure changes, that reduce the effectiveness of the catalysts and the reluctance to make the necessary mitigating operational changes. There are proprietary steady state models that can provide some cursory indication of performance enhancement during operation. These models have not been used widely and it is not certain whether they would be effective in simulating the process with disturbances over the run length of the process. All public domain dynamic hydrotreater research is based on pilot plant data that does not translate well to industrial applications. A unique and crucial part of this study is the use of publicly unattainable data, gathered from fourteen operating hydrotreaters.

A lumped parameter dynamic model, using both Excel® and HYSYS® software, for industrial refinery/upgrader VGO hydrotreaters has been developed. The model takes proprietary and public steady state hydrotreater models and successfully applies it to a commercial dynamic simulation package. The model tracks changes in intrinsic reaction rate based on catalyst deactivation, wetting efficiency, feed properties and operating conditions to provide useful information,

such as required operating temperature, outlet sulfur composition and chemical hydrogen consumed. The model credibly simulates local disturbances, and represents the three distinct operating zones during hydrotreater run length (start, middle and end). This correlative, partially predictive model can be applied to demonstrate the tangible economic benefits of increasing hydrogen use to improve the operation of a hydrotreater by increasing run length and/or improving crude processing.

It is the author's strong desire to have this model used to maximize refining assets in an effort to optimize the productive life of our society's current main energy source, oil!

Acknowledgements

I would like to begin my thesis by acknowledging some of the people and organizations who helped and guided me:

Dr. W. Svrcek, University of Calgary, Co-Supervisor: Great guy, great supervisor, great chemical engineer. Bill helped me maneuver through various obstacles and provided timely guidance to give me the opportunity to pursue my PhD aspirations.

Dr. B. Young, University of Auckland, Co-Supervisor: Brent provided much appreciated timely input and feedback even though we were separated by a few time zones and the Pacific Ocean.

Praxair: Thanks to Ray Drnevich for helping with selecting this topic, Dan Bonaquist for supporting my industrial scholarship and overall thesis, and Ram Watwe for serving as an external reviewer. I am very appreciative of the overall culture at Praxair R&D that helped reinforce my passion for further learning.

NSERC: Thanks for offering the IPS scholarship for individuals that wish to pursue their graduate education in concert with an industrial partner.

Data Sources: Special thanks to the six operators and respective catalyst vendors for taking the effort to implement and authorize the necessary secrecy

agreements allowing me to gather and analyze the data and then to publish the results for the improvement of the refining/upgrading industry.

Family: This should conclude my formal quest for education. It has been a challenge balancing a career, family, extra-curricular activities and this PhD pursuit. I would like to thank my family, Ramona, Rachel and Devin for understanding and helping with my “time management” challenge.

Table of Contents

List of Tables

List of Figures and Illustrations

List of Symbols, Abbreviations and Nomenclature

A = Frequency factor in Arrhenius Equation

AF = Activity Factor, dimensionless

Al = Aluminum

Anilpt = Aniline Point of Crude

API = American Petroleum Institute Gravity

b = Temperature Effect Factor, dimensionless

B = Temperature corrected, catalyst fouling factor

BPD = Barrel per Day

Bromine # = Bromine Number of Crude

C_i = concentration of species of i, mol/vol

C_p = heat Capacity, energy/(temperature)(mol or per unit mass)

CoMo = Cobalt Molybdenum

Crackstock% = components in crude that will crack

D = Molecular Diffusivity, ft^2/s

DBT = Dibenzothiophene

Derivative = Change in Catalyst Efficiency Factor

d_p = Particle diameter, mm or in.

E_{act} = Activation Energy, energy/mol

EF = Catalyst Efficiency Factor

EOR = End of Run

F' = Mass Flux, mass flow/(area)(time)

FAC = Temperature influenced Fouling Rate

FCC = Fluidized Catalytic Cracking

FR = Fouling Rate

G = H_2/Oil Ratio, SCFB

G_a = Galileo Number, dimensionless

g = H_2/Oil Ratio Effect Factor, dimensionless

g' = Gravitational acceleration, ft/s^2

ΔH = Enthalpy Change for a reaction, energy/mass

H_2 = Hydrogen

H_2S = Hydrogen Sulfide

HC = Hydrogen Consumption

HDS = Hydro-desulfurization

k = Forward reaction rate constant

k' = Thermal Conductivity, energy/(time)(length)(temperature)

Ki = Equilibrium Constant for a Reaction

KLa = Gas-Liquid Mass Transfer Coefficient

KSa = Liquid-Solid Mass Transfer Coefficient

L = Liquid mass flow rate, $lbs/(ft^2)(s)$

L/D = Length to diameter ratio

LHSV = Space Velocity, HR^{-1}

M = Mass Flow, weight/hour

Met% = Concentration of Metals deposited on Catalyst

MOR = Middle of Run

MW = Molecular Weight, lb/mol

N = Nitrogen, PPM

n_a = apparent reaction order

NiMo = Nickel Molybdenum

NOx = Nitrogen Oxide compounds

P = Pressure, PSIA

PCL = Percent Chlorides, %

PFR = Plug Flow Reactor

PHI = Catalyst Characteristic Factor

p = Pressure Effect Factor,dimensionless

pH_2 = Hydrogen Partial Pressure, psi

Q = heat sink or source, BTU/hr

q = Percent of blocked sites on catalyst, %

q_o = Maximum percent of blocked sites for completely deactivated catalyst, %

R = Universal Gas Constant, energy/(mol)(K)

RNC = Catalyst deactivation factor, catalyst properties based

RTD = Residence Time Distribution

r_i = Reaction Rate of component i, mol/(vol.)(time)

R_e = Reynolds number, dimensionless, (Ld_p/μ_L)

S = Bulk Sulfur, WT%

SCF = Standard Cubic Feet

SG = Specific gravity, dimensionless

Size = Catalyst diameter factor, in or mm

SOx = Sulfur Oxide compounds

SOR = Start of Run

Sp Gr = specific gravity of oil, dimensionless

VPSI = Catalyst deactivation factor – activity, efficiency, kinetics

VPSIC = Temperature corrected VPSI

T = Temperature, °R, unless specifically noted otherwise

t = time

u = superficial velocity, ft/s

V = Volume

VGO = Vacuum Gas Oil

WABT= Weighted Average Bed Temperature

WBP = Weighted Boiling Point, ^{o}F

Y = Catalyst Efficiency Factor

YC = Progressive Catalyst Efficiency Factor

Z = Packed bed length, ft

%asphaltenes = sum of asphaltenes in the feed, %

%aromatics = sum of aromatics in the feed, %

Greek Letters

ε = Bed void fraction

ϕ = Ratio of catalyst sites blocked

η = Wetting efficiency

μ = viscosity, Ns/ft^2

ρ = desnity, lbs/ft^3

τ = Catalyst pellet tortuosity, dimensionless

Symbols

c = catalyst

f = Feed

HDS = Hydrodesulfurization

i = Specific component

L = Liquid

m = metals

p = Product

s = Sulfur

0 = start of run

Chapter One: INTRODUCTION

1.1 Problem Statement

Hydrotreating is a process that uses hydrogen and a catalyst to remove contaminants, primarily sulphur from crude oil streams. Hydro-processing has become a key refiner/upgrader operation due to two key developments. First, transportation regulations for refined products have evolved to significantly reduce the maximum amount of sulphur allowed (ex. 30 ppm gasoline for US 2006)[1]. Secondly, it is becoming necessary for refiners to process heavier, more sour crudes due to reduced availability of "sweeter" (low sulphur) crudes. As a consequence, refiners/upgraders (operators) need to remove more sulphur than previously required.

Operators struggle to achieve desired run lengths (time from start up to shutdown) and crude throughput due to the occurrence of process disturbances reducing the effectiveness of the catalysts. The disturbance, in the form of crude flow changes, feed compositional changes (specifically contaminants such as sulfur) with a given crude[2] and from processing various crude types, or hydrogen partial pressure (H_2 PP) changes, is not typically preventable but the impact can be mitigated during the operation of the hydrotreater.

1.2 Opportunity

Most operators struggle to make the necessary changes to mitigate the impact of the disturbance to recover lost run length or crude through put since there is very little supporting evidence that they can rely on to provide mitigating steps.

Considerable research has been performed in the area of steady-state and dynamic hydrotreater models using pilot-plant results but reliably scaling up the results to the industrial level over an entire run length remains a challenge. Over the author's 10+ years gathering first-hand information at over 40 of North America's refineries/upgraders apprehension continues to exist as to whether hydrogen can be used as a tool to improve refinery operations. Most operators surveyed[3] agree in principle that improving hydrogen (H_2) partial pressure will improve hydrotreater operation (via improved conversion) but can not make a justifiable, economic case to attempt the increased used of hydrogen.

A representative model of an actual vacuum gas oil (VGO) hydrotreater based on commercial parameters that can track dynamically the performance, including various changes and disturbances in the operation would be an invaluable tool. Operators could use this tool[4] to

1. Design and critique new trickle flow reactor designs
2. Optimize control schemes
3. Run closer to multiple operating constraints
4. Plan necessary modifications due to changes in operating conditions
5. Train both plant operators and engineers

Chapter 3, Literature Review, illustrates that there are a few dynamic models for hydrotreaters in the public domain and that they are suited to represent short-term, single step changes in a laboratory environment. Currently, there are no such publicly available dynamically-based models validated over entire run

lengths for multiple operating units. There are commercial (eg. KBC and AspenTech) steady-state hydrotreater models that could be modified for dynamic simulation, but to date, the operation of these steady-state programs remains cumbersome[5]. As a result, operators do not have the tools necessary to optimise process variables for disturbances during operation.

Since more operators are dealing with, or considering, processing heavier crudes, an industrially validated model for vacuum gas oil hydrotreaters would provide significant value to refining/upgrading operators.

1.3 Objectives

The body of work performed by the author entailed gathering a substantial amount of relevant industrial data, specific to vacuum gas oil streams, and validating a theory based set of correlations that was optimized for the developed steady state hydrotreater model and then used in a HYSYS® dynamic model of the hydrotreater. The specific goals of this research project were to:

1. Develop a reliable model that simulates the process over the length of an industrial hydrotreater's run that incorporates the effects of catalyst activity specific to "start of run", "middle of run" and "end of run".
2. Apply the developed dynamic model to determine economic ways to improve the operation.

By using industrial data, and creating a model that responds to various disturbances and influences during an entire hydrotreater's operation,

refiners/upgraders will now have the necessary software tools to justify the use, and have the necessary confidence to introduce increased hydrogen (purity and thus partial pressure) to improve hydrotreater operation.

1.4 Summary

In this chapter, the main objective of the thesis was presented, namely creating an industrially validated vacuum gas oil hydrotreater dynamic model. The objective addresses the problem and opportunity presented from operators' dealing with increased sulfur feed and reduced sulfur specifications in the refined products. Chapter 2 will provide the required background information on hydrotreating, while Chapter 3 provides a literature review. Chapters 4 through 7 provide the details of the model theory and development, the data used to validate the model, the results from the model and the application of the model. Overall, this thesis will provide insight into the use of experimentation, correlation development and industrial level application of the results.

Chapter 2: Hydrotreater Background

Chapter 2 provides insight into the actual configuration of an industrial vacuum gas oil hydrotreater, where it fits in the operator's process, and the key considerations in operating a hydrotreater. Information in this section is used to guide the model development in Chapter 5 so as to create a realistic representation of an industrial VGO hydrotreater.

2.1 Refinery Feedstocks

Most refineries use crude oil as a feedstock although oil sand syncrudes are becoming an increasingly important feed stock in North America. Table 2.1 shows a typical crude elemental composition.

Table 2.1- Elemental Composition of Crude[6]

Carbon	84-87%
Hydrogen	11-14%
Sulphur	0-5%
Nitrogen	0.2%

Crudes are classified according to weight, impurities and types of organic compounds. The API gravity is given by Equation 2.1.

$$API = \frac{141.5}{SG} - 131.5 \quad @\ 60^{o}\text{F} \tag{2.1}$$

Crude API gravities range from approximately 8 to 50[7].

Organic compounds (containing carbon molecules) are generalized as paraffinic, naphthenic and aromatic. In general, crudes having less than 0.5% sulfur are considered sweet while higher sulfur content crudes are considered sour. Metals content varies from almost zero to 1000 ppm of primarily nickel and vanadium and these metal impurities tend to concentrate in the heavier ends of the crude (residual portions of the crude). Sulfur is contained in all fractions but in a higher percentage in the heavy fractions[6].

2.2 Hydro-Processing

In the most elementary sense, every refinery splits its crude stock into several fractions and upgrades these fractions by various processes in order to make them more suitable for their final application. Figure 2.1, on page 7, shows a typical refinery block flow diagram complete with the finished product slate and where the vacuum gas oil hydro-treating fits in the scheme. Hydro-processing can occur on almost any feed–fraction, either to improve the finished product

properties or to pre-treat the feed prior to some other processing step. Many refineries will have only a few of these processes[6-8,10].

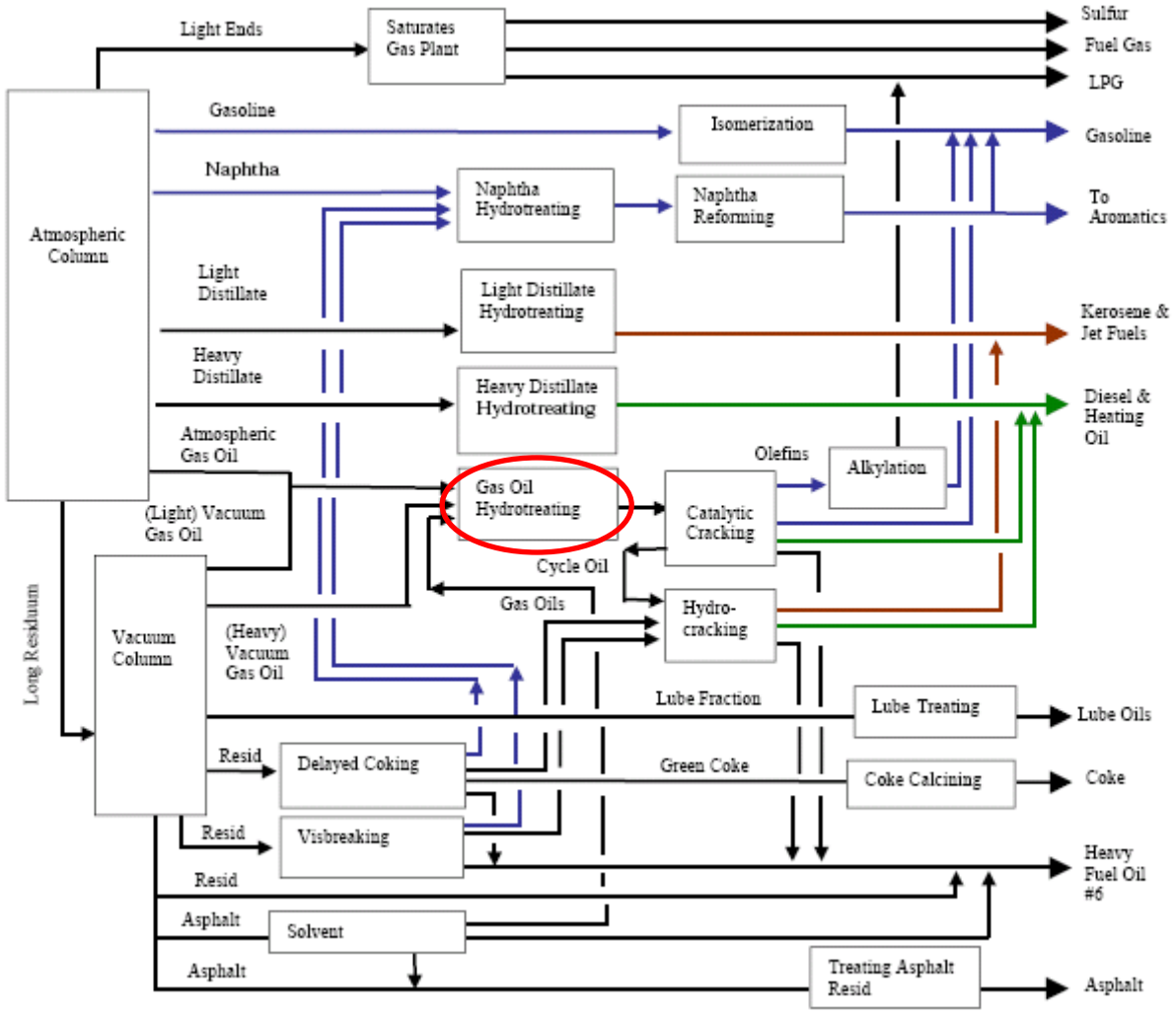

Figure 2.1- Refinery Process Diagram[8]. The typical location of the Gas Oil hydrotreating unit (circled in figure) is immediately downstream of the atmospheric and vacuum column and upstream of the catalytic cracking unit.

Hydro-processing improves the quality of a petroleum fraction by reacting it with hydrogen in the presence of a catalyst. The benefits of hydro-processing include

decreased pollution tendencies, improved odor, color, gum forming tendencies and storage stability. These benefits are the result of removing the sulfur, nitrogen, oxygen, metals, olefinic or diolefinic compounds, or by saturating the aromatic rings. Petroleum fractions generally treated are hydrogen plant treat gas, naphthas (straight run, cracked, etc), kerosene, jet fuel, heating oils, distillate fuels, catalytic cracking feed, lube oils, waxes, shale oils, tar sands products, and others. The two major objectives of hydro-processing are to meet product purity specifications (usually pollution) and to remove impurities that act as poisons for other refining processes (octane reforming, hydro-cracking).

2.3 Vacuum Gas Oils

With the increased processing of heavier crudes and the upgrading of bitumen, there are more vacuum gas oils that require hydro-treating. Gas oils have final boiling points up to 1050°F[2]. These may be used as industrial or home heating oils or as feedstocks for hydro-cracking or cat cracking processes for conversion to motor fuel products. Heating oils and motor fuel products need to be hydro-treated to remove sulfur and nitrogen impurities. Gas oils are also pre-treated prior to being used as feedstocks for fluid catalytic cracking (FCC) or hydrocracking. FCC pre-treating, accomplished in a VGO hydrotreater, reduces vanadium and nickel which would otherwise poison FCC catalysts. Nickel lay down on the FCC catalyst results in reactions that increase gas and coke production, while vanadium contributes to the destruction of zeolitic structures on regeneration of FCC catalyst[5]. In addition, sulfur and nitrogen removal reduces

FCC stack gas emissions of SOx and NOx pollutants. Typically feedstocks to FCC units require 1% or less sulfur and minimum metals[8].

Since the FCC unit provides the largest upgrade in value to a crude stream, the VGO hydrotreater must remove a multitude of components, including sulfur, and metals (vanadium and nickel) to reduce FCC catalyst deactivation.

2.4 Hydrotreating Processes

The catalytic reformer, which was introduced in the forties due to the development of the continuously regenerative catalyst, produced hydrogen from the dehydrogenation reactions. Refiners began to use this hydrogen for distillate hydro-treating[8]. They treated naphtha for gasoline, light distillate for kerosene and jet fuel, and heavier distillate used for heating oil and diesel fuel. The primary objective was desulfurization but there was a degree of ring saturation that improved kerosene smoke point and diesel Cetane Number (two indicators of quality of the crude product). In addition, hydrogen was employed to hydro-finish certain lube stocks to eliminate acid and caustic treatment as well as improve product quality. Removal of contaminants that destroy downstream catalysts is now a standard feature[8]. As more demands are placed on hydro-treating, the variety of hydrogen sources is widening. Over two dozen hydro-treating processes are offered by licensors[8], however the basic hydro- treating scheme, Figure 2.2, on page 10, provided by most licensed processes scheme is essentially the same.

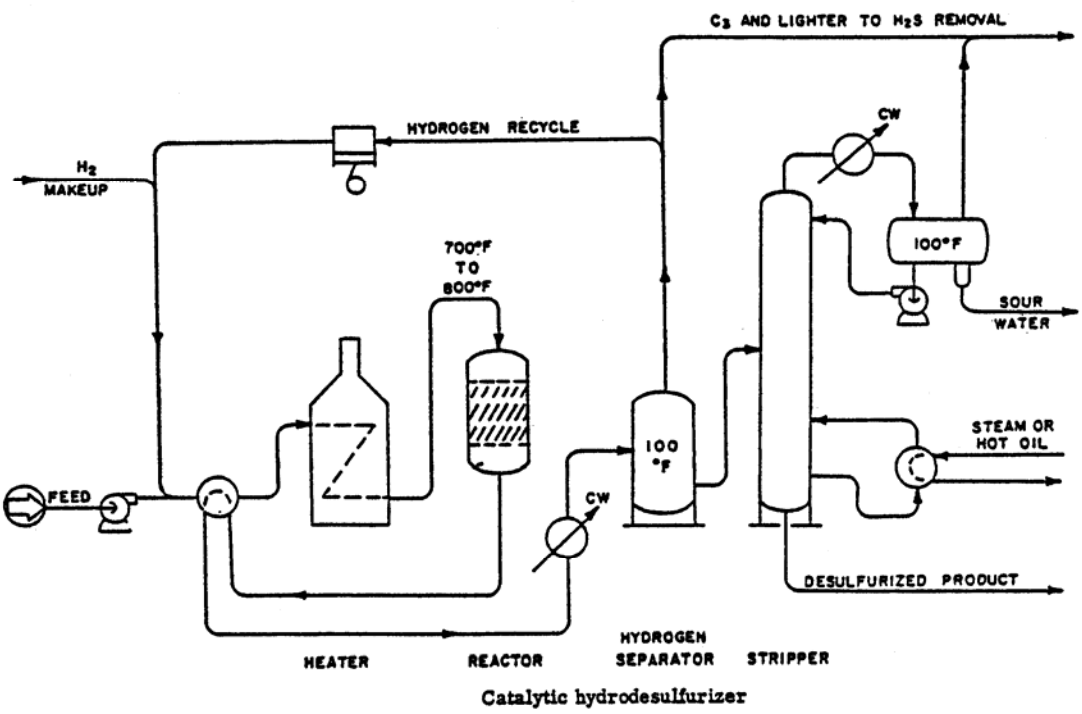

Figure 2.2 – Hydro-treating Process Schematic[6]

The procedure is to pump a heated feedstock and hydrogen through a fixed bed of catalyst. Multiple flash drums (hydrogen separator) provide a recycle hydrogen stream. A stripping column produce a liquid desulfurized product, and waste streams (sour water and light hydrocarbons). From various references[6-9], and personal surveys[3], typical critical operating conditions for hydrotreaters are:

Operating pressure from about 300 to 2200 psig (2065-15170 kPa)

Hydrogen to oil ratio may vary from 300 to 5000 SCF per barrel of oil (53 – 890 sm^3/m^3 of oil)

Bed temperature is typically between 500°F and 800°F (260 – 430°C)

Space velocity may range from 0.5 to 15 hr^{-1} LHSV

2.5 Vacuum Gas Oil Hydrotreating Process Description

Vacuum gas oil (VGO) hydrotreaters perform a vital role in refining operations. The two main functions of the VGO hydrotreater are to:

1. Remove sulfur in the crude by reacting the crude with hydrogen over a catalyst to meet end product specifications
2. Accumulate poisons (metals) on the catalyst to prevent metals from rapidly reducing the effectiveness of downstream catalytic operations (i.e. FCC units).

These two functions of the VGO hydrotreater are not complementary, since the accumulation of the poisons on the catalyst reduces the ability of the catalyst to meet sulfur removal objectives. The VGO hydrotreater's competing goals tend to make the unit expensive to operate due to short run-lengths (2-3 years)[7] resulting in frequent cost-intensive shutdowns. Also adding to the cost of the VGO hydrotreater, this unit requires a relatively pure (>75%, preferred over 90%)[7] hydrogen stream either produced from steam methane reforming or recovered from refinery hydrogen rich streams.

Desulfurization of gas oil can be achieved with a relatively modest decomposition of the crude oil at about 300 psig. Pressures as high as 1,500 psig can be employed to achieve the required sulfur removal for very heavy crudes, which is the focus of this study.

Figure 2.3 shows a typical process flow diagram of a vacuum gas oil hydrotreater. The model developed in Chapter 5 and used in HYSYS, is based on Figure 2.3. The unit will normally require two reactors of two beds, to provide a greater catalyst volume than in straight desulfurization service in order to obtain the necessary sulfur removal and metal removal for a reasonable liquid hourly space velocity [7-9]. Figure 2.3 shows that a feed is mixed with recycled and make-up hydrogen. The mixture is then heated in a furnace and fed to the first reactor. The temperature rise from initial hydrogenation in the top bed of the first reactor is such that a liquid quench is required immediately after. The quench is supplied from a low pressure separator, and is typical of a treated full range gas oil product.

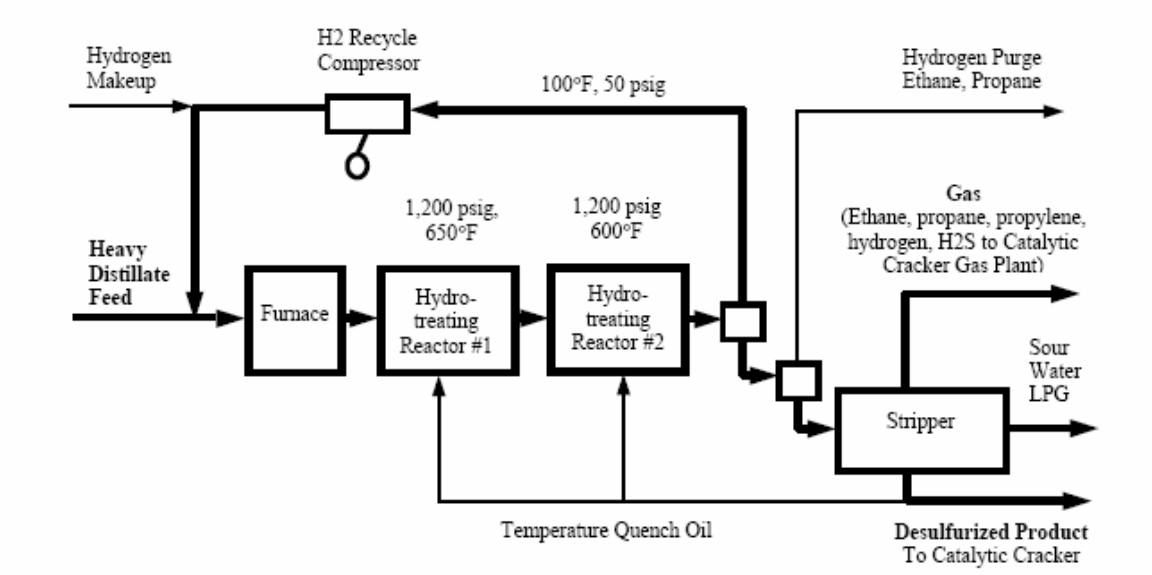

Figure 2.3 – Vacuum Gas Oil Hydrotreater Process Description[8]

Effluent from the second reactor is separated in two stages. The high-pressure separator provides a recycle hydrogen gas stream, while the low-pressure

separator light ends go to the hydrogen sulfide recovery unit. The liquid from the high pressure separator feeds the low pressure separator and the low pressure separator liquid is the feed to the stripper which produces a light ends over head product and a light distillate bottoms product. The stripper bottoms product is then sent to FCC.

The initial feed temperature is expected to be about 650^{o}F[7-9]. All desulfurization reactions are endothermic but only mildly so[10]. On the other hand hydrogenation is highly exothermic and care must be taken to avoid runaways, a topic of some importance and complexity. A cascade process control scheme is typically used[3,11] to control the reactor temperature. The hydrogen flow to the reactor is the manipulated variable to control temperature in the primary control loop but it is prone to disturbances, (primarily changes in hydrogen recycle and make-up flow). A secondary feedback loop controls the hydrogen flow and is required to mitigate the disturbances from the hydrogen delivery system.

The operating pressure of this system is about 1,200 psig (8275 kPa) at the first reactor inlet. For a given catalyst activity, the hydrogen partial pressure can be related to the amount of sulfur freed for conversion to hydrogen sulfide. The operation at 1,200 psig will also lead to 25% ring saturation, which will result in somewhat less than 95% sulfur removal[7-9].

The choice of operating conditions is determined by hydrogen availability. Note, gas oil units are more capital intensive than other types of hydrotreating units (light distillate or naphtha) because of the more intensive hydrogenation[8] that leads to such problems as quench, multi-stage separators and more complex strippers.

2.5.1 Trickle Bed Reactors

Most hydrotreaters are trickle bed reactors [3,6,7,10]**.** Figure 2.4 illustrates the various flow regimes possible for a fixed bed reactor.

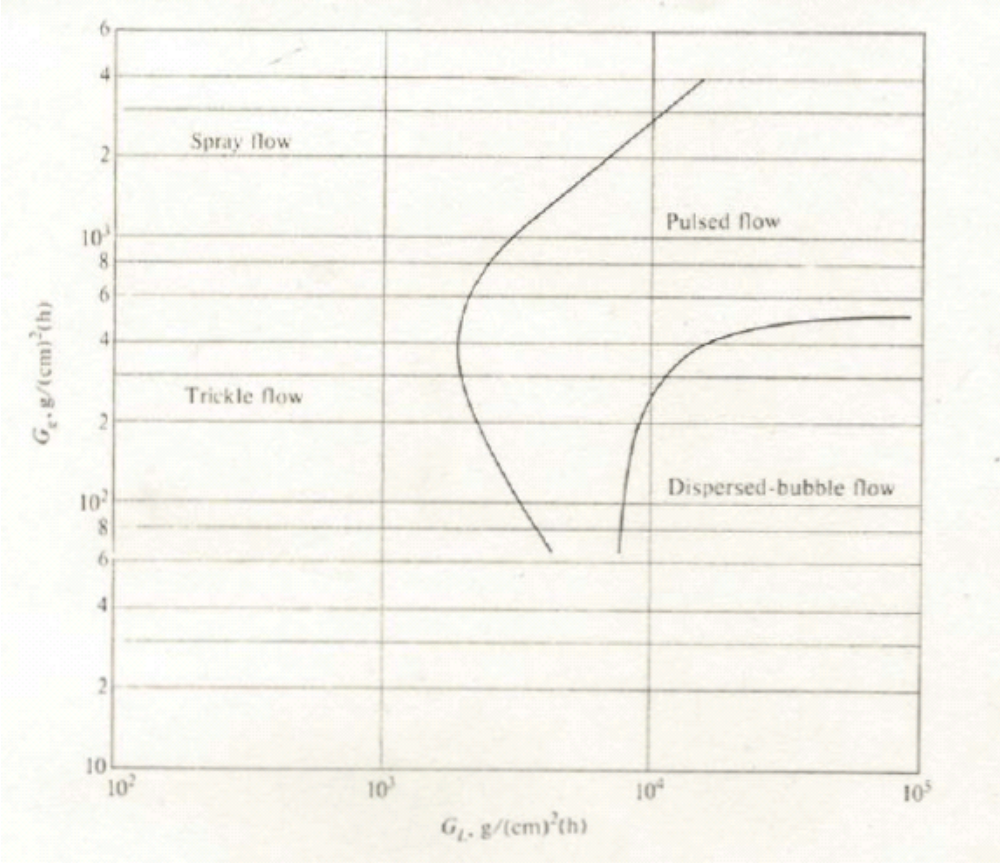

Figure 2.4 – Various Flow Regimes in a Fixed Bed Reactor[15]. Hydrotreaters operate in the trickle flow regime where the liquid and vapour flow is low.

The liquid (crude oil to be “treated”) and vapour (hydrogen) travel co-currently downward (pressure gradient and gravity) in very small quantities over a fixed bed of catalyst. At low liquid and vapor mass velocities, the gas phase is continuous and the liquid falls in rivulets (essentially laminar flow[10]) from one catalyst particle to the next (trickle flow regime).

Trickle bed reactors are chosen primarily because the crude oil has a low volatility and has a tendency to coke and crack. Complete vaporization of the crude is thus not practical for energy use reasons and the concern with significantly altering the crude oil via cracking and coking is not economic and feasible at this stage of the process.

2.5.2 Hydrotreating Catalysts

Two types of catalysts are generally used. Cobalt molybdenum catalysts are preferred for desulfurization and olefin saturation since they require less hydrogen consumption for a mild operation. Nickel molybdenum is utilized for nitrogen removal and aromatic saturation.

2.5.3 Trickle Bed vs Ebullated Bed VGO Hydrotreater Reactors

The principal alternative to a trickle bed reactor is an ebullating (or slurry) bed, in which catalyst particles are in motion and constantly replenished[8,15]. The major advantage of an ebullating bed is the ability to “regenerate” on line so that the catalyst deactivation phenomenon is removed[10]. The major disadvantages of the ebullated bed reactor are:

1. The lower degree of conversion versus a Trickle bed

2. Capital and operating costs for an ebullated bed are significantly higher

The trickle bed flow pattern is closer to plug flow, while the ebullated bed residence time distribution patterns are closer to a CSTR, thus making conversion in an ebullated bed lower relative to the trickle bed[10]. Ebullated beds require filters that need to be continually replaced, pumps for moving the slurry, and additional vessels to operate as intended. All these items increase the capital and operating costs. Operators have evaluated the costs and benefits for the two types of reactors and to date[3], the use of trickle-bed reactors for VGO hydrotreating is still far more prevalent than ebullated beds.

2.6 Hydrotreating Process Variables

The efficiency of the hydro-desulfurization process is measured by the degree of sulfur removal or, in other words, by the yields of sulfur-free products. However, there are several process variables that need special attention as any one of these variables can have a significant influence on the duration and effectiveness of the hydrodesulfurization process. The major process variables are: reaction temperature, hydrogen to oil ratio, reactor pressure (hydrogen partial pressure) and liquid hourly space velocity[7,10,12]. If these variables are not properly adjusted to process disturbances, the following problems may be exacerbated:

1. *Poor selectivity:* Some fractions of the feedstock will be cracked to undesirable low molecular weight (light hydrocarbon) products and conversion will be lower.

2. *Rapid catalyst aging:* Catalysts can sinter, losing surface area, activity and shortening run time length.

3. *Hot Spots:* When local reactor temperatures are well above 750°F (400°C)thermal cracking occurs.

Thermal cracking produces olefins, which add hydrogen, releasing heat. This increases the temperatures further, and thermal cracking rates continue to increase. These hot spots can easily reach temperatures higher than the safe upper limits for the reactor walls, and results can be catastrophic (vessel failure).

2.6.1 Temperature

Rates of all reactions in hydrotreating increase with increasing temperature. Increasing temperature will increase hydrogenation but hastens the deterioration in the number of active catalyst sites. Through the run, temperature control is used to offset the decline in catalyst activity. The maximum temperature is usually limited by process equipment design where most hydrotreating reactors have a metallurgical limit of some 800°F. Except for very high, pressure hydrogen operations, coke deactivation due to thermal cracking would prohibit operation above 800°F in any case.

There will be some temperature rise across the catalyst bed due to the overall exothermic nature within the hydrotreater reactor. In most industrial cases[3,7,10], the reactor is designed with a series of hydrogen quench points to smooth the reaction temperature profile resulting in close to isothermal conditions as possible, thus extend the end-of-run outlet temperature limitation. For any one

bed, a good rule-of-thumb[7] for determining average bed temperature (WABT – weighted average bed temperature) is provide by Equation 2.2.

$$T_{average\ bed} = 1/3\ T_{inlet} + 2/3\ T_{outlet} \qquad (2.2)$$

The WABT is used in this thesis to represent the temperature in the reactor for modelling purposes.

2.6.2 Pressure

Reactor pressures in hydrotreating vary depending on the requirements of the feed. Increasing pressure increases hydrogen partial pressure and retards coking deactivation[9,12] . This is of greater concern with heavier stocks, higher con-carbon stocks and cracked or coked stocks. Both sulfur and nitrogen removal is aided by higher hydrogen pressure [7,12]. Aromatics saturation is highly correlated with hydrogen pressure.

2.6.3 Hydrogen to Oil ratio

In order to insure adequate hydrogen pressure at the reactor outlet, hydrogen in excess of the chemical requirements must be charged to the reactor. Usual practise is to have two to three times the hydrogen required for reactions to assure efficient reactor performance[7]. High concentrations are required to prevent coke lay down on catalyst and poisoning the catalyst. This is particularly true for the heavier crudes containing traces of resins and asphaltenes that are subject to coking.

The overall effect of increasing the H_2:Oil ratio *(*or hydrogen partial pressure) is to increase the extent of the conversion through an increase in catalyst activity. As with the temperature variable, there are also limitations to increasing the H_2:Oil ratio. Use of excessively high H_2:Oil ratio may only serve to saturate the catalyst, and any further increase will only slightly affect the conversion.

2.6.4 Liquid Hourly Space Velocity (LHSV)

Liquid hourly space velocity (LHSV) is defined as volume of oil per volume of catalyst per hour. As used in refinery operations it is normally calculated as cubic feet of oil per cubic foot of catalyst per hour. In all hydrotreating reactions an increase in LHSV (oil feed rate) results in decreases in desulfurization, denitrogenation, aromatic saturation and other hydrogenation reactions [5,7,12].

A sample calculation of space velocity is as follows: A gas oil hydrotreater holds 240,000 lbs of catlayst and has a through put of 56,000 barrels per day. The catalyst is loaded at 42 lbs/ft^3. There are 5.73 ft^3 per 42 gallon barrel. Therefore,

$$\text{LHSV} = \frac{\left(5.73\ \text{ft}^3/\text{bbl}\right)\left(56{,}000\ \text{bbl/day}\right)\left(42\ \text{lb/ft}^3\right)}{\left(24\ \text{hrs/day}\right)\left(240{,}000\ \text{lbs}\right)}$$

$$\text{LHSV} = 2.3\ \text{h}^{-1}$$

The reciprocal of LHSV provides the residence time. In other words, since the catalyst volume for the trickle bed reactor is constant, LHSV will vary directly with the feed rate. To maintain a fixed rate of hydrodesulfurization, decreased LHSV (or increased feed rate) is usually compensated for by increasing the reaction temperature[4,9,12].

2.7 Hydrotreating Reactions

Oil fractions by their nature contain a large number of organosulfur, organonitrogen and aromatic species. The concentration and reactivity of the species vary widely from crude to crude. Unfortunately, oil fractions can seldom be fully characterised and doing so does not provide any better insight into processing the crude[13]. This makes analysing the hydrotreater performance

relative easy since the focus is on the reduction of total sulphur, not on the individual sulphur-bearing species. However, understanding the reactions of key sulphur components is necessary for a successful representation of the process. The analysis of the bulk crude stream can be based on the approximation that the number of species in an oil fraction is so large that the mixture can be treated as a continuum[6,13,14]. Petroleum properties are often measured as a continuous function of boiling point, and this feature is available in all simulation software[11,13].

Figure 2.5 shows some typical chemical reactions occurring in the hydrotreating process. Depending on the complexity of the feedstock compounds, more or less hydrogen may be consumed in removing the sulphur. Additional hydrogen is required due to solubility losses and other difficult to identify cracking or saturation reactions[17]. Most commercial reactors provide for a hydrogen make-up of two to ten times the hydrogen required for chemical reactions[18]. It is particularly important to provide additional hydrogen when dealing with highly unsaturated feed stocks such as coked or cracked feed stocks[5-10,20].

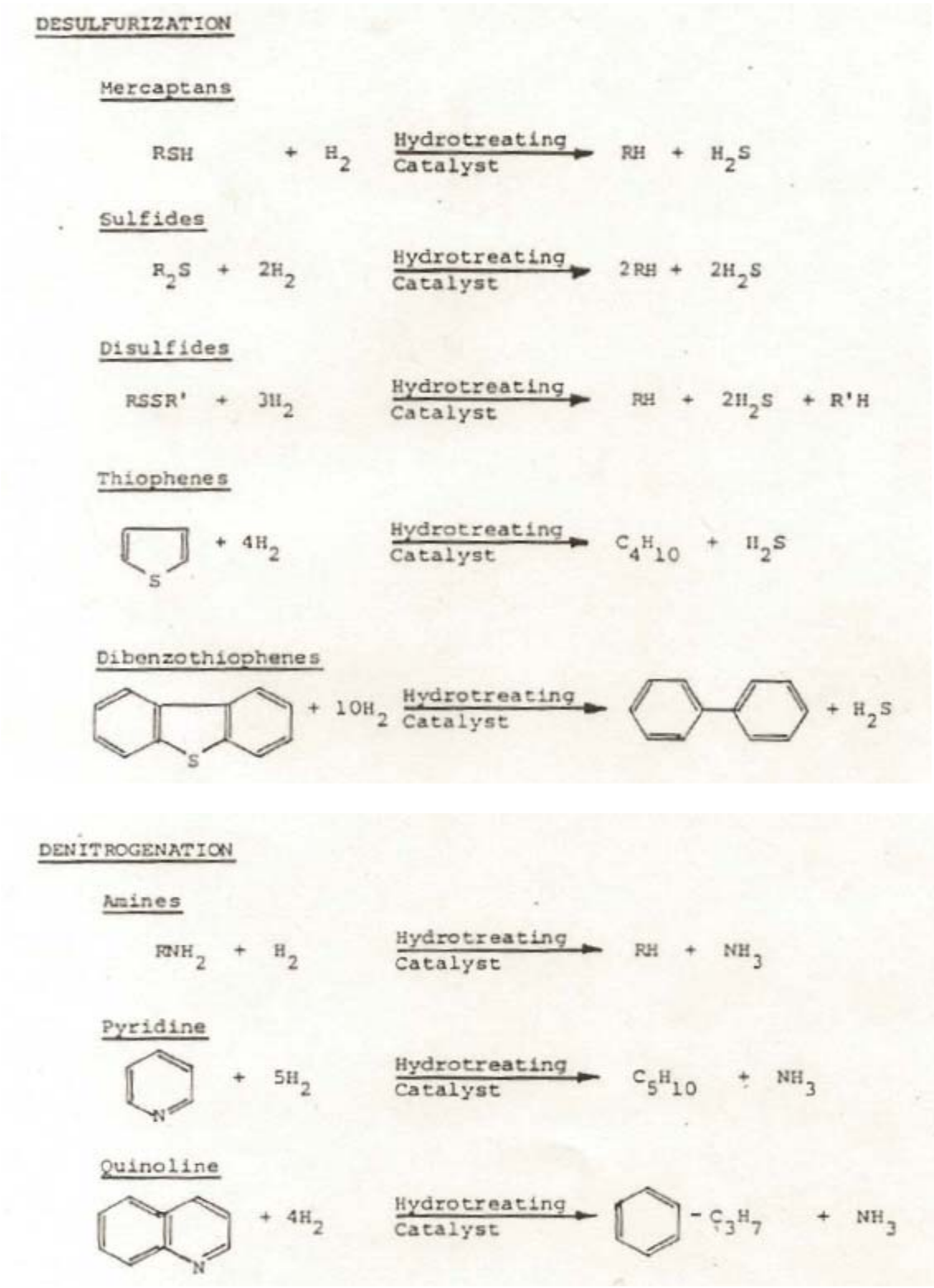

Figure 2.5 continued

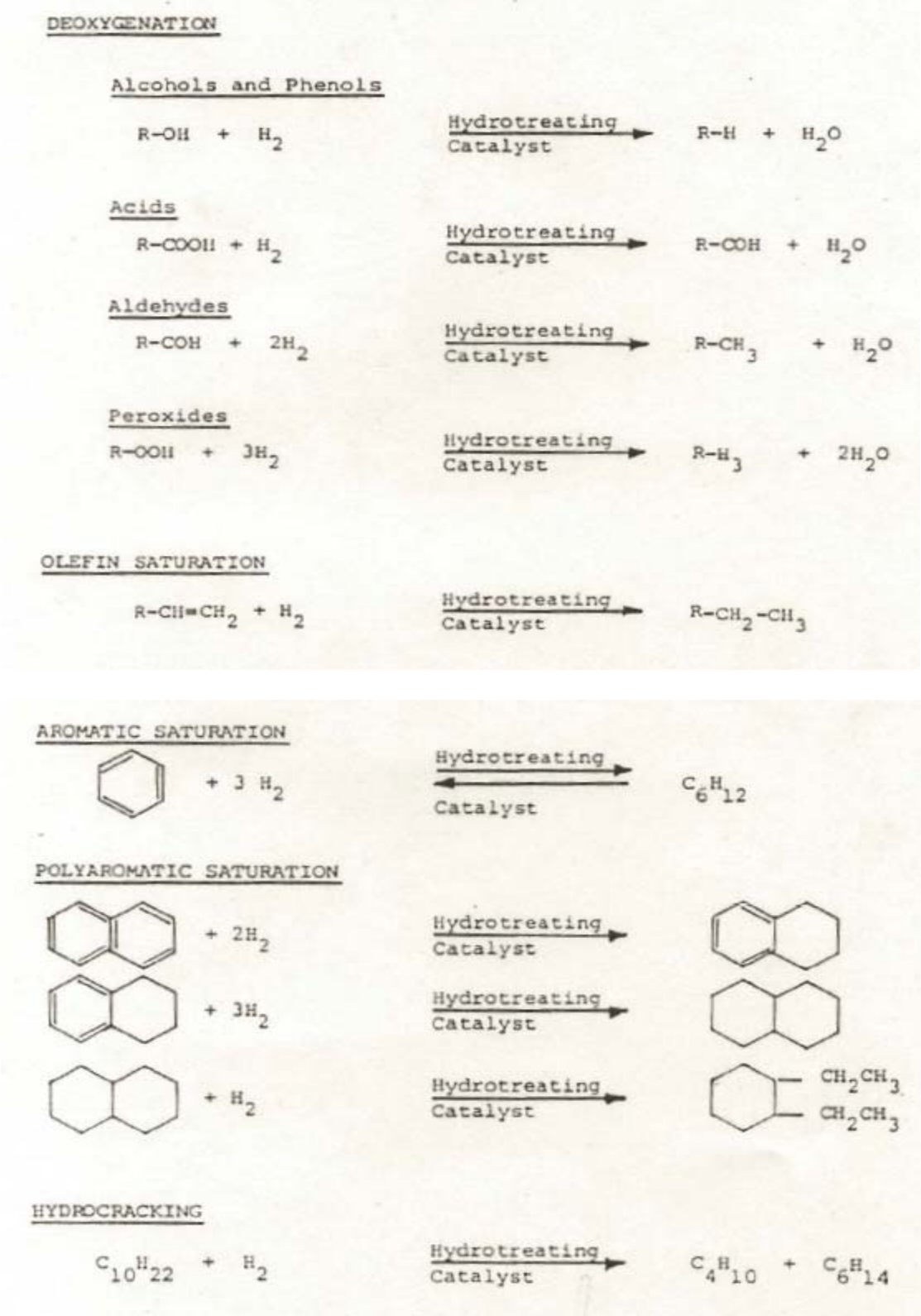

Figure 2.5 Typical Hydro-processing Reactions and Hydrogen requirements[7]

2.8 Catalyst Deactivation

Feed properties and operating conditions (severity of the reaction) determine the catalyst life in hydrodesulfurization. Catalyst deactivation is mainly due to metal deposits and coke accumulation on and within the catalyst pellet[19]. It is characterized by an initial rapid decline in activity (Start of Run – SOR), followed by a gradual loss in activity during the middle-of-run (MOR) operation, and finally a fast and sudden activity reduction during the end-of-run (EOR) operation.

Figure 2.6, on page 24, shows a qualitative illustration of how foulant material adds to the catalyst and what impact that has on catalyst activity. Line b shows the coke profile, where most of the coke deposit occurs early in the operation. Line c shows the metal profile which is mostly a consistent lay down of material. Line a shows the reduction in catalyst activity (typically the percentage of catalyst life remaining). Lines b and c when added together, can account for the shape of the catalyst activity line. The significant drop off in performance at the end can be attributed to two factors:

1. Increase in dehydrogenation reactions– temperature above a certain value, generally 750^{o}F[5,7,13,19,20], starts aromatics crossover[5], coupled with the accumulation of metals on catalyst results in dehydrogenation reactions competing with the desired hydrogenation reactions for sulfur removal
2. Pore-mouth plugging of Catalyst[15] – Coke and metal accumulation gets to a point where the catalyst surface for reaction is greatly reduced since the reactants are blocked from most of the internal catalyst surface area

In practice, the temperature of the reactors should be increased gradually during the operation in order to compensate for the effect of decreased reaction rates due to catalyst deactivation, and to maintain the sulfur content of the product within a specified range. Nevertheless, this increase in temperature is not indefinite. It is limited to a maximum allowable operating bed temperature where the catalyst is assumed to be completely deactivated.

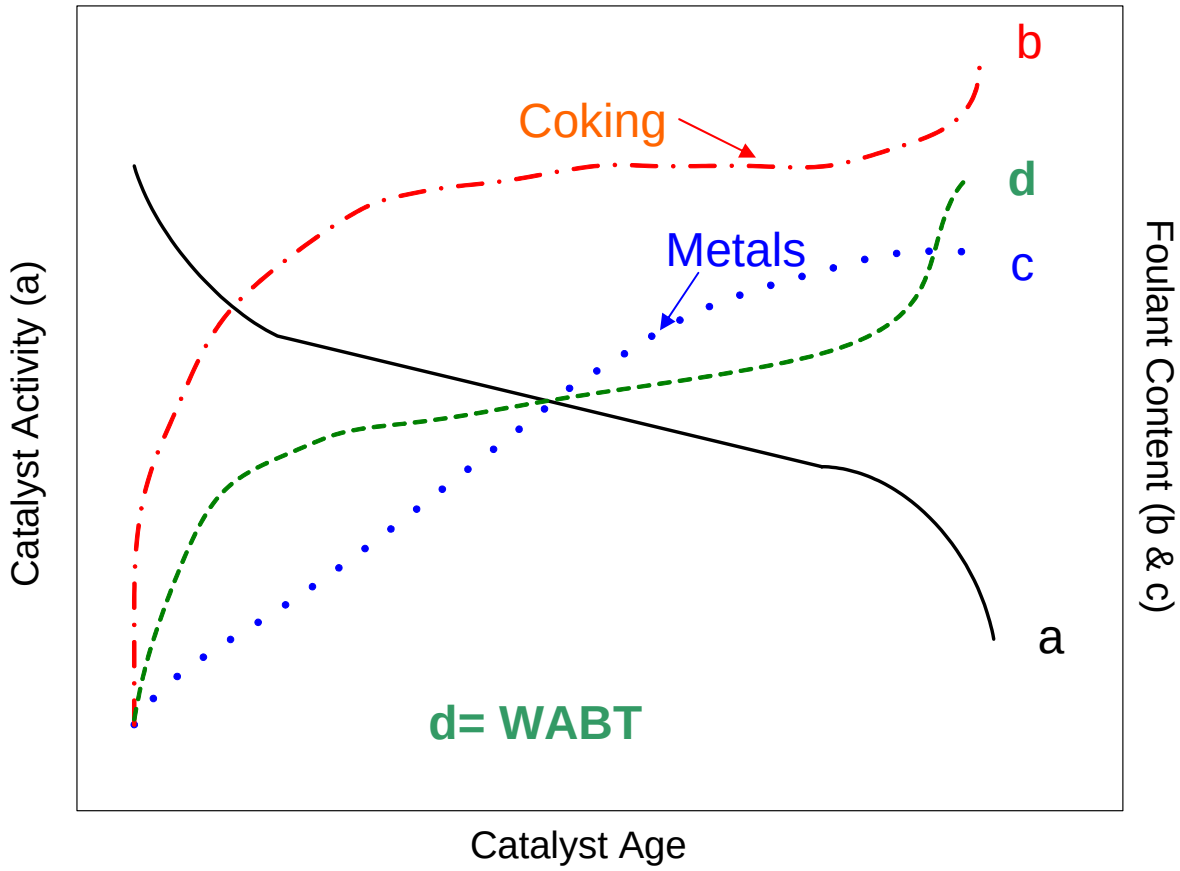

Figure 2.6 – Schematic Representation of time-dependant catalytic activity and coke and metals contents of the catalyst, a) Activity profile profile, b) Coke profile, c) Metal profile[20]. The representative WABT profile is shown as line d. It follows an s-shaped curve as well, but moves in the opposite direction to the overall catalyst activity profile. As a result, the WABT (a readily available plant measurement) acts as an indirect indicator of the reduction in catalyst activity during the reactor run.

In general, excessively high temperatures above 750 F[7] lead to deactivation of the catalyst much more rapidly than lower temperatures.

2.8.1 Metals impacting Catalyst Deactivation

Metals deposited on the catalyst from the feedstock may be nickel, vanadium, iron or arsenic, and greatly diminish the ability of the hydrotreater to remove sulfur. The VGO hydrotreater is specifically designed to remove these metals, as the metals can vary from a few parts per million in some Middle East crudes to several 1000 parts in say Venezuelan Orinoco crudes[15]. Usually a typical hydrotreating catalyst will show significant activity loss after 10% metals deposition on the virgin catalyst[22]. About 30% to 35% metals deposition is the maximum capacity for a typical catalyst[19-22].

2.8.2 Coke formation impacting Catalyst Deactivation

Catalyst deactivation by coke deposition is a serious problem in hydrotreater operation and if left uncontrolled can severely limited the operation. The rapid decline in the activity of the catalyst during initial operation of the process is caused by the initial coke formation, as shwon in figure 2.6. The initial coke reduces the surface area and porosity of the catalyst substantially[20], as coke does build up relatively rapidly to a maximum level within about 20% of the run cycle (SOR)[3,519,22], coinciding with the time at which a relatively constant activity is obtained.

A routinely cited coking mechanism, Figure 2.7, "hydrogen abstraction, carbon addition" (HACA) mechanism for adding rings to coke is shown as a possible route to consider for coke generation during thermal cracking in the VGO hydrotreater[23]. Figure 2.7 shows the most important steps:

1.Abstraction of hydrogen from the surface of the coke layer by a free radical,

2.Addition of a gas-phase olefin,

3.Cyclization,

4.The generation of radicals from olefinic sites, and

5. The dehydrogenation of unsaturated rings.

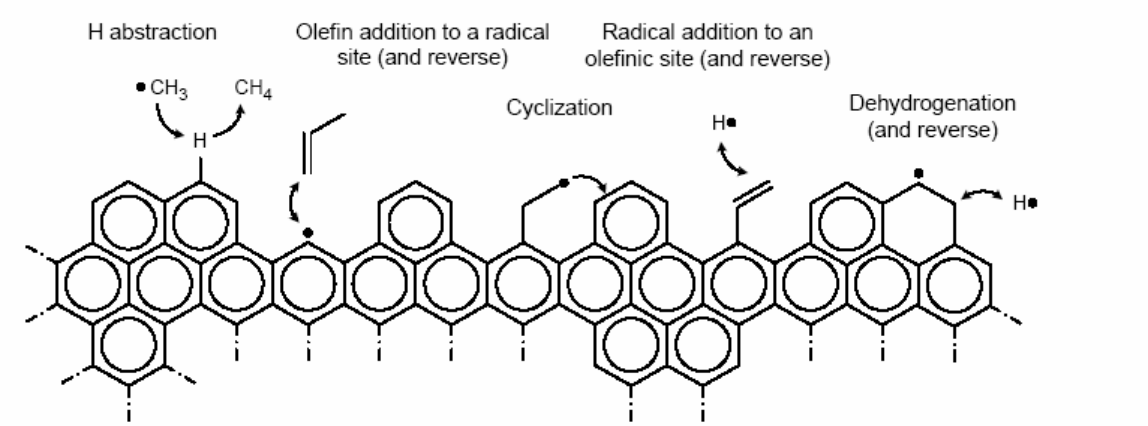

Figure 2.7- Radical Mechanism for Coke Growth in Hydroprocessing Units[24]

The impact of coking needs to be incorporated into the catalyst deactivation model. Note, the only benefit of coke formation is metals retention in the coke[19] .

2.9 Summary

Chapter 2 provided necessary background information on the function of a VGO hydrotreater and the importance of catalyst deactivation, through coking and metal deposition, in the process. The three stages of industrial hydrotreater operation need to be considered using at least the four primary key process variables (temperature, hydrogen to oil ratio, LHSV and hydrogen partial pressure) in any industrial based VGO hydrotreater model. Chapter 3 , Literature Review, discusses in depth the specific aspects cited in Chapter 2 required for the development the proposed hydrotreating model. The information from both Chapter's two and three will be used to develop a framework for the dynamic model to be presented in Chapter 5 (Model Theory).

3 Literature Review

The reactor type modeled in this study is the trickle bed reactor because it is the most commonly used in VGO hydrotreaters[3,6,7,10] and the mathematical models for trickle bed reactors are widely available in the literature. This includes both steady state and dynamic models. However, in most situations, the dynamic models show a simple exponential path to steady state when used in studying the dynamic responses or when used in advanced control applications. Furthermore, the models tend to be validated using only pilot plant data over a very short time period . A limited number of research publications did present investigations on the impact of catalyst deactivation on the dynamic behavior of trickle-bed reactors.

The current section will thus focus on the literature references that contain relevant theoretically based developments that can be used to enhance the effectiveness of the industrial correlations that were used as the basis for the dynamic model. This includes mathematical models for hydrotreating processes, concentrating on those involving catalyst deactivation.

In addition, information gathered from proprietary sources, specifically catalyst vendors, will be shared within the terms of confidentiality agreements.

Mathematical models cited in literature are listed in Table 3.1. Table 3.1 categorizes the literature references as steady state or dynamic, whether catalyst deactivation was considered and whether experimental (pilot plant or industrial) data was used in validating the developed models. Papers used as specific references in this thesis are appropriately noted.

Table 3.1: Summary on literature cited for the modeling catalytic reactors

REF No.	Reference	Model		Catalyst Deact.	Experiment P=Pilot I= Industrial	Application
		Steady State	Dynamic			
33	Levenspiel et al (1968)	X		X		Fixed bed reactor
32	Kodama et al (1980)	X		X		Residue desulfurization
31	Tamm Et al (1981)	X		X	P	Industrial Desulfurization, metals deposition
	Baiker and Bergougnan (1985)		X			Fixed Bed – 1-d vs 2-d modeling
37	Döhler and Rupp (1987)	X			P/I	VGO-treatment
	Chao et al. (1990)		X	X		Trickle Bed
	Barto et al (1990)		X			Fixed bed reactor
21	Chao et al. (1991)	X		X		HDS
	Barto et al. (1991)		X	X		Pellet Dynamics
	Miyauchi and de-Wind (1994)	X				Residue Hydrotreating
10	Lucien et al (1993)	X			I/P	Shell HDS process
	Froment et al (1994)	X			P	HDS, 1-d heterogeneous
	Borio and Schbib (1995)		X	X		Four stages reactor
29	Koyama et al (1995)	X	X		I	Vacuum Residue HDS
	Kulkarni and Dudukovic (1996)		X			Gas and solid phase fixed bed reactor
	Warna and Salmi (1996)		X			3-phase trickle bed reactor hydrogenation of toluene
13	Korsten and Hoffmann (1996)	X				HDS, 3-phase, Trickle Bed
	Recke and Jørgensen (1997)		X			Catalytic oxidation of hydrogen to form water
	Iliuta et al. (1998)		X		P	Residence time distribution
36	Lababidi et al. (1998)	X		X		Desulfurization
38	Juarez et al (1999)	X		X	P	H2S impact on HDS
34	Kokayeff (1999)	X		X	P	HDS Aromatic Saturation
35	Ho (1999)	X				HDS kinetics
28	Oballa (1999)	X		X	P	Hydrocracking
	Julcour et al (1999)		X		P	3-phase fixed bed
	Matos and Guirardello (2000)	X		X		HDS + HDM
35	Hu et al (2001)	X			I	HDS on Industrial data
	Chowdury et al (2002)	X			P	HDS of Diesel oil
	Lababidi et al. (2004)		X	X	P	Advanced control
4	Mederos et al (2006)		X		P	HDS, Trickle Bed

3.1 Steady State Models of Trickle Bed Reactors

A summary of the trickle bed reactor involving an ideal model was published by Charles Satterfield in 1975, and appears to be one of the more highly referenced articles for trickle bed reactors in hydro-desulfurization literature. This paper serves as a starting point for most trickle bed reactor analysis, since comparisons with slurry reactors, between pilot plant and industrial reactors, along with hydrodynamic impacts are provided. Satterfield also provides insight into mass transfer and contacting "impacts", since the HDS reactions are considered fast[25]. In 1992, Gianetto updated the trickle bed reactor summary of Satterfield to include research that developed correlations for determining when mass transfer, flow distribution and wetting efficiency effects should be considered. There still remains much work to be done on the reactor models and the correlations dealing with industrial data[26].

Based on pilot-plant data, Korsten and Hoffman[12] in 1996 proposed a three-phase reactor model for hydrotreating. The authors provided possible plausible explanations for the limitations of pilot plant models and suggested relationships applicable to industrial reactors when certain phenomena are applicable. In particular, the key process variables discussed (pressure, temperature, hydrogen-to-oil ratio) and the impact of wetting efficiency on reactor conversion of heavy crudes was considered crucial in any model development.

A residence time distribution (RTD) model to describe a trickle-bed reactor packed with porous particles and operated both under partially and fully wetted

conditions was proposed by Iliuta et al. (1999). They viewed the external liquid stream as divided into a dynamic zone where an axially dispersed plug flow pattern prevails, and an external stagnant (or static) zone contiguous to both the dynamic zone and the partially wetted porous particles. Experimental investigation of the residence time distribution was also reported by Iliuta et al. (1998). They examined the influence of imposed gas phase distribution along the packing bed on the axial mixing of liquid.

Literature from industrial research groups[13,27,28,29] (i.e. Exxon, Indian Oil, Novacor, Mizushima Oil) focus on developing a lumped approached (aggregation, asymptotic), for kinetic mass transfer and heat transfer effects for modeling purposes. The use of boiling points to characterize the crude helps to provide a theoretical means to explain the “peculiarities” and complexities of a hydro-desulfurization (HDS) process[13]. A one-parameter model was used in all cases.

A reaction order of 1.5-1.9 for hydro-desulfurization (HDS) reactions has been experimentally determined by various studies[28,30]. In addition, these studies[28,30] evaluated the benefit of choosing one sulfur species (ex. thiophene or dibenzothiophene) as the key representative reaction rate for the overall hydro-desulfurization reaction. Thiophene appears to be the most reactive, and is virtually absent from the product stream, while dibenzothiophene is mostly converted[27].

3.1.1 Catalyst Deactivation

The “s” shape curve representing the temperature profile in an industrial HDS reactor can be directly attributed to the three distinct zones of catalyst deactivation (start of run, middle of run, and end of run)[19,21,28,31]. Deepak and Thakur[19] provided a detailed review of the key contributors and considerations for catalyst deactivation. Metal deposition and coking during the entire reactor run can be represented in a pore-plugging model (effectively reducing catalyst surface area)[31,32]. Coking occurs rapidly at the start of run[33] reaching a steady state during middle of run, while metal deposition consistently increases during the start and middle of run[31]. Paul Robinson[5] discusses considerations for end of run deactivation (aromatics saturation[34], complete plugging of catalyst) which can be considered for dynamic model development.

3.1.2 Steady State Industrial HDS reactors

Applying a steady state model to monitor hydro-desulphurization unit performance[29,35,36,37] is the closest comparison to what is being attempted in this body of work. In each case, a steady state hydrotreater model incorporates catalyst deactivation factors and a summary of industrial plant data from one site. The studies model the middle of run performance well (when it is basically linear with no disturbances), but admit to not being able to model the start of run (SOR) and end of run (EOR) conditions[36]. In all three cases, weighted average bed temperature (WABT) is used as an indicator of catalyst deactivation and thus reactor performance, while maintaining desired sulfur outlet composition.

3.1.3 H2S Impact on Hydrodesulfurization

Various studies have shown that the inhibiting effect of H_2S on the main hydrotreating reaction is greater at lower temperatures and at start of run when the production of H_2S is the highest due to the initial high reactivity of the catalyst[12,19,20,26,20,38,39]. This information, mainly pilot plant based, is crucial in building the appropriate relationships to robustly simulate the start of run characteristics of an industrial HDS reactor.

3.1.4 Hydrogen Consumption in HDS Reactors

Very little public literature is found to model or correlate hydrogen consumption in the HDS reaction. In most industrial cases, operators run excess hydrogen to ensure that enough hydrogen is available[3,7,8,10] for the main HDS reaction. Narasimhan et al[27] (1999) provide a correlation to account for the various consumers of hydrogen (main HDS reactions, competing reactions, chemical and mechanical losses) while Haitham et al[36] (1998) provide a relationship for hydrogen consumption based on temperature and pressure. Both studies provided data for enhancing hydrogen consumption correlations obtained from industrial sources.

3.2 Dynamic Models

Research in dynamic modeling of catalytic reactors has been fairly extensive, however studies on trickle bed HDS reactors are not as readily available. The literature reviewed in this section and illustrated in Table 3.1 is of general interest in this area and serves as a comparison to the approach used in this research

study. The literature noted below deals with strictly first principle developments of dynamic models not necessarily for HDS reactors. Insight into applicability of one-parameter models, mass and heat transfer modeling, hydrodynamics (eg. Ignore radial effects), kinetics, mathematical solution approaches is provided in this literature.

The simulation and optimization of a set of industrial fixed bed catalytic reactors operating in deactivation-regeneration cycles was presented by Borio and Schbib (1995). They developed the dynamic mathematical models for the four stages of the process. The first model is for the dehydrogenation (deactivation by coking) stage, the second for steam purge, the third for the evacuation stage, and the last one for the regeneration stage. An iterative method was used to solve the simulation modules which operate in series, hence, it was possible to advance along the cycles starting from initial conditions of the bed until the overall mass and heat balances are satisfied. To prevent the permanent loss of the catalyst activity by sintering, an upper limit of temperature was imposed.

Dynamic models for three phase trickle bed and slurry reactors were formulated and presented by Warma and Salmi (1996). The proposed reactor models consisted of parabolic partial differential equations (PDEs), which were converted to ordinary differential equations (ODEs) by spatial discretization using finite difference formulas. The ODEs were solved by the backward difference method. The authors demonstrated their models through two examples; oxidation of $S0_2$ and hydrogenation of toluene. They concluded that the dynamic simulations

provided a meaningful path to the steady state of the reactor and gave valuable information on the reaction dynamics.

A first-principle dynamic model for a tubular fixed-bed reactor with a highly exothermic reaction was presented by Hua and Jutan (2000). They used this model in designing a nonlinear inferential cascade control. The dynamic behavior of the reactor was described by dimensionless, coupled, nonlinear PDE's, in which a pseudo homogeneous assumption was made. Their model neglected axial diffusion of reactants, wall capacity and heat losses. This model is then lumped using the orthogonal collocation method, followed by partitioning the model into three subsystems for control design purposes. The proposed dynamic model was used to simulate an industrial phthalic anhydride fixed-bed reactor.

Dynamics of recycle fixed bed reactors was investigated by Recke and Jørgensen (1997). In this type of reactors, un-reacted reactants or fraction of the outlet stream are recycled to improve the utilization of raw materials and reduce energy consumption. A pseudo homogeneous model with constant transport parameters was assumed, and radial effects were neglected. The model was developed for catalytic oxidation of hydrogen to form water. The model was discretized using orthogonal collocation.

A dynamic model of a three-phase fixed-bed reactor was reported by Julcour et al. (1999). Their model accounts for the limitations to heat and mass transfer at the gas liquid interface and catalyst surface, as well as the heat transport through the reactor jacket. It consists of a system of partial differential equations that were solved using the Gear method. The proposed model was tested by

comparing simulated transient axial temperature and concentration profiles with experimental responses obtained from a pilot reactor used for the consecutive hydrogenation of 1,5,9-cyclododecatriene on a Pd/AI203 catalyst. The authors concluded that a model with numerous parameters can be used to describe steady-state conditions and responses to moderate disturbances.

A dynamic two-dimensional pseudo-homogeneous dispersion model has been used by Kvamsdal et al. (1999) to simulate the performance of a fixed bed catalytic reformer. Baiker and Bergougnan (1985) presented both one-dimensional and two dimensional pseudo-homogeneous models to describe the dynamic behavior of a non isothermal, non-adiabatic pilot plant fixed-bed reactor, for the hydrogenation of toluene to methylcyclohexane on an industrial nickel catalyst.

3.3 Dynamic Models Considering Catalyst Deactivation

The variation of the reactor's performance with catalyst deactivation was addressed by Kunugita et al (1989). A dynamic model of a fixed bed reactor with catalyst deactivation was developed. First, the kinetic equations for the reaction of carbon dioxide with methane over a nickel catalyst were determined experimentally under negligible deactivation. Deactivating factors were then introduced to evaluate the effect of catalyst deactivation on actual reactor performance. The reactor dynamic model was expressed as a lumped-parameter model, represented by a system of nonlinear ordinary differential equations describing the energy and mass balances.

Effect of catalyst deactivation was also studied by Kunugita et al. (1989) using a transfer function between the manipulated variable and the reactor temperature. The transfer function was obtained by linearizing the dynamic model. In the proposed transfer function, the process gain and time constants are functions of the deactivating factors. Hence, as the catalyst deactivates, the parameters of the transfer function would vary affecting the dynamic response. The authors claimed that this approach is convenient for designing a control system, and stated that good agreement was found between the experimental data and simulation results under different catalyst conditions.

A nonlinear dynamic model for a fixed-bed reactor was utilized by Cheng et al. (1996a, b) to estimate catalyst activity as well as the temperature and concentration profiles. They proposed a scheme for state and parameter estimation in an industrial scale fixed-bed reactor with decaying catalysts where phthalic anhydride is produced by the partial oxidation of o-xylene. Their dynamic model is two-dimensional and pseudo homogeneous neglecting axial dispersion. They used a simplified deactivation reactivation model based on the balance of active sites. In their earlier publication, Cheng et al. (1996a, b) lumped the distributed parameter reactor model into a differential and algebraic system using orthogonal collocation on finite elements. The optimal estimation of the reactor state was formulated as a nonlinear program based on a moving horizon and solved by a sequential strategy. This formulation resulted in tracking the reactor behavior and inferring the catalyst activity profile using four real temperature measurements. However, the computing time required for the estimation is

longer than that for an optimal filtering method using a mechanistic deactivation model.

The dynamic behavior of a fixed bed reactor was examined by Megiris and Butt (1988), for a model hydrogenation reaction of benzene on a NiMo catalyst, poisoned by thiophene. Benzene hydrogenation reaction is usually used for deactivation studies because it involves large thermal effects, is irreversible, and subject to rapid poisoning by sulfur compounds, with a number of metal catalysts. In this study, the authors examined two types of dynamics; (1) constant temperature with variable conversion, and (2) variable temperature with constant conversion. They concluded that the constant conversion simulation results provided the means for identification of the catalyst poisoning mechanism, and the constant temperature dynamics provided a severe test for interpreting the traveling waves and cyclic operation.

In a later, two part publication, Megiris and Butt (1990 a, b) compared the simulation model with experimental results. The first part (Megiris and Butt, 1990a) explored a cyclic operating policy for the reactor operation, in which conversion is allowed to decline under deactivating conditions to a preset minimum and then readjusted to initial conditions by increasing the reactor temperature. They found that an integral guard bed, growing with time, is formed at the reactor entrance, which to a large extent governs the cyclic behavior.

Dynamic simulation and experimental results for a constant conversion policy was presented in the second part (Megiris and Butt, 1990b). They showed that the constant conversion operation is an “averaging” procedure that masks the

effects of all the important parameters that influence the dynamics of the reaction system. This remark is quite important because in practice, constant conversion operation is followed, and determination of intrinsic deactivation parameters in such conditions results in misleading conclusions.

Barto et al. (1991) addressed the influences of catalyst pellet dynamics on the overall bed dynamics. They studied the dynamic behavior of an isothermal axial dispersion fixed-bed reactor packed by catalyst pellets with Dirac delta distribution activity in the case of bimolecular Langmuir-Hinshelwood kinetics. They also discussed the influence of the active point location, the Thiele modulus and Damkohler number on the dynamic behavior. The model equations included pellet balances, reactor balances and reaction rate expressions. The authors showed that the heterogeneous model of the catalytic reactor behaved as a cascade of a number of individual catalyst pellets, with different reactant surface concentrations. They concluded that although there is some interaction between the pellets, the dynamic behavior of the reactor is governed by that of an individual pellet.

3.3.1 Residue Hydrotreating Reactors

The dynamic behavior of residue hydro-desulfurization reactors was studied by Chao[21] and coworkers and reported in a number of publications (Chao et al., 1986, 1987, 1989 and 1990). They examined the dynamic behavior of a one-dimensional pseudo-homogeneous model incorporating the effects of mass and heat dispersion. The parameters used in the simulation are primarily based on

the experimental data of Kodama et al[32] . The method of orthogonal collocation was used to obtain the solution of the coupled mass and energy balance equations. They also adopted the Kodama (1980) catalyst deactivation model in considering the interaction of demetallization and coking reaction on a catalyst. The performance of the reactor during the start-up period and that for long time operation was studied. The effect of stepwise changes in feed composition, feed rate, and inlet temperature on the dynamic behavior of the reactor were also investigated.

A combined system parameter estimation and deactivation model identification procedure was proposed by Chao et aI. (1990) to create what they called “a grey model” of an adiabatic residue hydro-desulfurization (RDS) trickle-bed reactor. Using the proposed grey model, the chosen objective function consisted of the predetermined reactor outlet sulfur content and the optimal set-point was the reactor inlet temperature. Five case studies using a dynamic simulator of an adiabatic RDS trickle-bed reactor were compared to pilot plant data.

Lababidi et al. (2004) studied the on line dynamic behavior of a pilot hydrotreating plant. A control strategy was implemented to optimize the degree of desulfurization by finding the optimal reaction bed temperature. Selected manipulated parameters are system pressure and reactor skin temperature. The authors highlighted the main factors affecting the operation and dynamics of the hydrotreating process. They concluded that advanced control techniques are promising in optimizing hydrotreating reactors where operating conditions are not stable due to catalyst deactivation.

As recently as April 2006 has seen the publication of the dynamic modeling research of a trickle bed hydrotreating reactor, validated with pilot plant data. Mederos et al[4] describe a dynamic heterogeneous one-dimensional model incorporating reactions for hydro-desulfurization, hydro-denitrogenation, and hydro-dearomatization. The model matched pilot plant data well, considering the short reactor length and all the wall effects specific to this size of pilot plant reactor. With no catalyst deactivation or wetting efficiency factors included, it is hard to imagine this model being valid for more than the 2300 seconds (38 minutes) it was validated for, and in an industrial setting.

3.4 Mass Transfer Considerations

Many studies have been performed to determine the impact of mass transfer[25,26,40,41]. There are potentially different transport steps (gas to liquid to solid) that may be rate determining in trickle bed reactor[40]. Fig 3.1, on page 40, illustrates the partial steps in trickle bed reactors. Numerous relationships for mass transfer coefficients are provided in the literature for use in developing HDS models. In the gas phase, the concentration of the reactant C_G (eg. Sulfur) is constant in the bulk part of the phase. As the reactant reaches the gas/liquid phase boundary, the concentration of C_G reduces to C_G^* governed by the gas phase mass transfer coefficient K_G. The reactant liquid phase concentration, C_F is the highest at the gas/liquid phase interface (C_F^*) and the reduction in concentration to the bulk liquid phase is governed by the liquid phase mass transfer coefficient K_G. C_F reduces to C_S across the liquid/solid boundary by the

liquid-solid mass transfer coefficient K_S. K_{FS} represents the overall mass transfer coefficient from the liquid to the solid phase. Within the catalyst, the reactant travels through pores to a point where the concentration of C reduces to zero. The point at which the reactant reaches zero within the pore varies and is governed by the mass transfer resistance within the catalyst pores.

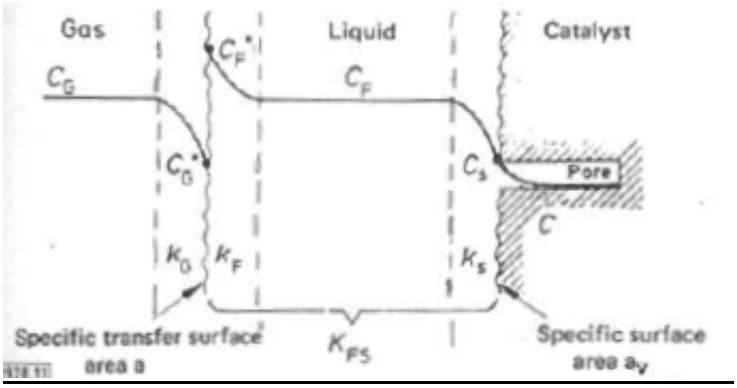

Figure 3.1 Partial steps in chemical reactions under trickling conditions[38]. The concentration profile of reactant C is shown in the gas phase, liquid phase and catalyst zone.

3.4.1 Gas phase Mass Transfer coefficient

It is generally theorized[7,25,26,40-44] and corroborated from lab studies that mass transfer resistance in the gas phase is not rate-limiting. The gaseous reactants (hydrogen and a few hydrocarbon non-condensables) are present in considerable stoichiometric excess and constitute a high mole fraction of the gas phase, hence it can be assumed that the transport processes in the gas film at the gas/liquid interface will not represent a rate-limiting step.

3.4.2 Gas-Liquid (KLa) Mass Transfer Coefficient

Studies have shown that the gas-liquid interface mass transfer coefficient is greater than the liquid-solid (KSa) interface mass transfer coefficient[26]. Gianetto and Specchia[26] and Hofman[40] appear to have developed useable correlations for the KLa in a trickle bed HDS reactor.

3.4.3 Liquid Phase Mass Transfer Coefficient

A few key papers elucidate when mass transfer phenomena through the liquid film should be considered. The relationship specific to hydro-desulfurization of middle distillates and VGO in industrial trickle bed reactors shows that mass-transfer in the liquid phase does not play an important role. An inequality was presented that if certain conditions were present than mass transfer in the liquid phase cannot be neglected[12,25,26,39] However, for pilot plant reactors where the liquid superficial velocity is 70 times smaller than that of an industrial reactor, this inequality is true, and thus mass transfer in liquid phase must to be considered[43].

3.4.4 Liquid-Solid (KSa) Mass Transfer Coefficient

KSa plays a minor role in the HDS conversion but still should be included in the model. Korsten and Hoffmann[12], Satterfield et al[41] and Iliuta et al[43] provide correlations that can be used in the HDS model.

3.4.5 Solid Phase

The main resistance inside the pellet is to mass transfer[45] with

mass-transfer limitations in catalyst pores more likely to occur if they are filled with a liquid than a vapor[10]. Typically, a Weisz-Prater criterion[26] is used to include the solid phase mass transfer resistance.

3.5 Wetting Efficiency

During this literature review, it was found that wetting efficiency (or contacting effectiveness) is a crucial phenomenon affecting the reaction rate in trickle bed reactors, which not only depends on the partial wetting of the external catalyst but also on external liquid renewal[12,25,26,40,42-44]. In these cases, the primary reactant feed is liquid, and if not volatile can go into depletion, accelerating catalyst deactivation[26]. Also, a decrease in the catalyst-liquid contacting reduces the surface for mass transfer between the liquid and catalyst causing a decrease in the reaction rate[44]. Figure 3.2 provides a representation for the flow pattern around a catalyst particle in the trickle flow regime under full wetted and partially wetted situations.

The wetting efficiency, η, (or sometimes called contacting effectiveness) is defined as the fraction of the catalyst pellet external area effectively wetted by the liquid flowing down the bed. Wetting efficiency is poor at low rates[10] at start-up and during upset conditions and thus should be included in any model attempting to simulate the entire run length of an industrial reactor.

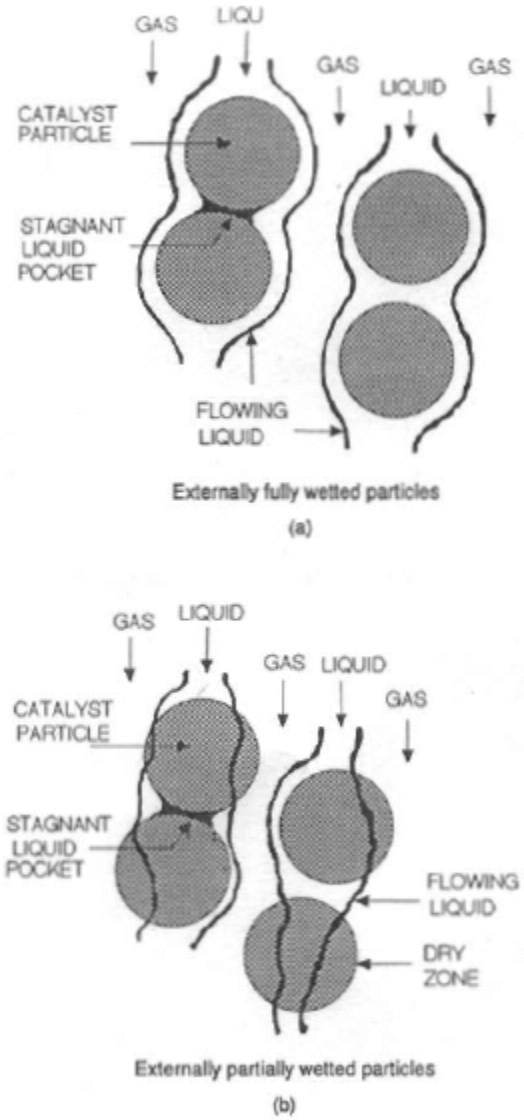

Figure 3.2 Schematic of flow patterns in trickle flow regime for a) externally fully wetted and b) externally partially wetted particles[44]

3.6 Industrial Information

Table 3.2 summarizes the experimental data for pilot sized reactors published in literature[4,12,20,24,30,38,40,41]. Table 3.2 also presents the same data for industrial reactor sizes gleaned from literature sources[29,35-37], and from the industry surveys[3].

Table 3.2 - Pilot Plant versus Industrial Reactor characteristics

Type	Superficial Liquid Velocity (kg/m^2s)	Superficial Gas Velocity(kg/m^2s)	Reactor Diameter (m)	Reactor Length (m)
Industrial	4-35	0.03-2.5	1.5-6	7-30
Pilot Plant	.08-3.5	.001-0.28	0.15-1	0.4 –2.5

Chapters four and five provide information from the industrial operators and catalyst vendors that signed secrecy agreements. The basis of the steady-state hydrotreater model is the proprietary correlations from the operators/vendors. Most proprietary correlations are similar to those available in the literature that are based on pilot plant data. A concerted effort was made to replace proprietary correlations with published information to allow a more transparent presentation of the model.

3.7 Summary

Nearly all literature for HDS dynamic models (Table 3.1) are solely based on validations using pilot plant data [4,21,32]. This approach does not transfer well to industrial applications for the following reasons:

1. Dynamic models only run from approximately forty minutes to three months in length [4,21,32]
2. Multiple variable disturbances and operator responses are not considered[4,12,21]
3. Low conversion occurs since the pilot plant reactor is 10-20 times shorter[7,12]

All the dynamic models developed were run over such a short time, that the accuracy of any catalyst deactivation factors, if included, cannot be ascertained.

In addition, the robustness of these models cannot be verified since the interaction of various variables (crude, temperature and hydrogen changes) is not demonstrated. Finally, non-validated correlations[40-44] have been developed to account for the incomplete catalyst wetting through contacting effectiveness that creates a lower sulfur conversion in pilot plants. As a result, there is little or no confidence in scaling up a pilot plant validated dynamic model to industrial scale conditions. Hence, there is a need to develop a VGO HDS dynamic model that is valid over an entire run length (at least 1.5 years).

There are a few papers [4,7] (Table 3.1) that attempted to show compatibility with industrial data by adding one or two commercial reactor data points from other literature to show how well the model could be applied in the industry setting. Note, almost any model can be made to match one or two data points. Also, these models showed at least one of the three noted deficiencies when trying to extend applicability to actual industrial conditions.

The literature review of dynamic modeling is still very important to this study as there are valuable insights that can be gleaned from a pilot-plant validated dynamic model, that can be used in the development of a novel industrially validated dynamical model for a vacuum gas oil hydrotreater model.

Chapter Four summarizes the data obtained from industrial VGO units that will be used to validate the model developed in Chapter Five. Chapters Six and seven provide the results from and application of the model, respectively.

Chapter 4: Data Acquisition

The primary objective of this thesis is to create a robust hydrotreater model that can be used to improve the operation of industrial HDS units. As noted in the literature review, there is very little industrial information available that can be used to validate an industrial focused model. Furthermore, pilot plants do not reflect how an industrial unit operates[12], so pilot plant data can not be used to validate the developed model. For this research to meet its primary objective, detailed industrial data from various sources was mandatory.

4.1 Sources of Data

Forty-five refineries/upgraders were visited to create a database of industrial hydrotreater data that could potentially be used in validating the developed HDS reactor model. Over a ten year period, a database of 24 hydrotreaters (HDS) in various services (Distillate, Vacuum gas oil (VGO), naphtha, kerosene) was developed. Of the 24 HDS in the database, 14 Hydrotreater units have the necessary process and equipment information to adequately build a representative model of the hydrotreater unit. For publishing purposes, confidentiality agreements with 6 of the refinery/upgrading operators (all in North America) have been obtained (labeled plants A-F). Multiple site visits to witness the data retrieval and operation for most of the units was also performed. The necessary data required from the operating plants for model development is as follows:

1. **Operating**- pressures, temperatures, (WABT = weighted average bed temperature), flows for an entire run length (SOR to EOR).

2. **Frequent/reliable compositional laboratory data** - crude (including aromatics, cracked gas, olefins) off gas, hydrogen, contaminants (including sulfur, nitrogen, chlorides, and metals (vanadium, nickel, iron), bromine #
3. **Equipment**- vessel size, pump sizes, piping sizes, control valves
4. **Catalyst**- suggested k (activity/equilibrium) values, size, shape,

Excerpts of the raw process data from all the units is provided in table format in Appendix B. Tables 4.1a and 4.1b, on page 51, provide a range of operating data from a large industrial sample of HDS trickle bed reactors. The column labeled "Industry Range of HDS Units" is taken from a personal database and information provided from reference 7. All six plants used in this research operate within the industry range developed. Three of the plants (A,E,F) have reactor pressures below 700 psig, while the other three plants (B,C,D) operate between 970 and 1550 psig. The average initial reactor temperature range was 630-685^{o}F. Plants B, E and F had hydrogen to oil ratios of less than 1000, while the other three plants had over 2500 scf/bbl for hydrogen to oil ratio. In all cases, a significant amount of hydrogen is required to obtain the necessary outlet sulfur specifications. All plants require outlet sulfur to be less than 0.05 wt%, with two plants requiring <0.03 wt% of sulfur. Product nitrogen for four plants needs to be less than 10 wppm.

Each of the six operating units differ to some degree from one another, and thus provide ample unique validation opportunities for the developed model. However,

as noted in Table 4.2, on page 52 all the plants are VGO (Vacuum gas oil) hydrotreaters. A concerted effort was made to obtain operating data from units processing at the same point in the refining process. The intent of this approach was to make the model manageable since different refinery streams have different hydrotreating processing schemes and requirements[6-8.]

Table 4.1a Hydrotreating Operating Conditions

	Industry Range of HDS Units	Plant A	Plant B	Plant C
Space Velocity, LHSV	.1 – 15	0.76	1.23	0.54
Reactor Pressure, PSIG	300 – 2200	675	1065	970
Temperature, °F average	500 – 800	630	645	666
Hydrogen to Oil, SCF/Bbl	300 – 5000	2500	840	3050
Product Sulfur	5 ppm-0.5%	0.04	0.05	0.03
Product Nitrogen	5 ppm-0.5%	<10ppm	<3 ppm	<0.3%

Table 4.1b Hydrotreating Operating Conditions

	Industry Range of HDS Units	Plant D	Plant E	Plant F
Space Velocity, LHSV	.1 – 15	0.41	0.88	1.63
Reactor Pressure, PSIG	300 – 2200	1550	460	475
Temperature, °F average	500 – 800	685	635	675
Hydrogen to Oil, SCF/Bbl	300 – 5000	4400	750	925
Product Sulfur	5 ppm-0.5%	0.03	0.04	0.04
Product Nitrogen	5 ppm-0.5%	<10ppm	<3 ppm	<0.1%

4.2 Reactor Information

Table 4.2, on page 52 shows a summary of catalyst/reactor information crucial for developing a hydrotreater model. The physical dimensions of the catalyst (volume, weight, bulk density, size) are provided. The catalyst particle size ranges from 1.87mm to 2.54mm, with the bulk density ranging from 38.4 to 53.2 lbs/ft^3. For purposes of this study, the catalyst shape is assumed to be cylindrical for all cases. The shapes of the catalysts used in the six plants do vary from the cylindrical shape but this information was unavailable from the plant or catalyst

vendors. Also, in the model development, a simplifying assumption was that the catalyst diameter and length are the only inputs used to define the catalyst particle. The reactor diameters are in the narrow range of 11 feet to 14 feet while the catalyst volume has a wide range (3415 – 6523 ft^3). For the 6 units, the catalysts are either nickel-molybdenum (NiMo) or cobalt-molybdenum (CoMo) on an alumina substrate. Typically, CoMo catalyst is used for "moderate" hydrodesulfurization, while NiMo catalyst is used for "severe" hydrodesulfurization (ex. Ultra low sulfur diesel) involving nitrogen removal and aromatic saturation. Porosity and tortuosity values were provided under secrecy agreement and have not been published in this document. The overall average reaction order ranged from 1.4 to 1.7 and activation energy ranged from 24500 to 32000 cal/mole for the key hydrodesulfurization reactions listed in Chapter 3[3]. Also shown in table 4.2 is the length of each unit's run which varied from a low of 1.1 years (significant disturbances during operation) to a high of 3.0 years (very minor disturbances during operation) and the typical sulphur feed (0.8-2.2 wt%) and product concentration of sulfur.

Table 4.2 – Catalyst/Reactor information

UNIT		Plant A	Plant B	Plant C	Plant D	Plant E	Plant F
REACTOR DIAMETER	ft	13	12	12.5	12	11	14
CATALYST TYPE		NiMo on Al	NiMo on Al	CoMo on Al	NiMo on Al	NiMo on Al	CoMo on Al
CATALYST VOLUME	cuft	4424.0	2865.0	5925.6	6523.0	2415.0	4189.0
CATALYST WEIGHT	lbs	207928.0	110016.0	266650.0	316650.0	128478.0	163371.0
CATALYST DENSITY	lbs/cuft	47.000	38.400	45.000	48.544	53.200	39.000
Cycle length	years	2.60	2.00	1.80	1.08	3.00	2.28
REACTION TYPE (HDS,HDN)?		HDS	HDS	HDS	HDS	HDS	HDS
DESIRED PRODUCT S	%WT	0.04	0.05	0.03	0.03	0.04	0.04
TYPICAL FEED S	%WT	1.70	0.80	1.50	2.20	1.40	0.90
SOR AVERAGE TEMP.	°F	605.0	590.0	660.0	580.0	631.0	610.0
TYPICAL LHSV	H-1	0.76	1.23	0.54	0.41	0.88	1.63
FEED TYPE (N,KERO,LGO,VGO)?		LGO	LGO	LGO	LGO	LGO	LGO
SUGGESTED REACTION ORDER	-	1.65	1.5	1.6	1.7	1.55	1.4
ACTIVATION ENERGY	CAL/MOLE	27000	29000	32000	24500	26500	27500

Figure 4.1 provides more detailed information on how the catalyst beds are

arranged for one of the reactors (plant B).

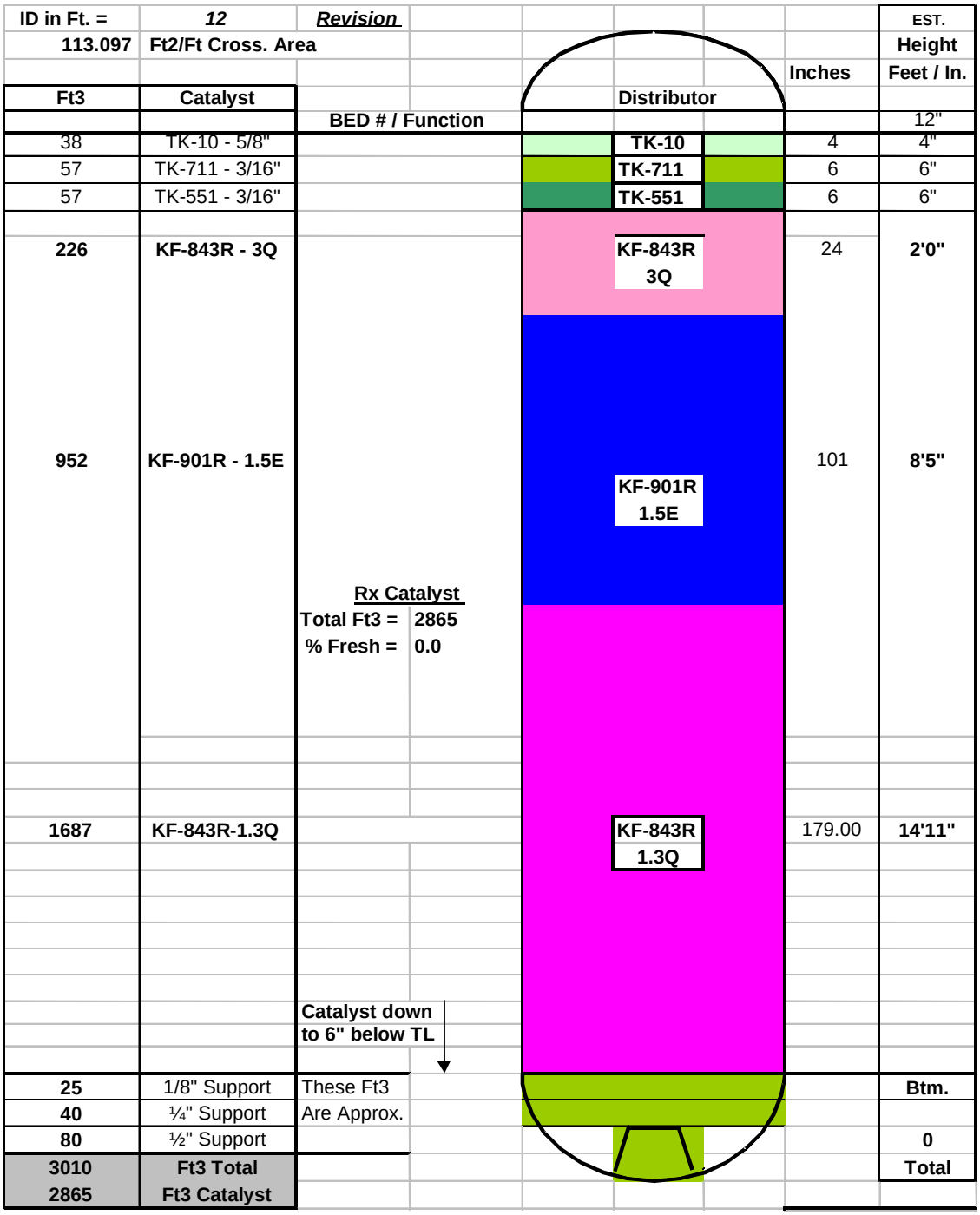

Figure 4.1 Plant B catalyst configuration in reactor. An example of the detailed catalyst bed info used in the research. Type and volume of catalyst is noted. Appendix A contains the same information for each of the six units that were evaluated. For each of the catalysts a volume has been provided for use in both

the steady state and dynamic model. This information is not readily available in the public domain.

4.3 Representative PFD

All six units used in this evaluation are trickle bed reactors with a single reactor scheme. Figure 4.2, on page 55, illustrates a portion of Plant B's actual PFD (process flow diagram). The other 5 plant PFDs are available on the thesis CD. As noted in Figure 4.2 and explained in Section 2.5, the feed to the Hydrotreater reactor is pre-heated in the furnace to the required feed temperature. The HDS reaction takes place in a single trickle bed reactor with at least four beds of catalyst (five beds in Plant B, Figure 4.2). Each bed has a hydrogen quench to control the temperature of the reaction along the length of the reactor. The hydrogen flow is on a cascade control loop, with the main control variable being the bed temperature and the secondary control variable being the flow of hydrogen. Figure 4.2 illustrates this cascade control loop and is implemented on all six plants that were evaluated.

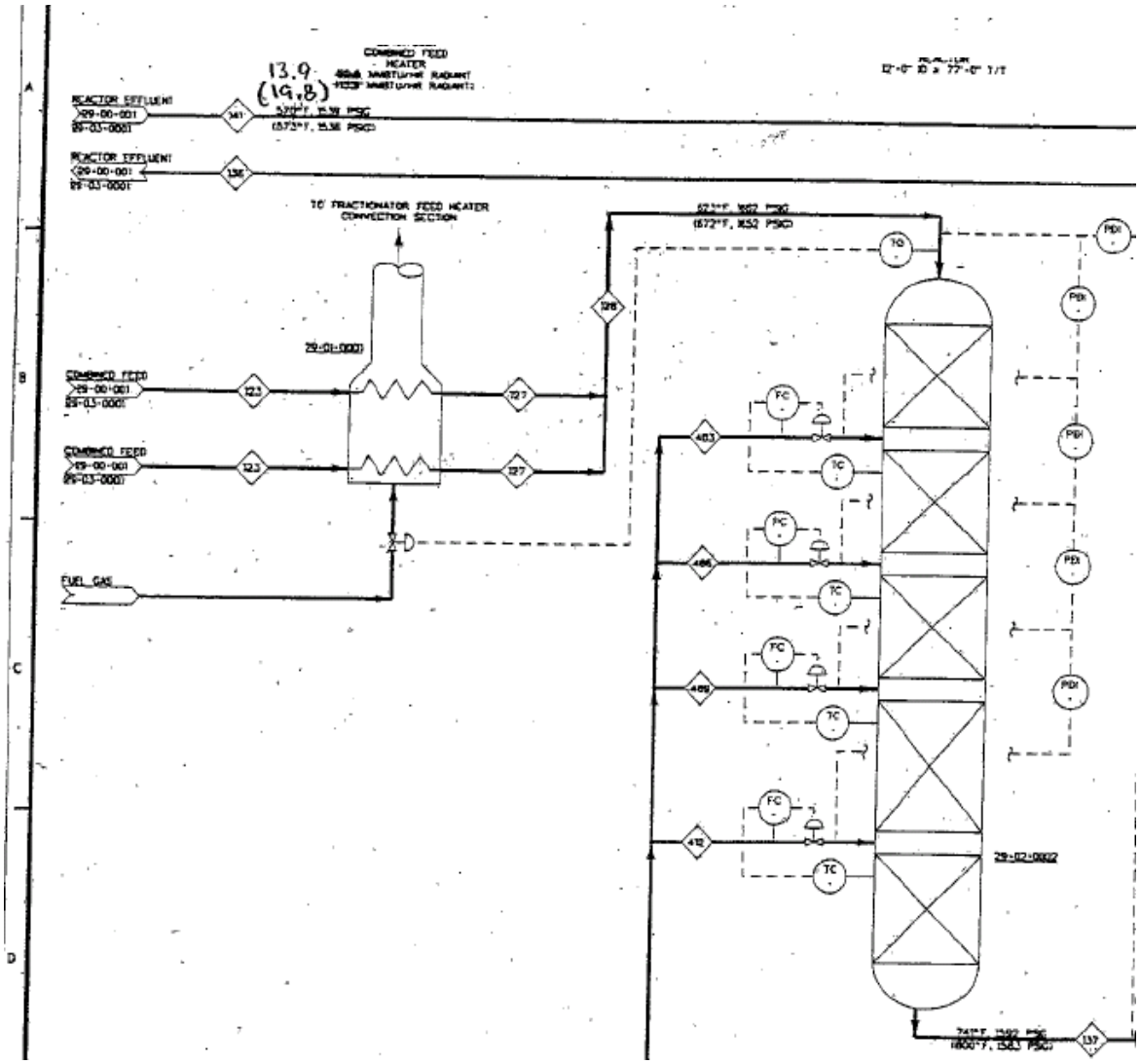

Figure 4.2 – Plant B – Representative Portion of PFD for HDS Reactor. Picture is taken from an actual PFD from Plant D. HDS reactor with 5 fixed catalyst beds and intermittent hydrogen injection are shown. Also shown is the feed furnace.

4.4 Plant Data Obtained

This section provides an illustration of the process data obtained and evaluated. Appendix B contains all the process data tags and some data points in tabular form. Every data point from every plant is provided on the attached thesis CD. Figures 4.3-4.8 show some of the key process variables and how they trend through out the operation. Understanding how the reactor responds to various

disturbances is crucial in building a robust model. The main requirement for an HDS reactor is to control the outlet sulfur to just below a specified maximum limit (Table 4.2). When the inlet sulfur increases above the normal expected amount (a disturbance), the reactor WABT responds as shown in Figure 4.3 for Plant D. The resulting increase in WABT (weighted average bed temperature) is required to try to maintain the outlet sulfur concentration specification. As the reactor temperature increases, the activity (conversion) of the catalyst increases but the impact on longer catalyst activity needs to be considered. Note, the reactor temperature profile over the run length is the inverse of the catalyst deactivation profile. The reactor temperature is a readily available measurement (with multiple temperature indicators in each bed) and thus is used as a key indicator of how well the model matches the operation of the actual plant. The response presented in Figure 4.3, on page 57, occurred when the inlet sulfur went from an expected 2.2% to 4.2% and the plant operator gradually increased the reactor bed temperature from 630 to 647 F) in response to the feed sulfur increase.

Figure 4.4, on page 57, shows the overall inlet and product sulfur measurements for plant D. Thus the model must be able to accurately calculate the outlet product sulfur content. Figure 4.4 shows that as the inlet sulfur increases, the reactor struggled to maintain the same level of outlet sulfur concentration as in the start of the run. The reactor could not handle the increased sulfur, with the WABT increases not adequate to stimulate sufficient catalyst activity. Some other variable needed to be adjusted to get sulfur product with specification.

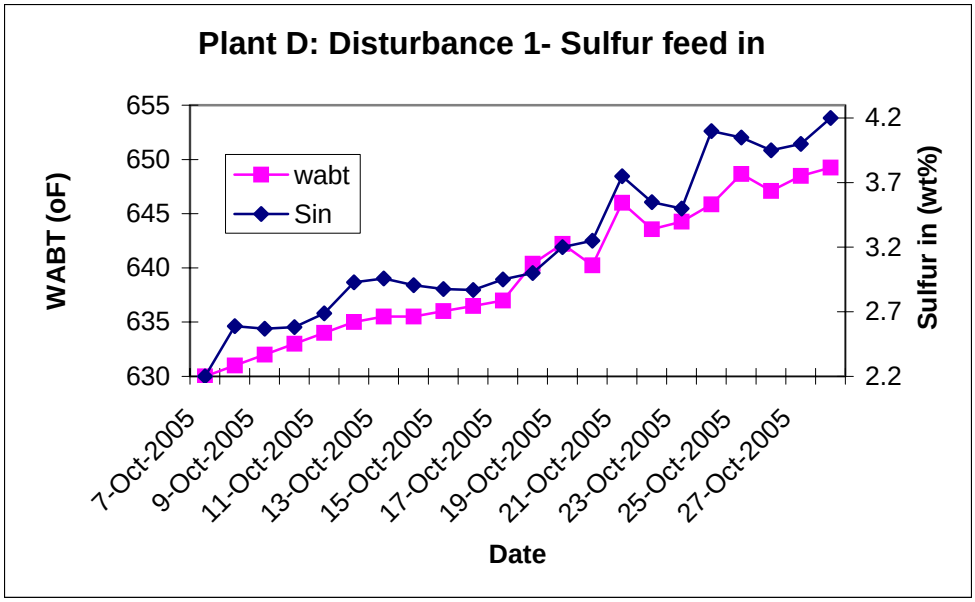

Figure 4.3 Plant D: Example of Feed Sulfur Disturbance and Temperature Response. The inlet sulfur went from 2.2 to 4.2 wt% in a span of 20 days. The WABT was increased from 630 to 650^{o}F to increase activity of catalyst.

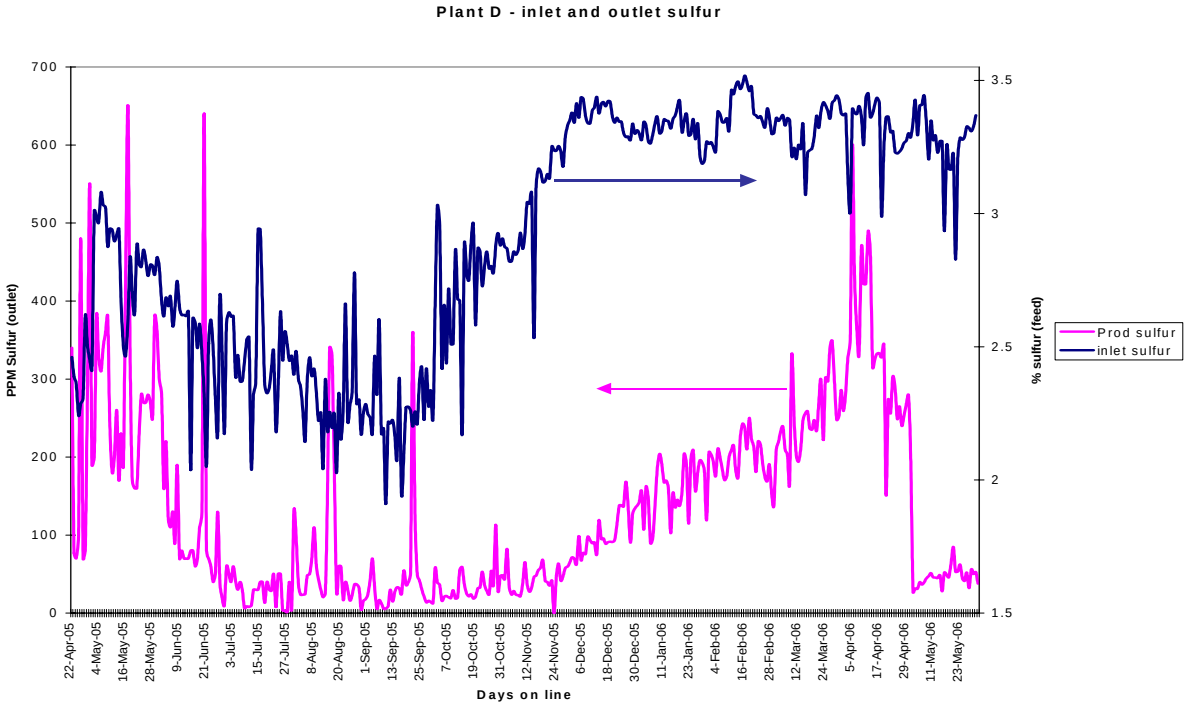

Figure 4.4 – Plant D: Inlet and Outlet Sulfur. 400ppm is the sulfur product specification. The inlet and outlet sulfur values are shown for the entire run length for plant D.

Figure 4.5 provides an illustration of key disturbances on WABT, thus on the operation. It is these disturbances, with all the necessary information provided by the operator, which allowed for the development of a correlative, partially predictive dynamic model. The figure shows three disturbances impacting the overall run length and crude processing, and outlines what happens in the process as a result of the first sulfur disturbance, namely that the catalyst life is shortened, crude charge is reduced, and the WABT must be increased to increase catalyst activity.

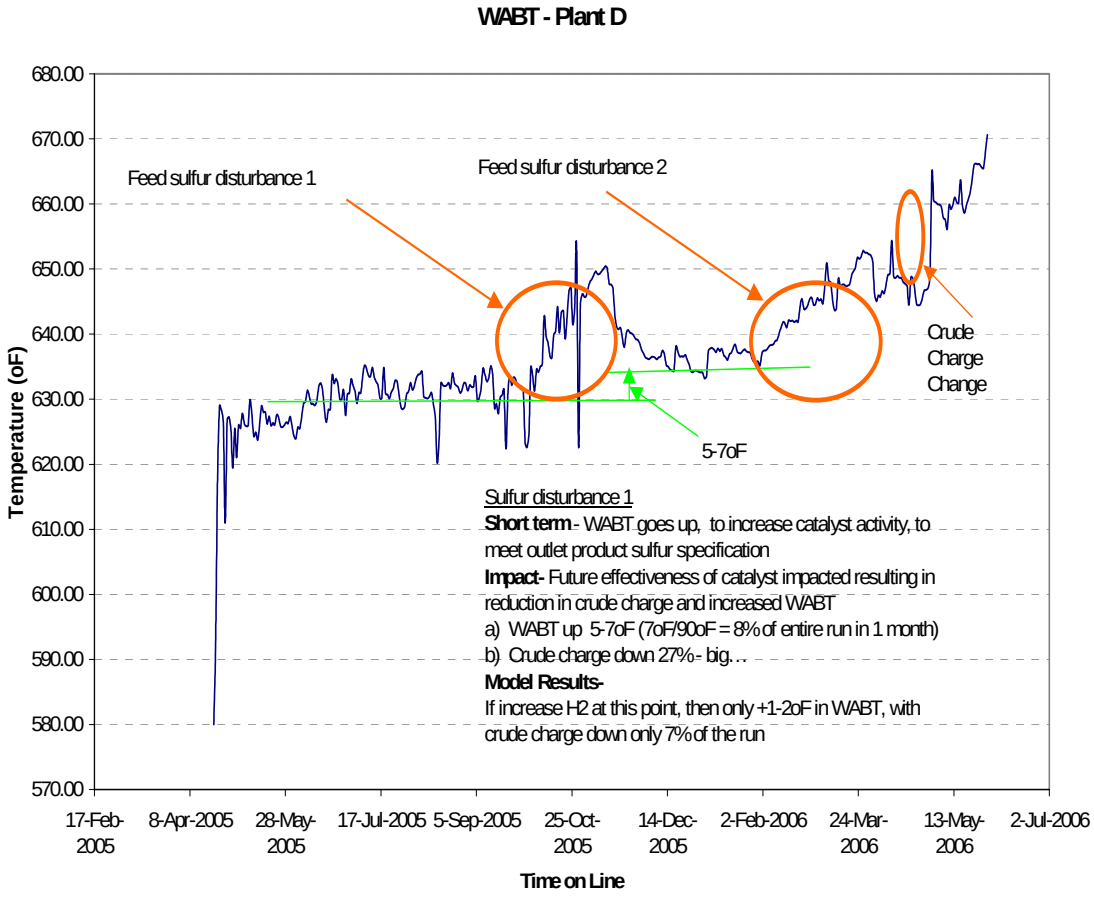

Figure 4.5 Major disturbances and WABT for Plant D. The WABT for platn D for entire run length is shown. Two sulfur disturbances and one crude change are noted, with the effect being an increase in WABT. The model developed in this thesis needs to simulate the WABT response to the major disturbances noted.

The other two disturbances noted in Figure 4.5 are another sulfur distrubance and an increase in crude flow.

In all cases, the WABT increased in response. Figure 4.6 adds the crude flow to the WABT shown in Figure 4.5.

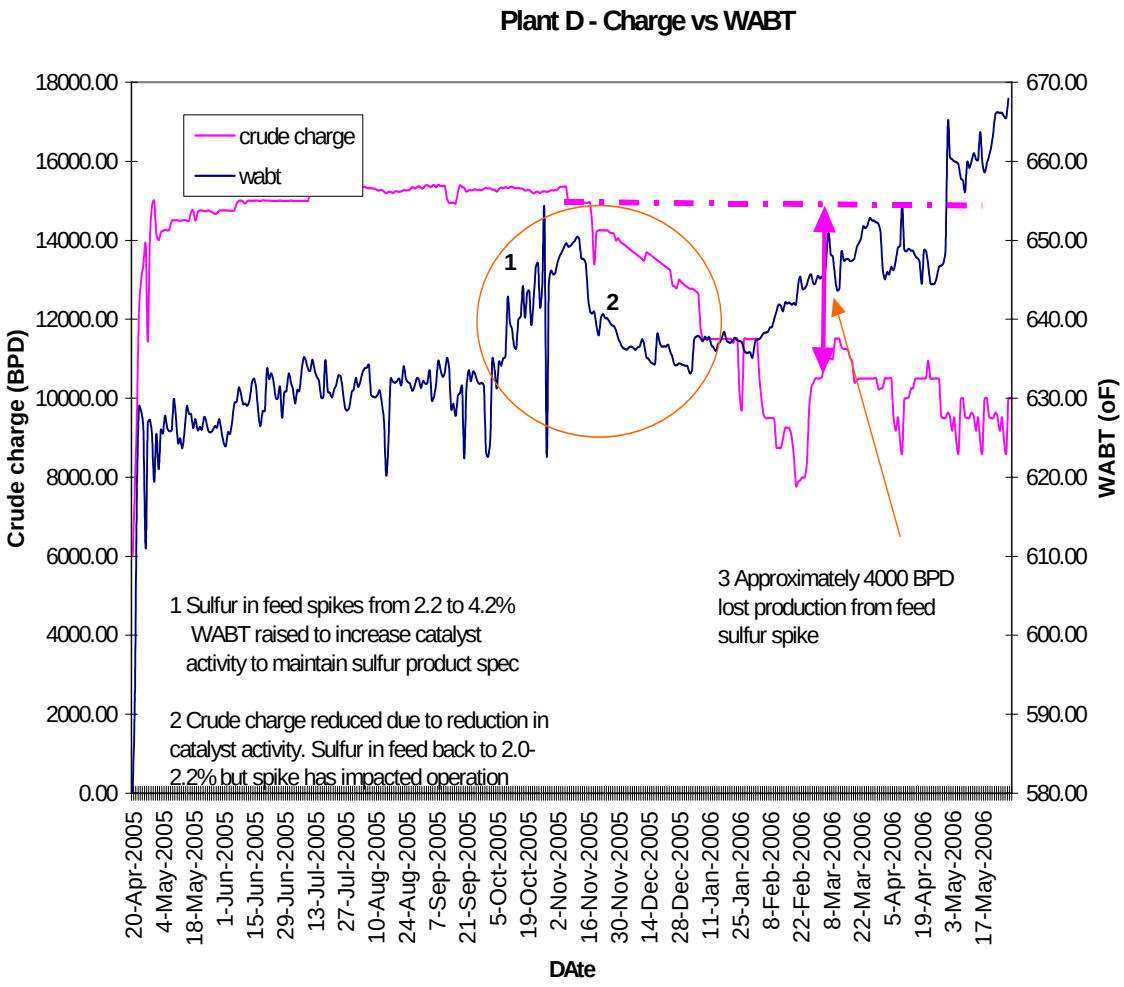

Figure 4.6 – Plant "D" Crude and WABT from Start of Run (SOR) to End of Run (EOR). The crude flow is reduced since the increase in WABT was not obtaining the desired outlet sulfur values. The crude was reduced by approximately 4000 BPD. WABT was also reduced concurrently (November to December 2005) to try to "extend" reactor run length.

For the first disturbance, the crude flow was reduced since the rapid increase in temperature to increase catalyst activity severely impacted the performance of the reactor. As a result, the amount of crude that could be processed was reduced (on average 4000 BPD). If the reactor operation can mitigate the impact of various disturbances, for this case, a maximum increase in throughput of 4000 BPD could be obtained.

Figures 4.7 and 4.8 (on page 61) show two other key reactor process variables, namely pressure, hydrogen purity and hydrogen to oil ratio. For these two key variables,

there does not appear to be a change to optimize the operation due to these disturbances.

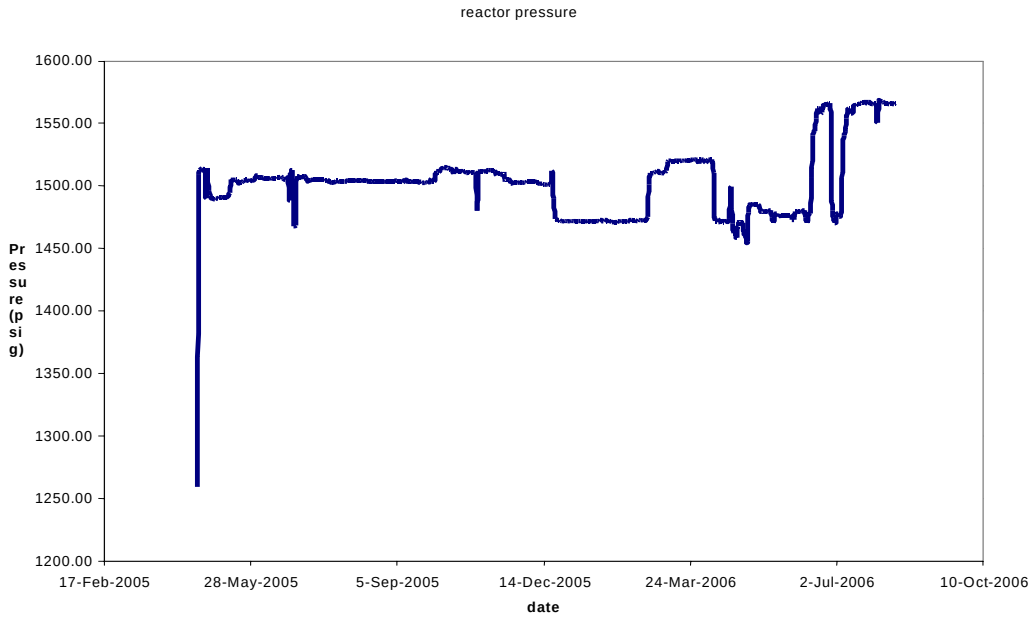

Figure 4.7 Plant D Reactor Pressure. Pressure is shown for the entire run length.

However, the hydrogen purity and hydrogen to oil ratio tend to trend downward near the latter half of the run when an increase or at least maintenance of these values would be expected to maintain the reactor performance. This would suggest that there may be an opportunity to use these variables to mitigate the impact of the disturbances.

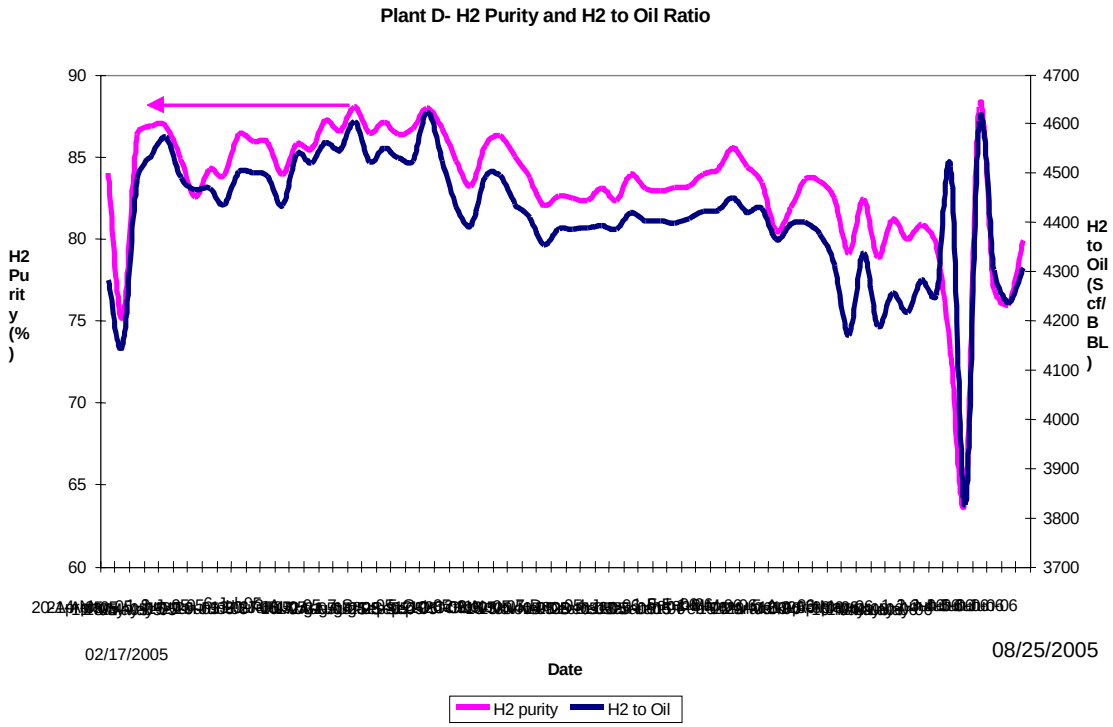

Figure 4.8- Plant D -Hydrogen Purity and H_2 to Oil ratio. Data is shown for the entire run length

4.5 Limitations/Benefits of industrial data

4.5.1 Benefits

The obvious benefit of obtaining extensive industrial data from multiple operating units, is the ability to validate a model with industrial data. Actual crude and the real contaminants are used on the specified catalyst at the required operating conditions. In the public domain, researchers have little access to industrial data

to validate their pilot plant based models. In addition, the suggested/expected performance of the hydrotreater is provided as a starting point for creating a representative model for the entire industrial run length. There are no scale-up issues as there is when using pilot plant data and there is no concern with developing/improving a model that has not been properly validated in an industrial setting. However, if classical theory from pilot plant research can be used to simulate the desired trend as a starting point for the model development, operators will have confidence in the output of the model.

The model developed in this study uses lumped parameters (explained further in Chapter Five) which match well (R^2 of 0.90-0.935 for WABT) with the type of information gathered from the industrial plants. For example, crude compositions are provided as boiling point ranges and the sulfur composition is provided as an overall sulfur value, not on a sulfur species basis. Laboratory testing of a typical feed sample for a distribution of sulfur species has been provided for each operating unit, in order to obtain an appreciation for what sulfur bearing compounds are in the feed stream.

In most literature, the pilot plant explores the impact of a single disturbance and the resulting new steady state. In an industrial environment, the operating objectives differ significantly, with multiple operating variables changing in response to a disturbance to move to a new stready state rapidly. A model of an

industrial unit must incorporate this operating reality while also understanding the limitations of a lumped approach when individual effects may be missed.

4.5.2 Limitations

A key drawback to using solely industrial data is that there is little quality control of the received data. In a pilot plant, the location of sample points and process measurements can be set by the researcher to obtain the desired information. In addition, pilot plant tests can be re-run multiple times to develop confidence in a certain cause/effect relationship. No such luxury is available in an industrial setting. Different operators in an industrial setting will run the plant slightly differently, that is, there is no way to account for the variances in operating philosophy from shift to shift. It must be assumed that over the entire run length, the impact of differing operating philosophies (conservative versus aggressive versus inexperienced etc.) will be small compared to the overall response of the reactor to external disturbances.

4.6 Summary

There is very little industrial data published that can be used for steady state and dynamic model development. Detailed industrial data, under confidentiality agreement, was obtained from six refiners/upgraders. Catalyst, process and laboratory data, and equipment information was among the needed and gathered data. Hence a significant objective of this study was obtaining the necessary industrial data to enable the development and validation of a model ready for use

in an industrial setting. This chapter clearly showed that the objective to gather quality industrial data was attained and that the benefits of using industrial data should out weigh its limitations, but the limitations need to be considered when evaluating output from the derived model.

Chapter five takes the relevant data from this chapter and presents the development of the steady state HDS model and the application of the developed dynamic model. Chapter 6 uses the process data summarized in this chapter, and provided in Appendices A, and B to validate the model. Chapter 7 discusses the application of the model to industrial opportunities and chapter 8 provides the conclusions and recommendations for further studies.

Chapter 5: Model Development

5.1 Model Basis

The model in this study was developed to meet the objective of creating a dynamically functioning VGO hydrotreating model that can be used successfully in industrial settings. Process data, equipment specifications, and catalyst information from actual commercial-scale VGO hydrotreaters were used in building and validating the model.

5.1.1 Model Platform

Since this model is developed for industrial settings, and to be used by refiners/operators, the software considered for the model had to have the following features:

1. Should be readily available to the operators
2. Users should be familiar with tool(s)
3. Relatively inexpensive
4. User friendly

All refiners/operators use spreadsheet based software for various functions such as linear programming to optimize plant economic objective function, and evaluate operating data. Excel® (with Visual Basic®) was chosen as the primary tool to store, and calculate the various parameters of the VGO hydrotreater model and to display the output. For the dynamic portion of the model, HYSYS® was chosen. All operators[3] are familiar with HYSYS®, and use a simulator (HYSYS®, Aspentech, PROII (SIMSCI), VMGSim) to provide plant/unit

calculations and sensitivity analysis. Refiners/operators do not readily use dynamic simulation tools due to the difficulty in using them[5,7,46]. If a dynamic model is to be accepted and used by the refiner/operator, using an extension of a familiar tool should provide the operator confidence that using a dynamic model can be taught and benefits realized. Both software packages chosen are common tools used by the expected users, so implementation at an operating unit should be feasible. Figure 5.1 shows a simple schematic of the communication between Excel® and HYSYS® developed model. All the necessary kinetic relationships, and correlations are stored in Excel® for the calculation of the outlet sulphur composition, and hydrogen consumed at each time

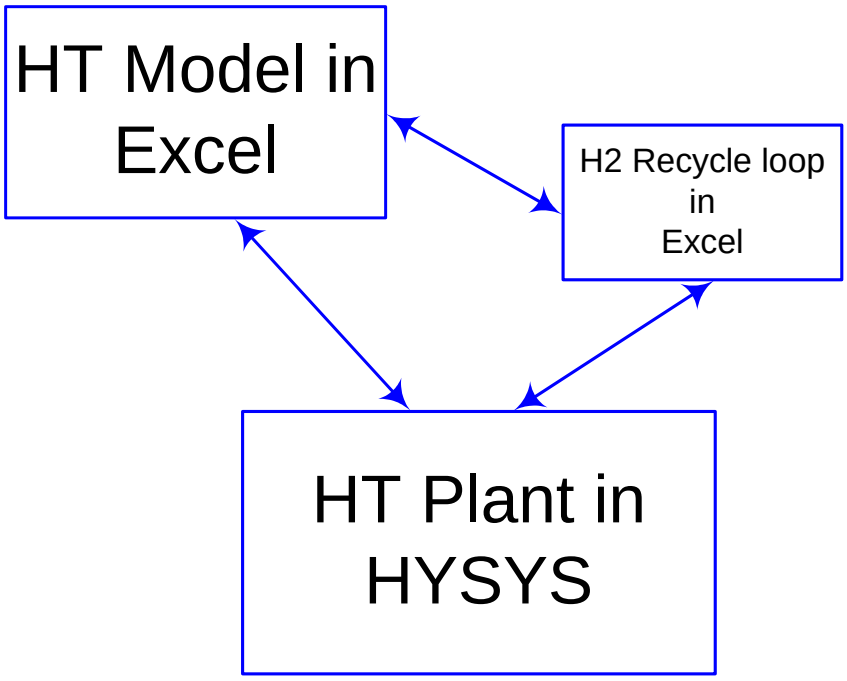

Figure 5.1- Model Platform – Software Interaction between Excel® and HYSYS®. The hydrogen recycle loop and the hydrotreater model reside in Excel® while the entire plant was simulated in HYSYS®. The H_2 recycle and reactor temperature are used to ensure closure between the two programs for each time step.

step. HYSYS® is used to simulate the entire unit and run the model dynamically. A detailed explanation of the calculation routine is provided in Section 5.9.

5.1.2. Lumped Approach

Data obtained from industrial operations is routinely in a “lumped” format. As stated earlier, crude oil is defined and measured based on boiling point ranges, while sulphur is typically measured and reported as an overall %, that is, not by specific component. Hence, the model must reflect the lumped nature of the data available at the industrial unit. Lumped crude properties are used in both the steady state and dynamic portions of the model. To address the lumped sulphur composition provided from the industrial units, dibenzothiophene (DBT) was chosen as the sulphur component to base the overall sulphur reaction kinetics on. Figure 5.2 shows the possible reaction routes for DBT. K_1 in Figure

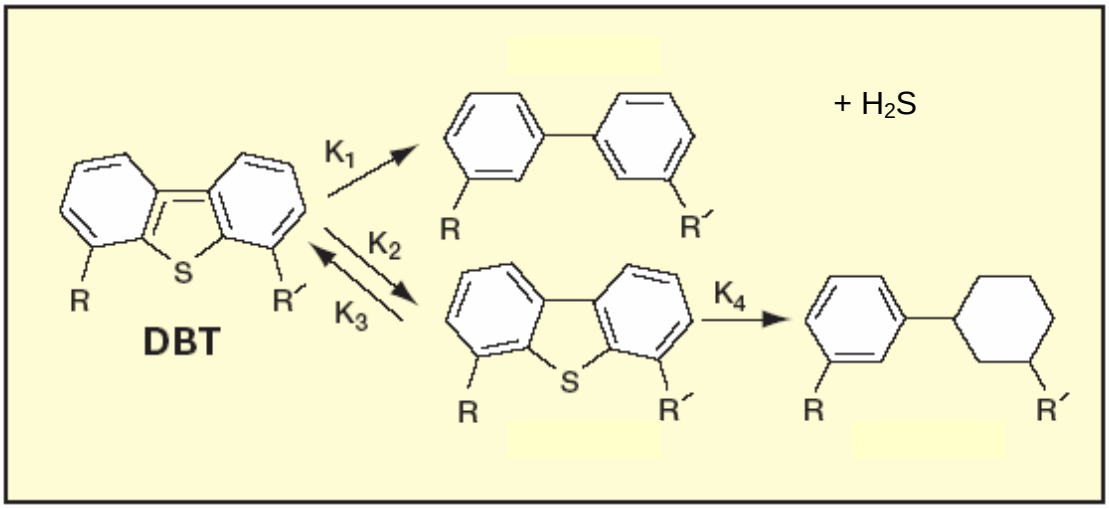

Figure 5.2 – A proposed HDS Mechanism by Hu[35]. A fast direct route for conversion of DBT is shown by K_1, and the slower indirect/hydrogenation route is shown by K_2,K_3,and K_4. For the lumped model in this research, the slower hydrogenation route for DBT (dibenzothiophene was considered).

5.2 represents the direct route for conversion of DBT to H_2S and its removal. Most sulphur-based components follow this route: mercaptans, sulfides, di-sulfides and thiophenes[7,32,33,35,46] . The hydrogenation route (K_2,K_3,K_4) is a slower route, requiring partial hydrogenation of aromatic rings in the DBT structure prior to removal of sulphur. It is hypothesized that by using the slower DBT hydrogenation route to represent the overall sulphur conversion, treating all the sulphur as DBT should provide the representative conversion of all the sulphur. All the sulfur species that are easier to convert than DBT, will be lumped as being converted as of DBT. The reversible dehydrogenation portion of this reaction provides a realistic representation of the reduced driving force of hydrodesulfurization at higher temperatures[35,46]. A limitation of this assumption is the possibility of faster products starting to react with the slower ones.

5.1.3 Commercially available tools

There are no readily available dynamic models for industrial scale HDS operations[5,35,46], and no work has been done for VGO hydrotreaters, but the requirement for research has been suggested numerous times[7,21,32-35,46]. KBC has a correlation-based, steady state industrially focussed hydrotreater model and is tuned with linear offsets from a base case[5]. Aspentech has a fully rigorous, equation-oriented, steady state industrially focused hydrotreater model which is difficult to use and difficult to tune[5,7]. The model being developed in this study provides a practical and useable industrial HDS model that is not currently available to refiners/operators.

5.2 Dynamic simulation

Industrial plants are never truly at steady state[3], as feed and environmental disturbances, fouling, and catalytic degradation continuously upset the conditions of a smooth running process (i.e. a pilot plant). The design and optimization of a VGO hydrotreater involves both steady state and dynamic behavior. As opposed to a steady state simulation vastly more information in the form of detailed equipment specifications are required. Furthermore a plant dynamic simulation can be used to study[47]:

- **process optimization**
- controller optimization
- safety evaluation
- **transitions between operating conditions**
- Start up / Shutdown conditions

5.2.1 Use of a Commercial Dynamic Simulation

The dynamic model in HYSYS® simulates thermal, equilibrium, and reactive behavior of the VGO hydrotreater in a similar manner to the steady state model. The HYSYS® dynamic model shares the same physical property packages as the steady state model. From my past experience[56] in modeling crude units and corroborated by Kaes[60], the Grayson-Streed thermodynamic package in HYSYS® was used. For these reasons, and the familiarity of the program by operators, HYSYS® was chosen as the dynamic simulation tool for this study.

The dynamic model in HYSYS® necessarily uses a different set of conservation equations from the steady state model, time changes in variables are all important in a dynamic simulation. Hence, the equations for material, energy, and composition balances include an additional “accumulation” term. Non-linear differential equations are formulated to approximate the conservation principles, since an analytical solution method does not readily exist for the complexity of this reactor operation. Therefore, numerical integration is used to determine the process behaviour at distinct time steps.

5.2.2 Distributed and Lumped Models

Most chemical engineering systems have thermal or component concentration gradients in three dimensions (x,y,z) as well as in time. A set of partial differential equations (PDEs) is used to characterize such a distributed system mathematically. If the x, y, or z gradients are ignored, the system is “lumped” and all physical properties are considered equal in space and only the time gradients need be considered in such a plant model. For purposes of this study, the z gradient (one-dimensional) and time gradients are considered in the model. This approach allows the process to be modeled using ordinary differential equations (ODE’s), thereby saving calculation time. In addition, the lumped mathematical representation fits the lumped data available from an industrial plant.

HYSYS® uses lumped models for all of the unit operations, including the reactor. A modified version of the standard plug flow reactor (PFR) can be used to

represent the trickle bed reactor (tubular, packed bed reactor) as this reactor model does have thermal and concentration gradients with respect to the length of the vessel. In the solution algorithm, the reactor models can be subdivided into several sub-volumes to match the number of packed beds in the reactor which are considered to be lumped; that is, the reaction rate, temperature and compositions are constant through each sub-volume (packed bed), varying only with time. In essence, therefore, the key modeling characteristics of the PFR, though inherently distributed (with respect to the length of the vessel), still uses a lumped analysis to obtain the solution. Using the PFR model appears to be a starting point for this lumped parameter analysis since it can consider time and z dimension gradients, mimics the tubular nature of the actual reactor and can be coupled to the model developed in Excel® and is linked to HYSYS® for dynamic simulation of the HDS. The issue of mass transfer considerations when using an ideal PFR will be need to be addressed when using the PFR model as a base model.

5.2.3 Holdup Model

Dynamic behaviour arises from the fact that plant equipment has material inventory or holdup. A holdup model is necessary to correctly model changes in an inlet stream due to typical changes in the composition, temperature, pressure or flow of this stream to a vessel with volume (holdup). The Holdup model in HYSYS® was reviewed to understand and determine the logic so as to set the

necessary time steps and whether any modifications (in HYSYS® or Excel®) were needed to maintain calculation consistency between the two software packages.

The necessary holdup model calculations in HYSYS® include:

1. material and energy accumulation
2. thermodynamic equilibrium
3. heat transfer
4. chemical reaction

There are several underlying assumptions that are made in the hold up model calculations:

1. each phase is assumed to be well mixed
2. mass and heat transfer occur between phases in the holdup

The “lag response” that is observed in any unit operation holdup is the result of the accumulation of material, energy, or composition. To predict how the conditions change over time in HYSYS®, a recycle stream is added in addition to the feed streams.

The stream is not a physical stream in the unit operation, rather, it is used to introduce a lagged response in the output. Essentially, the recycle stream represents the material already existing in the equipment. It becomes apparent that a greater amount of material in the holdup means a larger recycle stream and thus, a greater lagged response in the output.

The holdup model was used to calculate material, energy, and composition accumulations. The following calculation steps were set as defaults in HYSYS®[46]:

1. Material accumulation was calculated at every integration time step
2. The energy of the holdup was calculated at every second time step.
3. The composition of the holdup was calculated at every tenth time step.

This study used the same the calculation sequence for material accumulation and energy as defaulted in HYSYS® but the composition was set to every integration time step to ensure enough data points (at least 10 is suggested in literature to ensure a disturbance can be captured over the calculation sequence)[47] were calculated for the given time constant. Each time step was set to five minutes (data was available in 1-minute, 5-minute, hourly and daily averages), which provided approximately a range of 10 to 34 time steps for each calculated time constant. The 1-minute data set increased the computational time without gaining any increase in model performance, while any time greater than five minutes would not provide the necessary calculation times for a time constant. As a result, for the 5-minute time step there was sufficient data points calculated for the given time constant providing confidence that any process disturbance and subsequent response would be adequately captured by the model. The time constant is normally defined as the time it takes for a designated response variable to reach approximately 63% of its steady state value from a change in an input. Table 5.1, on page 74, shows the LHSV, residence time and determined time constant for each plant. The time constant was in the range of 115-128% of the residence time for the six plants published.

The determined time constants published in Table 5.1 are based on industrial operation where multiple input variables are changing at any given time impacting the output response variable (i.e. sulfur product). As a consequence,

Table 5.1 – LHSV, residence time and determined time constant for each plant published in this research.

Plant	LHSV (1/hour)	Residence time (hour)	Determined Time Constant (hour)
A	0.76	1.31	1.67
B	1.23	0.81	0.93
C	0.54	1.85	2.22
D	0.41	2.41	2.82
E	0.88	1.13	1.44
F	1.63	0.61	0.79

the time constant may not be exactly as stated since a steady state may never actually occur in the industrial reactor. The data was evaluated for a scenario where temperature, and crude flow remained fairly constant so as not to impact the outlet sulfur value so a temporary steady state could be found. As an example, the calculated time constant from plant B is shown in Figure 5.3, on page 75. The inlet sulfur is typically 0.8%, and in this case, a change in inlet sulfur occurred, from 0.4 to 0.75 wt%. The inlet sulfur stayed in the 0.65 to 0.75% range for the duration of the evaluation (3 hours). The crude flow, and reactor temperature remained fairly stable since operations did not feel the need to change the operation in response. As a result, the product sulfur (response) increased from one tentative steady state (0.025 wt%) to another tentative steady state (0.045 wt%). The time to get to 63% of the total change in response was 56 minutes or 0.94 hours, thus the calculated time constant.

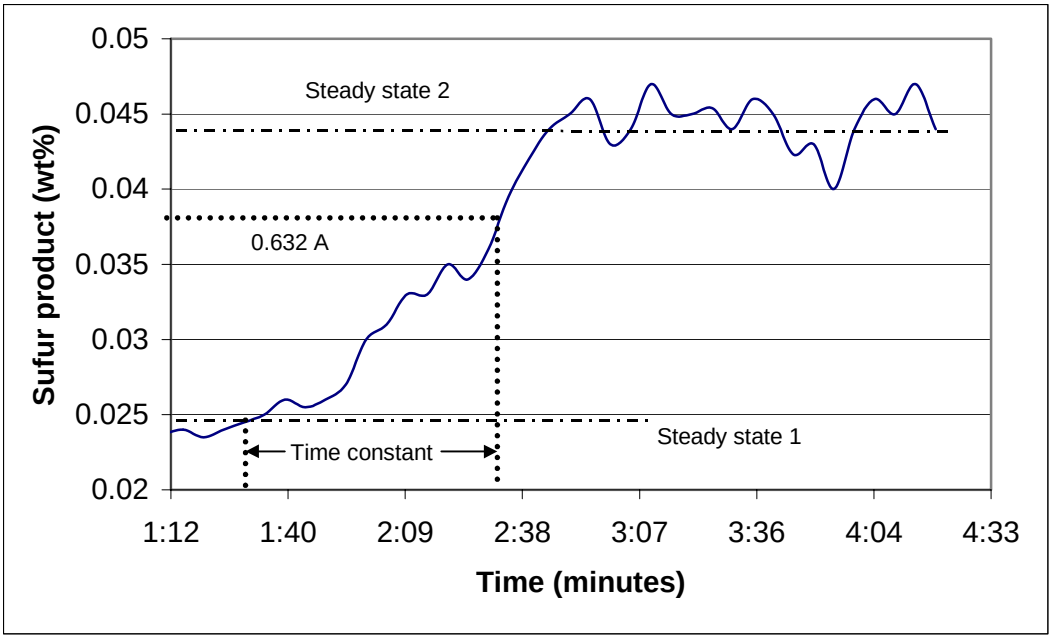

Figure 5.3 – An example of a time constant determination using data from Plant B on November 24, 2005. The inlet sulfur concentration spiked from 0.45 to 0.76 weight percent at 1:05pm and stayed constant and relatively stable until 5:00pm. The product sulphur (response variable) went from 0.025wt% (tentative initial steady state) to 0.04wt% (tentative second steady state). The time constant was determined as 0.94 hours (63% of the response change from steady state 1 to steady state 2).

5.2.4 Assumptions

The conventional hydrotreating unit is a trickle-bed reactor, that is, a cylinder containing a fixed bed of catalyst, through which a mixture of gas and liquid flows co-currently downwards. The reactor is adiabatic, so there is no radial transport of heat. Since the ratio of reactor length to diameter is very large, the liquid distribution within the catalyst bed is assumed to be essentially uniform (no radial gradients). The fluid pattern can be approximated by a laminar flow since the Reynold's number calculated for each plant was in the 200-300, approximately a factor of 10 less than the laminar/turbulent crossover point calculated at a Reynold's number of 2000. However, the catalyst particles cannot be assumed to

be fully wetted.

Assumptions made in deriving the mathematical model of the reactors can be summarized as:

- The reactors operate adiabatically.
- The flow pattern is described by laminar flow with factors for degree of mixing included. Radial dispersion effects of mass and heat are negligible.
- Resistances to transport of mass and heat between the external fluid phase and the particle surface are neglected.
- The temperature of the catalysts is assumed to be the same as that of external fluid at the same position.
- The fluid velocity, density, and mixing coefficients are taken to be independent of axial distance and temperature.
- There is no mass or heat dispersion outside the reactor.
- Sulphur is converted to hydrogen sulfide in the desulphurization step
- Total metal concentration is considered. Metal content (concentration) accounts for both vanadium and nickel.

5.3 Kinetic Modeling

The kinetic model for the hydrotreating reactions quantizes the effect of process variables on the rate of reaction or activity. This is required for predictive and diagnostic purposes. For example, one can use a kinetic model to predict how the product sulphur will vary with, say, space velocity, or hydrogen-to-oil ratio or hydrogen in the feed or purity and reactor pressure. The desired output for this research from the kinetic model is the bulk product sulfur composition.

5.3.1 HDS Kinetics

As is well known, kinetic behavior is determined from experimental data for all compounds. The experimental data is obtained in lab-scale or pilot plants operated as batch reactors[3,7,8,10,15,16,26] (no in or out flow of material). Once the specific reaction rate has been determined from the batch experiment, the kinetics derived from the batch reactor are applied to the appropriate flow reactor design equation (continuous stirred tank reactor (CSTR), Plug flow reactor (PFR) or some combination)[7,8,15,16]. This is the accepted method for developing a representative model for a reactor (eg. hydrotreater) in academia, and industry, even though the models used for deriving kinetics and reactor design are different. For this research, accepted reactor research standards were followed, the kinetic expression is derived from batch reactor data, while the reactor model chosen is a modification of an ideal CSTR/PFR model.

In the case of complex petroleum feeds where mixtures of organic compounds are reacting at different rates, experimentally determined kinetics are relied on to make sense of the products obtained. Seldom can a completely definitive prediction be made for these types of complex mixtures. However, approximate predictions (lumping parameters) can be made which, in most cases, are more than adequate for industrial scale refinery unit operations[34-39].

For purposes of understanding operating hydrotreating kinetics, it is useful to review some basic theory. Consider the following two second order

reaction mechanisms (second order when two molecules react) shown in Equations 5.1 and 5.2:

$$2A \rightarrow C+D \tag{5.1}$$

$$A+B \rightarrow C+D \tag{5.2}$$

where A and B are reactants, C and D are products and the coefficients represent the number of moles of each component taking part in the depicted reactions. The reaction rate information for the reactions 5.1 and 5.2 will normally be extracted from experiments run in a batch reactor. The mole balance for reaction 5.1 in an experimental batch reactor is noted by the two terms on either side of the left equal sign in Equation 5.4. The rate of disappearance of A, for Equation 5.1, is given by the right hand side of Equation 5.3 when the reaction takes place in a batch reactor, as was done by the catalyst vendors for the VGO hydrotreater data obtained in chapter 4 and used in this research:

$$-r_A = \frac{-dc_A}{dt} = kc_A^2 \tag{5.3}$$

and for the reaction shown in Equation 5.2, by Equation 5.4:

$$\frac{-dca}{dt} = kc_A c_B \tag{5.4}$$

where the lower case c's are concentrations, t is time, and k is the reaction rate constant. Equation 5.4 is a combination of the batch reactor mole balance and the expected rate law expression. In Equation 5.4, for the special case where concentrations of A and B are equal, the rate of disappearance of A shown in

Equation 5.4 reduces to Equation 5.3. Assuming that either Equation 5.1 or the special case of Equation 5.2 applies, combining with Equation 5.3 and separating variables results in Equation 5.5;

$$-\int_{c_o}^{c_1} \frac{dc_A}{c_A^2} = k \int_{t_o}^{t_1} dt \tag{5.5}$$

where c_o is the concentration of A at t_o and c_1 is the concentration at t_1.

Integrating Equation 5.5 results in Equation 5.6.

$$\frac{c_o - c_1}{c_o c_1} = k\left(t_1 - t_o\right) \tag{5.6}$$

Dividing numerator and denominator on the left by c_1 and letting $t_1 - t_0 = t$ results in Equation 5.7.

$$\frac{1}{c_1} - \frac{1}{c_o} = kt \tag{5.7}$$

Equation 5.7 is a straight line with slope k passing through the origin. In interpreting hydro-treating data, the term t is replaced after integration by the reciprocal of liquid hourly space velocity, a value that is readily calculated from plant data and used in plant operations. For sulphur concentration data, c can be replaced by %S in Equation 5.7 to become Equation 5.8;

$$\frac{1}{S_p} - \frac{1}{S_f} = k(LHSV)^{-1} \tag{5.8}$$

where S_p represents the bulk product sulphur weight % taken from operating laboratory data and S_f represents the bulk feed sulphur weight % taken from operating laboratory data.

Equation 5.8 can be re-organized to Equation 5.9, an expression for a bulk sulphur reaction rate.

$$k = LHSV \left(\frac{1}{S_p} - \frac{1}{S_f} \right) \tag{5.9}$$

Since k is only a function of temperature, values of $1/S_p - 1/S_f$, calculated from feed and product sulphur data, will show a linear relationship to $LHSV^{-1}$ if the desulphurization follows the apparent second-order rate law. If the plotted curve passes through the origin, additional justification exists for application of the second-order equation. For sets of data obtained at different temperatures, curves may be drawn and their slopes calculated. The slope (k) of a curve representing a particular temperature is the desulphurization rate constant for that temperature. With $LHSV^{-1}$ in units of hours and S as %S, k will have the units, $(hr)^{-1}$ $(\%S)^{-1}$. The same procedure can be followed for other assumed reaction orders. The general form of Equation 5.9 can be written as Equation 5.10.

$$k_{HDS} = LHSV\ f\ (S_f, S_p) \tag{5.10}$$

where f (S_f,S_p) is a function determined by the order of the reaction. Table 5.2, on page 81 shows forms of this function (Equation 5.10) for first, one-and-one-half, and second order kinetics[7,13,15,28].

The assumed kinetic equation for sulphur does exhibit a fractional value, with many industrial researchers finding 1.5 as the best fit for heavy oil hydrotreaters[7,13,28,30,49-52]. A 1.5 reaction order was considered as a starting point for the development of the model in this research.

Table 5.2 Apparent Kinetic Order for 1st, 1.5 and 2nd order reactions

Apparent Kinetic Order	f (S_F/S_p)
1st	ln (S_p/S_f)
1-1/2	$\frac{1}{\sqrt{S_p}} - \frac{1}{\sqrt{S_F}}$
1-1/2 to 2nd	$\frac{1}{(S_p)^{n-1}} - \frac{1}{(S_f)^{n-1}}$
2nd	$\frac{1}{S_p} - \frac{1}{S_F}$

Fractional orders appear to be a practical way to kinetically model mixtures of compounds reacting at widely varying rates in a trickle bed reactor[49-52].

5.3.1.1 Calculation for Product Sulphur in the Model

Temperature is an important variable in the conversion of sulphur in an industrial VGO hydrotreater[7,8,9,15,13,20,28,32-35,42-44]. If the Arrhenius relationship, Equation 5.11, is applicable in the temperature range investigated, a plot of ln k

$$k = A \exp (- E_{act}/RT) \qquad (5.11)$$

against reciprocal absolute temperature will also be linear. From such a plot, for a standard catalyst, k may be read for any temperature. In Equation 5.11, A is the frequency or pre-exponential factor, E is the energy of activation, R is the gas constant and T the absolute temperature. Equating Equations 5.10 and 5.11 can be combined into Equation 5.12 which can then be re-written as Equation 5.13.

$$A \exp(-E/RT) = LHSV\,[\,f(S_f, S_p)\,] \tag{5.12}$$

$$\exp\left[a - \left(\frac{b}{T}\right)\right] = LHSV\left[f\left(S_f, S_p\right)\right] \tag{5.13}$$

To dynamically track catalyst behavior when calculating outlet sulphur composition of an industrial hydrotreater, from known or observed results, Equation 5.13 formulated as a ratio, becomes Equation 5.14

$$\frac{\exp\left(a - \frac{b}{T_1}\right)}{\exp\left(a - \frac{b}{T_2}\right)} = \frac{LHSV_1\left[f\left(S_f, S_p\right)\right]}{LHSV_2\left[f\left(S_{f_2}, S_{p_2}\right)\right]} \tag{5.14}$$

where subscript 1 represents a discrete environment in the system, while subscript 2 represents a different discrete point in the system. The formulation for Equation 5.14 is taken from the ideal gas law comparison between states where conditions from two states are determined by ratioing the ideal gas law equation at two different states. In this derivation (which is a multiphase system), the concept of ratioing is borrowed from the ideal gas law, with the understanding that the research is not dealing with an ideal gas, the two states of Equation 5.14 are considered at two different times. Knowledge of key variables in one state

are used to determine a specific variable in the second state. For this research, the first state is treated as a previous point in time, while the second state is treated as the current point in time. Since catalyst deactivation builds on previous process conditions, the ratioing of the two states to determine the current sulfur product value seemed a reasonable approach and this concept, for consistency in derivation, is used in the development of the catalyst deactivation correlations in this research.

Using a 1.5 reaction order as starting point based on findings in literature, adding key variable parameters[7] (based on matching data from plant d – correlative) and rearranging, the nominalized Equation 5.15 results. Full derivation of Equation 5.15 is included in Appendix C.

$$S_{pi} = \left\{ \left[\left(\frac{1}{\sqrt{S_{p(i-1)}}} - \frac{1}{\sqrt{S_{f(i-1)}}} \right) \frac{LHSV_{i-1}}{LHSV_i} \left(\frac{P_{i-1}}{P_i} \right)^p \left(\frac{G_{i-1}}{G_i} \right)^g e^{\left(\frac{b}{T_{i-1}} - \frac{b}{T_i} \right)} + \frac{1}{\sqrt{S_{fi}}} \right]^{-1} \right\}^2 \tag{5.15}$$

Substituting the 1.5 order form of Equation 5.10 into Equation 5.15, provides another useable form, Equation 5.16;

$$S_{pi} = \left\{ \left[k_{i-1} \frac{LHSV_{i-1}^2}{LHSV_i} \left(\frac{P_{i-1}}{P_i} \right)^p \left(\frac{G_{i-1}}{G_i} \right)^g e^{\left(\frac{b}{T_{i-1}} - \frac{b}{T_i} \right)} + \frac{1}{\sqrt{S_{fi}}} \right]^{-1} \right\}^2 \tag{5.16}$$

where the subscript, i refers to the nominal (or desired value), i-1 refers to the previous (observed) value, S_p is the product sulphur in weight percent, LHSV is space velocity, T is the absolute temperature, and S_o is the feed weight % S.

Equations 5.15 and 5.16 are based on a proprietary steady state catalyst vendor correlation for outlet product sulfur shown in Equation 5.17[3]:

$$S_p = \left[(LHSV^{-1} e^{(a-\frac{b}{T})} P^p G^g + \frac{1}{\sqrt{S_f}})^{-1} \right]^2 \quad (5.17)$$

The pressure and hydrogen to oil ratios are multiplied to the kinetic expression portion of the equation, since theses variable directly influence the rate of reaction[7,8,9,15,13,19,28,32-35]. The constants are experimentally determined and vary with feedstock. Typical b values are 18,000 to 25,000^{o}F[3,7,28] and hydrogen pressure and hydrogen to oil exponents are in the range of p = 0.008 to 0.02 and g = 0.05 to 0.1[7,20] in the steady state format of Equation 5.17.

For the "dynamically" functioning sulfur product equation developed in Equation 5.15, the additional factors for correcting pressure and hydrogen ratios external to the impact on reaction rate (k_i) have been added to provide additional parameters to better match each unique industrial hydrotreater operation. The two parameters added, pressure (P) and hydrogen to oil ratio (G), were the two important hydro-treating parameters not already included in Equation 5.15. The general format for the p and g parameters is taken from the catalyst vendor steady state design correlation (variable to an exponent multiplied to the kinetic portion of the equation) in Equation 5.17. However, a ratio of the variables (P_{i-1}/P_i and G_{i-1}/G_i) was considered to match the ratioing done to the rest of the equation to get it into "dynamic" format. The ratio of variables was then set with an exponent similar to what was done in the steady-state design Equation 5.17. In

using the ratio concept to develop the sulfur product equation, parameter “a” (temperature dependent) was removed from the calculation, reducing the number of parameters to be considered.

The other two important hydro-treating parameters, as noted in chapter 2, are temperature and Liquid Hourly Space Velocity, and are embedded in Equation 5.15. Having all the important variables incorporated in Equation 5.15, with the suggested format, should positively impact the accuracy of the model.

Temperature and space velocity corrections can be made with some confidence within reasonably close ranges of operating conditions. Pressure correction should be done with a measure of caution and preferably within the range of actual operating data limits[7,12]. Chapter 6, Table 6.1 does provide results of the new parameters for each plant data set evaluated.

5.3.1.2 Calculation for Product Nitrogen in Model

Nitrogen is converted to ammonia in the denitrogenation step[12,21]. Examples of nitrogen containing compounds are pyridines and pyrroles[7,21]. As the feeds become heavier, denitrogenation becomes more significant, particularly for heavy distillate and vacuum gas oil hydrotreating[9]. Nitrogen removal requires about four times as much hydrogen as the equivalent sulphur removal[21-24], since the amount of nitrogen molecules is typically greater than the sulfur and the complexity of the nitrogen-embedded crude oil molecules tends to be, in general, higher than for the sulfur molecules[20,21-24]. For the nitrogen product, the same

approach for the sulfur equation was used. A steady state design equation for nitrogen product is shown in Equation 5.18.

$$N_p = e^{\left[\ln N_f - \left(\ln kLHSV^{-1} e^{\left(a - \frac{b/T}{}\right)} P^p G^g\right)\right]} \tag{5.18}$$

was converted to a format that uses two time points, with the parameter arrangement changed to a ratio format to mimic the modifications made. 1st order kinetics was used [7,53-56] as the initial choice for the reaction order. Both 1.5 order and 2nd order relations were tested but the material balance for the plant would not close for these cases, so a first order derived equation was used. The derivation steps for Equation 5.19 is the same for Equation 5.15 found in appendix G so they are not reproduced in this document.

$$N_{pi} = \exp\left\{\ln N_{fi} - \left[\ln k_i \frac{LHSV_{i-1}}{LHSV_i}\left(\frac{P_{i-1}}{P_i}\right)^p \left(\frac{G_{i-1}}{G_i}\right)^g e^{\left(\frac{b}{T_{i-1}} - \frac{b}{T_i}\right)}\right]\right\} \tag{5.19}$$

5.4 Mass Transfer Limitations

The time constant to reach equilibrium between liquid and gas phase is approximately slightly the same or greater than the reactor space time[7,41-45] so the overall HDS reaction can be considered moderately fast[10,12,15,25,26,]. Based on available literature[33,45,47] there is evidence to suggest that the hydrotreater sulfur reaction is moderately fast. A moderately fast reaction may have competing controlling resistances. In this case, both kinetics and mass transfer appear to

compete as controlling resistances in the reactor. As a consequence, kinetics should not necessarily be considered the sole controlling resistance for the HDS reaction[47]. As a result, equations have been developed[12,26,41] and used to model mass transfer in VGO hydrotreaters and have been used to determine whether the mass transfer limitations are negligible for fixed bed trickle bed HDS reactors. Equations 5.20[25] and 5.21[45] have been taken from literature to determine whether it is necessary to consider mass transfer external, and internal to the catalyst, respectively, in the model. For Equation 5.20, if the inequality is true then external mass transfer needs to be considered.

External Mass Transfer $$\frac{10d_p}{3S_f}\left(-\frac{r_s}{V_c}\right) > m \qquad (5.20)$$

Equation 5.20 was developed from pilot plant studies on trickle bed reactors and was compared to an industrial plant data set. Basically, the inequality compares the mass transfer coefficient on the right of the inequality to the kinetics for the reaction on the left hand side. The variables included are d_p (particle diameter), S_f (Sulfur in feed), r_s (reaction rate), V_c (catalyst volume) and m (mass transfer coefficient). All variables in this relation are readily available from plant data or can be calculated at each time step. The mass transfer coefficient was calculated using the following correlation, Equation 5.20a, published by Gota and Smith[25] and has been cited in many literature sources.

$$m = \rho_c^{0.267} T^{0.2896} \left(\frac{G_L}{\mu_L}\right)^{d_p^{0.4}} \sqrt{\frac{\mu_L}{8.93x10^{-8}\rho_L\rho_c}} \qquad (5.20a)$$

where ρ_c is the catalyst density, T is temperature, G_L is the liquid mass flux velocity, ρ_L is the crude oil density, and μ_L is the crude oil viscosity.

The m values from this correlation using my plant data were the same or lower (0.03-0.05 versus 0.03-0.23) than what is stated in literature, so using this inequality correlation should tend to predict the need to consider external mass transfer more readily. As result, this inequality was used to determine whether external mass transfer should be considered.

If the inequality shown as Equation 5.21 is true then internal mass transfer can be neglected.

Internal Mass Transfer $$\frac{\left(\pi d_p^2 r_s\right)}{\left(DS_f \varepsilon\right)} < 1 \qquad (5.21)$$

Equation 5.21 was developed by Froment and Bischoff to provide an indication if diffusion within the catalyst is rate limiting. The correlation was developed experimentally in a pilot setting. The variables in Equation 5.21 are τ (pellet tortuosity- provided by catalyst vendor under secrecy agreement, so no validation provided), d_p (pellet diameter), ε (catalyst porosity), D_s (sulfur molecular diffusivity), S_f (feed sulfur) and r_s (reaction rate). No other literature was found that provided a criteria for determining if internal mass transfer should be considered in the model development. If the inequality is rearranged to separate catalyst properties from reaction characteristics the following comparison in Equation 5.21a can be considered:

$$\frac{\left(\pi d_p^2\right)}{\left(\varepsilon_i\right)} < \frac{DS_f}{r_s} \qquad (5.21a)$$

The left hand side has catalyst features and the right hand side of the equality has the reaction rate. If the catalyst features are substantial compared to the reaction rate, internal mass transfer should be considered in the model.

Using the plant data obtained, Equation 5.20 shows that mass transfer limitations do not play an important role outside the catalyst in industrial VGO hydrotreaters while Equation 5.21 shows that mass transfer limitations do exist inside the catalyst. Table 5.3 presents these calculations for each plant data set. For mass transfer limitations on reaction kinetics outside the catalyst, the value of the

Table 5.3 Determining whether mass-transfer limitations are negligible

PLANT -->	1	2	3	4	5	6
Outside Catalyst (5.20)						
Left hand side, cm/s	3.51E-03	4.25E-03	4.35E-03	6.50E-03	4.10E-03	4.00E-03
Right side – Average m , cm/s	3.30E-02	4.50E-02	4.00E-02	5.80E-02	4.90E-02	3.80E-02
Ratio (right side/left side)	9	11	9	9	12	10
Inside Catalyst (5.21)						
Left hand side	30	65	104	56	73	48

inequality on the left-hand side of Equation 5.20 is approximately an order of magnitude greater than the right hand side for the entire operating life of the reactor. This result, along with larger m literature values, provide confidence that mass transfer limitations outside the catalyst do not need to be incorporated into the lumped parameter developed model. On the other hand, Equation 5.21 results range from 30 to 104, which is significantly greater than one, implying that this model should incorporate the impact of mass transfer limitations within the catalyst. Since the validity of correlation used for internal mass transfer

importance could not be substantiated, incorporating it is a safe assumption, even though the results from Equation 5.21 indicated internal mass transfer should be considered. If possible, since the basis of the model is a lumped approach, a lumped relationship for intra-catalyst mass transfer limitations should be used.

5.5 Wetting Efficiency

Chronologically, in the development of this model, wetting efficiency was incorporated to account for the impact of intra-catalyst mass transfer limitations. It did aide in matching the sharp increase in catalyst deactivation at the start and end of the catalyst run life. This would indicate that using wetting efficiency for this lumped parameter approach is a useful approach in modeling any intra-catalyst mass transfer impacts. Figure 3.2 shows impact of wetting efficiency on the coverage of liquid on the catalyst.

Equation 5.22[44], taken from Dudokovic's research, is a correlation used to describe this phenomenon and was incorporated in the developed model.

$$\eta_e = 1.104\,\mathrm{Re}_L^{1/3}\left[\frac{1+[(\Delta P/Z)/\rho_L g]}{G_{aL}}\right]^{1/9} \qquad (5.22)$$

Dudokovic used tracer techniques to determine the impact of various operating conditions on wetting efficiency in trickle-bed reactor catalyst beds. An additional purpose of the research was to relate wetting efficiency in a pilot plant to industrial scale operations. The data for the correlation developed was at industrial operating pressures so there is a basis for using it in a model of an industrial HDS. In addition, all the terms in Equation 5.22 can be readily calculated from plant data, which is a benefit for the model being generated.

Equation 5.22 is based on a flow regime indicator (Reynolds number (Re_L)), pressure drop ΔP, reactor length (z), gravitational acceleration (g), ρ_L, the crude oil density liquid density and the Galileo number given by Equation 5.23.

$$G_{aL} = \frac{d_p^3 \rho_L^2 g \varepsilon^3}{\mu_L^2 (1-\varepsilon)^3} \tag{5.23}$$

The Galileo number may be regarded as proportional to gravity forces divided by viscous forces. The Galileo number is typically used in viscous flow and thermal expansion calculations, for example to describe fluid film flow over walls. The variables in the Galileo number have been defined in Equations 5.20-5.23.
The Galileo number incorporates the catalyst surface, so as the catalyst deactivates due to metal and coke deposition, the wetting efficiency is impacted and is reduced accordingly. For this lumped model, the wetting efficiency parameter is being used to address the impact of internal mass transfer resistances. Wetting efficiency provides an overall indication of how much catalyst is being covered for reaction. Internal mass transfer resistance deals with the resistance to mass transfer of the fluid within the catalyst. If there is no reactant within the catalyst then the amount of internal mass transfer resistance can be considered to be so high that the reaction cannot proceed. So, the wetting efficiency will capture this portion of the internal mass transfer resistance. However, the sections of the inner catalyst that do have reactants and there is mass transfer resistance, the wetting efficiency will not account for this. Again, being a lumped model, the wetting efficiency (calculatable with industrial data)

will provide some level of indication of internal mass transfer resistance but not address all of the internal mass transfer resistance. In this research, this is where a compromise is made between developing a lumped model and the need for a detailed representation of the fluid interaction on a micro-level. The wetting efficiency provides some capture for the internal mass transfer resistance.

In Equation 5.24 the wetting efficiency is used to change the reaction order of the model;

$$n_a = 2\eta_e \tag{5.24}$$

where n_a represents the wetting efficiency adjusted apparent kinetic reaction order and 2 (two) is maximum reaction order demonstrated[7,20,26,33-35] for the lumped HDS reaction. Since industrial reactors typically have a wetted efficiency[12] of 0.7 – 1.0 and industrial research has shown that 1.5 is a viable reaction order for industrial HDS reactions, Equation 5.24 should result in reaction orders in the range of 1.4 – 2.0. The reaction order range of 1.4 - 2.0 covers the expected reaction order range provided by the catalyst vendors and operators for each plant well in table 4.2 (1.4 – 1.7). In the event that the wetting efficiency goes outside the expected range, and it is a true indication of performance, the model is not limited by a fixed, previously determined reaction order.

Since reaction rates do vary and reaction orders for a specific plant are not exactly 1.5, it was considered necessary to attempt to vary the reaction order for

the HDS reaction in the model. Equation 5.24 can be combined with the developed model by including and updating the wetting efficiency for the overall lumped kinetic HDS model during the entire reactor run length. Incorporating Equation 5.24 into the sulphur product equations for a generalized fractional reaction order (eg. 1.1 to 2.0), Equation 5.25i, results in Equations 5.25a and 5.25b. The complete derivation for Equation 5.25i and the addition of Equation 5.24 creating 5.25a and 5.25b can be found in Appendix C.

$$S_{pi} = \left\{ \left(\frac{1}{S_{p(i-1)}^{n_i-1}} - \frac{1}{S_{f(i-1)}^{n_i-1}} \right) \frac{LHSV_{i-1}}{LHSV_i} e^{\left(\frac{b}{T_{i-1}} - \frac{b}{T_i}\right)} \left(\frac{P_{i-1}}{P_i} \right)^p \left(\frac{G_{i-1}}{G_i} \right)^g + \frac{1}{S_{fi}^{n_i-1}} \right\}^{\frac{1}{1-n_i}} \quad (5.25i)$$

$$S_{pi} = \left\{ \left(\frac{1}{S_{p(i-1)}^{2\eta_{ei}-1}} - \frac{1}{S_{f(i-1)}^{2\eta_{ei}-1}} \right) \frac{LHSV_{i-1}}{LHSV_i} e^{\left(\frac{b}{T_{i-1}} - \frac{b}{T_i}\right)} \left(\frac{P_{i-1}}{P_i} \right)^p \left(\frac{G_{i-1}}{G_i} \right)^g + \frac{1}{S_{fi}^{2\eta_{ei}-1}} \right\}^{\frac{1}{1-2\eta_{ei}}} \quad (5.25a)$$

$$S_{pi} = \left\{ k_{hds(i-1)} \frac{LHSV_{i-1}^2}{LHSV_i} e^{\left(\frac{b}{T_{i-1}} - \frac{b}{T_i}\right)} \left(\frac{P_{i-1}}{P_i} \right)^p \left(\frac{G_{i-1}}{G_i} \right)^g + \frac{1}{S_{fi}^{2\eta_{ei}-1}} \right\}^{\frac{1}{1-2\eta_{ei}}} \quad (5.25b)$$

Equation 5.25a is the form of the sulphur product equation used in the model in this research.

5.6 Catalyst Deactivation

The reaction rate is not constant during the run life of a hydrotreater. In addition to the wetting efficiency impacting the HDS trickle bed reaction rate, the following factors impact the reaction rate[7,9,10,12,15,20]:

1. Catalyst deactivation
2. Catalyst type
3. Temperature
4. Pressure

5. Feed

6. % hydrogen

7. Recycle

Thus, in a high fidelity dynamic model, the reaction rate must accurately track the catalyst deactivation process. Hence a crucial step in developing an accurate hydrotreater model is developing a realistic representation of catalyst deactivation and including it in the reaction rate expression, Equation 5.26

$$k_i = k_{actual} = f(Catalyst\_activity) * k_{hds} \tag{5.26}$$

where

$$f(catalyst\_activity) = 1 - \frac{q}{q_o} = 1 - \phi \tag{5.27}$$

The variable q represents the concentration of blocked sites (or concentration of poisons of catalyst) from metals deposition and coking, and q_o represents the maximum concentration corresponding to complete deactivation of the catalyst[15].

Since it is difficult to determine q_o and q, industrial operators and catalyst vendors have developed a series of correlations to determine the life remaining in a catalyst[3,7] in industrial and pilot plant settings; (1-ϕ), or sites that are not poisoned. These correlations tend to provide a downward trend in catalyst activity similar to a MOR catalyst activity profile in a sterile environment (free of any disturbances). Figure 5.4, on page 91, shows an application of three correlations that have been used and referred to in research and industry to track catalyst deactivation. Correlations from a catalyst vendor[3] (representing

proprietary steady state calculation), Robinson[5] (representing industrially focused consultant's model), and Chao et al[21] (representing comprehensive academic research model) were evaluated and shown in Figure 5.4. In addition, the catalyst deactivation profile from this research is provided for comparison purposes. Data from plant D was used to attempt to simulate the catalyst

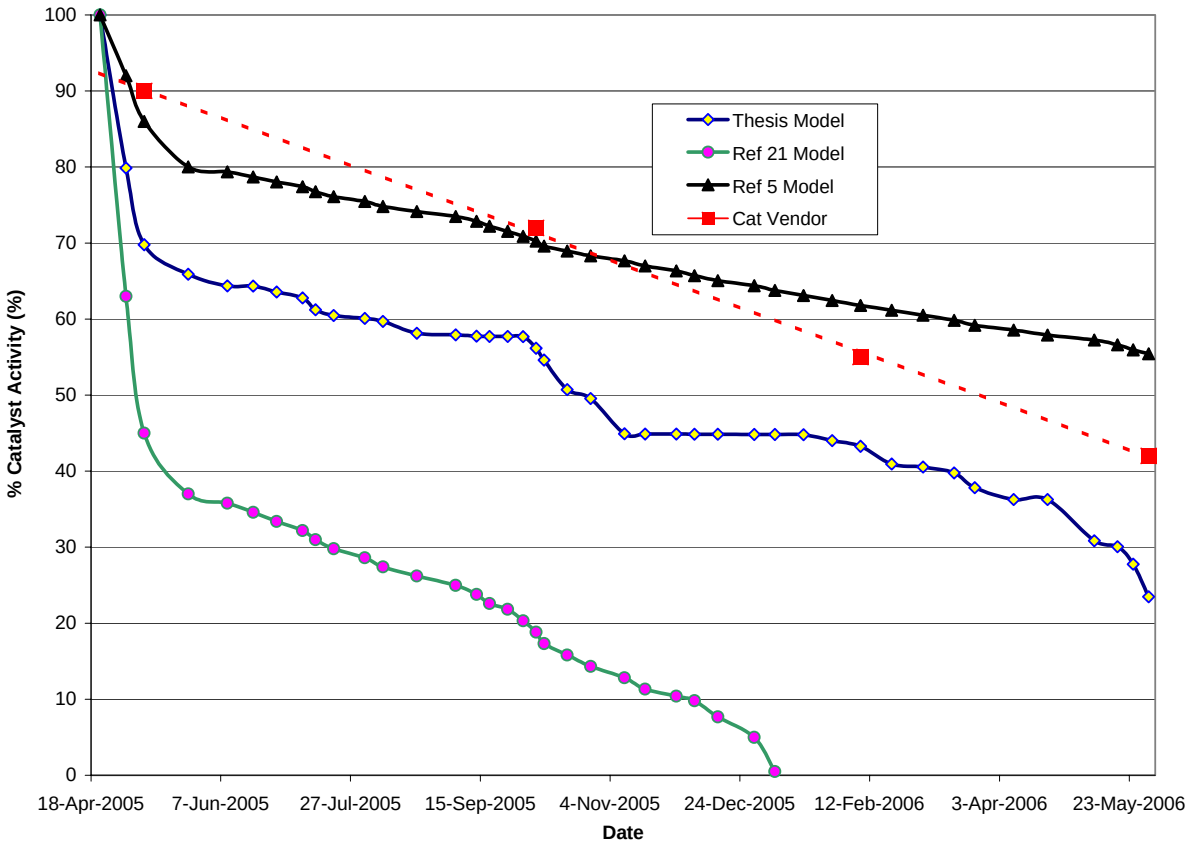

Figure 5.4 – Catalyst activity profiles generated from various models evaluated incorporating catalyst deactivation using Plant D data. Reference 21 line based on publicly available literature has a very steep SOR and exhibits an s-shaped curve for catalyst deactivation predicting EOR prematurely. The Reference 5 line is from an industrially focused consultant. There appears to be a factor for SOR deactivation but the remainder of the curve is an essentially a negatively sloped straight line. The catalyst vendor line is four data points generated from a prorated evaluation of a steady state design set of correlations. The catalyst activity profile from this research is included for comparison purposes. This model appears to capture and represent disturbances in the reactor.

deactivation for all the correlations. The purpose of this exercise was to determine which style of deactivation model was to be used, modified or improved or if a new approach was needed for this research.

Each of the three correlations evaluated had severe limitations when considering the goal of the research is to create a lumped parameter VGO hydrotreater model based on industrial data. Chao's model appeared to be the best one available in literature to consider in this research since it contained provisions for metals and coking deposition and start of run accelerated catalyst deactivation . All other models in literature appeared to have limited catalyst deactivation models developed. Listed below are the pertinent shortcomings from the Chao model:

1. For SOR uses Levenspiel model for rapid deactivation – too aggressive
2. Metals Deposition broken into two parts – assumed linear in each section
3. Coking – fixed proportion to volumes of carbonaceous compounds and catalyst, no consideration for coking tendency
4. Data needed to run model not available or easily calculated from plant data

Overall, Chao's model did not have the ability to address real changes in hydrotreater reactor conditions as shown in Figure 5.3 (Ref 21 data points). The model does generate an S-shape curve which is the generally accepted overall trend for catalyst deactivation. However, with the very simplistic representation for coking and metals deposition and the need to calculate pore radius and metal

deposition thickness, this model (and other models found in literature) does not lend itself well for converting or modifying for this research since the data available in the plant is not sufficient enough for frequent updating of the key parameters in the model. All the models reviewed in literature were compared to catalyst deactivation data that resembled a smooth S-shaped curve. It has been argued that a good curve fitter could create a relationship to match the smooth S-shaped curve. This may speak to the challenge of using rigorous, fundamentally based calculation models to model industrial data. If the industrial data has multiple disturbances, these models are not equipped to address these disturbances.

Industrially based models were also investigated. Results for the industrial based model (Ref 5 line in figure 5.4) were obtained by using Robinson's WABT calculation model that includes catalyst deactivation. The EOR predicted was similar to the 3 year run length expected by the catalyst vendor. In reality, plant D ran for just over a year. As a result, the calculated line (Ref 5 line) from this model in figure 5.4 resembles a MOR profile for most of the plant d data set evaluated. As per Chao's model, a nice S-shaped curve can be generated from this model. Details of the model were not published but appear not to respond to any changes in process conditions during the run. As a result, no further investigation was taken into this type of model .

Also investigated was a catalyst vendor correlation package[3] created primarily for designing VGO hydrotreater reactors. The calculation was run at a few time points and prorated to account for the different time span between SOR and EOR, so as some comparison could be made. The overall expected catalyst deactivation based on plant D data was 75% over 3 years[3,7]. The correlation package was not designed to calculate catalyst activity during the run, since there is no provision for the accumulation of deactivation but only a total expected catalyst deactivation over the entire run. Included in the correlation package is a catalyst deactivation factor that uses plant available data to determine impact of coking and metals deposition, but as configured does not track catalyst deactivation to determine remaining catalyst activity at a given time point. As a result, the set of correlations from the catalyst vendor as currently configured can not be used for this research.

However, with the key parameters developed to use plant data, these catalyst vendor steady state correlations were evaluated to determine if they could be improved and changed to respond to disturbances and track the activity over time. In addition, the parameters used in the catalyst vendor steady state form are similar to the Thiele Modulus and effectiveness factor relationships used historically for generating the S-shape catalyst deactivation curve[20] when mass transfer gradients occur within the catalyst as illustrated in the Chao model[21].

The Thiele Modulus quantifies the ratio of the reaction rate (n= reaction order) to the diffusion rate in the pellet for a hydrotreater reactor as noted in equation 5.a[22]:

$$\Phi \equiv \frac{reaction\_rate}{diffusion\_rate} = d_p \sqrt{\frac{\rho_{cat} A_{os} k_s^{n-1} C_H C_s}{\rho_{oil} D_{as}}} \qquad (5.a)$$

The variables used for the Thiele modulus are $d_{p,}$ catalyst diameter; ρ_{cat}, catalyst density; A_{os}, effective catalyst surface area (=f(coking and metals deposition)); k_s, sulfur reaction rate; C_H, hydrogen concentration; Cs, sulfur concentration; $\rho_{oil,}$ crude oil density; D_{AS} effective diffusivity of sulfur.

The effectiveness factor uses the Thiele Modulus to create a fractional factor that is multiplied to the reaction rate at the particle surface conditions to provide a measure of how far the reactant diffuses into the pellet before reacting. It is a dimensionless number that essentially measures how effectively the catalyst is being used. The effectiveness factor ranges from 0 to 1, and may be derived from material balances of the reacting species on a spherical catalyst pellet[7,11,22]. A low effectiveness factor value ($E_f \rightarrow 0$) means the pellet is reacting at a low rate. The reactant is unable to penetrate significantly into the interior of the catalyst pellet and thus a large portion of the catalyst is not used to convert the reactant. For a high effectiveness factor ($E_f \rightarrow 1$), the entire volume of the catalyst is being used for reaction since the reactant can diffuse quickly into the entire pellet. Equation 5.b illustrates the generic relationship for the effectiveness factor

with the diffusion limited reaction rate r_{sd}, ratioed to the kinetically controlled reaction rate r_s (located in the denominator).

$$E_f \equiv \frac{r_{sd}}{r_s} \qquad (5.b)$$

Table 5.4 shows the effectiveness factor for various catalyst particle shapes, with all of them using the Thiele Modulus as the sole variable.

Table 5.4 – Effectiveness factors derived for various particle shapes[22]

Sphere	$\eta = \frac{1}{\Phi}\left[\frac{1}{\tanh 3\Phi} - \frac{1}{3\Phi}\right]$
Cylinder	$\eta = \frac{1}{\Phi}\frac{I_1(2\Phi)}{I_0(2\Phi)}$
Slab	$\eta = \frac{\tanh \Phi}{\Phi}$

Figure 5.5, on the next page, illustrates the relationship between the effectiveness factor and the Thiele modulus.

The desired S-shaped curve is generated representing the overall trend for catalyst deactivation in a hydrotreater reactor. For a pilot plant where only a single variable (ex. sulfur concentration or hydrogen concentration) may be adjusted to determine impact on a catalyst activity, the Thiele modulus provides a reasonable representation for catalyst activity due to internal mass transfer resistances.

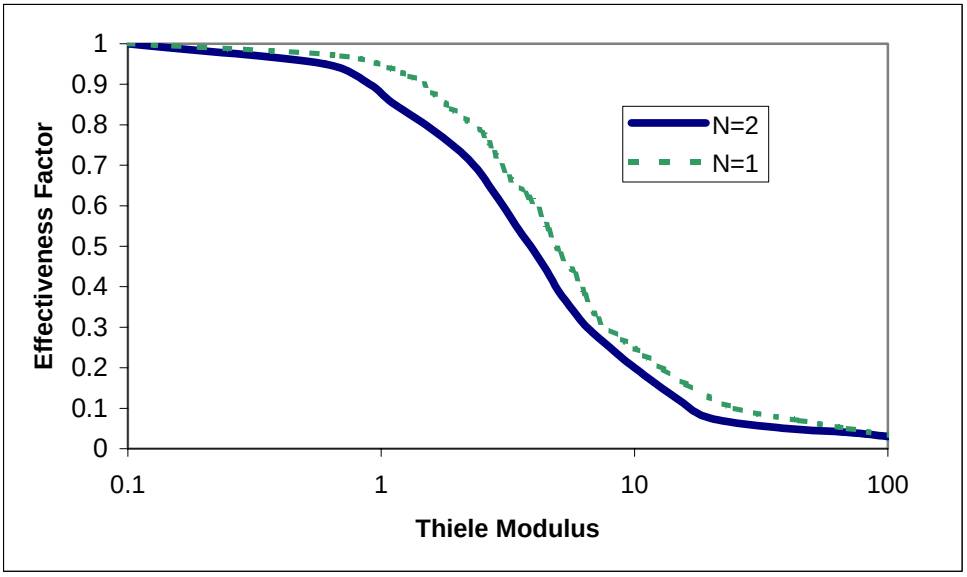

Figure 5.5 – Thiele Modulus Φ vs. Effectiveness factor E_f for reaction orders of N=1 and N=2 for hydrotreater reactor, the typical boundaries for sulfur hydrotreater reaction orders. Relationship follows the classical S-shaped curve for catalyst deactivation and is used in pilot plant research to match the general trend of the SOR-MOR-EOR catalyst deactivation witnessed in a non-industrial environment.

Even though the use of the Thiele Modulus and effectiveness factor are used to calculate conditions within the catalyst particle and do not directly fit the lumped approach for the model in this research, the key variables used in calculating the Thiele Modulus and effectiveness factor ($d_{p,}$ catalyst diameter; ρ_{cat}, catalyst density; A_{os}, effective catalyst surface area (=f(coking and metals deposition)); k_s, sulfur reaction rate; C_H, hydrogen concentration; Cs, sulfur concentration; $\rho_{oil,}$ crude oil density; D_{AS} effective diffusivity of sulfur.) are included in the catalyst deactivation model developed in this research. In addition, the wetting efficiency concept considered in this research to capture reactant contact to the catalyst for this lumped approach provides a similar function to the effectiveness factor used in classical catalyst intra-particle deactivation models. As a result, there is

confidence in evaluating and using the basis of the steady state catalyst vendor correlations for application in the catalyst deactivation model in this research to develop a “dynamic-oriented” representative industrial catalyst deactivation model that is based on classically-based deactivation research.

5.6.1 Catalyst Deactivation - Middle of Run (MOR)

Formulating mechanisms to explain rates of poisoning is as difficult as establishing mechanisms for the main reaction itself[7,13]. As noted in the literature review, three distinct catalyst deactivation regimes/zones occur (start of run, middle of run and end of run), and each regime/zone should be treated differently in a catalyst deactivation model. The MOR has a gradual catalyst deactivation trend due to continuous, steady metal deposition with the coke deposition at an “intermediate” equilibrium. The basis for catalyst deactivation representation in the model developed in this research is based on the MOR which is typical of most hydrotreater catalyst deactivation models[7,19-21,32].

The basis for catalyst deactivation representation in the model is based on proprietary steady state catalyst deactivation correlations derived by catalyst vendors. The correlations developed provide an overall representation of the impact of two key contributors to the catalyst deactivation: metals deposition (part of the objective in VGO hydrotreater) and coke deposition. Equation 5.28a[7] is used for MOR catalyst deactivation in steady state calculations by catalyst vendors with q_o representing the total expected degree of catalyst deactivation over the total run. The impact of SOR, and EOR is lumped into the steady state equation of 5.28a. The catalyst vendor deactivation equation would under predict

during SOR and EOR, and over predict during MOR[3].The purpose of the catalyst vendor catalyst deactivation correlation is to understand the overall impact of catalyst deactivation on the life of the reactor under different scenarios (ex. crude flow, hydrogen partial pressure, sulfur and contaminants in the stream) for design purposes. Equation 5.28a is a proprietary steady state vendor catalyst deactivation relationship calculating the amount of total expected deactivation on the catalyst between SOR and EOR.

$$q_o = \left(\frac{\left(\frac{VPSI * RNC}{EF * K} - 1 \right)}{VPSIC} - \frac{B_t}{8} \right)_t \qquad (5.28a)$$

The above correlation is based on readily available plant operating data which is a benefit when applying/building a lumped model. It was decided to focus on altering the catalyst vendor steady state correlations to a form that could be used at various time intervals. As shown in figure 5.4, the currently available literature based catalyst deactivation models[5,21], appear to be too inaccurate and would be difficult to convert to use operating data as the only inputs to the model. Another Benefit of using and modifying “previous generation” proprietary industrial correlatons for MOR and developing specific add-on SOR and EOR factors is the ease of programming in Excel® solver. When catalyst deactivation is included with a 2nd order type rate law, coupled differential equations need to be solved which increases the complexity of the calculation without any assurance that a solution (regardless of accuracy) will be obtained.

For the dynamic portion of the model, a relationship needed to be created representing the catalyst life remaining at each point in time a calculation was to be made. In other words the catalyst activity for each point in time needed to be determined so a representative kinetic relationship could be used to calculate the sulfur product out of the reactor . This relationship developed for remaining catalyst activity is denoted by (1-ϕ) and is shown in Equation 5.28b. using the initial condition of, at t=0, B_0=1.

$$1-\phi = 1-\left(\frac{\left(\frac{VPSI * RNC}{EF * K}-1\right)}{VPSIC}-\frac{(B_t - B_{t-1})}{8}\right)_t * \left(\frac{\left(\frac{VPSI * RNC}{EF * K}-1\right)}{VPSIC}-\frac{B_t}{8}\right)^{-1}_{t=0} \quad (5.28b)$$

Equation 5.28b uses 5.28a in the denominator which is the steady state catalyst deactivation relationship from the catalyst vendor. The denominator (q_o), as provided by a catalyst vendor, calculates the expected total deactivation of the catalyst from SOR to EOR. In discussions with various catalyst vendors[3], and hydrotreating modeling experts[3,61,62], and some trial error with the plant D data set, Equation 5.28a was modified to represent q, the numerator in Equation 5.28b (the amount of catalyst deactivation to this point). A B_{t-1} term was added as a subtraction term to try to represent the change in temperature impacting on catalyst deactivation between each data point. Without this modification, the catalyst deactivation would be under-predicted (based on initial analysis of plant D data and then subsequently with the remaining data sets) and thus catalyst activity would be over predicted. Subtraction was chosen since it can capture the

difference in fouling tendency for a change in temperature that was trying to be represented.

The following Equations 5.29 to 5.55 are the correlations necessary to obtain the deactivation values for the catalyst vendor steady state variables in Equation 5.27a and the developed time-varying catalyst deactivation Equation 5.27b. The equations noted by “a” are taken from a catalyst vendor, with the “b” and “c” equations noting the modification made by the author (if applicable) to the “a” equation to make it suitable for the catalyst deactivation factor used in this research. The intent of the modifications presented in Equations 5.27b-5.55b is to accumulate incremental loses in catalyst activity at each time step to create an overall representative catalyst deactivation profile.

Equations 5.29 to 5.31 provide a relationship for temperature and fouling factors for catalyst deactivation over the entire run length for use in Equations 5.28a and 5.28b. B_t was included by the catalyst vendor to shift the deactivation profile to match data from their database of VGO hydrotreater data. There is no 5.29b needed, since the modification for this factor is embedded in Equation 5.28b.

$$B_t = \frac{(FAC - 1)}{9} \text{ for t>0} \tag{5.29}$$

FAC is a fouling activity correlation, and in the steady state form 5.30a provided the impact of fouling over the entire design temperature range. For this research, 5.30a was used to determine the maximum catalyst deactivation for the denominator of 5.28b, and was modified to provide an accumulating fouling catalyst deactivation factor at each time step for the numerator in Equation 5.28b.

The T_{eor} was changed by the author to T_i to obtain the accumulating fouling activity correlation (from SOR to point in time being calculated).

$$FAC_0 = \frac{(T_{EOR} - T_{SOR})}{FR_{T0}} \text{ for t=0} \quad (5.30a)$$

$$FAC_i = \frac{(T_i - T_{SOR})}{FR_{Ti}} \text{ for t>0} \quad (5.30b)$$

$$FR_T = FR + AF_T * FR_{size} * FR_{crack} * VPSICO \quad (5.31a)$$

$$FR_{Ti} = FR_i + \frac{AF_{Ti} * FR_{sizei} * FR_{crack_i} * VPSICO_i}{derivative_i} \quad (5.31b)$$

FR_T in Equation 5.31a represents a catalyst vendor's overall fouling expected on the catalyst during the run based on the design conditions of the crude. A derivative term, Equation 5.32b with Equation 5.32c, was created to modify 5.31a to create, 5.31b, to track this relationship for fouling from the impact of changing crude properties on the reaction over each time interval. In a mathematical sense, a rate of change is calculated by taking the derivative of a function. In the absence of a function, a derivative factor was created. Equation 5.32b has a difference term in the numerator with a constant denominator. The denominator represents the change in time or the time between data points which has been set to 5 minutes (5/60).

$$Derivative = \frac{\partial Y}{\partial t} \approx \frac{(Y_{i+1} - Y_i)}{0.08} \quad (5.32b)$$

The database gathered for this research and data from various catalyst vendors was used to fit the data to create Equations 5.32b and 5.32c. From a physical

point of view, Y_i represents the impact of crude properties on catalyst deactivation. The terms included in Equation 5.32c, are from existing catalyst vendor steady state relations provided below and are multiplied together to obtain Y_i. The three terms multiplied together defined further below (AF = catalyst activity factor , EF = efficiency factor, and PHI = physical properties factor) all calculate a contribution to the impact of crude properties at a given time on catalyst deactivation. These items are not additive but appear to be multiplicative based on fitting with the research data base.

$$Y_i = AF_{Ti} * EF_i * PHI_i \tag{5.32c}$$

Equations 5.33 to 5.55, with the exception of 5.37b and 5.39 (developed by author for this research), are taken from a catalyst vendor to calculate the necessary variables for the key catalyst deactivation relationships developed in this research (main catalyst deactivation factor, 1-ϕ, 5.28b and impact of crude properties on deactivation, Y_i, 5.32c).

Equation 5.33 represents the fouling rate parameters specific for metals deposition and the potential for cracking (indicator for coking). This relation is taken from a catalyst vendor and is used for both Equations 5.31a and 5.31b.

$$FR_i = \frac{Vc_i * \varepsilon * WABT_i}{876000 * Met\%_i} \tag{5.33}$$

while V_c is the Catalyst volume, ε , is the void space in the catalyst bed (provided by catalyst vendor), Met% , defined in Equation 5.34, is the concentration of metals deposited on the catalyst feed (typically vanadium and nickel, but can include nickel and others), with WABT as the overall reactor absolute temperature and C_m representing metals in the feed (ppm).

$$Met\%_i = 36500 * \left[\left(\frac{100000 * M_i}{\rho_{ci} * V_c} \right) * \left(\frac{C_{mi}}{1e6} \right) * 42 * \left(\frac{1179.88}{API_i + 31.5} \right) - 0.0101578 \right] \qquad (5.34)$$

In Equation 5.31b, FR_{cracki} represents the potential impact of crude cracking in the reactor, based on the presence of asphaltenes[7,12,20] and aromatics[7,12,20] which are precursors to coking of the catalyst.

If Crackstock% = 0, FR_{cracki} =1 (5.35i)
If Crackstock%>0,

$$FR_{cracki} = 1 + \frac{(\%asphaltene_i + \%aromatics_i)}{100} \qquad (5.35ii)$$

FR_{size} in Equations 5.31a and 5.31b include the size of the catalyst into the catalyst deactivation as shown in Equations 5.36i and 5.36ii.

If d_p (catalyst diameter) < 0.0625, FR_{size}= 0.5 (5.36i)
If d_p >0.0625

$$FR_{size} = 1 - 13.33(0.1 - d_p) \qquad (5.36ii)$$

$VPSICO_i$, in Equation 5.37a, is included in Equations 5.31a and provides the impact of crude properties and hydrogen partial pressure on the catalyst fouling

rate. As hydrogen purity is increased the tendency to coke is reduced[7,9,12,21,32-35] , Equation 5.37a;

$$VPSICO = \left(\frac{pH_2}{1000}\right)^{-3} * e^{(0.0015*\%Ashphalt+560*PCI)} * \left(\frac{WBP}{1000}\right)^{1.5} * e^{\left(14.5-\frac{30900}{T_{sor}+460}\right)} \quad (5.37a)$$

Equation 5.37b is a modification of the steady state relationship in 5.37a by converting T_{sor} into the reactor temperature at each time interval.

$$VPSICO_i = \left(\frac{pH_{2i}}{1000}\right)^{-3} * e^{(0.0015*Ashphalt_i+560*PCI_i)} * \left(\frac{WBP_i}{1000}\right)^{1.5} * e^{\left(14.5-\frac{30900}{T_i+460}\right)} \quad (5.37b)$$

where WBP is the weighted average boiling point (T_{10}+T_{30}+T_{50}+T_{70}+T_{90}) from the distillation curve provided in the lumped crude analysis. Asphalt is the percent asphaltene in the feed and PCL is the percent chlorides in the feed, if any are present (otherwise, PCL is set as 1).

VPSI in Equations 5.28a and 5.28b are defined by Equation 5.38.

$$VPSI_i = AF_T * EF * e^{\left(\frac{E_a}{RT}\right)} \quad (5.38)$$

where

$$\frac{E_a}{RT} = LHSV^{-1} LN \frac{S_{p(t-1)}}{S_{f(t-1)}} \quad (5.39)$$

Equation 5.39 was considered, based on a basic relationship to the Arrhenius equation in Equation 5.11 from what the catalyst vendor provided, noted as Equations 5.40i and 5.40ii below. The previous time interval values for sulfur were used since the ratio of sulfur is fairly constant. By using the previous sulfur values an iterative loop is removed at the current time interval.

$$e_i^{\left(\frac{EA}{RT}\right)} = e^{\left(25-(26558+\left(\frac{B}{R}\right)_i * \frac{LN\left(\frac{S_F}{S_P}\right)}{(T_I+460)}\right)} \quad (5.40i)$$

$$\left(\frac{B}{R}\right)_i = e^{\left(7.49-\frac{6260}{WBP}+\frac{17.29}{Anilpt}+1100-T_i+460\right)} * e^{\left(\frac{9.472*\frac{(pH_2-57.93)}{pH_2}}{\left(\frac{1100}{T_i+460}\right)}\right)} \quad (5.40ii)$$

The VPSI term factors in variables that influence catalyst deactivation through activity, and effectiveness factors and a temperature factor based on the Arrhenius relationship. The activity factor relationship, Equation 5.41, incorporates feed properties, hydrogen partial pressure, physical properties of the catalyst (density and surface area), and whether the operating unit has an H_2S scrubber. Without an H_2S scrubber, H_2S is recycled back to the reactor where it inhibits the desulphurization reaction. Each activity factor is calculated using Equations 5.42 through 5.46.

$$AF_{Ti} = AF_{FEEDi} * AF_{pH_{2i}} * AF_{scrubi} * AF_{areai} * AF_{\rho i} \quad (5.41)$$

$$AF_{pH_{2i}} = e^{\left(\frac{-173.2}{pH_2}\right)} \quad (5.42)$$

$$AF_{\rho i} = \frac{\rho_c}{53.5} \quad (5.43)$$

$$AF_{area} = \frac{SA_c}{142} \quad (5.44)$$

A_{scrub}= 0.966 if scrubber in the unit (5.45i)

A_{scrub}=0.883 if no scrubber in the unit (5.45ii)

$$AF_{FEEDi} = \frac{e^{\left(\frac{18393}{WBPi} - \frac{9.77*\%Cracki}{T_i+460} - 3.285\right)}}{\left(1 + \frac{0.2*\%asphalt_i}{1000} + \frac{0.06356*N_{2i}}{1000} + \frac{0.01536*PCI_i}{1000}\right)} \quad (5.46)$$

The efficiency factor, Equation 5.47, tracks the change in catalyst performance over each time interval time period, with PHI, Equation 5.48 as the primary variable (function of temperature, catalyst and feed properties). This efficiency factor relationship resembles the Thiele Modulus and provides similar features for representing the overall S-shaped trend for catalyst deactivation.

$$EF_i = \frac{\left(e^{PHI_i} - e^{-PHI_i}\right)}{e^{PHI_i}} + \frac{e^{PHI_i}}{PHI_i} \quad (5.47)$$

$$PHI_i = 0.788*Size*\sqrt{\frac{1100*AF_{area}}{460*T_i} * \frac{300*SG_i}{MW} * e_i^{\left(\frac{EA}{RT_i}\right)}} \quad (5.48)$$

$$SG_i = \frac{141.5}{API_i + 131.5} \quad (5.49)$$

$$Size = \frac{\theta_c}{0.1} \quad (5.50)$$

RNC is defined by Equation 5.51 is also found in Equations 5.28a and 5.28b. RNC uses the fouling rate and catalyst properties to create an acceleration factor (based on a ratio of the residue theorem for evaluating a cross-sectional surface)[57] to the MOR catalyst deactivation. Equations 5.52 through 5.55 are used to calculate the value for RNC.

$$RNC_i = \frac{\left(e^{YC_i} - e^{(-YC_i)}\right)}{\left(e^{YC_i} + e^{(-YC_i)}\right)} * \frac{1}{YC_i} \tag{5.51}$$

$$YC_i = YC_{FACTi} * PHI_i \tag{5.52}$$

$$YC_{FACTi} = (1 + \exp(-100 + 16 * ALPHA_i * VPSIC_i^{0.75}))^2 \tag{5.53}$$

$$ALPHA_i = \frac{FR_{INITi}}{T_i - T_{SOR}} \tag{5.54}$$

$$VPSIC_i = ALPHA_i * (VPSI_i - 1) \tag{5.55}$$

5.6.2 Catalyst Deactivation – End of Run

During the operation of an HDS unit the catalyst deactivation accelerates after a certain point bringing on a quick end to the catalyst run life. The refiner is keenly interested in staying away from this acceleration point and also interested in knowing when it will occur and how much time is left before product specifications cannot be met by manipulating process parameters (crude flow, hydrogen partial pressure). Using a middle of run (gradually trending) catalyst deactivation model is not adequate for modeling the accelerated reduction in catalyst activity[12,21,28]. The refiner, to successfully operate the HDS, must know when the rapid catalyst deactivation will occur. Time indicators[28] have been developed, and can provide an estimate of when the catalyst activity may rapidly beginning deteriorating. Since DBT is used as the indicator compound in the lumped approach, information from the equilibrium curve for DBT is being used

as the indicator of catalyst deactivation acceleration. Figure 5.6, on the next page, shows the DBT desulphurization equilibrium.

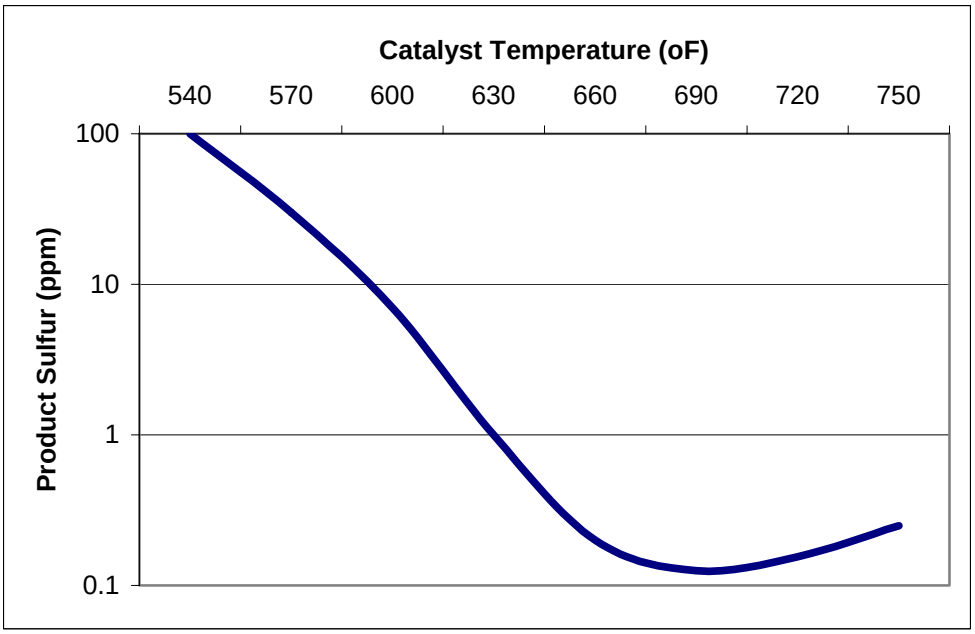

Figure 5.6 – DBT Equilibrium[7,58] supplied by catalyst vendor based on VGO stream. The product sulfur tends to begin to increase after reaching a minimum at approximately 685°F. Contributors to this increase in product sulfur is aromatic saturation reversibility, coke core-plugging, H_2S competing for H_2 molecules and increased hydrogenation reactions.

Note, DBT in the product begins to increase after 685°F. This reduction in sulphur conversion after 685°F is typically attributed to the following four concerns:

1. The impact of core plugging from coking that blocks access to remaining internal catalyst surfaces[15,20,30-32]
2. The impact of metals on the catalyst creating increased dehydrogenation or selective poisoning becomes a major contributor to deactivation after certain amount of material is on the catalyst surfaces [5,20,30]

3. The impact of H2S as a competitor for hydrogen[20,27,30,31,34]

4. The saturation of aromatics is reversible [5,30,34]

An enhancement to the lumped MOR portion of the proposed catalyst deactivation model is to include a “rapid deactivation term” that would include the applicable EOR features noted above. In Equation 5.41, an additional term in the activity factor model has been included by the author to model EOR deactivation and results in Equation 5.56. The EOR factor was added to this activity factor, due to the ease of multiplying another term to the relationship to increase the deactivity witnessed and also it adds another key activity variable to the relationship.

$$AF_{Ti} = AF_{FEEDi} * AF_{pH_{2i}} * AF_{scrub} * AF_{area} * AF_{\rho i} * AF_{EORi} \quad (5.56)$$

AF_{EOR} is defined in Equation 5.57. Equation 5.57 is used to calculate the increased coking tendency and change in sulphur equilibrium. Below a temperature of 685^{o}F, the AF_{EOR} is set to 1, while above 685^{o}F Equation 5.57 is used to calculate the AF_{EOR}.

$$AF_{EOR_i} = \eta_{ei} e^{-\left(\frac{H_2S_{t-1}M_{fi}\%Cracki}{850(T_i+460)}\right)} \quad (5.57)$$

The AF_{EOR} factor is embedded in Equation 5.27b of the MOR deactivation model and acts to increase the rate of catalyst deactivation at the end of run.

The format for the AF_{EOR} equation was based on other activity factor correlations developed by the catalyst vendor. Since the activity factors when applied to the

modified MOR model appeared to represent the phenomena they were set up to match based on comparison to plant D and F data, an exponential format was used as a starting point with the following variables investigated:

1. Coking represented by the amount of coke precursors in the crude (%crack * Mf)
2. Metals represented by %met
3. H_2S representing amount of H_2S generated
4. Wetting efficiency

Plant F data was used to determine whether the format for the equation was reasonable and also was used to determine what constants would be needed to match the plant data. Figure 5.7, on page 116, shows a comparison of the plant WABT in the EOR region to the various versions of the EOR activity factor considered. The coking and H_2S relationship appeared to exhibit the necessary sensitivity to the plant data while the metals factor was rather insensitive. H_2S and coking were placed in the numerator so that as these values increased, the activity would reduce. The temperature was placed in the denominator since as it is increased, catalyst activity increases. The wetting efficiency was included to incorporate the concern with incomplete wetting adding to the reduced activity and subsequent increase in coking potential. Figure 5.7 shows a few of the options considered for the AF_{eor} factor. Equation 5.57 provided the closest match to the data. When the metals impact was included, it appeared to dominate the entire relationship and reduce the sensitivity of the model to changes in the plant data . The coking variable appeared to represent the core plugging that blocks

the remaining catalyst sites which have been cited many times as the primary contributor to catalyst deactivation at EOR[20].

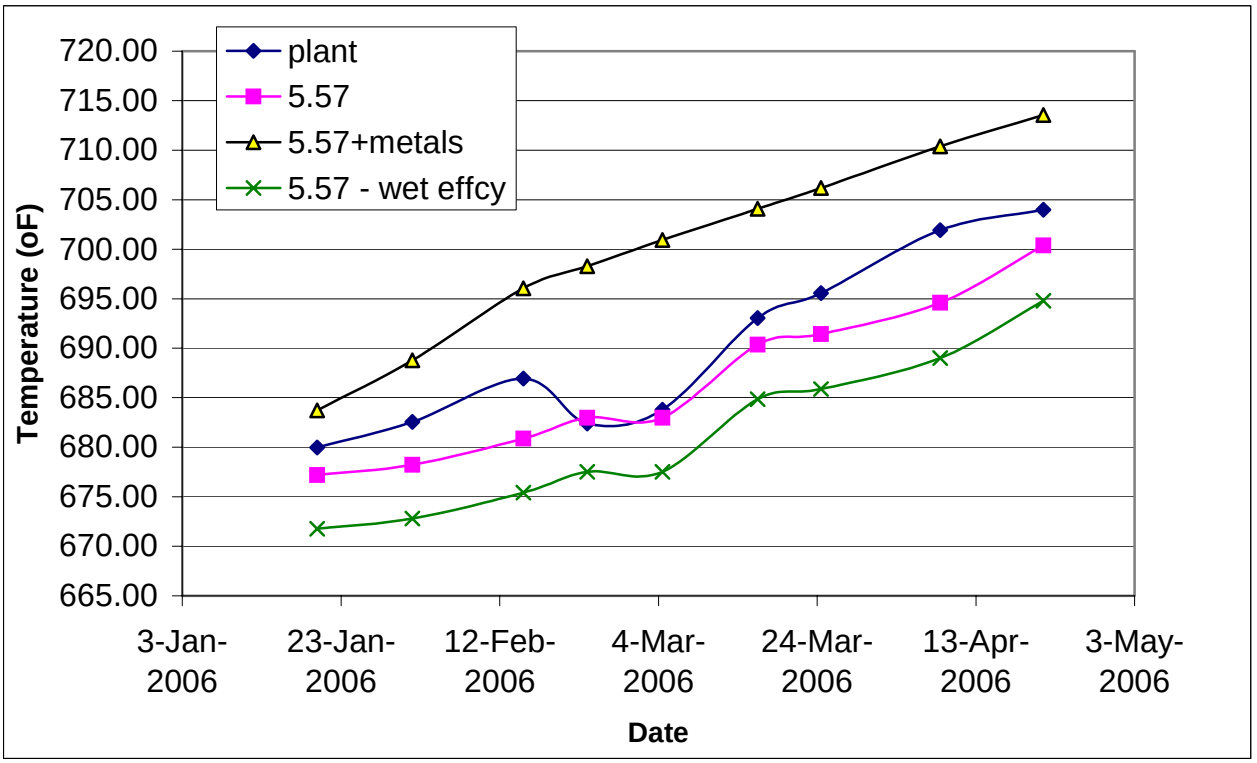

Figure 5.7 – Development of EOR activity factor for catalyst deactivation based on plant F EOR information. Variations to Equation 5.57 were preliminarily evaluated to determine the best fit to the plant d plant data. Adding metals impact (data 5.57+metals) to the activity factor reduced the sensitivity of the factor to the other contributors to catalyst deactivation, while not having wetting efficiency (data 5.57-wet effcy) in 5.57 reduced the fit of the overall model.

The wetting efficiency (range of 0.6-1) was added to shift the model closer to the plant data. The wetting efficiency when multiplied in Equation 5.57 acts to reduce the activity in this factor as what would be expected in real operation. When the catalyst is not fully wetted, the active sites are reduced and the catalyst activity is reduced. In addition, un-wetted locations tend to increase tendency for coke formation permanently reducing the catalyst activity for the rest of the plant run.

The EOR factor is applied to the model when the temperature reaches 680^{o}F, just before the point where the sulfur product begins to increase in Figure 5.6 or when the catalyst has been deactivated by 70%. At 70% deactivation, the pore plugging of the catalyst tends to occur and the rapid decline in activity can result[5,7,20,35,36].

5.6.3 Catalyst Deactivation - Start of Run (SOR)

In industrial scale reactors, the initial temperature rise is faster than in a pilot plant reactor due to rapid coke equilibrium being established on the catalyst[36]. The MOR model needs to incorporate this rapid coking that is the cause of accelerated catalyst deactivation (nearly a vertical line from day zero for the first 20-30 days or the first 30-40^{o}F temperature rise) during the SOR. To model this initial deactivation Equation 5.58, FR_{crack_initi} has been developed by the author to meet the model development objectives of providing a representative hydrotreater model over the entire run length. Features from Equation 5.35ii, FR_{cracki}, were considered when developing Equation 5.58. Again, the pre-cursors to coke formation are included in the fouling rate (%ashphaltene and %crack – asphaltenes and hydrocarbons with cracking tendencies) but this new factor emphasizes the first 30-40^{o}F temperature rise after SOR. Wetting efficiency is also evaluated and included since a poor wetting efficiency will exacerbate the catalyst deactivation because a catalyst particle not completed wetted will tend to coke quicker than a completely wetted catalyst particle[20,26,44]. For this factor, the wetting efficiency was used as an exponent to accentuate the impact of the

coking precursors. As the wetting efficiency increases, the impact on coking decreases from the inverse exponent as expected. Various wetting efficiency multipliers were attempted but the desired trend required additional constants to be added and could not provide the rapid change in catalyst deactivation desired. The exponent required no other adjustment constants based on a correlation fit to data of plant D with reference to the other plants' data sets. Figure 5.8 shows a comparison between the two of the types of wetting efficiency factors investigated.

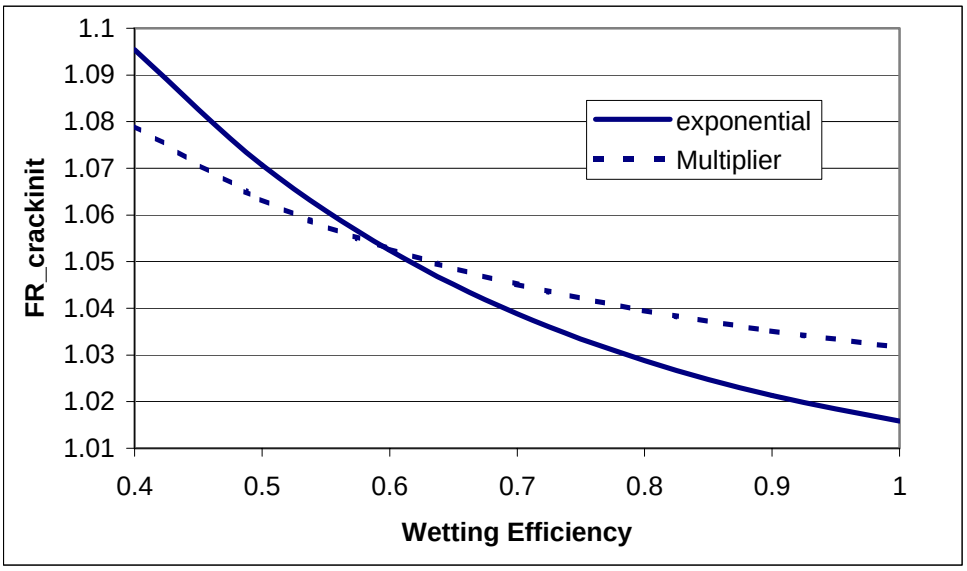

Figure 5.8- Comparison of wetting efficiency factors considered for the SOR catalyst deactivation factor. The figure uses a temperature difference of 10^{o}F, a 5% value for the sum of % ashphaltenes and % crack. The wetting efficiency multiplier considered requires an additional constant to get in the value range expected for this variable during SOR, and the absolute value of its slope is not as aggressive as catalyst deactivation during SOR. The exponential wetting efficiency provides the desired absolute slope and is in the desired range to correlate to the plant data.

The wetting efficiency as an exponent provides a more rapid change in SOR fouling factor due to wetting efficiency than the multiplier and thus provides a

better fit for matching the rapid changes in catalyst activity during SOR. The variables included (coking precursors to simulate the coke build up (%ashpaltenes and %aromatics) and temperature to match the length of time that the reactor is in the SOR region) are primarily the ones that have been cited in literature as being important in the SOR region[20]. A key feature for the use of this SOR factor is when and how to reduce its impact to match the situation in the reactor. As the temperature increases to a point where the coking reaches equilibrium, the $(T_i - T_{sor})^{\wedge 0.5}$ factor was considered (via inspection) to make the FR_{crack_init} small relative to the other MOR factors when the reactor is in the MOR region, so it only impacts SOR as intended.

$$FR_{crack\_init} = 1 + \frac{(\%asphaltene + \%aromatics / 100)^{\frac{1}{\eta_e}}}{\sqrt{(T_i - T_{SOR})}} \tag{5.58}$$

FR_{crack_init} is now added in Equation 5.31b, the fouling rate expression, resulting in Equation 5.59 which incorporates the SOR catalyst deactiviation into the overall MOR catalyst deactivation model.

$$FR_T = FR + AF_T * \frac{FR_{size} * FR_{crack} * VPSICO * K}{Derivative} * FR_{crack\_init} \tag{5.59}$$

The fouling rate expression 5.31b was considered as the location to place the SOR factor since an existing coking factor FR_{crack} is part of the equation. FR_{crack} tracks the MOR coking tendencies, so it was decided not to adjust that factor but to add another factor that would be effective in the SOR range. The choice of the

format of the factor originated from inspection of the key variables involved and the desired shape for the equation output and was checked/optimized by trial and error matching plant D and F data.

5.6.4 Catalyst Deactivation Summary

Section 5.6 provides a description of the catalyst deactivation model used in this research. Basically, a group of proprietary steady state design correlations were converted and improved by the author to represent catalyst deactivation over the entire run portion. Enhancements to the base MOR correlations were made to better represent SOR and EOR catalyst deactivation in a HDS. Variables that should be impacting catlayst deactivation in the SOR and EOR regions were evaluated and input into a format that resembled previously successful correlation formats. An algorithm was created to determine when to apply the appropriate SOR and EOR features in the catalyst deactivation model. The algorithm is shown in figure 5.9, on page 121. As a result, a catalyst deactivation model for the entire run length of an industrial VGO hydrotreater has been developed.

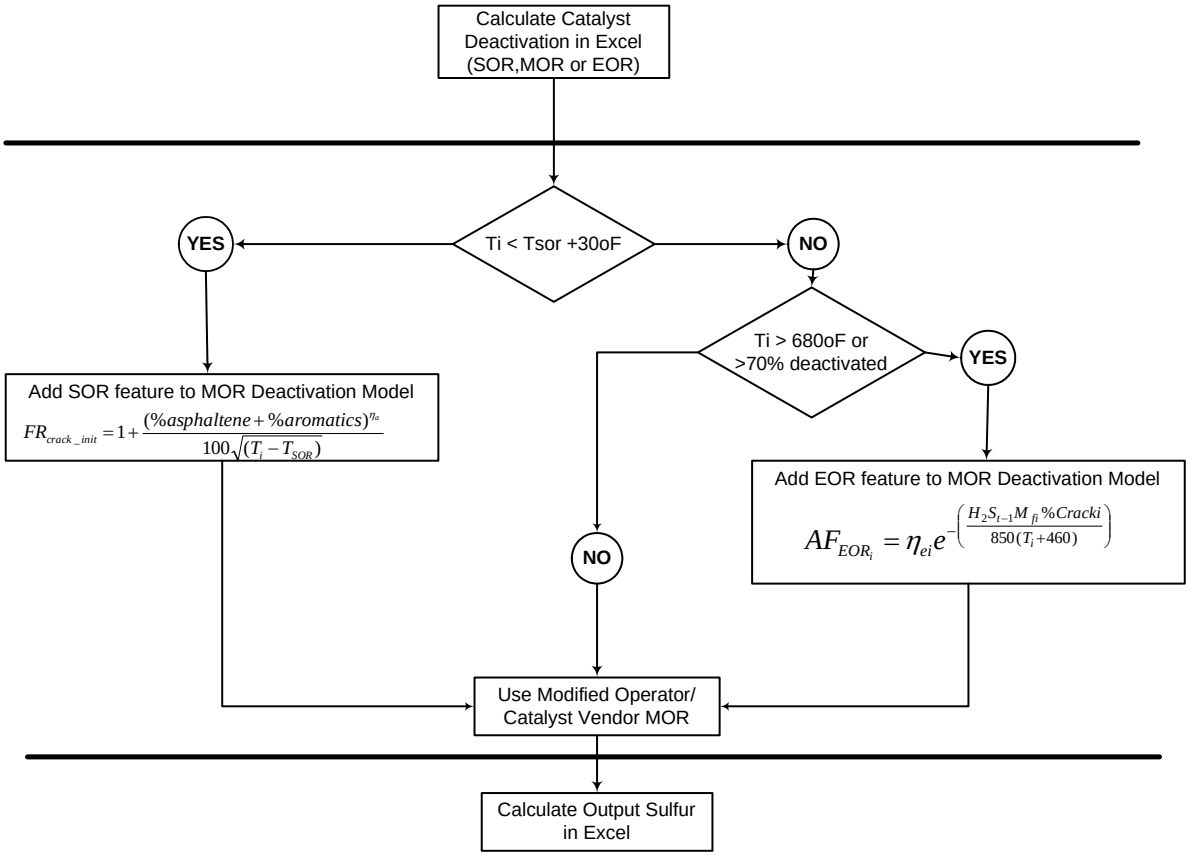

Figure 5.9 – Algorithm illustrating how the NEW SOR and EOR catalyst deactivation features are used in the catalyst deactivation portion of the model. When the temperature remains less than 30^{o}F after SOR, the SOR catalyst deactivation feature is incorporated into the overall catalyst deactivation calculation. When the temperature is above 680^{o}F or the catalyst deactivated by over 70%, the EOR catalyst deactivation feature is activated and added to the overall catalyst deactivation

5.7 Hydrogen Consumption

The hydrogen balance is key to properly operating an HDS. Hydrogen is consumed/lost in the light gas purge, absorbed in the hydrocarbon liquids and in the sulphur/nitrogen removal reactions. Most of the hydrogen is consumed in the desulphurization reactions. However the hydrogen lost via the light gas purge is approximately half that used for desulphurization, while hydrogen lost on the hydrocarbon liquids is negligible. Hence, the hydrogen must be accurately

tracked to ensure adequate hydrogen is provided for the main desulphurization reactions. Equations 5.60-5.65b were updated from the catalyst vendor Equations 5.60-5.65a[3,7] to track hydrogen in the HDS reactor. New coefficients were considered. The coefficients of olefins, nitrogen and aromatics were increased while the sulfur coefficient decreased. For heavier crudes with greater and more complex olefinic and aromatic compounds, increased hydrogen consumption to obtain desired hydrodesulfurization seems reasonable. Increased hydrogen consumption for nitrogen is acceptable, however, the reduction in the sulfur coefficient could not be explained but was found necessary to match the plant hydrogen consumption. In discussions with the catalyst vendor[3], the sulfur relation may have been the primary variable that was adjusted in the original correlations to compensate for low values from the other contributors.

$$HC = F\left(sulfur + N_2 + Olefins + Crack + Aromatics + purge\right) \tag{5.60}$$

$$F(N_2) = \left(\frac{N_F - N_P}{100}\right) * 5237 * \left(\frac{1179.89}{API + 131.5} - 0.010578\right) \tag{5.61a}$$

$$F(N_2) = \left(\frac{N_F - N_P}{100}\right) * 5685 * \left(\frac{1179.89}{API + 131.5} - 0.010578\right) \tag{5.61b}$$

$$F(Sulfur) = \left(\frac{S_F - S_P}{100}\right) * 1700 * \left(\frac{1179.89}{API + 131.5} - 0.010578\right) \tag{5.62a}$$

$$F(Sulfur) = \left(\frac{S_F - S_P}{100}\right) * 1492.3 * \left(\frac{1179.89}{API + 131.5} - 0.010578\right) \tag{5.62b}$$

$$F(olefins) = 0.925 * Bro\min e\# * \left(\frac{1179.89}{API + 131.5} - 0.010578\right) \tag{5.63a}$$

$$F(olefins) = 0.97125 * Bro\min e\# * \left(\frac{1179.89}{API + 131.5} - 0.010578\right) \tag{5.63b}$$

Bromine# is a measure of the amount of aliphatic unsaturation in the crude stream. It is twice the actual olefinic concentration in the crude stream. The Bromine number is measured as part of the regulary plant laboratory analysis.

$$F(aromatics) = 450 * \frac{\%aromatics}{MW} * \left(\frac{1179.89}{API + 131.5} - 0.010578 \right) \quad (5.64a)$$

$$F(aromatics) = 477.5 * \frac{\%aromatics}{MW} * \left(\frac{1179.89}{API + 131.5} - 0.010578 \right) \quad (5.64b)$$

$$F(purge) = F(aromatics + olefins + sulfur + N_2) \quad (5.65a)$$

$$F(purge) = \eta_a * F(aromatics + olefins + sulfur + N_2) \quad (5.65b)$$

For the purge, an observation from the data was that the hydrogen losses appeared higher than what Equation 5.65a was providing and increased when the reactor was at higher conversions. Based on these two pieces of information, the wetting efficiency was applied to match the reality of the data. A possible explanation is that as conversion increases, there are more lights gases produced and the drive for hydrogen to come out of solution increases, resulting in more hydrogen in the purge gas. The wetting efficiency can be related to the conversion in the reactor so it was applied to the purge relationship.

Hydrogen consumption relationships in literature were evaluated. Lumped hydrogen consumption based on temperature and pressure was of initial interest due to the lumped nature of the model. However, the hydrogen consumption values generated were an order of magnitude greater [3,5,7,19,33] than what would be expected and also calculated from Equations 5.60-5.65 For example, here is an equation developed by Labibidi[25] that was evaluated:

$$HC = 8.91x10^{-6}P + 4.16x10^{-6}(T - 273) - 1.4x10^{-3} \quad (5.66)$$

Model was not able to close its material balance with Equation 5.66. Equation 5.66 is based on pilot plant data and thus translating the equation to industrial scale may have not feasible. The material balance for the entire plant D data set closed when Equations 5.60-5.65a were used during initial development of the model. As a result, these correlations were used and improved to match the plant D data set. No further changes to these hydrogen consumption correlations (5.60-5.65b) were made during the evaluation of the other plant data (A,B,C,E,F). Equation 5.66 could be altered to fit the data however, the existing set of correlations 5.60-5.65 were adequate in the initial development.

5.8 Conservation Relationships

5.8.1 Reactor Model Choice

Two ideal flow reactors exist that are used for reactor model development:

1. CSTR (continuously stirred tank reactor) = molecules completely mixed and
2. PFR (plug flow reactor)= all molecules leaving reactor have been inside the reactor exactly the same amount of time (flat velocity profile with no axial mixing).

The model of a (non-ideal) reactor needs to portray the real reactor with some realism. The principal characteristics of the reactor that cause its behavior to deviate from the ideal much be reflected accurately in the model. The proper choice of a model to represent a real reactor has been stated as more art than science[15].

In addition, when choosing a model, the equations that describe a chemical reactor must be solvable since there is no benefit to having a situation very accurately described by a set of highly coupled integrodifferential equations with complex boundary conditions if the solutions to this system is virtually unobtainable[15,16]. Mathematical tractability is practiced by modeling a non-ideal reactor as a combo of ideal reactors or by making slight modifications to an ideal model by adding in a correction factor or dead volume, bypass stream or a recycle stream [15,16].

Industrial reactors, in particular trickle bed reactor, typically operate as non-ideal reactors. Three concepts are used to describe non-ideal reactors[7,11,15]: the distribution of residences in the system (RTD = residence time distribution) , the quality of mixing, and the model used to describe the system. The three concepts can be regarded as characteristics of the mixing in non-ideal reactors.

As a first approximation, non-ideal reactors can either be represented as an ideal CSTR or PFR. In real reactors, however, non-ideal flow patterns exist that represent a loss of conversion and this needs to be accounted for in the reactor model. Macromixing information (i.e RTD) can be used as an improvement to the initial approximation of an ideal reactor. A third level or approximation is using information on a microscale (micromixing) to make predictions about the conversion of a non-ideal reactor. Since the model being developed is a lumped model, general RTD profiles were evaluated to provide insight into choosing a

model to represent the non-ideal reactor in this research. RTD of a reactor is a characteristic of the mixing that occurs in the chemical reactor [11,15].

There is no axial mixing in a plug-flow reactor, and this omission is reflected in the RTD which is exhibited by this class of reactors. The CSTR is thoroughly mixed and possesses a far different kind of RTD than the plug flow reactor.
The RTD exhibited by a given reactor yields distinctive clues to the type of mixing occuring within it, and is one of the most informative characterization of the reactor.

Typically, an RTD is determined experimentally by injecting an inert chemical (tracer) into the reactor at some time. RTD analysis on these types of reactors shows that laminar flow tubular reactors, and CSTR's have similar profiles while CSTR's with dead space/bypass and packed bed reactors tend to have similar RTD profiles. Figure 5.10, on the next page, shows typical RTD distributions and thus provides some indication which model or models can be used for this research.
Trickle bed reactors have been calculated as having laminar flow. Plants A-F all exhibit laminar flow, with Reynolds numbers (150-300) well below the laminar/turbulent boundary of 2000. For laminar flow in a tubular reactor, the velocity profile is parabolic, with the fluid in the center of the tube spending the shortest time in the reactor. The RTD begins to resemble a CSTR so there could be an argument that a CSTR could be used as model. Also, the RTD for CSTR

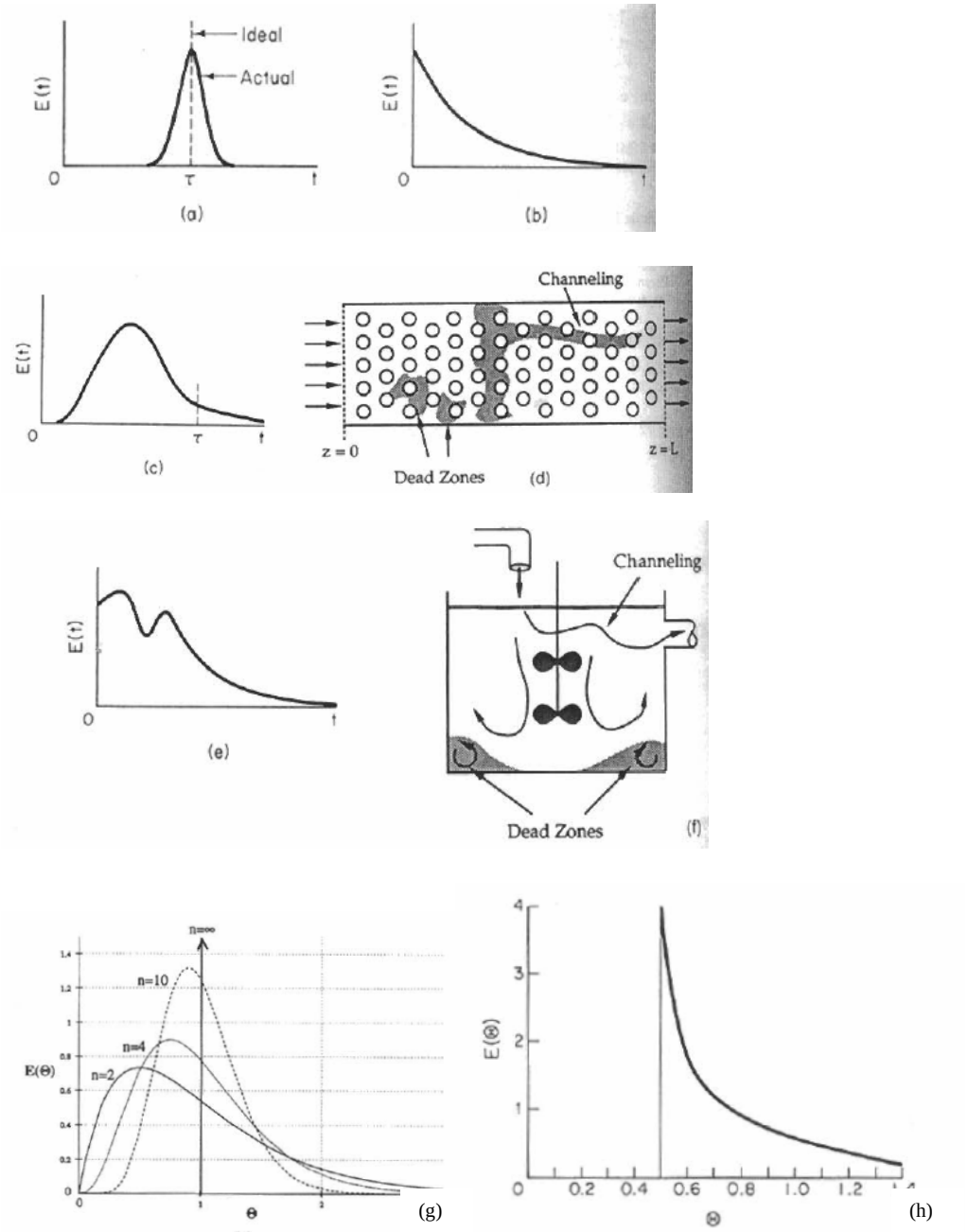

Figure 5.10[16] – Examples of typical RTD distributions for various types of reactor models. a) RTD for near plug flow reactor; b) RTD for near perfectly mixed CSTR; c)RTD for packed bed reactor with dead zones and channeling; d) packed-bed reactor description of c) RTD; e) RTD of CSTR with bypass and dead space; f) CSTR with dead zone description of e) RTD; g) RTD for CSTR in series h) RTD curve for a laminar flow reactor

in series resembles a packed bed reactor RTD. It can be surmised from RTD information that an ideal PFR should not be used to represent a packed bed reactor. It should be cautioned, that RTD analysis cannot be used to completely explain the choice of the model but provides insight into what models may be used (CSTR in series, packed bed with dead zone and channeling) and which ones should not be used (ideal PFR).

Another piece of information to consider when choosing a model is to look at the speed of the reaction. In general, for slow reactions, modeling the reactor as a CSTR is a good first approximation[15,16,26]. For fast reactions, mass transfer resistances (intra- and inter- particle control the reactor), applied to CSTR's or PFR's models with dispersion/mixing factors included are typically used[15,16,26]. Most literature states that a PFR is the typical starting point for tubular reactors. Based on available literature there is evidence to suggest that the hydrotreater sulfur reaction is moderately fast[3,7,10,15,16,24-26]. A moderately fast reaction may have competing controlling resistances. In theory and in this research, both kinetics and mass transfer (internal) appear to compete for reactive "control" of the reactor.

In this particular research, we have access to a significant amount of industrial process data, albeit lumped, so a choice was made to modify an existing ideal model by developing some lumped parameters that would represent the plant

data. Conversion comparison between different models was performed to assist in deciding what model to use in this development process.

Most literature starts[7,15,16] with assuming fluid moves through a trickle bed reactor as a PFR and every molecule spends an identical length of time in the reaction environment. Here, the velocity profile is flat and there is no axial mixing. Both of the assumptions are false to some extent in every tubular reactor, more so, when the tubular reactor is filled with fixed beds of catalyst. Two models are suggested to factor in the non-ideal nature of a trickle bed reactor – a series of identically sized CSTR's or modify the plug flow reactor by imposing a dispersion/mixing relationship. It has been shown that conversions (X) for various reactor models follow the following hierarchy in Equation 5.67[7,11,15,16]:

$$X_{PFR}>X_{seg}>X_{series}>X_{CSTR}>X_{CSTR\_dead}>X_{mm} \quad (5.67)$$

Using already developed derivations from literature for conversion[16], table 5.4, on page 123 shows the various conversions from each model reviewed. There are two cases that are close to the plant data average conversions for each plant (PFR with performance factor and CSTR with bypass/dead space). It should be noted that the desired model in this research is a lumped model so the choice of model should reflect this simplification due to the type of data available for inputting into the model.

The conversion relationships used for table 5.5 (on page 131) results were based on 2nd order reactions. Time variables were changed for $LHSV^{-1}$ since LHSV is readily available from data set. Also, the catalyst deactivation model developed

for this research was also used for all different models evaluated. The conversion relationships are noted below in Equations 5.68-5.73.

CSTR:

$$X = \frac{(1+2LHSV^{*}SA^{*}k_{hds}S_{in}) - \sqrt{(1+2LHSV^{*}SA^{*}k_{hds}S_{in}) - (2LHSV^{*}SA^{*}k_{hds}S_{in})^{2}}}{2LHSV^{*}SA^{*}k_{hds}S_{in}} \quad (5.68)$$

CSTR with dead space and bypass:

$$X = 1 - \frac{S_{in}(-1+\sqrt{1+4LHSV*SA*k_{hds}S_{in}})}{2LHSV*SA*k_{hds}} \quad (5.69)$$

CSTR in series: As N (number of tanks) increases, the RTD and conversion approaches that of a PFR. N=2 and N=4 were chosen to do the conversion evaluation for this style of reactor

$$X = 1 - \frac{1}{(2LHSV*SA*k_{hds})^{n}} \quad (5.70)$$

CSTR with segregated mixing parameter :

$$X = \frac{k_{hds}S_{in}LHSV^{-1}}{1+k_{hds}S_{in}LHSV^{-1}} \quad (5.71)$$

CSTR with maximum mixing parameter: Integration was difficult so Euler method was used to obtain the following conversion relationship

$$X_{i+1} = X_i + \Delta LHSV^{-1}\left(\frac{X_i}{1-X_i} - k_{hds}S_{in}(1-X_i)^{2}\right) \quad (5.72)$$

where at t=0, $X_i = X_{design}$

PFR:

$$L = \frac{v}{k_{hds} S_{in} SA}\left[2n(1+n)\ln(1-X) + n^2 X + \frac{(1+n)^2 X}{1-X}\right] \quad (5.73)$$

For the PFR with wetting efficiency , the wetting efficiency was applied to the ideal PFR model in Equation 5.73.

Table 5.5 Summary – Conversion values for actual plant data (A-F) and model options considered. Plant data conversions provided in top 4 rows. Conversion values from models considered provided in bottom 8 rows. The PFR with wetting efficiency and CSTR with dead space+bypass were the models with the closest results to the plant average conversion.

	A	B	C	D	E	F
Conversion (Design)	0.976	0.938	0.980	0.986	0.971	0.956
Conversion (minimum)	0.600	0.760	0.902	0.543	0.733	0.760
Conversion (maximum)	0.994	0.979	0.996	0.988	0.992	0.979
Conversion (average)	**0.946**	**0.933**	**0.973**	**0.872**	**0.937**	**0.932**
MODEL OPTION AVERAGE						
Conversion (PFR)	0.991	0.967	0.994	0.998	0.988	0.964
Conversion (CSTR in series with n=4)	0.987	0.965	0.99	0.976	0.985	0.961
Conversion (CSTR dispersion via Segregation)	0.984	0.961	0.989	0.975	0.983	0.96
Conversion (CSTR in series with n=2)	0.983	0.954	0.984	0.966	0.981	0.953
Conversion (CSTR)	0.979	0.951	0.978	0.947	0.977	0.941
Conversion (PFR with wetting efficiency)	**0.942**	**0.936**	**0.967**	**0.876**	**0.918**	**0.916**
Conversion (CSTR with dead space + bypass)	**0.932**	**0.922**	**0.956**	**0.862**	**0.887**	**0.883**
Conversion (CSTR dispersion via Max. Mixing)	0.865	0.842	0.845	0.835	0.843	0.848

The model chosen for this research was a modified Plug flow reactor model considering the results of the conversion evaluation, the speed of the reaction, the RTD evaluation and the shape of the actual reactor (packed bed tubular). Based on the conversion analysis, the CSTR with dead space/bypass model could also be considered as a possible simplification to the model.

The modification or deviation factor applied to the ideal PFR was the wetting efficiency factor considered in the previous section. Since the model used in this research uses a lumped approach with data available at a macro level (outside

the reactor and at a limited locations within the reactor), applying the wetting efficiency as an indicator of overall particle interaction appears to be reasonable based on the matching of results in this thesis. The wetting efficiency provides an indication to what extent the reactants can access the catalyst to initiate and complete the reaction. The trickle bed reactor does deviate from a PFR since a parabolic velocity profile (laminar flow) and axial mixing are expected to be present. Degrees of segregation and mixing factors have been added to PFR's to represent real tubular reactors. These models are based on analyzing RTD data, and thus cannot be applied for this research. However, the concept of degree of mixing and segregation impacting the extent of reaction can be translated to the concept of wetting efficiency, a value that can be calculated with the data used in this research.

5.8.2 Material Balance

By including the rate expression with catalyst deactivation into the modified PFR model, the overall VGO hydrotreater model can be developed. Figure 5.11 on page 133 provides a sketch of the model inputs and outputs. The conservation relationships are the basis of mathematical modeling for both the Excel® and HYSYS® portions of the model. The dynamic mass, and energy balances that are derived in the following section are based on the steady state material and energy balances with the exception of the accumulation term required in the dynamic material and heat balance.

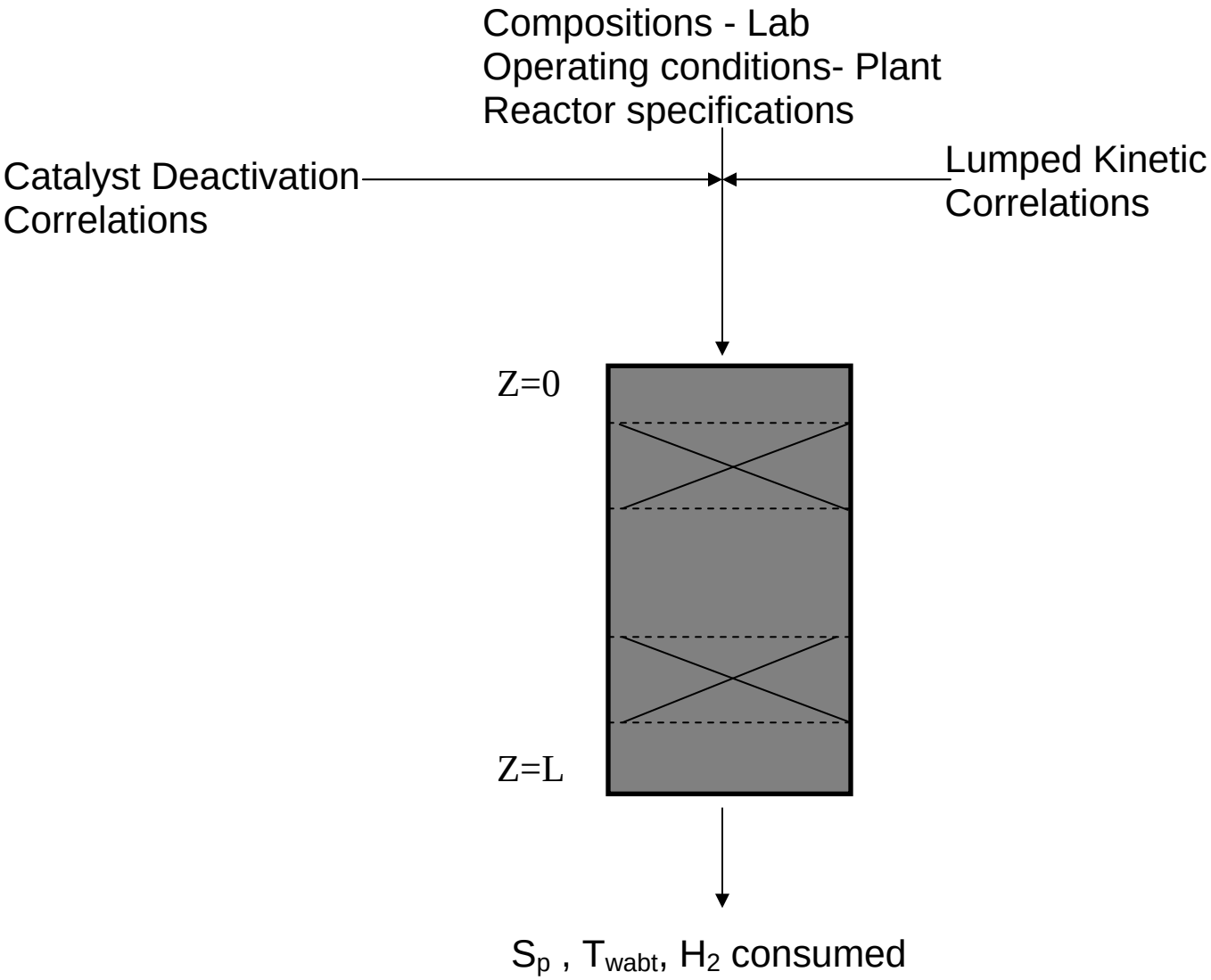

Figure 5.11 - Representation of VGO Hydrotreater Model Set-up. A modified PFR, over a length L was used with product sulfur composition, temperature and hydrogen consumed as the output from the model.

In the most general form the mass balance can be written as follows:

Rate of Accumulation Of Mass Within the system	=	Rate of flow of Mass into the system	-	Rate of mass generated in the system	+	Rate of mass Consumed in the system	-	Rate of mass flow out of the system

In mathematical terms the general mass balance for species i in a system is presented in Equation 5.74.

$$\frac{\partial C_i}{\partial t} + \nabla \bullet (-D_i \nabla C_i + C_i u) = r_i \qquad (5.74)$$

In Equation 5.74, C_i denotes the concentration of species i, D_i denotes the diffusion coefficient of species i, u denotes the velocity, r_i denotes the reaction term and ∇ represents $(\frac{\partial}{\partial x}, \frac{\partial}{\partial y}, \frac{\partial}{\partial z})$. The reaction term can accommodate arbitrary kinetic expressions for the reactants and products. The term within brackets represents the flux for species i. The first flux term describes the transport by diffusion while the second term represents the convective flux. The flux vector, j, is expressed here as mass flux, F', given by Equation 5.75.

$$F' = -D_i \nabla C_i + C_i u \qquad (5.75)$$

Boundary conditions for mass balance are provided by the following equations:

- Flux conditions

$$F'_i = f_o, \text{ at } z=0 \qquad (5.76a)$$

- Diffusion layer condition

$$F'_i = k_c (C_i - C_o) \qquad (5.76b)$$

- Insulation or symmetry conditions

$$F'_i=0 \qquad (5.76c)$$

- Concentration conditions

$$C_i=C_{i,0} \qquad (5.76d)$$

5.8.3 Energy Balances

Energy balance models are necessary to describe non-isothermal systems involving exothermic or endothermic reactions along with equipment for unit operations such as heat exchangers. Energy balances are in most cases coupled to momentum or mass balances. In the most general case, it is assumed that heat is transported by convection and conduction and arbitrary reaction mechanisms can be introduced as heat sinks or sources. In the most general form the energy balance can be written as follows:

Rate of Accumulation Of energy Within the system	=	Rate of flow Of Heat to The system From the surroundings	-	Rate of work Done by the System on The surroundings	+	Rate of energy Added to the system by mass flow into the system	-	Rate of energy Leaving system By mass flow out of the system

In mathematical terms the general energy balance is presented in Equation 5.77.

$$\rho c_p \frac{\partial T}{\partial t} + \nabla \bullet (-k'T + \rho c_p T u) = Q \qquad (5.77)$$

Where c_p denotes heat capacity, T is the absolute temperature, k is the thermal conductivity and Q is a heat sink or source. The expression within brackets is the heat flux vector, which in this case includes the contributions from convection and conduction, respectively, as per Equation 5.78.

$$q = -k\nabla T + \rho c_p T u \tag{5.78}$$

Boundary conditions for energy balance are provided by Equations 5.79a to 5.79c:

- Flux conditions

$$Q = Q_o \text{ at } z=0 \tag{5.79a}$$

- Insulation or symmetry conditions

$$Q = 0 \tag{5.79b}$$

- Temperature conditions

$$T = T_o \tag{5.79c}$$

5.8.4 Dynamic Material Balance

The dynamic material balance is based on the general mass balance Equation 5.74 describing convection-diffusion-reaction in the bed at the macro level. For simplicity, the diffusion flux will not be considered. This reduces the material balance equation to the pseudo-homogeneous one-dimensional balance shown in Equation 5.80a. The conservation equations may be written for a single reaction occurring in a cylindrical tube (flow is in z-direction) as

Equations 5.80a to 5.80c:

$$\frac{\partial C_A}{\partial t} - \frac{\partial (u_S C_A)}{\partial z} = \rho_B r_A \qquad (5.80a)$$

and

$$\rho c_p \frac{\partial T}{\partial t} + u_S \rho_g c_p \frac{\partial T}{\partial z} = (-\Delta H)\rho_B r_A + Q_u \qquad (5.80b)$$

With the following initial conditions:

$$\left.\begin{array}{l} C_A = C_0 \\ T = T_0 \end{array}\right\} \text{at } z = 0 \qquad (5.80c)$$

In Equation 5.80a, C_A is the concentration of a reference component, A, r_A is the rate of reaction of component A, u_s is the superficial velocity, and ρ_B is the catalyst bulk density. For the heat balance Equation 5.80b, Q_u represents heat transfer from/to the system, $(-\Delta H)$ is the heat of reaction, ρ_g is the gas density, and c_p is the specific heat of the fluid.

The dynamic material balance for the external fluid phase can be written for the sulphur species, Equation 5.81:

$$\varepsilon_1 \frac{\partial C_s}{\partial t} - \frac{\partial}{dz}(D_{as} \frac{\partial C_s}{\partial z}) + u_1 \frac{\partial C_s}{\partial z} = -\rho_1^{-1} r_s \qquad (5.81)$$

In these equations, C_s is the concentration of sulphur in the bulk fluid, D_{as} is the axial mass dispersion coefficient of sulphur; z is the distance from the reactor inlet; ε_1 is the volume fraction occupied by the liquid in the bed, ρ_l is the fluid density; u_l is the superficial velocity of liquid fluid and r_{si} is the rate of sulphur

removal. The solution of the above equation requires the boundary conditions shown in Equations 5.82a and 5.82b:

$$C_s = S_{in} \text{ at } z=0 \qquad (5.82a)$$

and

$$\frac{\partial C_s}{\partial z} = 0 \quad \text{at } z=L \qquad (5.82b)$$

Note, in Equation 5.81, r_s represents the lumped parameter rate equation for the desulphurization reactions.

5.8.5 Solution Methodology

The Implicit Euler Method[47] is used to convert the material and energy balances into algebraic equations for solution in the Excel® portion of the model. HYSYS® uses this solution method as well, so both parts of the model are using the same equation solver format. A brief description of the Euler differential equation solution method is provided and taken from reference 47. The next step value Yn+1 is based on the previous value Yn and the derivative as shown in Equations 5.76 and 6.77.

$$Y_{n+1} = Y_n + \int_{t_n}^{t_{n+1}} f(Y)dt \qquad (5.83)$$

where,

$$\frac{dY}{dt} = f(Y) \qquad (5.84)$$

Ordinary differential Equations are often integrated using the Implicit Euler method[47]. The Implicit Euler method is simply an approximation of Yn+1 using rectangular integration[47]. Graphically, a line of slope zero and length h (the step

size) is extended from tn to tn+1 on an f(Y) vs. time plot. The area under the curve is approximated by a rectangle of length h and height $f_n=(Y_{n+1})$:

$$Y_{n+1} = Y_n + hf_{n+1}(Y_{n+1}) \qquad (5.85)$$

The method is implicit because information is required at time T_{n+1}. Integration parameters such as the integration time step can be specified in the Integrator view from the simulation menu in HYSYS®. The integration time step can be adjusted to increase the speed or stability of the model solution.

5.9 Complete Model

5.9.1 Nonlinear Regression

Statistical analysis can be used to fit unknown model parameters and to evaluate the uncertainty associated with the fitted model as well as to compare several candidate models[59]. One common approach is to use optimization theory to derive least-squares estimates for the model parameters. A commonly accepted method of determining the best fit is to calculate the values of the model parameters than minimize the sum of the squares of the errors, ε', Equation 5.86:

$$\min_{a_j} \varepsilon' = \sum_{i=1}^{N} e_i^2 = \sum_{i=1}^{N} (y_i - \hat{y}_i)^2 \qquad (5.86)$$

where a_j are the parameters to be estimated, N is the number of data points, y_i is the measurement and $\hat{y}_i$ is the corresponding model prediction.

If the model is linear with respect to the model parameters, then linear regression is used, otherwise, nonlinear regression rather than linear regression can be used. For example, suppose that a reaction rate expression of the form $r_A = kC_A^n$

is to be fit to experimental data. Here r_A is the reaction rate of component A, C_A is the reactant concentration, and k and n are model parameters. This model is linear with respect to rate constant k but is nonlinear with respect to reaction order n, which is also the case for model development in this study. Equation 5.87 presents the general form for a nonlinear model:

$$\hat{y} = f(x_1, x_2, ..., a_0, a_1, ...) \qquad (5.87)$$

where $\hat{y}$ is the empirical model output, the x_i are inputs, and a_j are the parameters to be estimated. In this case, the a_j are not linear multipliers of the input functions. These parameters are estimated by minimizing the sum of squares error equation, Equation 5.86.

The nonlinear regressions performed in this study will be carried out using the Excel Solver®. The Solver is an "add-in" and part of a suite of commands sometimes called "what-if" analysis tools. The Solver can be used to find an optimal value for a formula in one cell, called the target cell, on a worksheet. The Solver is attached to a group of cells that are related, either directly or indirectly, to the formula in the target cell. It adjusts the values in the specified changing cells, called the adjustable cells, to produce the result specified from the target cell formula. Constraints can be applied to restrict the values the Solver can use in the model, and these constraints can refer to other cells that affect the target cell formula.

The Solver will be used to minimize the sum of squares error for the model equations represented in the form shown in Equation 5.87. The sum of squares

error is determined in the target cell, whilst values of the parameters to be estimated are allocated in the adjustable cells.

5.9.2 Model Steps

As stated in section 5.1, both Excel® and HYSYS® have been used to develop the model. The following sixteen steps summarize the model operation:

SET UP

Step 1 - Input equipment parameters specific to the plant into HYSYS®
= reactor, heater, vessel , pump, valve dimensions

Step 2 - Input catalyst physical characteristics into the Excel® model

ITERATIVE

Step 3 - t=i, Input the process variables (crude flow, lab compositions) into Excel® and perform mass balance for unit. It within tolerance, go to

Step 4 Provide an initial estimate for the reactor outlet temperature

Step 5 - Calculate the catalyst deactivation in Excel®
- impact of metals in crude and coke generated

Step 6 - Calculate the output sulphur in Excel®

Step 7 - Calculate the hydrogen consumption in Excel®

Step 8 - Import H_2 consumption, sulphur in product into HYSYS® ®

Step 9 - HYSYS® takes process data (crude flows, lab composition) and output from Excel® in step 7 and calculates reactor output temperature

Step 10 - HYSYS® calculates and adjusts Hydrogen composition and flow in Recycle loop to meet heat and material balance

Step 11 - Export the reactor temperature and hydrogen recycle values (flow, composition) back to Excel®

Step 12 - Compare HYSYS® outlet temperature to that estimated in step 4.

Step 13 - Compare hydrogen make-up purity between HYSYS® and Excel®

Step 14 - Return to step 4 if error tolerances for hydrogen consumption and temperature are not met. Otherwise,

Step 15 - Record time, and all process variables for t = i

Step 16 - Go to step 3 for t= i+1 until the entire run is completed

Figure 5.12, on page 143 shows the model process (16 steps from above) in algorithm form.

Figure 5.13 on page 144 shows the input and output sections of the Excel® model portion of the VGO hydrotreater model. In the output section of this section of the spreadsheet, the acceptability of closure between the Excel® and HYSYS® output results for each time interval is determined. If the error tolerance (as noted in Figure 5.13) is not met, then new estimates for temperature and hydrogen consumption are provided and another iteration is made.

Figure 5.14 on page 145 illustrates the hydrogen recycle loop used in the Excel® portion of the model, while Figure 5.15 on page 145 shows the hydrotreater unit HYSYS® model. Figure 5.15 is based on the generic hydrotreater HYSYS® simulation developed by Gerald Kaes[60]. A cascade control loop for the hydrogen flow is included to represent the actual VGO hydrotreater operation. A hydrogen tracking function is included in the simulation and is fed back to Excel® for iteration closure purposes.

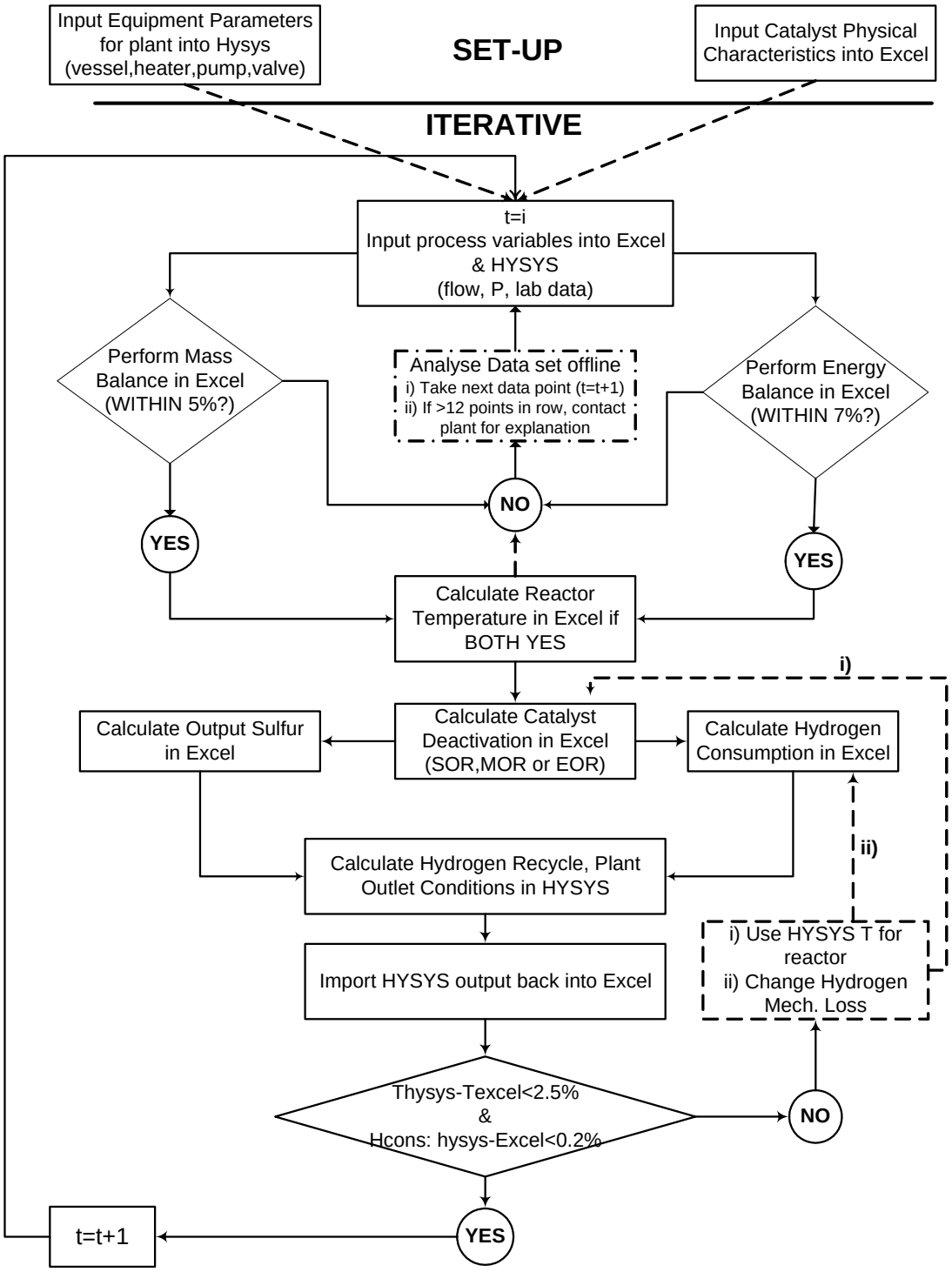

Figure 5.12 – Algorithm shows the process within the model to calculate the required sulfur product, temperature and hdyrogen consumption. The Figure shows data is input into the model, calculated in both Excel® and HYSYS® and how info is transferred between software packages. A single time step is show in this algorithm with the provision for calling the next set of data at the next data point.

MODEL INPUT							
						Iteration #	6
ASTM Distillation, F			API Gravity		29		
LV%	D-1160		Aniline Point, F		50		
0	255		Elem. Assay, Wt%				
5	325		Sulfur, Wt%		1.5		
10	375		Nitrogen, ppm		50		
30	475		PCI, ppm		55		
50	500		Asphaltenes, ppm		70		
70	550		Molecular Weight		190.092	Calculated	
90	600		Metals, ppm		0.1		
95	650		Cracked Stock, LV%		50		
100	675		Bromine Number		20		
WBP	2650						
			Catalyst Information				
Density	54		Size	0.1		Area	155
Volume	6210			H2S Scrubbing (Yes/No)			YES
OUTPUT -FROM MODEL							
			KINETIC CALCULATIONS			TEOR Gue	795
Activity Advantage		379.4795	F	TSOR	655		
Fouling Factor		1		Ti	725	<- latest guess	
Eff. Factor		0.510188		FR Init	0.00111		
Metals:							
Loading, Wt%/Yr		% Interstitial		°F/Wt% Metals		Fouling Rate, °F/Hr	
0.10739		50		20		0.00012	

OUTPUT -TRANSFER TO EXCEL							
			PROCESS CONDITIONS				
MBPOD	32		pH2	800		Sp	0.005
LHSV	1.2058						
CLOSURE BETWEEN HYSYS AND EXCEL							
			HYDROGEN CONSUMPTION				
	Export	From hysys	New Export				
Sulfur	163.782	163.5	163.5				
Nitrogen	2.08673	2.01	2.01				
Olefins	146.071	146.2	146.2				
Cracking	25	24.6	24.6				
Aromatics	92.2106	92.11	92.11				
Losses	37.6	37.6	37.6				
Total	466.75	466.02	466.02				
% DIFFERENCE		0.156413	If > 0.2%, change H2 chem and mech loss in hysys				
			if<0.2%, HYSYS value becomes new value for export				
			REACTOR OUTLET TEMPERATURE				
	Export	From hysys	New Guess				
Temp oF	725	700	708.5	<-- 66.7% of error added to hysys value			
% DIFFERENCE		-3.57143	if> 2.5% provide new guess and go to next iteration				
			if<2.5%, HYSYS value is used for T guess-stop iteration				

Figure 5.13– Input and Output Sections in Excel® Portion of Model (Lab compositions not shown. All the pertinent input variables are shown along with the output variables, including results from the tolerance check for temperature (<2.5% between values) and H_2 consumption (<0.2% between values)

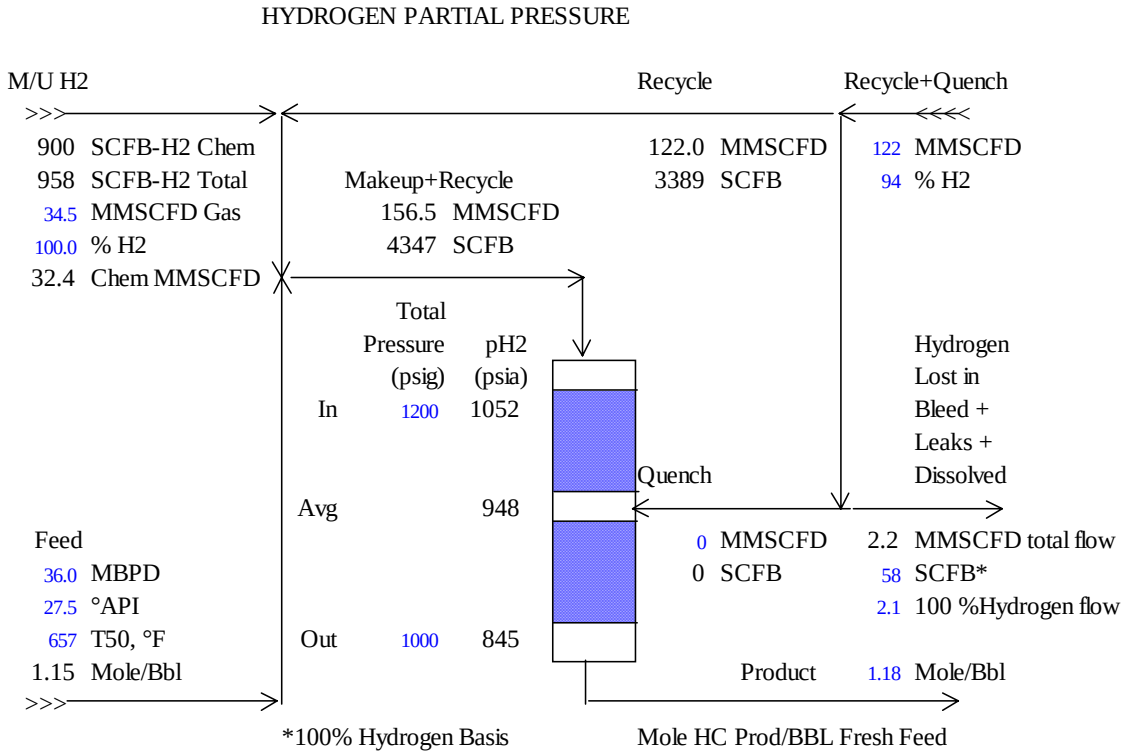

Figure 5.14 - Hydrogen Recycle Loop as configured in Excel®

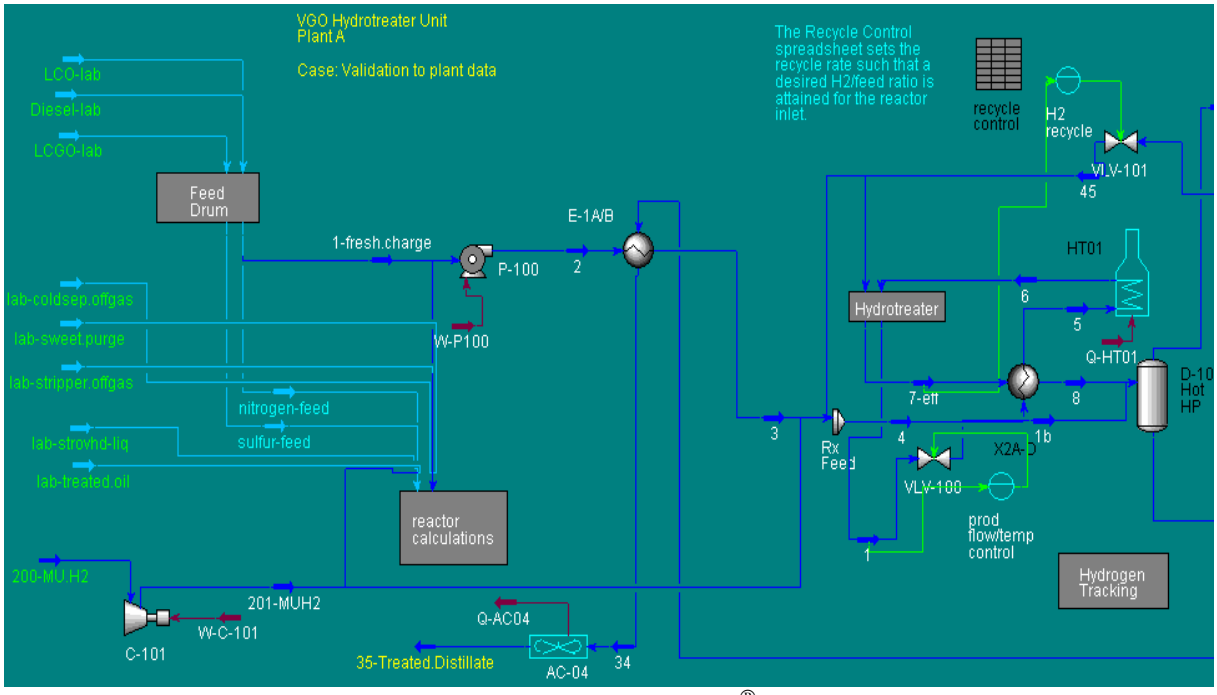

Figure 5.15 – Dynamic Simulation Set-up in HYSYS®

Figure 5.16 shows the composition input used for the HYSYS® portion of the model. Various labs provided a breakdown of components for each representative crude sample. This distribution analysis was used to breakdown the lumped sulphur lab sample at each time interval. Since HYSYS® provides a means to enter a separate sulphur species, the disposition of the unconverted sulphur species was tracked in HYSYS®. As noted for the lumped model approach, all sulphur compounds are treated as DBT to obtain the outlet sulphur, and all crude components are defined based on boiling point.

Composition	Crude in	H2 in	Composition	Crude in	H2 in
NBP 289	8.76E-07		METHANE	3.46E-07	0.1131
NBP 313	1.13E-06		ETHANE	1.09E-06	0.0025
NBP 338	1.83E-06		PROPANE	1.84E-06	0.0038
NBP 362	3.40E-06		IBUTANE	3.06E-06	0.001
NBP 386	6.41E-06		BUTANE	2.35E-06	0.0006
NBP 410	1.20E-05		IPENTANE	4.03E-06	0.0004
NBP 434	2.25E-05		PENTANE	3.13E-06	0.0001
NBP 458	4.46E-05		HEXANE	8.12E-06	0.0003
NBP 483	8.60E-05		H2O	4.26E-05	
NBP 509	0.000167		H2	0	0.8519
NBP 534	0.000319		THIOPHENE	0.004	
NBP 559	0.000618		BENZOTHIOPHENE	0.004	
NBP 587	0.001563		DIBENZOTHIOPHENE	0.004	
NBP 617	0.003812		DIPHENYLBENZYLTHIOPHENE	0.004	
NBP 647	0.010699		CARBONYL SULFIDE	0.001	
NBP 680	0.038492		DIMETHYL SULFIDE	0.001	
NBP 716	0.082755		DIETHYL SULFIDE	0.001	
NBP 752	0.110176		METHYLETHYL SULFIDE	0.001	
NBP 788	0.119854		DIMETHYL DISULFIDE	0.001	
NBP 824	0.121974		DIETHYL DISULFIDE	0.001	
NBP 860	0.120388		ETHYL MERCAPTAN	0.001	
NBP 896	0.115399		METHYL MERCAPTAN	0.001	
NBP 932	0.104449		BENZYL MERCAPTAN	0.001	
NBP 968	0.083461		H2S	0	0.0287
NBP 1003	0.052968		NITROGEN		0.0072
NBP 1041	0.025187		AMMONIA		
NBP 1080	0.006425		ASHPHALTENES		
NBP 1124	0.00099		AIR	9.15E-07	
NBP 1174	5.68E-05		NBP 119	4.41E-09	
NBP 1224	2.66E-06		NBP 140	1.42E-08	
NBP 1275	1.27E-07		NBP 167	2.40E-08	
NBP 1325	6.73E-09		NBP 192	3.83E-08	
NBP 1373	4.57E-10		NBP 216	8.19E-08	
NBP 1413	1.55E-11		NBP 240	1.82E-07	
NBP 1588	7.26E-16		NBP 265	4.50E-07	

Figure 5.16 – Compositional Input used in HYSYS®

5. 10 Summary

In this chapter a first-of-a-kind dynamical oriented lumped industrial based VGO hydrotreater model was developed. Steady state correlations from a catalyst vendor were used as a basis and then modified and improved for the middle of run (MOR) portion for the catalyst deactivation model. New SOR and EOR factors were developed to address the deactivation phenomena in these operating zones.

Improvement to and conversion of the catalyst vendor correlations (steady state catalyst deactivation and H_2 consumption) and the development of new correlations was based on the compilation of proprietary industrially VGO hydrotreater data (described in chapter 4). The developed model also incorporates key variables (similar to the Thiele Modulus) to provide an accurate representation for industrial conditions. A new algorithm was developed to account for the different zones in the catalyst activity profile.

Again the model is lumped to match data available from industrial operations and necessarily uses a mix of industrial correlations, kinetic reaction rate theory, and pilot plant findings. It uses plant data (to correlate parameter in the model) that contains changes in operating conditions in response to disturbances in operation. A unique feature is the incorporation of a changing reaction rate, wetting efficiency, catalyst deactivation for all three catalyst deactiviation zones. By including all key variables and being dynamic the model can provide representative values for plant performance at the plant site, namely WABT, hydrogen consumption and outlet sulphur

composition. Finally the model has been built using familiar software (Excel® and HYSYS®) for easy translation into existing operations and acceptance by users.

Chapter 6 validates the model developed in this chapter by using the operational data presented in Chapter 4 . Chapter 7 then uses the validated model in various scenarios to determine what steps can be taken to improve increased reactor run length with increased or at least maintaining the crude production rate.

Chapter 6: Results and Discussion

In this chapter, the model developed in Chapter 5 is validated using the acquired plant data presented in chapter 4, and the results of this evaluation are presented. The statistical value termed R^2 is used to illustrate how closely the developed model matched the acquired operating data and is the proportion of variability in a data set that is accounted for by the statistical model[63]. In this definition, the term "variability" means variance or, equivalently, sum of squared errors. More, there are several common and equivalent expressions for R^2, with the most common version seen in statistics texts is based on an analysis of variance decomposition as presented in Equations 6.1 and 6.2.

$$R^2 = \frac{SS_R}{SS_T} = 1 - \frac{SS_E}{SS_T}. \tag{6.1}$$

SST in the above definition is given by Equation 6.2.

$$SS_T = \sum_i (y_i - \bar{y})^2, SS_R = \sum_i (\hat{y}_i - \bar{y})^2, SS_E = \sum_i (y_i - \hat{y}_i)^2. \tag{6.2}$$

That is, SS_T is the total sum of squares, SS_R is the regression sum of squares, and SS_E is the sum of squared errors. More simply, R^2 is often interpreted as the proportion of response variation "explained" by the regressors in the model. Thus, $R^2 = 1$ indicates that the fitted model explains all variability in *y*, while $R^2 = 0$ indicates no 'linear' relationship between the response variable and regressors. An interior value such as $R^2 = 0.7$ may be interpreted as follows: "Approximately seventy percent of the variation in the response variable can be explained by the explanatory variable. The remaining thirty percent can be explained by unknown, lurking variables or inherent variability"[63] . When dealing with industrial plant

data, with inherent field measurement inaccuracies, an R^2 of over 0.85 should be considered as an extremely good match of the plant data by the model[3,7,48,61,62]. However, it should be appreciated that R^2 does NOT tell whether:

- the independent variables are a true cause of the changes in the dependent variable
- omitted variable bias exists
- the correct regression was used; or
- the most appropriate set of independent variables has been chosen

R^2 does provide an indication of how well the simulation matches the plant data. Appendix D contains the equations and data for the R^2 calculations reported in this chapter.

6.1 Parameter Sensitivity Analysis

For the outlet sulphur composition from the VGO hydrotreater, Equation 5.25a, the parameters b,p,g were tested with the operating data from all 14 plants to determine a feasible way to represent these parameters for each VGO hydrotreater. Table 6.1, on page 151, shows the final parameter values used for the fourteen plants from which significant data were obtained. The parameters were evaluated separately with the data sets and then together to check for cross-correlation between the parameters. The parameters were adjusted during the simulation run for each plant.

$$S_{pi} = \left\{ \left(\frac{1}{S_{p(i-1)}^{2\eta_{ei}-1}} - \frac{1}{S_{f(i-1)}^{2\eta_{ei}-1}} \right) \frac{LHSV_{i-1}}{LHSV_i} e^{\left(\frac{b}{T_{i-1}} - \frac{b}{T_i}\right)} \left(\frac{P_{i-1}}{P_i} \right)^p \left(\frac{G_{i-1}}{G_i} \right)^g + \frac{1}{S_{fi}^{2\eta_{ei}-1}} \right\}^{\frac{1}{1-2\eta_{ei}}} \quad (5.25a)$$

where

b = Temperature Effect Factor (exponent determined from operating data)

g = H_2/Oil Ratio Effect Factor (exponent determined from operating data)

p = Pressure Effect Factor (exponent determined from operating data)

Plants A through F have provided approval to publish all operating data and results, while the remaining eight plants noted in table 6.1 (R through Z) have agreed to allow their data to be used in the model but not published. For the parameters developed for Equation 5.25a, plants R through Z permitted the publishing of the parameter values in Table 6.1. The addition of the eight units increased the number of data points used to support the statistical significance of equations developments for the parameters.

Table 6.1 – Average calculated parameters for sulphur product composition

Plant	Average **p**	Average **g**	Average **b** (oF)	APIsor	Viscosity (SSU @ 100oF)
A	0.46	0.50	21500	30.1	58
B	0.63	0.54	23700	27.3	478
C	0.51	0.64	23350	19.5	453
D	0.89	0.53	23100	27	243
E	0.38	0.47	21700	30.8	46
F	0.39	0.55	24700	25.8	1525
R	0.41	0.51	24400	29.2	1310
S	0.59	0.63	23270	20	430
T	0.36	0.53	23000	26.7	300
U	0.53	0.59	24000	23	1000
W	0.44	0.56	24000	25	900
X	0.38	0.60	24600	22.3	1650
Y	0.37	0.52	23400	28	500
Z	0.78	0.63	24600	21	1568

Note for the pressure factor, p, the value ranged from 0.36 to 0.89 for the 14 plants analyzed. Equation 6.3 provides a calculation to determine parameter p,

based on hydrogen partial pressure (psig) and wetting efficiency. Both these variables are crucial in converting sulfur in the hydrotreater, and thus are incorporated in the calculation for parameter p.

$$p = (\frac{P_{H_2}}{4500})e^{\eta_e} \quad (6.3)$$

Equation 6.3 was based on a steady state catalyst vendor correlation[3] for this parameter ($p= P_{H_2}/2200$) in VGO hydrotreater service. The decision to keep partial pressure of hydrogen as the primary variable for this parameter was based on literature stating that hydrogen partial pressure is a significant contributor to the reaction performance. The wetting efficiency factor was included since the overall reaction relies on having reactants contacting the catalyst for the reaction to proceed. A reduction in contact will reduce the impact of the any hydrogen partial pressure benefits. The relationship between wetting efficiency and partial pressure are included in equation 6.3 as noted. The wetting efficiency is included in the equation as a raised exponent to an exponential function, to reflect the situation that as wetting efficiency decreases, the impact of the given hydrogen partial pressure reduces resulting in a higher value for parameter p. Parameter p is an exponent on a pressure ratio term, so as p increases, the outlet sulfur increases as expected. The wetting efficiency exponential function added to the p parameter was correlated against the plant data evaluated. Figure 6.1, on page 153, shows an example comparison between the wetting efficiency exponential and the wetting efficiency multiplier for parameter p. The range of parameter p for the exponential multiplier fits better with the operating data. The multiplier is linear and the value can generate sulfur

product values well outside what is shown in the lab results. The exponential function keeps the p parameter in a range that allows a good fit with the sulfur product for all the plant data sets.

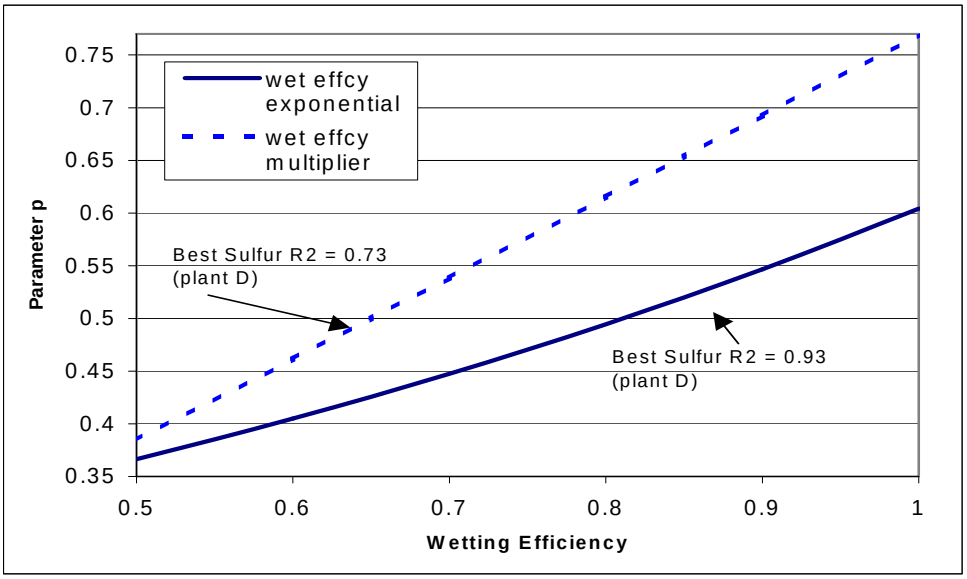

Figure 6.1 – Comparison between the wetting efficiency factor used as a multiplier and an exponent for use in developing parameter p. The multiplier, as expected creates a linear relationship between the wetting efficiency and parameter p, with an R^2 of 0.73 when the model product sulfur is compared to the plant data. Any value of p, above 0.65 and below 0.3 results in sulfur product from the model well outside the plant data. On the other hand, the exponential use of the wetting efficiency provides a parameter p within an acceptable range (0.35-0.63) providing an R^2 of 0.93 for the statistical evaluation between model and plant sulfur product.

For the temperature factor b, there appears to be a relationship to the crude's viscosity and the viscosity for each crude at start of run is included in Table 6.1. Figure 6.2, on page 154, shows the relationship between viscosity and the parameter b. A logarithmic relationship, with a R^2 of 0.978 for the 14 plant data set (R^2 of 0.980) for the six plants published in this study), has been fit, equation 6.4

$$b = 866.24Ln(\mu) + 18162 \quad (6.4)$$

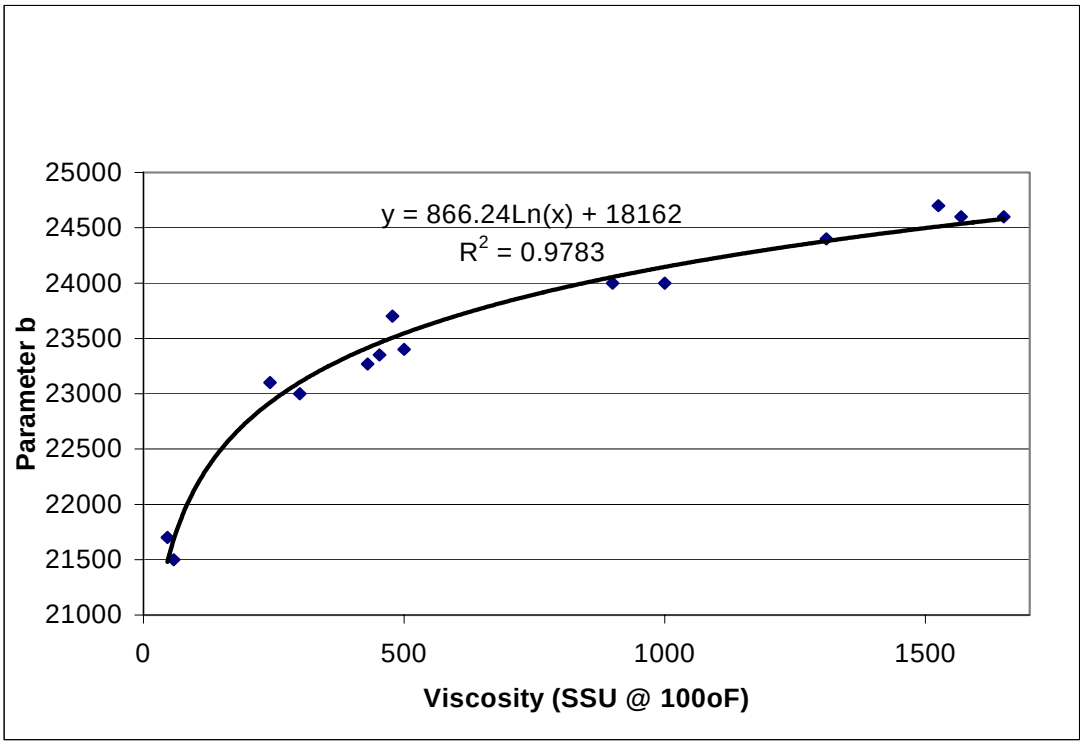

Figure 6.2 Parameter b (Temperature Effect vs. Viscosity). A logarithmic relationship between viscosity and parameter b can be created when evaluating the data from 14 industrial plants. A wide range of viscosities were found in the data set (~100 to over 1550 SSU @ 100^{o}F). The relationship provides an R^2 of 0.9783 giving confidence that knowing a VGO hydrotreaters feed viscosity, a reasonable parameter b in the sulfur product equation can be determined. The range of parameter b is 21500 to approximately 24600 which represents a 12.6% change from the low viscosity to high viscosity in the data base.

Since this is a lumped model, and viscosity measurements are not part of the daily analysis for the six plants, the b value cannot be adjusted daily based on viscosity. However, there are relationships for viscosity that are a function of regularly measured plant data (API (via Specific gravity of crude)), and temperature). Since viscosity is a function of temperature, it is not surprising there is a relationship between the b parameter and viscosity. Equation 6.5,

Glaso's correlation[12] can be used to update parameter b as the API and temperature changes during hydrotreater operation.

$$\mu = 3.141 * 10^{10} (T - 460)^{-3.444} (\log_{10}(API))^{a} \quad (6.5)$$

where $$a = 10.313(\log_{10}(T - 460)) - 36.477 \quad (6.6)$$

and T is provided in degrees Rankine. Viscosity does not change appreciably in the range of temperature operation for the VGO hydrotreaters evaluated (605-720oF), so the Glaus correlation was sufficient to capture any small changes in viscosity for SOR to EOR. The Glaus correlation was not evaluated for accuracy or against other correlations since it used readily available variables and the model was insensitive to the apparent small change in viscosity from SOR to EOR. However, the absolute viscosity number at SOR was in fact important in setting the value of parameter b. Any changes in viscosity and thus the parameter b during the run, were too small (< 0.5% from SOR to EOR) to be concerned with (difference is an order of magnitude less than the accuracy of the viscosity and temperature measurements)[3].

As shown in Figure 6.3, on page 156, parameter g, hydrogen-to-oil ratio, appears to be linearly related to the API of the crude, i.e. the more dense the crude, the larger the required hydrogen to oil ratio.

Typically, more hydrogen is needed for hydrotreating heavier crude[5,7,8], since the types of sulphur molecules are embedded in the heavier crude molecules and more hydrogen is required. As a result, the relationship between hydrogen to oil ratio and API is appropriate.

The linear relationship between parameter g and the API gravity of the crude feed can be described by equation 6.7 (R^2 of 0.9854).

$$g = -0.0141API + 0.9146 \quad (6.7)$$

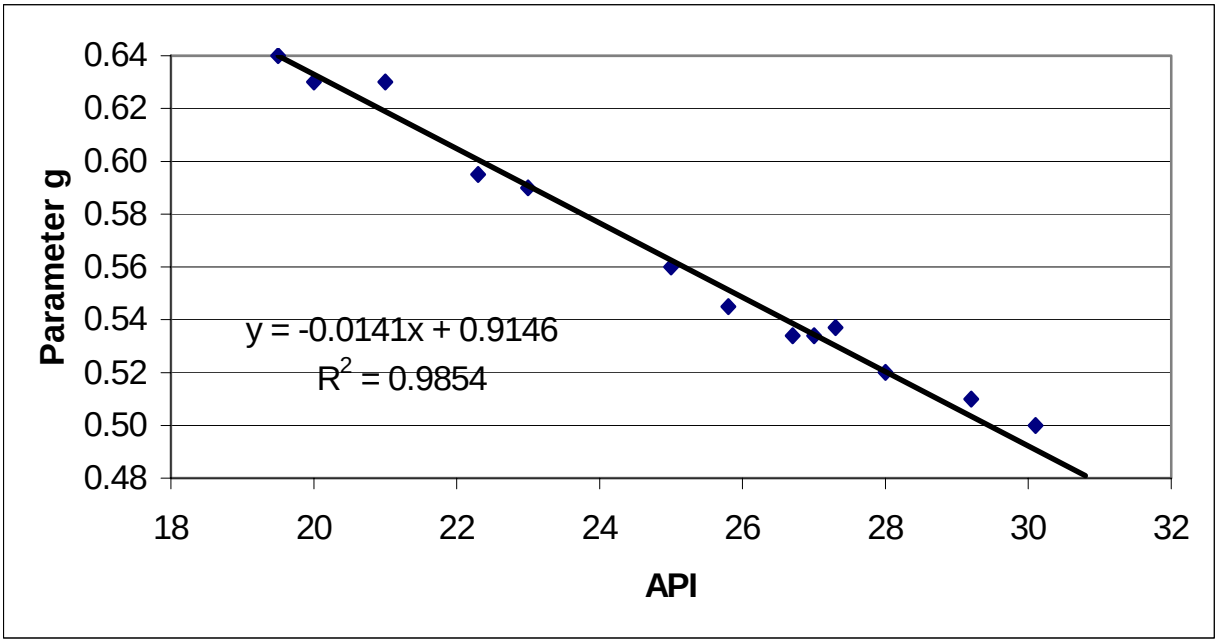

Figure 6.3 Parameter g (H_2:Oil Ratio) vs API. The 14 data sets for the VGO hydrotreaters in this research were used to correlate a linear relationship between API and parameter g (R^2 of 0.9854). As the API increases (density of crude decreases) and the parameter g decreases (less need for hydrogen to convert sulfur in "lighter" crudes[9]).

NOTE, this linear relation (equation 6.7) does not apply for ULS (ultra low sulfur) applications. The sulphur product specification for the VGO hydrotreaters studied was in the range of 300 to 500 wppm, well above the ULS specifications of less than 10 wppm.

Other variables were tested with parameter g but no correlation was found. Also, no other relationships between API and this parameter g (hydrogen to oil ratio) were uncovered in literature for evaluation in this research.

6.2 Model Development Progression

The model was developed and improved in nine distinct steps (versions). The final version, nine, results are used in the model validation and are presented in this chapter. The first 3 versions were primarily performed in the steady state mode, while the remaining versions were tested in the dynamic mode. A summary of the key development features in each version is noted below:

Version 1 – Initial MOR Catalyst deactivation model

Version 2 – EOR Catalyst deactivation factor – metals impact

Version 3 – SOR Catalyst deactivation – coke impact

-Obtain basic shape of SOR-EOR temp. curve
-R-squared = 0.75 for plant D (for all 6 plants = 0.65-0.75)

Version 4 – Reaction Kinetics

- Add impact of Nf, Np, Sf, Sp, space velocity, catalyst properties

Version 5 – Optimize specific parameter - temperature

Version 6 - Optimize specific parameter – H2 PP

Version 7 - Optimize specific parameter – H2/oil ratio

Version 8 – Optimize all process, reaction parameters simultaneously

-R^2 WABT= 0.86 for plant D (0.81-0.86 for 6 operating units.)

Version 9 – Include wetting efficiency, SOR/EOR catalyst deactivation enhancements

- Re-optimize all parameters
- R^2 WABT= 0.93 for Plant D (0.91-0.935 for 6 operating units)

Figures 6.4 shows versions 3 and 9 for plant D illustrating the progression of the model match to the operating data. Note, version 3 is the type of model that is

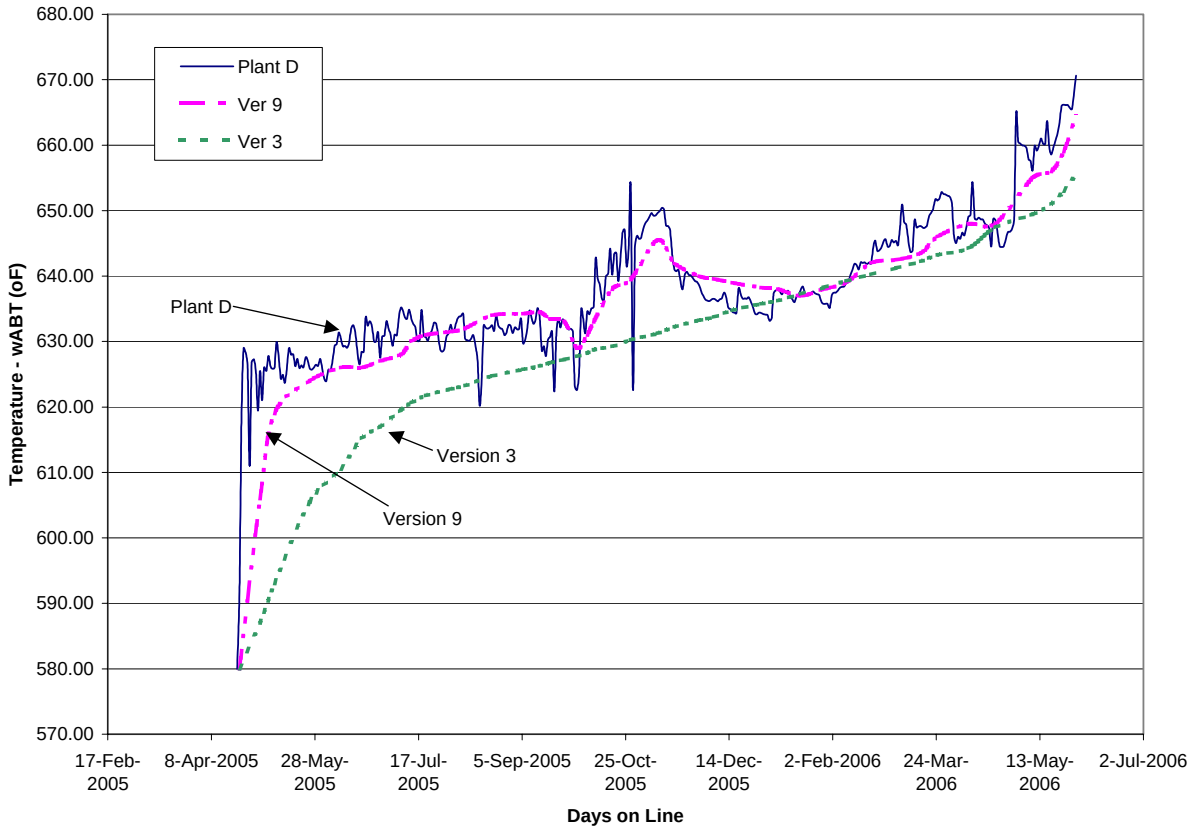

Figure 6.4 – Versions 3 and 9- Plant D, WABT vs. Time. A comparison between the final model (version 9), and a preliminary version (3) to the plant D reactor temperature from SOR to EOR. Version 3 provides the classical S-shaped trend for the temperature profile, while version 9 provides a closer fit to the plant data and a responsiveness to the major disturbances, thus increasing the accuracy of the model developed. Version 9 R^2 for WABT was 0.935, while version 3 provides an R^2 of 0.75.

typically provided by consultants and researchers for industrial operations, namely a steady state model used in a quasi-dynamic mode[5,9,27,34,35]. The three catalyst deactivation zones (SOR,MOR,EOR) are present, following the general trend of the catalyst deactivation. However, there are no response capabilities to

actual changes in operation or other disturbances. Between versions three (R^2 = 0.75) and eight (R^2=0.86) a successful dynamic component was added such that an improved match to actual operating data was made. Version three can be used to make a "rough" estimate of catalyst life but it is very limited in its ability to capture the impact of actual disturbances and changes in operating variables. Further tuning of the model (Version nine) provided the best match with an R^2 of 0.91 to 0.935 for WABT when compared to Version three at an R^2 of 0.65-0.75.

6.3 Model Validation – Specific Disturbances

For a model to match the plant data over an entire run length of an industrial hydrotreater (one to four years)[3], the model must, first, be able to accurately represent the impact of short-term disturbances. Once the short-term disturbances are matched, then long term issues such as catalyst deactivation and process changes can be added to improve the overall model response. Two of the three representative disturbances from Plant D, shown back in figure 4.5, page 58, were chosen to illustrate how the model responded over the short term. Disturbances one and two are feed sulphur spikes (only one is illustrated in this chapter), while disturbance three is a crude reduction due to increased catalyst deactivation. Figures 6.5 (page 160) and 6.6 (page 162) show how the model matches each of these two types of disturbances.

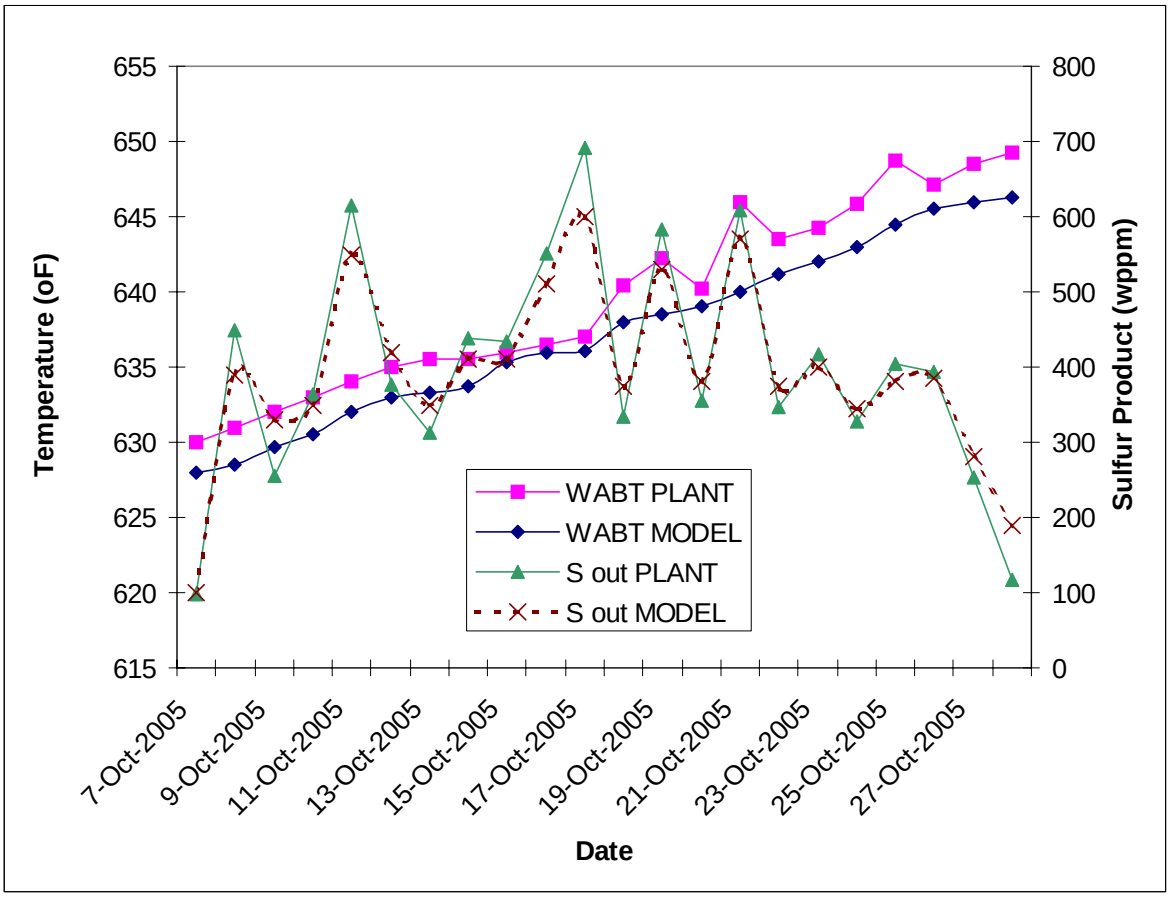

Figure 6.5 – Plant D, Local Disturbance 1, Feed Sulphur increase, version 9 . A sulfur spike of 2.0% occurred, starting on October 7th, 2005. The WABT was increased to increase the catalyst activity. Minimal changes to crude and hydrogen were witnessed, so the responsiveness of the model to a change in feed sulfur composition was evaluated. This disturbance was modeled to determine how well the model matched the two outputs from the model: WABT and product sulfur. The WABT R^2 was 0.94 and the sulfur product was 0.95.

Figure 6.5 shows data from October 7th through October 30th, 2005, where the sulphur in the feed increased from a typical 2.2% to a high of 4.2%. The VGO Hydrotreater operation maintained the outlet sulphur specification by increasing the reactor temperature from 630 to 645°F. The crude flow rate, another variable that operations can use to control sulphur product specification was relatively

constant during this time period. The crude flow had an average flow rate of 15355 BPD with a range of 15188 to 15275 BPD (1.1% and 0.5% difference from average, respectively). The hydrogen to oil ratio was increased from 4432 to 4495 scf/bbl, in an apparent attempt to mitigate catalyst deactivation. Using the plant data provided, the model provided a very good match to the reactor temperature (R^2 = 0.94) and the outlet sulphur product (R^2=0.95).

The above disturbance and operations response reduced the calculated life of the catalyst by 7.5%, which would translate into a run length of only 306 days (0.84 of a year). This sulphur excursion had serious implications on the hydrotreater run length, that is not well understood by operations. Reducing the crude flow rate during this time period or further increasing the hydrogen partial pressure may have helped the long term operation of this VGO hydrotreater.

Figure 6.6, on page 162, shows the impact of a continuous crude flow reduction (disturbance) from 10945 BPD on April 22, 2006 to 8619 BPD on May 6, 2006. The WABT went up from 648 to 660^{o}F, while the outlet sulphur specification was maintained during the 15 days of crude flow rate reduction with the outlet sulphur dropping from approximately 275 wppm to just under 50 wppm. Note, the model WABT R^2 is 0.97, and outlet sulphur R^2 is 0.95; both are very good. Inlet sulphur remained relatively constant and the hydrogen to oil ratio was reduced to match the crude flow rate. The plant data (Plant D) show that the hydrogen partial pressure (to save hydrogen operating cost) was used to offset the benefit

of reducing catalyst deactivation instead of allowing the temperature to remain constant. Catalyst life continued to decrease at a constant rate.

Figure 6.6 does show that the developed model is very effective in matching process disturbances over a short period of time. The bigger challenge was using the model from the beginning of run and matching the operation over an entire run with multiple disturbances and operational changes that impact catalyst deactivation.

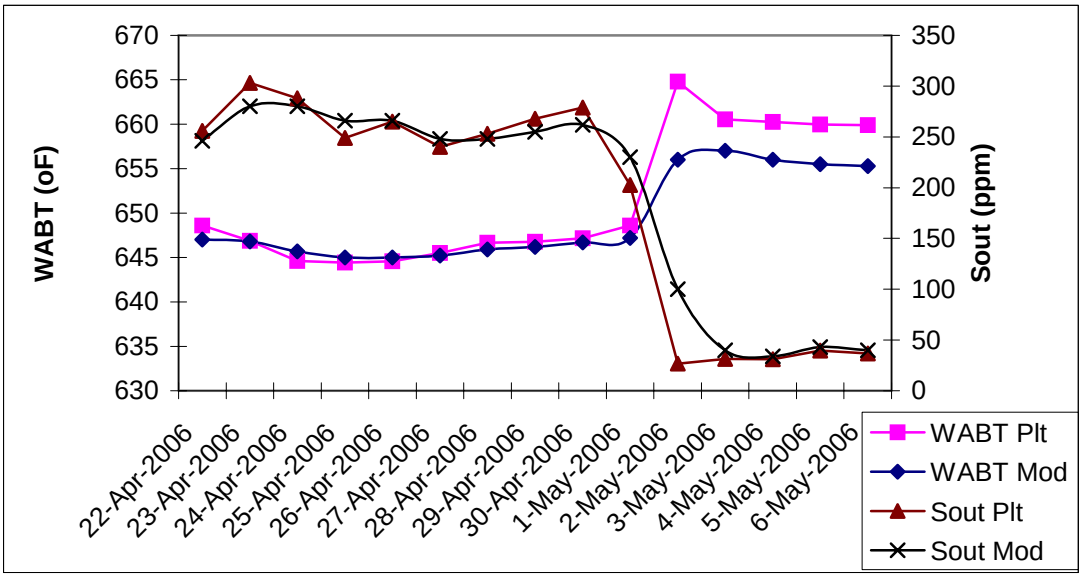

Figure 6.6 – Plant D, Local Disturbance 3, Crude Feed Decrease, version 9 Crude feed rate to Plant D was reduced from 10945 to 8619 BPD. The model was compared to the plant WABT and Sulfur output; R2 respectively of 0.97 and 0.95. As the WABT went up, the sulfur product went down. Model matched the trend and the actual data points well for this local “disturbance” to the plant D VGO hydrotreater.

6.4 Plant Results – Entire Run Length

The model output provides the reactor temperature (WABT = weighted average bed temperature) and sulphur outlet product, both variables that are constantly measured by industrial operations. The sulphur in the product is the primary

specification for the VGO hydrotreater, while the reactor temperature is directly related to the catalyst activity (as catalyst activity goes down, reactor temperature goes up).

6.4.1 Plant D Results

Plant D operated its VGO hydrotreater for 1 year and 4.5 months, well below the desired run length of four years. Figure 4.5, on page 58 showed the numerous major and minor disturbances that severely reduced the ability of the VGO hydrotreater to meet the crude production targets over the anticipated run length of four years. The results of the model predictions, figure 6.7, on page 164, for the product sulphur concentration and figure 6.8 (page 165) for the WABT, with an R^2 of 0.93 for the product sulphur and slightly better (R^2 =0.957) for product sulphur in the 20 to 130 ppm range. Above 130 ppm, the model shows a R^2 of 0.895, at times struggling to fully match the “spikes” in product sulphur plant data. Also, for the very low product sulphur values of less than 20 ppm, the model R^2 of 0.85 was acceptable but not outstanding. This trend in variation in R^2 values in the model product sulphur prediction was the same for all the plants analyzed. This variation in R^2 can be attributed to the accuracy of lab measurements and quality of the lab samples.

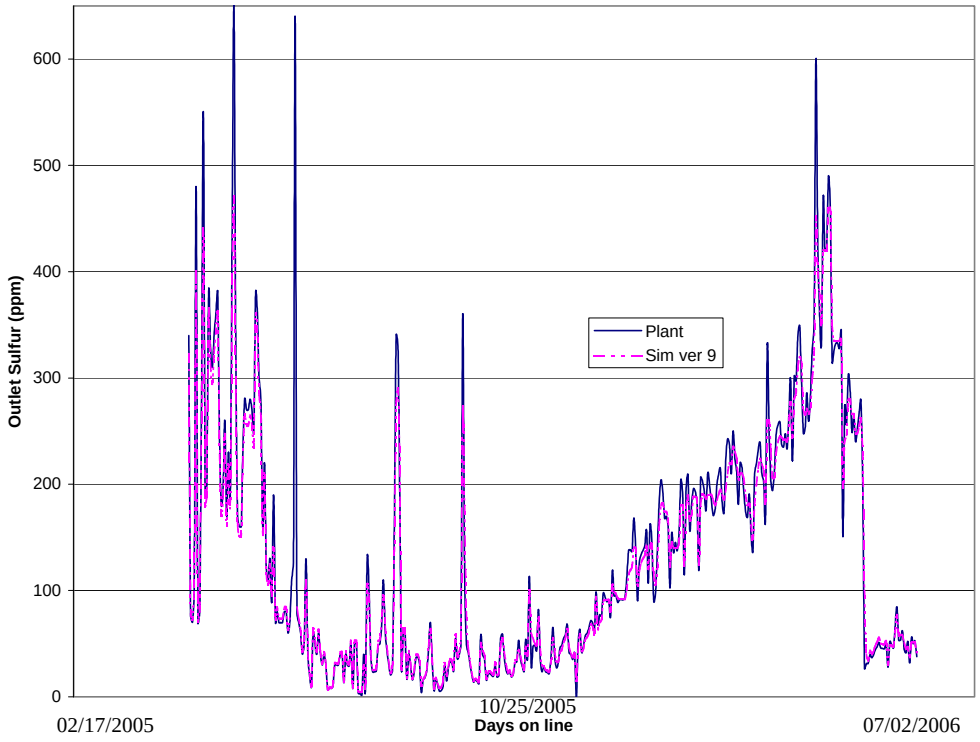

Figure 6.7 – Plant D – Product Sulphur Composition, Model vs. Plant Data. Version 9 Sulfur product values are compared to the plant sulfur product laboratory values. The overall R^2 calculated was 0.93, with the model capturing all the trends in the plant data. Between 20 and 130 ppm, the model matched the model better with an R^2 of 0.957. For less than 20 ppm, the R^2 was 0.85, while above 130 ppm, the R^2 was 0.895. The model was not as effective in capturing the spikes above 130 and below 20 ppm. The lumped approach in the model and the inaccuracy in the lab samples at the extreme points are likely contributors to the increased deviation by the model outside the 20-130 ppm range.

Figure 6.8 shows how the model WABT predictions compared to the Plant D data. The R^2 of 0.927 would indicate a very good model prediction. There are dates (time periods) during the run where the model predictions does not match the plant data. The data anomaly around March 24, 2006, does provide such an example. The plant data WABT trends up 5-7^{o}F and the model does not respond accordingly. None of the key process variables tend to indicate a direct reason

for the discrepancy (i.e. changing crude flows, sulphur inlet concentration, hydrogen purity or flow). Note, just prior to, and just after this date two large disturbances are noted and accurately tracked by the model. A few explanations can be considered, such as the catalyst deactivation had more of a long- term impact from the previous sulphur inlet disturbance than what was considered in the model or the operators raised the WABT as regular practice or to increase activity in anticipation of a disturbance.

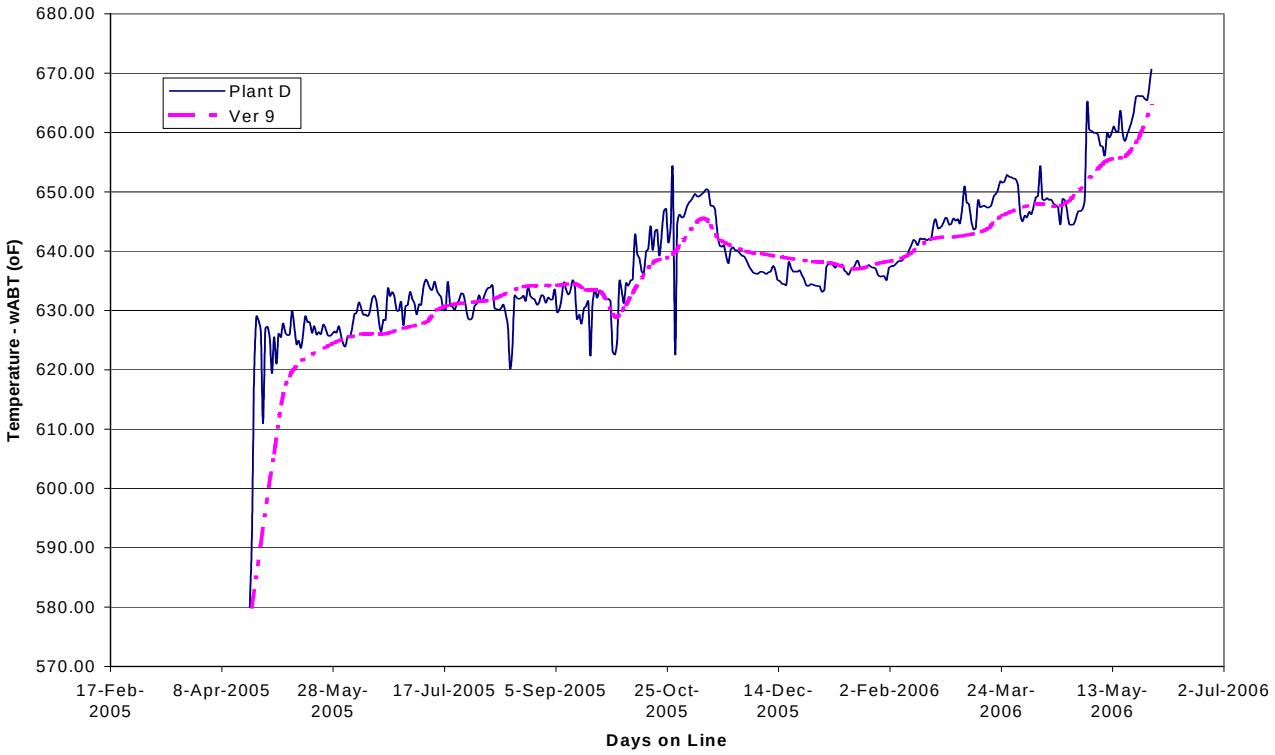

Figure 6.8 – Plant D – WABT, Model vs. Plant Data. Version 9 of the model is used to compare the values of WABT to the Plant D data. The WABT comparison has an R^2 of 0.927.

However, the model did accurately predict the temperature rise at the time of the disturbances. Discussion with the operator did not reveal anything specific regarding the events around March 24, 2006. Possibly, some human operating

factor may have been the result of a deviation from the normal temperature response. Or one could simply attribute this excursion to normal plant data quality. Considering this plant had the most significant disturbances of any studied, with such an uncharacteristically short run time, having a model that can get an R^2>0.9 is considered a very satisfactory model match.

6.4.2 Plant E Results

Plant E operated for three years as intended. Figure 6.9, on page 167, presents the plant E data and model predictions (R^2 of 0.95) for the product sulphur composition. Figure 6.10 (page 167) shows the WABT profile for the model predictions and plant E data (R^2 of 0.935).

The plant E temperature profile shows a more consistent rise when compared to the three distinct zones shown for plant D in Figure 6.8. "Adjustments" in temperature performed by operations (examples, February 23, 2003 and June 10, 2003) are highlighted. These "adjustments" are confirmed by the lack of supporting plant data/disturbances to support the changes, and corroborated by plant engineers during interviews[3]. These situations cannot be reflected in the model and thus will create an obvious reduction in the R^2 for the model. However, for this temperature profile, the R^2 for the model WABT was still a very acceptable 0.935.

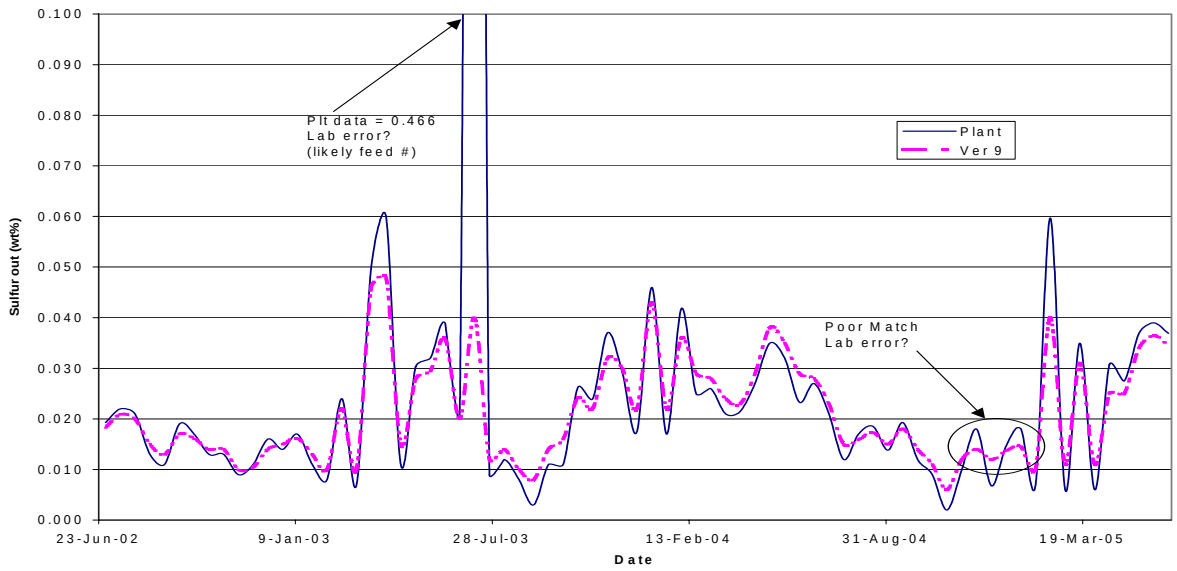

Figure 6.9- Plant E – Product Sulphur Composition, Model vs. Plant Data
Version 9 Sulfur product values are compared to the plant sulfur product laboratory values. The overall R^2 calculated was 0.95, with the model capturing all the trends in the plant data. In July 2003, the lab result is actually greater than the feed sulfur in, so a lab error is a likely explanation.

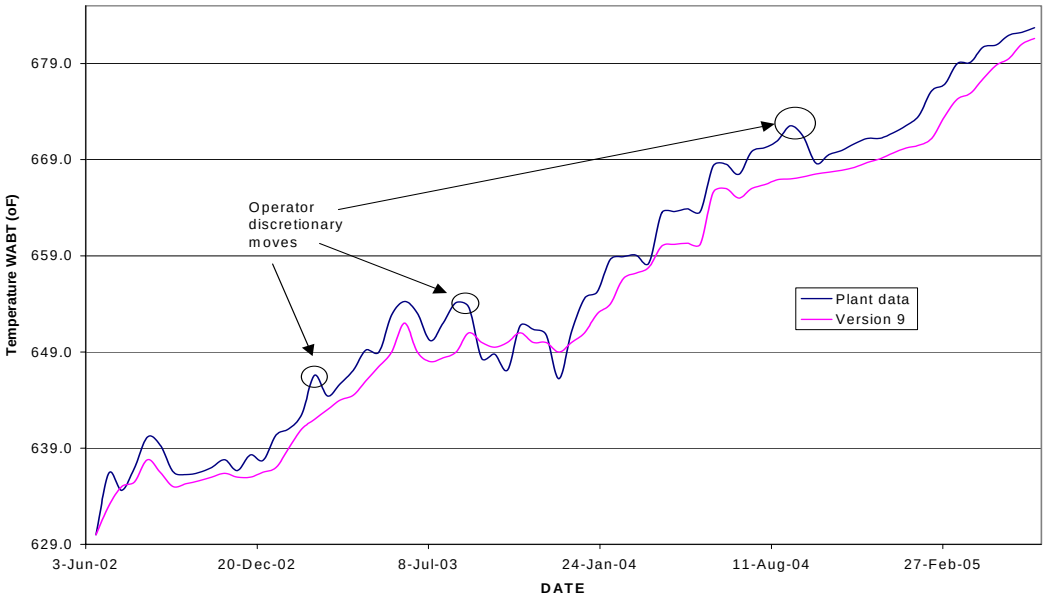

Figure 6.10 – Plant E – WABT, Model vs. Plant Data
Version 9 of the model is used to compare the values of WABT to the Plant E data. The WABT comparison has an R^2 of 0.935. A few situations are noted where plant operations made unjustifiable (based on feed conditions) increases in temperature. The model is not meant to capture these arbitrary changes.

6.4.3 Plant F Results

Plant F was on line 2.3 years, short of its three-year anticipated run length. The product sulphur composition and model predictions (R^2 = 0.88) are presented in Figure 6.11. For this plant, sulphur product trends upward throughout the run. It became more difficult for the model to match the product sulphur specification, when crude flow is decreasing and temperature increasing.

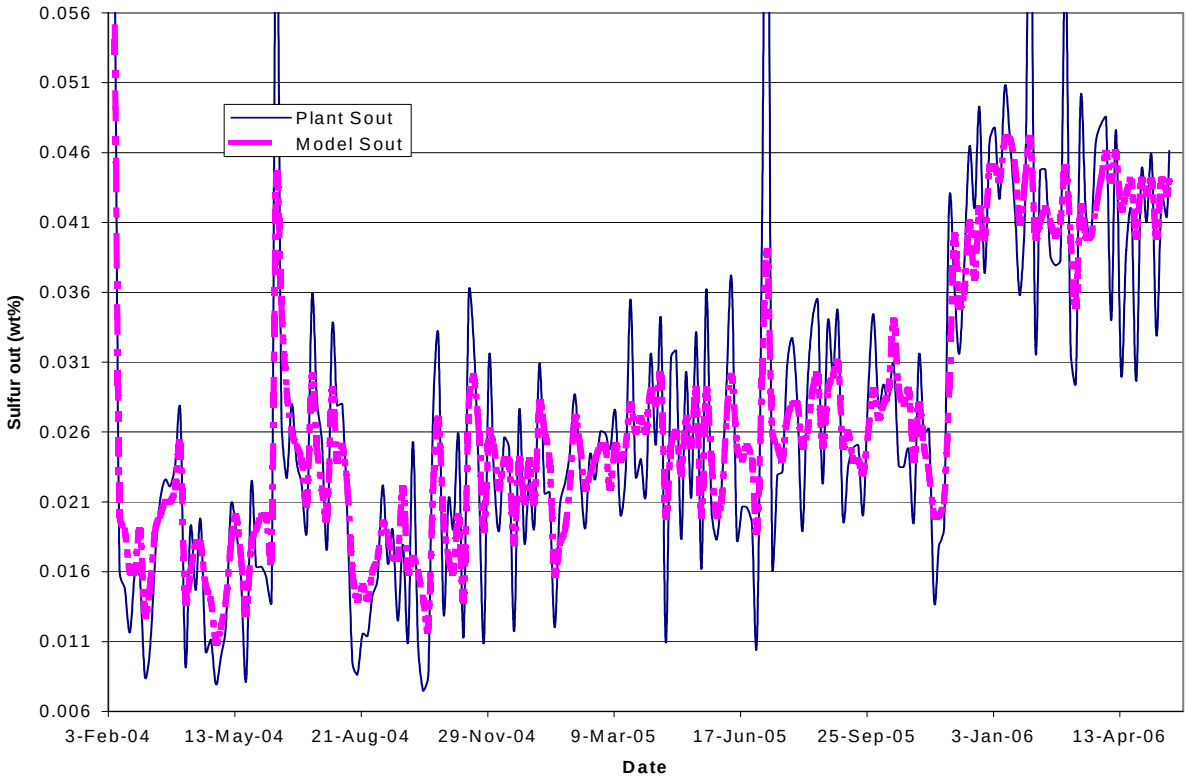

Figure 6.11 Plant F – Product Sulphur Composition, Model vs. Plant Data
Version 9 Sulfur product values are compared to the plant sulfur product laboratory values. The overall R^2 calculated was 0.88, with the model capturing all the trends in the plant data. In July 2003, the lab result is actually greater than the feed sulfur in, so a lab error is a likely explanation.

Figure 6.12, on page 169, shows the results for WABT for Plant F for the model (R^2 = 0.916) versus plant WABT data.

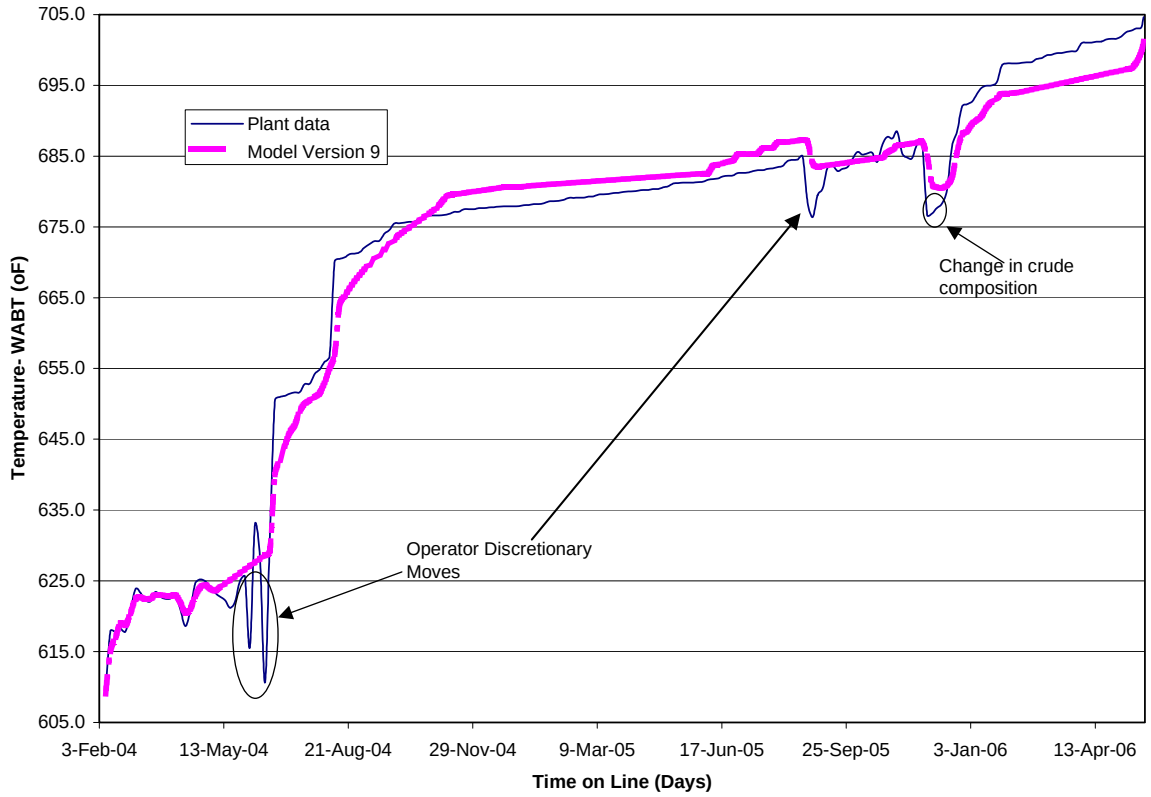

Figure 6.12 – Plant F – WABT, Model vs. Plant Data
Version 9 of the model is used to compare the values of WABT to the Plant F data. The WABT comparison has an R^2 of 0.916. A few situations are noted where plant operations made unjustifiable (based on feed conditions) increases in temperature. The model is not meant to capture these arbitrary changes. A distinct change in crude flow is noted in January 2006. The model responds well by adjusting the temperature accordingly.

The model trends the temperature profile well, except for the "discretionary" operational adjustments in the June 2004 time frame. Operators modified the temperature in the reactor without a real process reason. Except for these unexplainable moves[3], the profile and the accompanying disturbances are easy to explain and model. For example, the inlet sulphur composition doubles from mid-July to mid-August 2004, resulting in a desired rapid increase in WABT to increase activity of the catalyst to meet product sulphur specifications. In Figure

6.11, the product sulphur spikes during this time period, indicating the temperature adjustment helped in the short term, but wasn't entirely effective. Crude reductions were required due to the long-term impact on catalyst activity during this time of high sulphur feed.

Also, near the end of run (starting around December 2005), another feed sulphur spike occurred but was accompanied by an increase in feed metals. A change in crude blend was the reason for the disturbance[3]. Operations had to also lower the crude flow since the catalyst was not responding to small increases in WABT. Both WABT and crude flow had to be altered to try to meet sulphur product specifications. Note in Figure 6.11 the increased product sulphur composition (50+% increase from 2005 sulphur product results) indicates that the reactor was struggling to meet the necessary product sulphur specifications.

6.4.4 Plant A Results

Plant A ran for 2.6 years, just short of the target of three years before a shut down was required. Figure 6.13, on page 171, shows a comparison of the product sulphur composition for the plant and for the model predictions. The operation ran very close to the product specification of 0.04 wt% for the majority of the run time. The R^2 for the model predictions versus plant data comparison was 0.86, the lowest for the six plants. The model had difficulties with the both the extremely high and low sulphur values. Laboratory errors may have been the cause but

regular calibration had been performed as per the laboratory reports[3]. For all the product sulphur spikes, the model did indicate the correct trend, but did not calculate the measured extreme value. Another major cause of error is likely poor sampling and sample preparation. Also, the lumped nature of the model will not be able to address severe changes and extreme highs and lows with great accuracy.

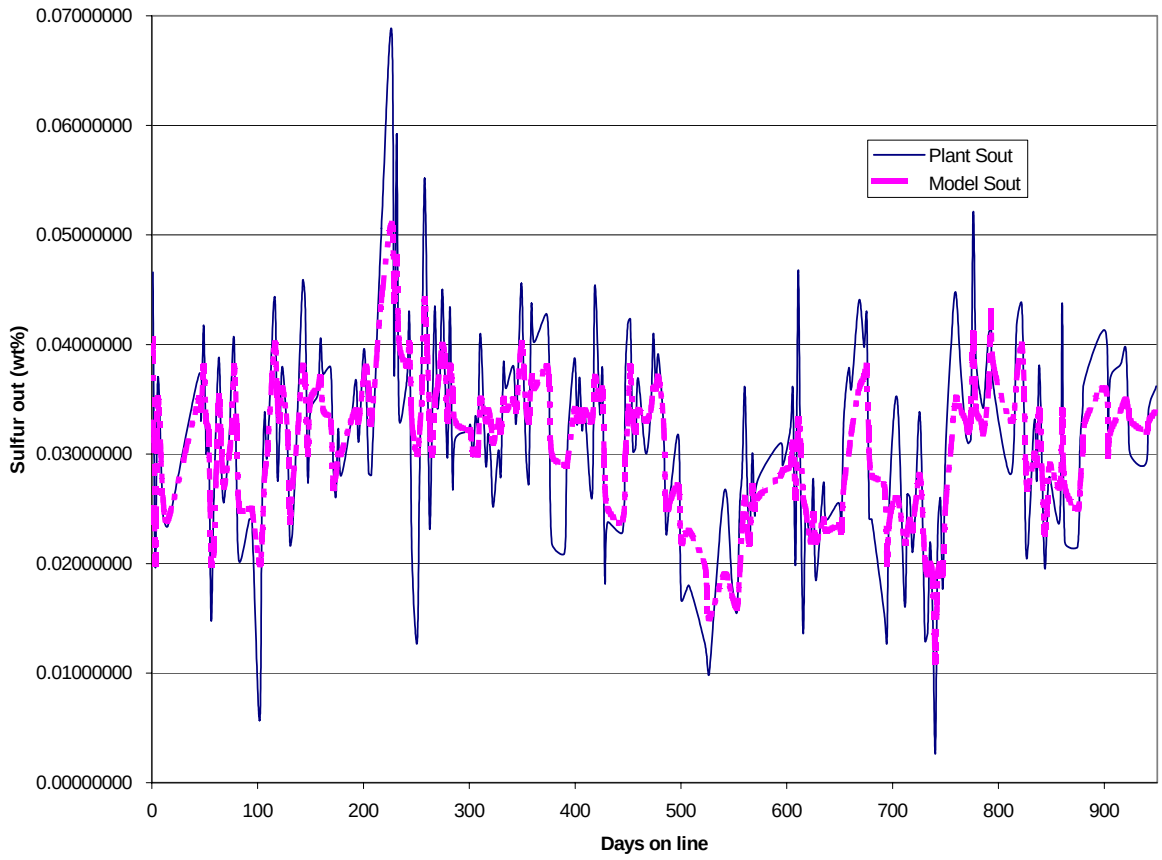

Figure 6.13 Plant A – Outlet Sulphur Composition, Model vs. Plant Data Version 9 Sulfur product values are compared to the plant sulfur product laboratory values. The overall R^2 calculated was 0.86, with the model capturing all the trends in the plant data but not able to match the extreme low and high sulfur values.

Figure 6.14 presents a comparison of WABT model predictions (R^2 = 0.91) to the plant WABT measured data. The model predictions were an acceptable reflection of the impact of disturbances.

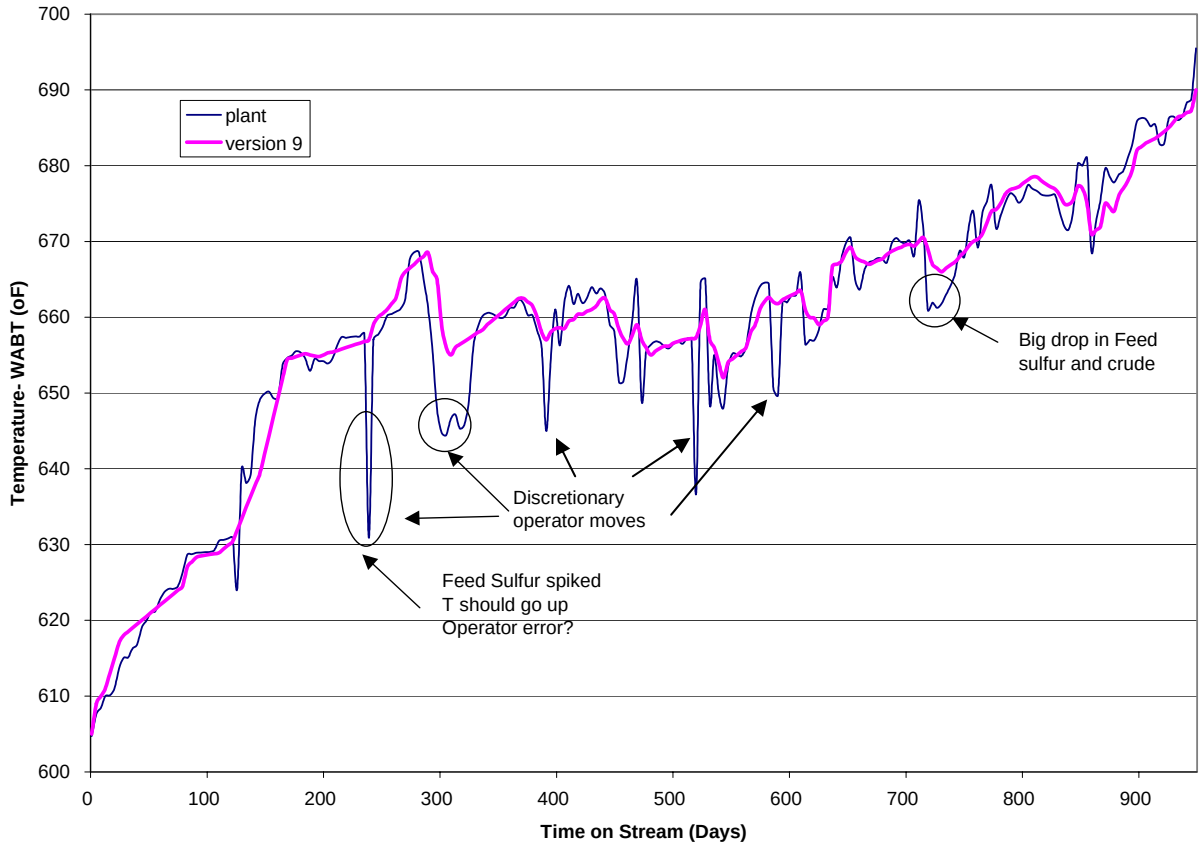

Figure 6.14 – Plant A – WABT, Model vs. Plant Data
Version 9 of the model is used to compare the values of WABT to the Plant F data. The WABT comparison has an R^2 of 0.916. A few situations are noted where plant operations made unjustifiable (based on feed conditions) increases in temperature. The model is not meant to capture these arbitrary changes. A distinct change in crude flow and sulfur composition is noted around Day 700. The model responds well by adjusting the temperature accordingly

However, there were operator adjustments that the model was unable to track.

These adjustments can be considered disturbances, since they impact the

catalyst activity. These operator changes can also be used to explain why the model product sulphur predictions

did not match as well as for the other plants. The unpredictable changes in temperature by the operators, for example on day 220, caused the reactor to operate in a way that was counter to what was taking place in the crude feed, namely a feed sulphur spike, which would require a decrease in crude flow rate or an increase in temperature and/or hydrogen partial pressure. In this case, the temperature went down (under operator control), the crude flow stayed fairly constant and there was no change in hydrogen partial pressure. The correct action would have been to raise the temperature in an attempt to mitigate the additional sulphur in the feed. However, the product sulphur increased to “off spec”, while the model only showed a marginal increase in product sulphur . Taking into account the many questionable operator adjustments during this run, the product sulphur results from the model are actually quite good (R^2= 0.86). The temperature profile for this plant followed a typical hydrotreater temperature profile (except for the operator adjustments). As a result, the model predictions were able to track the temperature profile fairly accurately (R^2=0.91).

6.4.5 Plant B Results

Plant B operated for 2 years, short of the desired three-year run length. However, the LHSV of 1.1 for this plant was higher than the designed value[3] of 0.8-0.9 hr^{-1}, which can partially explain the reduced run length. Run length was sacrificed for increased crude through put. For most of the run time, the product sulfur was well below the specification 0.05 wt%. When the sulfur product composition was

above specification, due to increased crude flow rates, the WABT was rapidly increased to try to bring the product sulfur down to the required product specification of 0.05 wt%. Rapid catalyst deactivation and the requirement to reduce crude flow were the result. Figure 6.15 presents a comparison of the model predictions (R^2 = 0.92) and the plant data for the product sulfur composition.

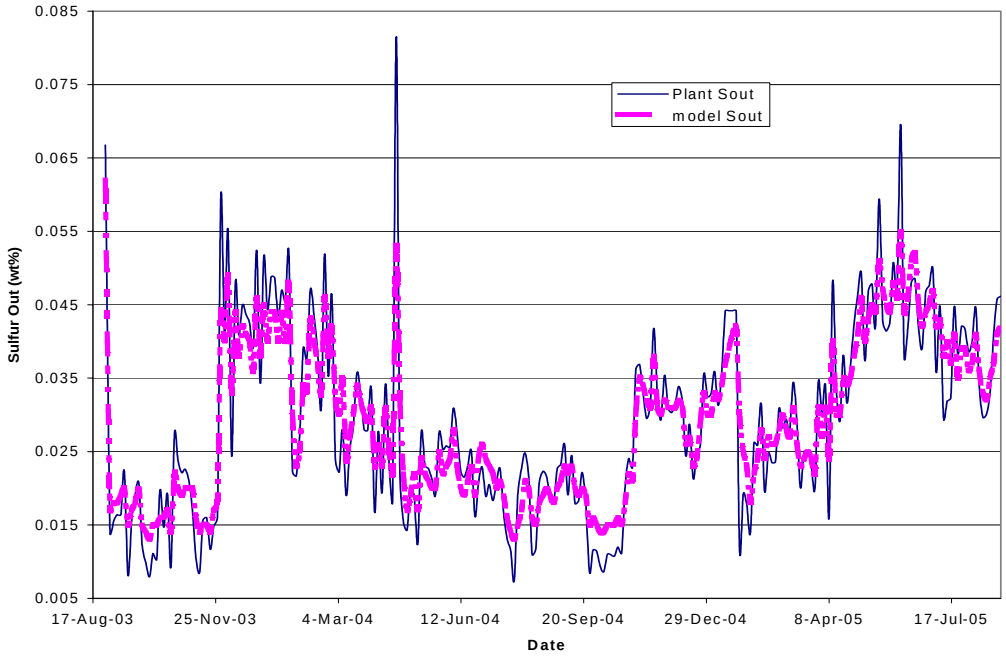

Figure 6.15 Plant B –Outlet Sulfur Composition, Model vs. Plant Data

Version 9 Sulfur product values are compared to the plant sulfur product laboratory values. The overall R^2 calculated was 0.92.

Figure 6.16, on page 175 shows a comparison of the model predictions (R^2 = 0.925) and plant data for the WABT for plant B. There were a few rapid increases in temperature different from the typical single SOR and EOR rapid increase. The causes of these multiple rapid increases (crude flow increases) were correctly identified and predicted by the model. It appears that the operator was trying to

process as much material as possible with catalyst life a secondary objective. In addition,

there were some crude changes that resulted in large drops in the feed sulfur composition (noted on Figure 6.16). There was a discrepancy between the model and what temperature the operators decided to choose in response to the changes in feed sulfur content. The operators tended to over correct by reducing the temperature more then required. As noted in figure 6.16, temperature was readjusted upward by operations rather quickly to prevent/minimize “off-spec” product. These examples (March 30th and July 5th) illustrate the value of the model as a tool to set the appropriate operating conditions due to changes in the feed composition.

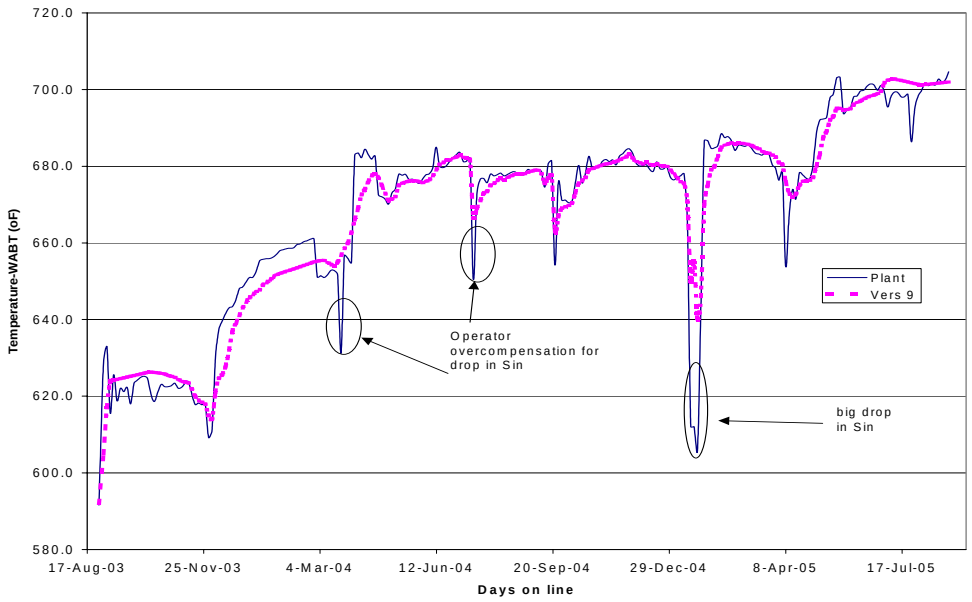

Figure 6.16 – Plant B – WABT, Model vs. Plant Data
Version 9 of the model is used to compare the values of WABT to the Plant B data. The WABT comparison has an R^2 of 0.925. A few points are noted where apparent operator overcompensation for drops in sulfur occur.

The model could be used as a guide to limit product sulfur specification excursions, along with increasing catalyst life but not exposing the catalyst to such sudden swings in temperature thus increasing run life of the catalyst or reducing the level of deactivation.

6.4.6 Plant C Results

Plant C operated for only 1.8 years well short of the expected three-year run length. Figure 6.17 presents a comparison of model predictions (R^2 = 0.90) and plant data for the production sulphur composition.

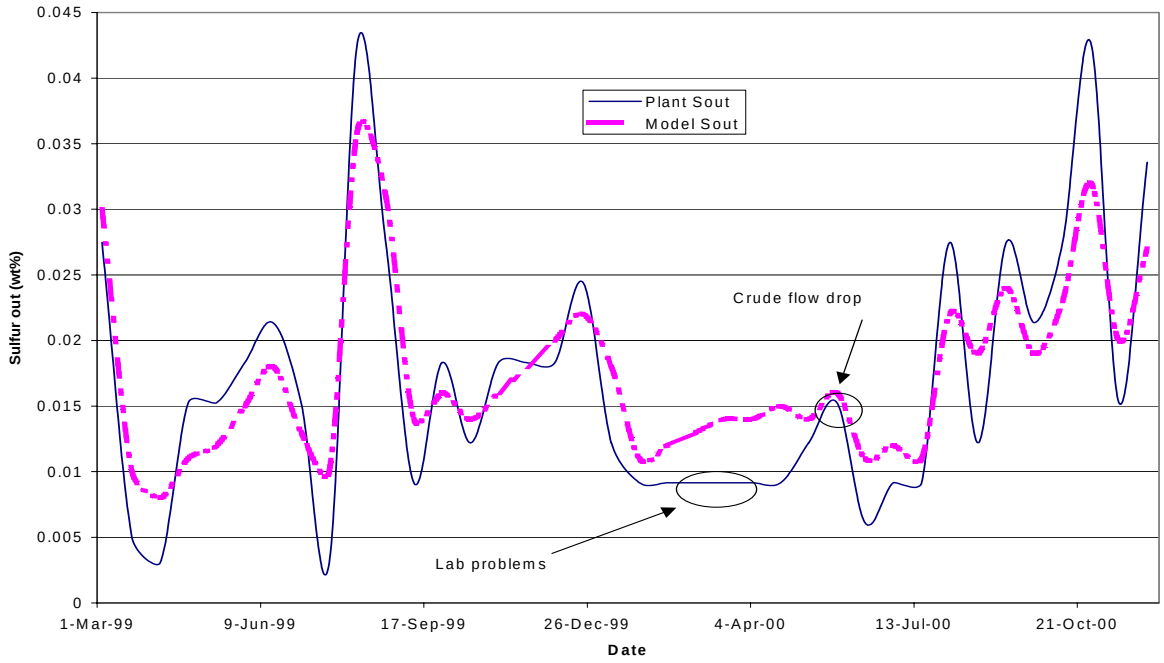

Figure 6.17- Plant C – Product Sulfur Composition, Model vs. Plant Data Version 9 Sulfur product values are compared to the plant sulfur product laboratory values. The overall R^2 calculated was 0.90. This plant experienced a lab malfunction in March-April 2000, with the model providing an indication of what the product sulfur values were.

The largest mismatch between the plant data and model predictions was the

laboratory analysis that showed for a span of three months that the product sulfur composition was a constant. However during this time period, the reactor temperature was adjusted in an attempt to maintain the product sulphur composition, which would also impact the comparison between plant data and model WABT predictions. The model predicted a higher product sulfur during this laboratory "problem". In a separate event, in June 2000, there was a feed crude change to an essential low sulfur content feed. Both the product sulfur and WABT predicted by the model and shown by the plant data decreased as would be expected.

In August 1999, a large increase in the feed sulfur resulted in a huge increase in product sulfur and a corresponding accelerated increase in WABT. Catalyst life was severely reduced during this disturbance and was the single largest factor in reducing the run length 3 years to 1.8 years. Being able to predict the impact of disturbances on catalyst life can aid operations in readjusting the operation to try to maintain or at least partially recover the original economic operating objectives (crude produced on specification over a given time period).

Figure 6.18, on page 178, shows a comparison of Plant C's WABT model predictions (R^2 = 0.925) and plant data. The temperature profile for Plant C does nicely match the SOR-MOR-EOR profile. However, the SOR WABT portion gradient is not as severe as would be typically expected.

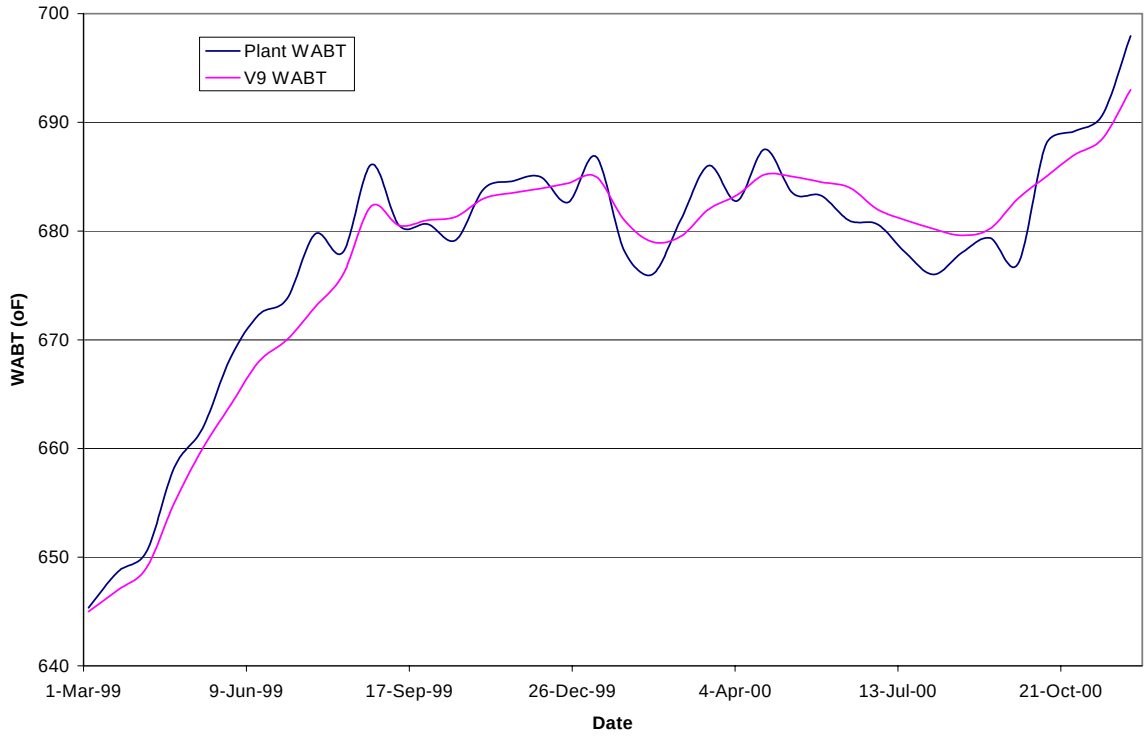

Figure 6.18 – Plant C – WABT, Model vs. Plant Data
Version 9 of the model is used to compare the values of WABT to the Plant C data. The WABT comparison has an R^2 of 0.925.

6.5 Predictability of Developed Correlative Model

The developed model in this research is correlative. The following process was used to develop the model parameters:

a) 8 unpublished data sets used to develop/update parameters b,p,g

b) then Plant d data used in entirety to correlate the parameters b,p,g

c) 1st 100 days (SOR = 30 to 40 days and part of MOR) for each remaining plant (a,b,c,e and f) used to optimize the parameters to complete remaining run length (300 to 800 days of data) for each plant

An exercise was performed to determine if the model could also be considered partially predictive. A new data set was obtained from plant d which had a different catalyst (updated version of existing catalyst) and a different starting temperature. The parameter correlations (b,p,g shown as equations 6.3-6.7) developed from the entire sets of plant data obtain were used.

Tables 6.2a and 6.2b (page 180) below compare information from the two plant D runs. The biggest difference between the two runs is the catalyst type and the starting temperature. The model was able to deal with a different catalyst and starting temperature while using the same model parameters from a different data set. The parameters from the previous data set of plant d were very close to the ones calculated for the latest plant d data set

Table 6.2a – Comparison of catalyst and reactor information for Plant D between the two data sets obtained for this research

UNIT		Plant D-base	Plant D-2nd
REACTOR DIAMETER	ft	12	12
CATALYST TYPE		NiMo on Al	**NiMo on Al***
CATALYST DIAMETER	in	0.091	**0.087**
CATALYST VOLUME	cuft	6523.0	**6510.0**
CATALYST WEIGHT	lbs	316650.0	**321594.0**
CATALYST DENSITY	lbs/cuft	48.544	**49.400**
Cycle length	years	1.08	**2.5 expected**
REACTION TYPE (HDS,HDN)?		HDS	HDS
DESIRED PRODUCT S	%WT	0.03	0.03
TYPICAL FEED S	%WT	2.20	**2.35**
SOR AVERAGE TEMP.	°F	580.0	**602.0**
TYPICAL LHSV	H-1	0.41	**0.45**
FEED TYPE (N,KERO,LGO,VGO)?		LGO	LGO
SUGGESTED REACTION ORDER	-	1.7	1.7
ACTIVATION ENERGY	CAL/MOLE	24500	24500

* a newer version of the catalyst was used for this latest hydrotreater run.

Table 6.2b Performance comparison between the two data sets for plant D. Parameters used are essentially the same, and the statistical evaluation results are comparable.

	D- base	D- new run
Time Started	apr 05	nov 06
Time End	jul 06	?
T start (oF)	580	602
T end (oF)	670	?
R2 sulfur	0.917	0.927
R2 temperature	0.916	0.934
SOR range (oF)	580-630	602-655
SOR T delta (oF)	50	53
Catalyst type	Version 7	Version 8b
Viscosity (SSU-100oF)	243	243
API SOR	27	27.1
Parameter b (average)	23000	23000
Parameter p (average)	0.9	**0.92**
Parameter g (average)	0.54	0.54

The parameters used for the new data set for plant d were not developed from the new data. The g (temperature) and b (hydrogen to oil) parameters used were from the previous plant d data set. The p parameter (hydrogen partial pressure) was slightly higher due to the increase in hydrogen partial pressure on the reactor. The correlation developed from the other data sets was used to calculate p for this data set. The key point for this evaluation is that the model calculations do not rely on any correlative analysis with this data set.

Figures 6.19, on page 181, and 6.20, on page 182, show the graphs of WABT and Sulfur comparing the data from the two plants and the model results. The R^2 for the sulfur and temperature are 0.937 and 0.934 respectively which is slightly higher than the original plant D sulfur and WABT (shown in table below) statistical values. It is expected that the R^2 for both Sulfur and WABT for the new data set will reduce when the EOR is factored in but should be close to the final R^2 statistical evaluation as the existing plant. At the same point in the time (in

the middle of the run) for the first plant D data set, the R^2 for the sulfur was 0.931 and for the WABT was 0.929 which is very close to the current R^2 values for this run. Differences in model performance between the two data sets will likely be attributed to different types and degrees of disturbances on each data set, the quality of data acquisition between the two sets and any other limitations from the lumped model.

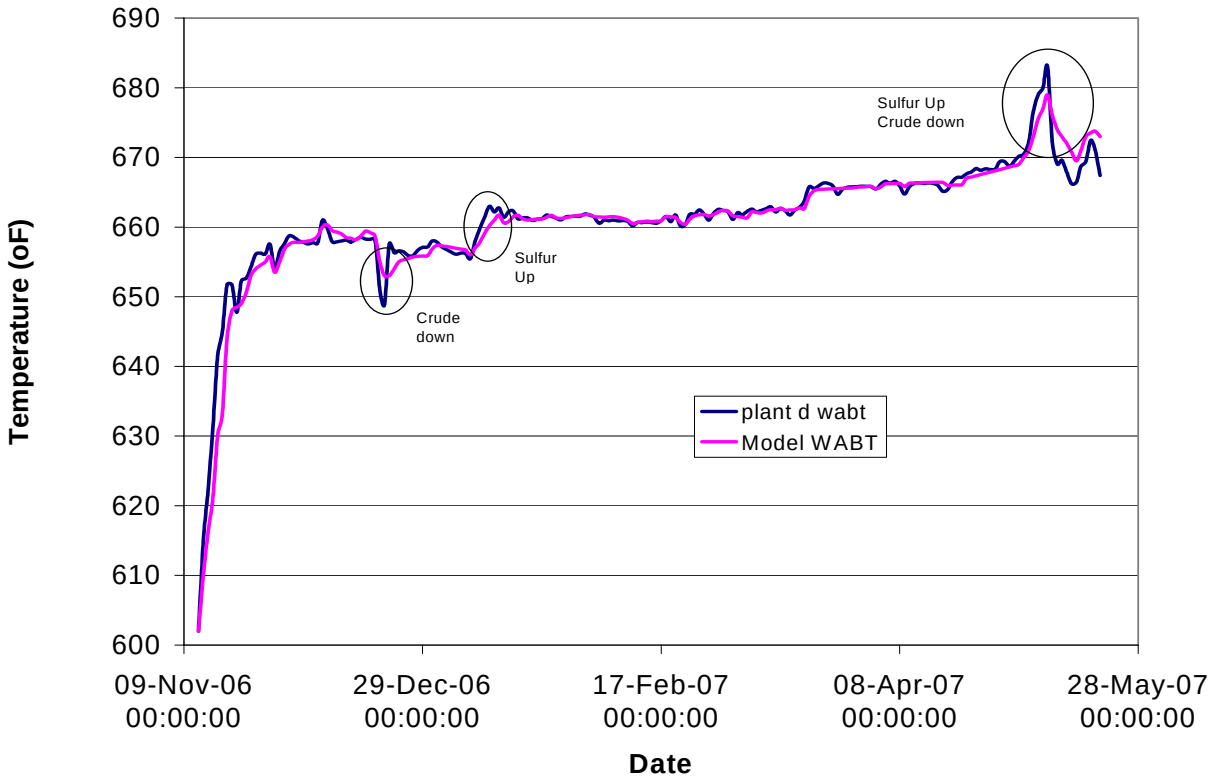

Figure 6.19- Comparison of WABT between plant data and model for a recent run of plant D. This graph shows how the model responds when parameters from a different data set are used on a different set of plant data. The model is able to capture the trend for temperature in the reactor for the changes noted in the table (crude change, sulfur spike in feed). The R^2 for the WABT was calculated to be 0.934.

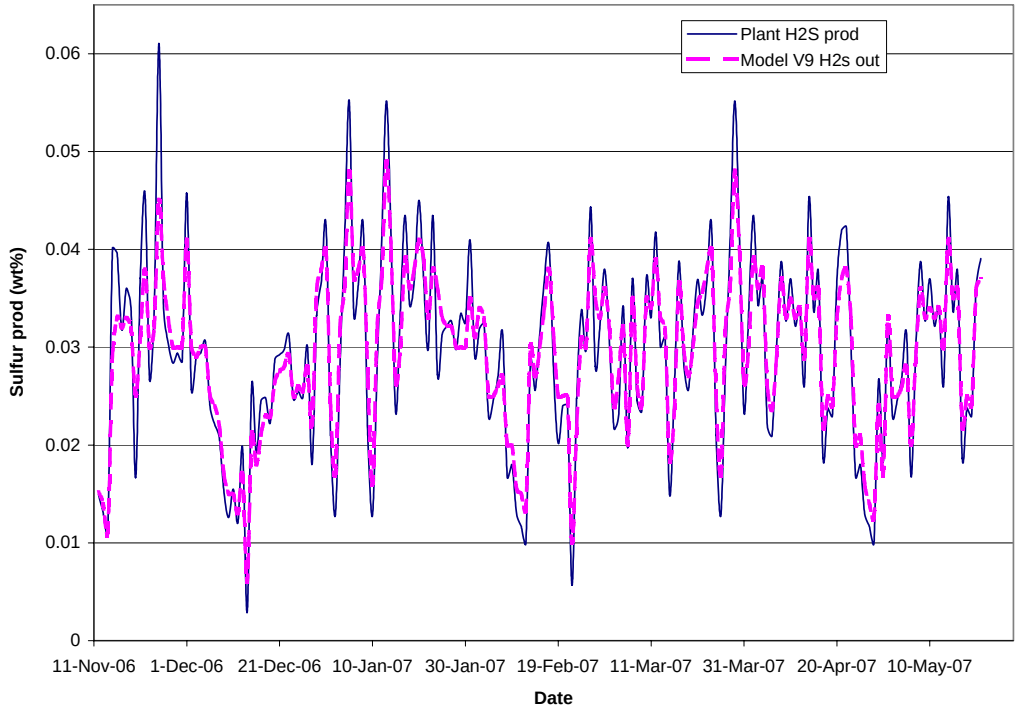

Figure 6.20- Comparison of product sulfur between plant data and model for a recent run of plant D. This graph shows how the model responds when parameters from a different data set are used on a different set of plant data. The R^2 calculated for the comparison between plant and model was 0.937.

Based on catalyst activity profile to date, the model predicts a run length of 2.4 years, just short of the 3 year design rate, but more than double the previous data set (1.08 years). Catalyst is considered fully deactivated to meet operating goals when activity goes below 25% and when the maximum allowable operating temperature (mechanical integrity concerns) is reached[3,7,12,23].

6.6 Summary

6.6.1 Model Results

Data for six plants were compared to model predictions for the plant WABT and product sulfur composition. Table 6.2 provides a summary of the statistical analysis used to compare the model predictions to the plant data. For the

Table 6.3 – Statistical Results for each Plant – Model vs. Plant

	Plant A	Plant B	Plant C	Plant D	Plant E	Plant F
Sulfur R^2	0.86	0.92	0.90	0.93	0.95	0.88
WABT R^2	0.91	0.925	0.925	0.927	0.935	0.916

product sulfur, the model showed a R^2 of approx. 0.86-0.88 for two plants (A,F) and over 0.90 for the other four plants. For the WABT, the model had an R^2 in the range of 0.91 to 0.935. Overall, the model does provide a credible match of the overall plant operation, especially when considering that the model uses a lumped parameter approach, that there are inaccuracies in the measurements and operator choices (on temperature) which as shown are not always the best method of mitigating a disturbance.

6.6.2 Catalyst Activity

Catalyst activity is directly related to the WABT and is a primary variable for operations to control the catalyst activity or rate of deactivation. Analyzing the catalyst activity profile, however, is helpful in making the decision as to when to schedule a unit shutdown, and how to mitigate further deactivation. Figure 6.21

shows the catalyst activity/deactivation profile for plant D. This figure does show very clearly the impact of the disturbances the life of the catalyst. Disturbance 1, a rapid increase in sulfur causes a 7.5% reduction in catalyst life. If the impact of the disturbance can be mitigated during the disturbance, catalyst life can be extended. The two disturbances noted in Figure 6.21 reduce the catalyst life by

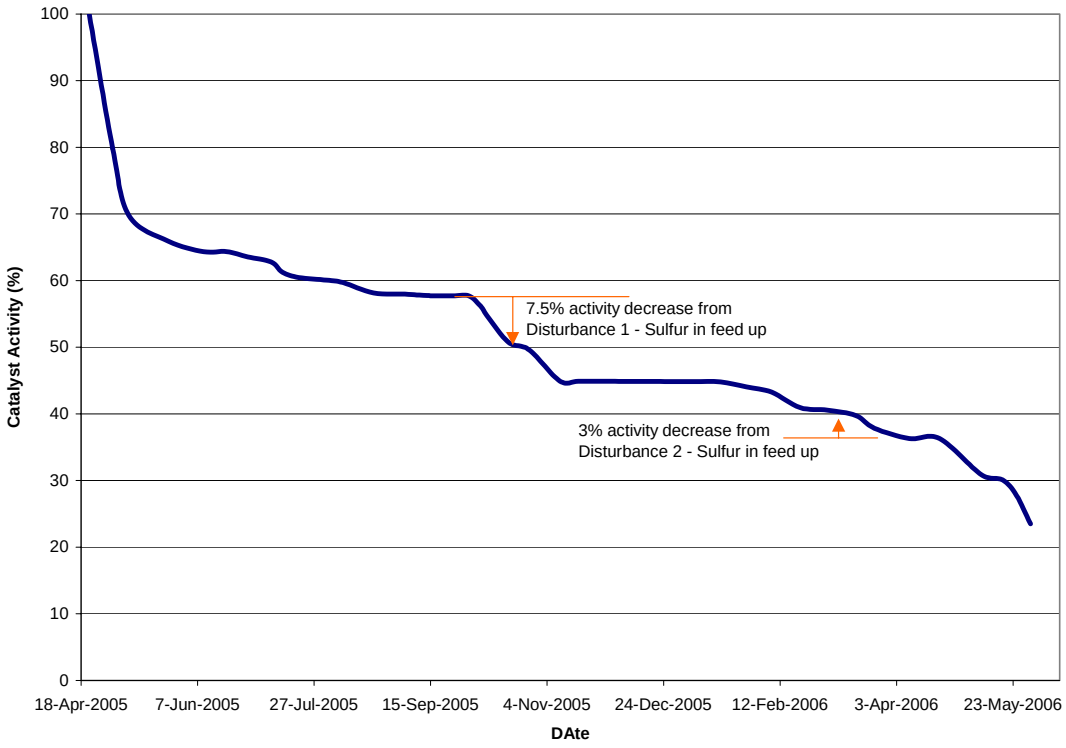

Figure 6.21 – Catalyst Activity Profile for Plant D
The deactivation of the catalyst calculated from the model is shown. The impact on catalyst activity is illustrated for two disturbances. The two disturbances together represent a 10% reduction in catalyst activity, which for a 3 year run length is approximately 4 months of operation.

10.5%, or 4 months. This information can be critical in deciding what steps operations can make to improve the performance or prepare for a shut down.

6.6.3 Sensitivity Analysis

Sensitivity analysis or model validation tuning of the Wetting efficiency, SOR and EOR increased the overall WABT R^2 for the model predictions from a range of 0.81-0.86 in version 8 to a range of 0.89-0.93 in version 9, an improvement of 6 percentage points. For the developed model correlations, any further adjustments in the model parameters resulted in the model to over predict the plant data, resulting in an overall poor match of the plant data trends. Figure 6.22 shows an attempt, for plant D, to aggressively track the steep SOR and EOR profiles and the steep changes in temperature during this run.

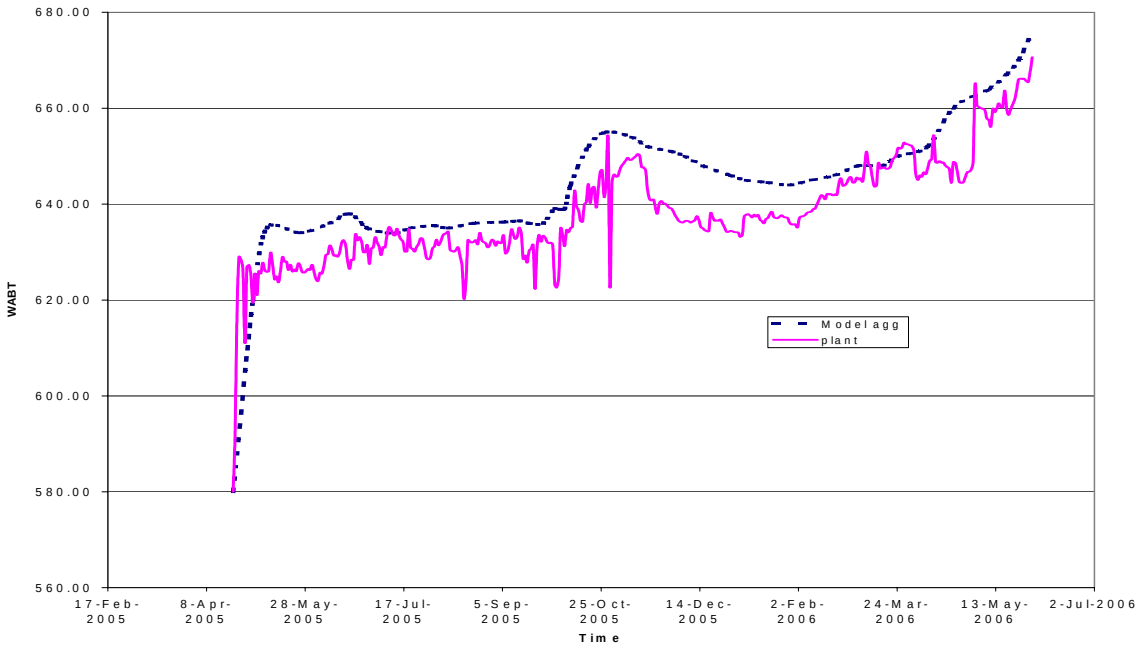

Figure 6.22 – Sensitivity analysis – Aggressive use of Parameters, Plant D, WABT, Entire Run. The model parameters were adjusted to determine the point at which the model could not be further improved past version 9. This WABT shown here is an example of when the model uses parameters not from equations 6.3-6.7.

As a result, the model became less sensitive to the downward trends in temperature, in other words, when catalyst deactivation stabilized and crude

flows decreased or hydrogen partial pressure increased the model predictions showed an R^2 of 0.85 for version 8, versus an R^2 of 0.93 for version 9. Consequently, it was decided to maintain the same sensitivity for all the operating scenarios (both upward and downward trends) rather than forcing a tighter match on the upward trending disturbances. In a pilot plant scenario where one variable is being manipulated, focusing on this one variable can provide a very good match. The challenge in using plant data is managing multiple variables in a dynamic system. For this lumped parameter approach, version 9 was chosen as it provided a balanced response to both trends in temperature while tracking the overall temperature profile for the entire run.

Further refinement of the model may be possible; however the type, accuracy and quality of data from an industrial site is considered, along with using a lumped approach, and R^2 values well over the 0.9 for the developed model (version 9) does not justify further refinement as the developed model is representative of the industrial unit operation. Note, there was no plant data available that could be used to account for/model short term localized hot spots or flow mal-distribution that could impact catalyst activity. Had this type of data been available then further refinement of the model would be justified and could possibly be used to model short term excursions.

In presenting the model results to the operators, their perception is that anything that provides a generic trend of performance with some ability to account for changes in operation is more than what can be expected in an industrial setting. The value of the model as a tool to set the appropriate operating conditions due to changes in the feed composition was also illustrated. The gross operator errors can be avoided and optimum variable set point choices can be made to improve the economic performance of the VGO hydrotreater by using the model predictions.

Refiners/operators are keenly interested in making economically sound decisions that extend the catalyst life of their hydrotreaters. Of the six plants for which data is presented, only one (plant E) met its desired run length target. However, even plant E did not meet its total capacity through put requirement.

Refiners/operators now have a tool (chapter six positive results), that responds to and reflects actual industrial plant operation, that can be used to determine whether changing operational variables will improve VGO hydrotreating operation is economically feasible. Since operators struggle to meet run length targets, a tool to realistically analyze options was required.

As stated in chapter six, the primary outputs to the developed dynamic lumped parameter model are the sulfur outlet composition (main specification) and WABT (directly related to catalyst deactivation and readily available to operators to track performance of process). In this chapter the hydrogen partial pressure via hydrogen purity is adjusted to determine it's impact on the long-term performance of the hydrotreater.

7.1 **Specific Applications**

Two plants (D and F) were selected to study the effect of changes in hydrogen purity on the operation of industrial VGO hydrotreaters. Each of the six plants

could benefit from timely increases in hydrogen purity, however only plants D and F will be studied in detail.

7.1.1 Plant D Model Application

Using the validated dynamic model of the process, various scenarios for plant D were evaluated to determine what mitigating steps in the process could be used to improve the operation. For Plant D, hydrogen purity was increased to 99.9% from an average of 90.9%, while keeping the recycle gas flow rate constant. Access to third party on-the-spot 99.9 % pure hydrogen was assumed (as per availability of industrial gas pipeline networks in Gulf Coast, Louisiana, California, and soon-to-be Edmonton). The test (scenario 1) involved increasing the hydrogen partial pressure from 1900 to 2050 psig at the point of the 1st major disturbance while maintain same run length. The model predicted WABT from version nine was held constant as well.

Increasing the hydrogen partial pressure has been shown to improve desulfurization by reducing the impact of coke formation[20]. As shown in Figure 7.1, on page 190 the crude charge could be increased by an average of 3200 BPD of crude for approximately seven months (204 days). During actual operation, the inlet sulfur feed disturbance (Disturbance #1) triggered the steady decline in crude flow in order to maintain outlet sulfur specifications. The addition of hydrogen did enable a slower catalyst deactivation, and thus allowed the operator to increase crude flow more than what actually occurred. The benefit to

the operator based on $25/bbl ($55/bbl crude into refinery, and $80/bbl product out plant) upgrade[3] is $16.3MM ($25/bbl x 3200 BPD x 204 days). The cost is the higher purity hydrogen (90.9 to 99.9%). Market price (March 2007) for Edmonton area spot hydrogen is $0.84/kscf. The recycle flow of 88% hydrogen has to be further purified or diverted to another area such as “fuel ”, and/or flaring . Using a simple cost analysis, 35 mmscfd of 99.9% is required at a cost of $6.0MM for the 204 days, resulting in a net value to the refiner of some $10.3MM.

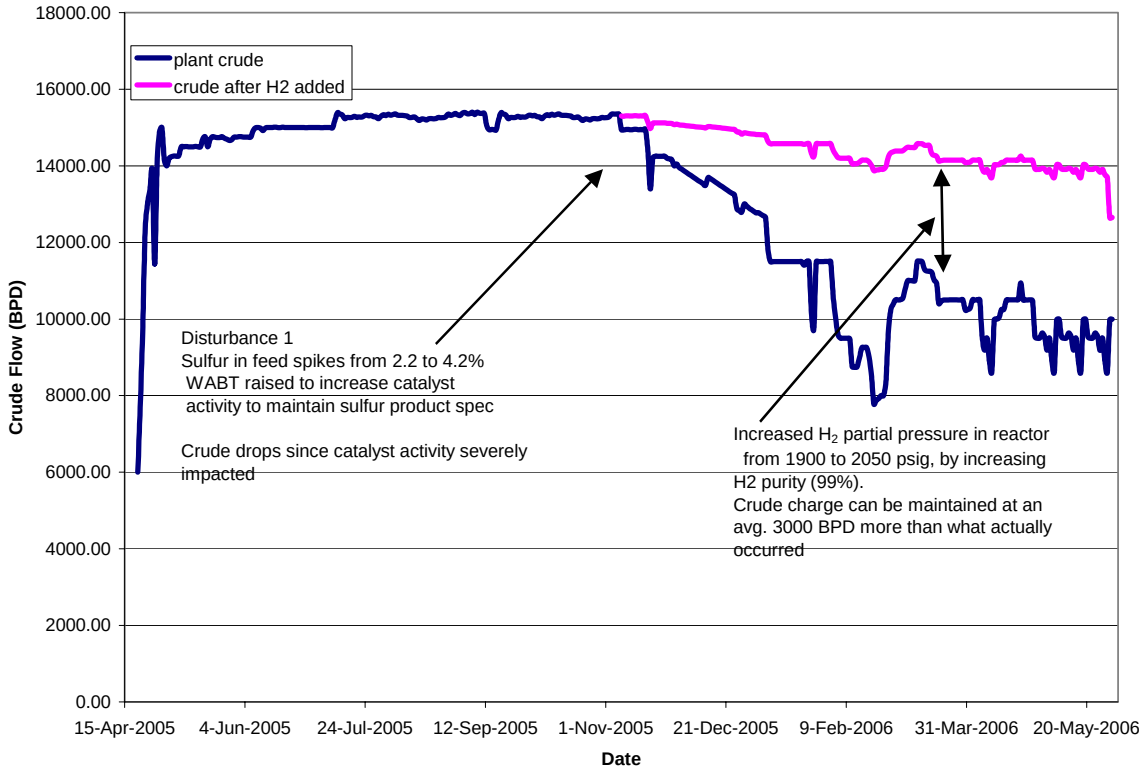

Figure 7.1 – Plant D- Impact of adding H_2 on Crude Production. Figure shows the crude flow feeding the VGO hydrotreater for the entire run length of plant D. Hydrogen partial pressure is increased to 2050 psig from 1900 psig at the first disturbvance in the plant in late October 2005. The result is an increase in crude production after November 2005 of 3000 BPD on average.

Hydrogen partial pressure positively impacts deactivation due to coke formation and the model accounts for this catalyst phenomenon. In contrast, increased hydrogen partial pressure in the model negatively impacts catalyst deactivation by metal deposition[20] . For this case, the crude flow rate dropped significantly at the EOR reflecting the impact of metals deposition accelerating catalyst core plugging.

Another way to illustrate the benefit of increased hydrogen partial pressure is to compare the catalyst activity between the base case model and the model with increased hydrogen (only variable changed). Figure 7.2, on page 192, shows that at the point of the first disturbance, a higher purity hydrogen feed creates a reduced drop in catalyst activity of 3% (versus the 7.5% catalyst activity in the base case). The long-term effect of the higher purity hydrogen is a 13% higher catalyst activity by the end of the run. The increased catalyst activity can be translated into an increased crude flow, Figure 7.1.

Another interesting scenario (scenario 2) that was evaluated was to increase hydrogen partial pressure for the entire run to determine increased run length for the same plant crude production pattern. Scenario 1 did show that crude production could be increased by an average of 3200 BPD after disturbance 1 so scenario 2 was looking at increased run length benefits. The initial coke deposition on the catalyst is mitigated by the increase in hydrogen partial pressure, that is catalyst deactivation will not be as rapid and the WABT will not be as high with the increased crude. The net result for no change on crude

throughput and other variables extrapolated was a run length increase of 45% (Scenario 2).

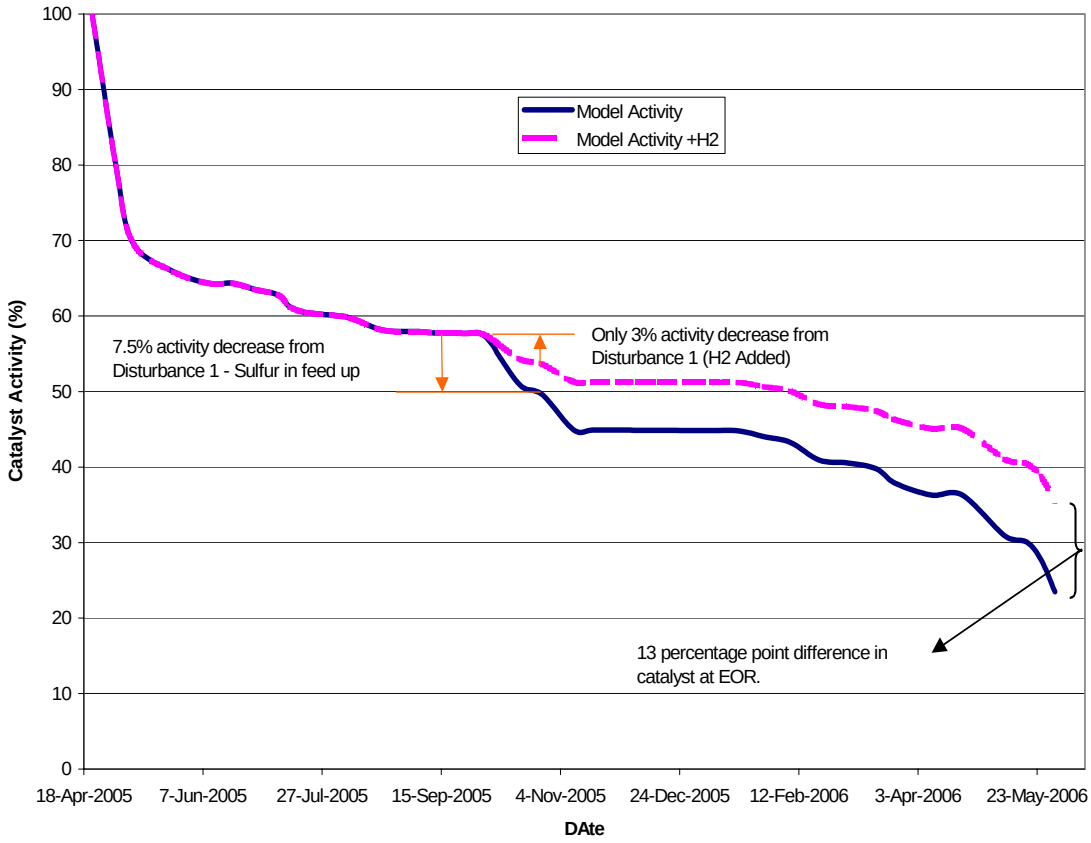

Figure 7.2- Catalyst Activity change due to Increased Hydrogen purity. This figure shows the impact on catalyst activity when the hydrogen partial pressure is increased (2050 from 1900 psig) in October 2005 in response to Disturbance 1 (increase in Sulfur feed). A 3% activity decrease is calculated by the model as opposed to the 7.5% calculated at the given hydrogen partial pressure. Over the remaining life of the run, the model calculates a 13 percentage point increase in catalyst activity remaining with the increased hydrogen partial pressure.

Figure 7.3, on page 193, shows the WABT and the increased run length for two scenarios (2 and 3). Scenario 3 shows an increase of 15% in run length if the crude production increase from scenario is maintained.

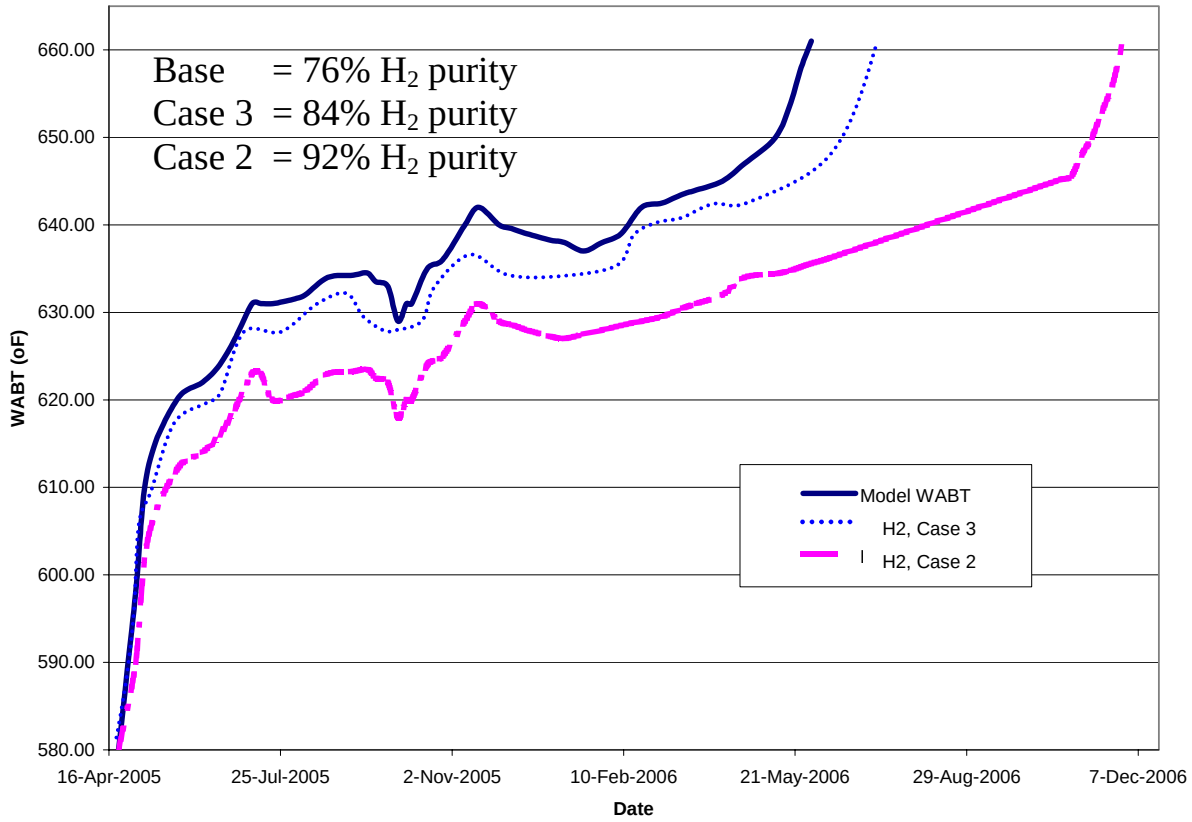

Figure 7.3 – Plant D, Increased Hydrogen Purity for Entire Run Length
Case 3 shows an increase in run length of 45%, when the hydrogen purity of the gaseous feed is increased to 92% from the plant actual of 76%. Case 2 shows an increase in run length of 15% when hydrogen purity is increase to 84% from the plant actual of 76%. For both case 2 and 3, the only variable changed in the model was the hydrogen purity and thus hydrogen partial pressure of the reactor.

However, with no operational data beyond the plant run length, scenario 1 illustrates an increase in crude production from the increased hydrogen partial pressure for the same run length is the best demonstration of the model. The trade off between crude charge and run length needs to be decided by the plant manager so both options were evaluated.

7.1.2 Plant F Model Application

Plant F struggled to maintain product sulfur below specification, in particular after January 6, 2006 (Figure 6.10 and 6.11). A crude change occurs with increased sulfur and metals in the feed. The crude rate is slightly reduced and the WABT is further increased to compensate for this change in feed. However, both these process variable adjustments do not add to the overall goal of maximum crude throughput for the longest possible run length. The model can be used to determine the economic benefit of adding higher purity hydrogen feed (from an average of 90.9% to 99.9%) to the reactor. Figure 7.4 shows that increasing hydrogen purity to 99.9% will keep the sulfur product below the 0.4 wt% specification for the remainder of the run (with one exception),

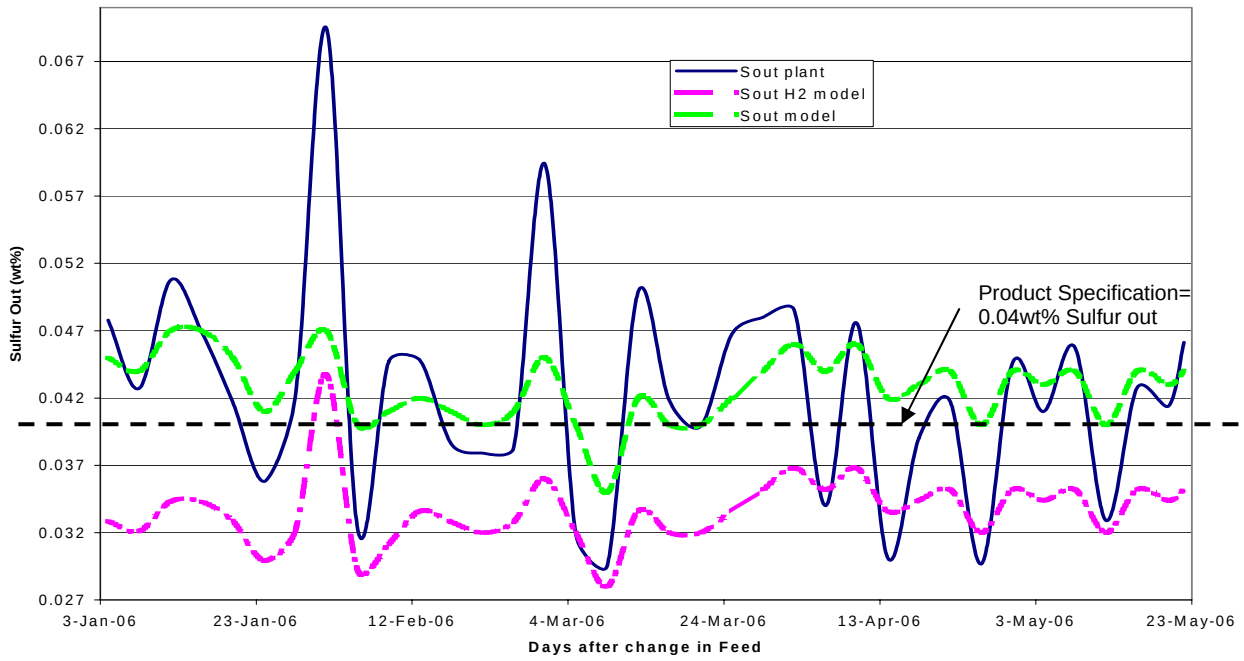

Figure 7.4- Plant F Sulfur product with Hydrogen Addition. In this evaluation, the impact of increasing hydrogen purity from 90.9% to 99% is related to the output sulfur. The product specification is 0.04 wt% sulfur. By increasing hydrogen purity, the model calculates that Plant F would have been able to meet product specification more readily.

far better result than if the hydrogen purity was not increased. Keeping product sulfur within specification is crucial for downstream units, specifically the fluidized catalytic cracking (FCC) unit where the catalyst is more sensitive to contaminants (ex. sulfur and metals) than the VGO hydrotreater. In addition, the increased purity hydrogen (average of 48.6 mmscfd) mitigates catalyst deactivation for the hydrotreater, as shown by the slower catalyst deactivation in figure 7.5, on page 196. At the end of run, catalyst activity was 4.6% higher for the case with increased H_2 purity and thus increased hydrogen partial pressure. The increased catalyst activity can be translated into an increased crude flow for the same run length and WABT. The crude flow can be increased by an average of 1250 BPD to 23,500 BPD for 36 days. The value of this increased crude flow is some $0.67MM using the same cost data ($25/bbl upgrade and $0.84/kscf) as for the crude and hydrogen as in the Plant D.

As previously demonstrated for Plant D, if hydrogen purity is increased right from start up, more crude can be processed for plant F and the value of adding hydrogen would be larger. However, for this example, the intent was to show the benefit of lowering the outlet sulfur composition to minimize catalyst degradation on downstream units (eg. FCCU), with the secondary benefit being improvement in the VGO hydrotreater effectiveness (eg. increase crude flow).

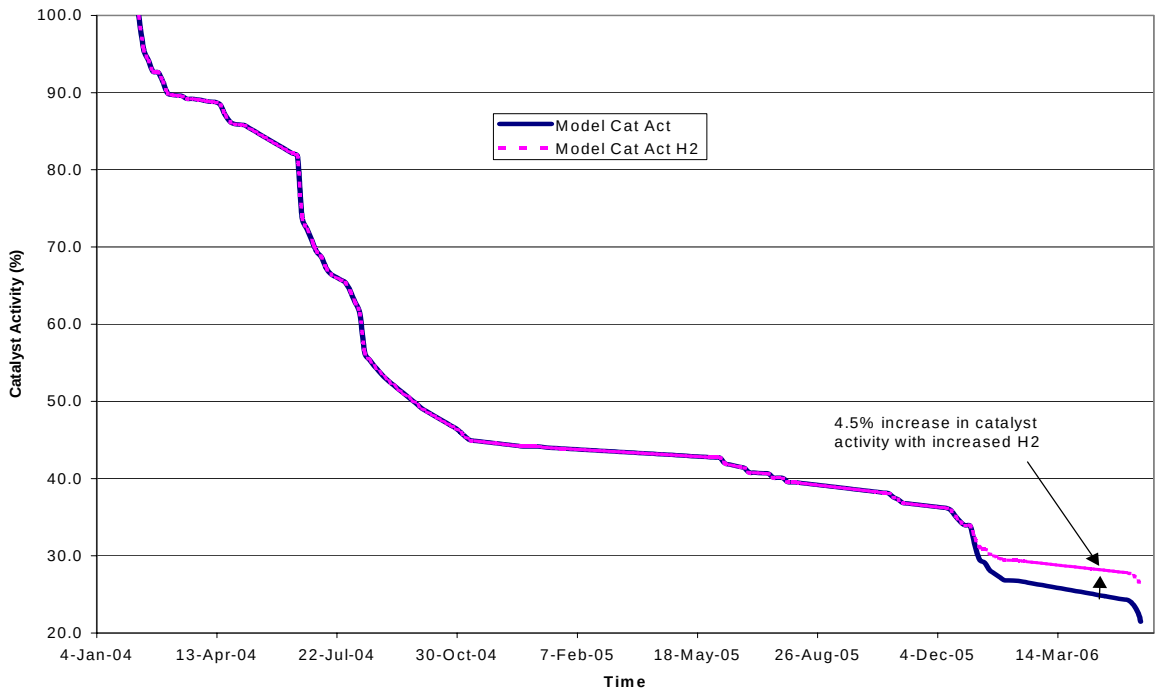

Figure 7.5 – Plant F Catalyst Activity with Hydrogen added. Using the model developed in Chapter 5, hydrogen purity was increased from 90.9% to 99% in December 2005. The model calculates an increase in catalyst activity at the actual end of run of 4.5%. this increase in catalyst activity can either be used to increase crude production for the same run length or increase run length (both valuable scenarios for the operator).

7.2 Application – Increase Run length

Typically, for justification of proposals for the improvement of hydrotreater operations, increasing run length of a hydrotreater to match overall refinery/upgrader mechanical shut down schedules is an understandable, tangible and large enough benefit. Justifying a disturbance mitigation tool, even though it can provide the largest economic benefit, is difficult since the counter argument is; “there are our well trained operators present to prevent disturbances from causing short and long term detrimental impact”. The application of the model developed in this study can provide tangible evidence to justify the benefit

of using more hydrogen to improve hydrotreater operations by increasing run length.

Using the model on plant C (data on shutdown and hydrogen costs were made available for evaluation), table 7.1 (page 199) and figure 7.6, on page 198 show that run length can be doubled by increasing the H_2 partial pressure (via increased hydrogen purity). Figure 7.6 does show three WABT profiles for plant C, with all plant inputs set to an average (all disturbances removed) but using the existing run length as a starting point (1.8 years with 77% H_2 purity). The intent of this analysis is to show the effect of hydrogen purity on the run length of the hydrotreater in a close to "ideal" scenario, namely maximum likely run length since disturbances are removed. The WABT profiles thus follow a typical curve for a hydrotreater. When the hydrogen purity is increased to 87%, the run length is increased to 3.3 years, nearly double the base case run length. Hydrogen purity of 87% was picked since two other plants(D and E) used in this study were operating at this level, and thus is an achievable value. For the second study (Curve 2 in Figure 7.6), 92% hydrogen purity was chosen, since this was the highest purity used in the operating plants from which data was available. The run length for plant C with 92% hydrogen purity was 3.93 years. Increasing hydrogen purity (if it also increases hydrogen partial pressure) definitely has a positive, tangible benefit of increasing the hydrotreater run length based on the developed model results. However, in most cases, refiners will struggle to get to the point where they can use 99% pure hydrogen unless the displaced low purity

hydrogen can find another use such as fuel gas or flaring. However, the flaring option will not be an economic option since the value of the displaced low purity hydrogen will be assigned no value.

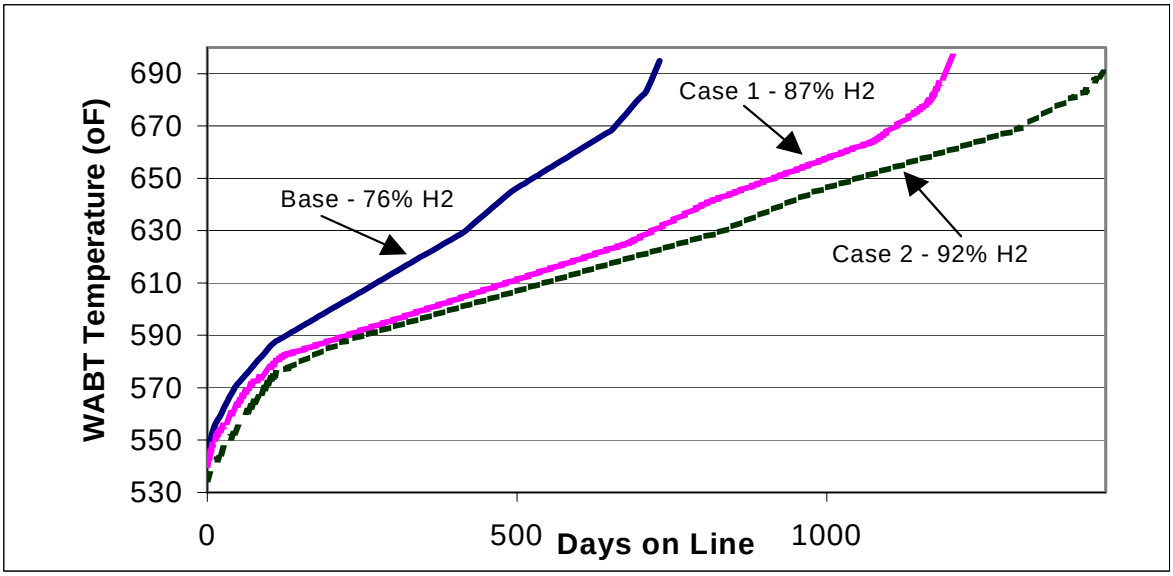

Figure 7.6 - Plant C run length impacted by increase in H_2 purity (ideal case, no disturbances). Two cases were run with the 87% and 92% H_2 purity cases generating a run length of 3.3 and 3.93 years, respectively. The actual base plant run length was 1.71 years. Without and disturbances, the model creates a classical s-shaped curve (as per the Thiele modulus) for the WABT.

Table 7.1 shows a more in depth analysis of the case study presented in figure 7.5 for plant C. Purity 1a and 2a in table 7.1 reflect the WABT profiles for case one and two of figure 7.5. Purity 1b and 2b evaluate the impact of reduced recycle rate (reduced operating cost savings) and thus hydrogen partial pressure on hydrotreater run length. Purity alone cannot improve hydrotreater operation. The flow of hydrogen is also necessary to obtain the required increase in hydrogen partial pressure.

From these case studies the following conclusions can be summarized: the higher the hydrogen partial pressure, the longer the run length[7,9,20,24,26] . The cost of hydrogen was set at $0.84/kscf and the recycle stream was blended with 99% pure hydrogen to obtain the increased recycle hydrogen purity. The benefit was calculated as the net present value of a shutdown that was not necessary due to the increased run lengths. The cost of a recent Plant C VGO hydrotreater shut down is approximately $30MM[3]. Incorporating all the costs, the operational cost savings value of up to $24MM (Net Present Value) for Case 1a if a shutdown can be avoided every two years.

Table 7.1– Application of Model: Vary H_2 purity and H_2 recycle to increase Hydro-treater run length

Application of Dynamic model	Base	Purity 1a	Purity 1b	Purity 2a	Purity 2b
VGO Hydrotreater					
Charge Rate	14.4	14.4	14.4	14.4	14.4
Recycle Purity	76.8%	92.0%	92.0%	87.0%	87.0%
Recycle Rate MMSCFD	28	28	17.1	28.0	17.1
Average H2 Partial Pressure	560	675	578	631	571
% Change in Deactivation Rate	Base	~ 50% Decrease	~15% Decrease	~40% Decrease	~10% Decrease
Cost: Increased H2 cost (base 1.8 yr run length)		$4.8MM	$5.4MM	$4.5MM	$4.8MM
Benefit: Extend run length to x years	Base	4	2.3	3.3	2.2
S/D savings		Save 1 every 2yr	Save 1 every 16 yr	Save 1 every 6 yr	Save 1 every 22 yr
$ Value (NPV) $30MM for S/D		**$24 MM**	$1.1MM	**$8.7MM**	$-1.1MM

7.3 Application – Increased Crude Flow

Table 7.2, on page 200, shows a summary of the economic benefits that can occur by using increased hydrogen purity at the same hydrogen flow rate (and thus higher hydrogen partial pressure) for all 6 plants. The developed model provides a valuable software tool that can be used to understand the impact of

changing a key process variable on the overall economics of the VGO hydrotreater operation. Refiners/operators, as noted earlier, do require confidence, and reliable justification before considering a project that might improve operations. The developed model does provide the necessary confidence to refiners/operators for VGO hydrotreater economic analysis because of the incorporated features and was validated using actual plant data from multiple refiners/operators. For this analysis, the run lengths, hydrogen flow, sulfur outlet composition and WABT were left the same as those in the plant data. No extrapolation of plant data past the run length was attempted. With increased H_2 purity (up to 99.9%) catalyst deactivation was reduced (for coking, but not for metals deposition), and the model translated this benefit into increased crude flow. Table 7.2 includes the average increased crude production over the run length. As described in previous sections, certain disturbances provided the opportunity to recover more crude production however, over the entire run, this positive impact is not sustained but still positive.

Table 7.2 – Value of Increasing H_2 purity via Increased Crude Throughput

Plant	Avg %H2	H2 Flow mmscfd	Avg Crude KBPD	Avg Crude Increase KBPD	$MM for entire run length	$MM /yr over run length
A	83	33	15.8	2.5	33.7	13.0
B	77	21	13.5	3.2	45.3	22.6
C	76	28	14.4	2.2	20.3	11.3
D	88	35	13.1	2.5	13.5	12.5
E	86	23	11.3	1.5	20.0	6.7
F	91	48.6	26.5	3.6	39.9	17.5

For the value calculation in Table 7.2, an average price of $0.84/kscf for 99% pure hydrogen and a $25/bbl crude upgrade value was used. The additional

crude that could be processed ranged from an average of 1.5KBPD to 3.6 KBPD with value (revenue from added crude production – cost of 99% pure hydrogen from a third party) for each plant ranging from $13.5 MM to $45.3MM CAD over the run length for each plant (or $6.7MM-22.6MM per year). These values may not make the top of a refiner's/operator's economic project priority list, but the values are certainly large enough that strong consideration should be made for providing a method to increase the hydrogen partial pressure (via increased hydrogen purity) where possible. A value was not assigned to the benefits to downstream units having less sulfur and/or metals in the feed.

7.3.1 Increase Recycle pressure to improve Catalyst Activity

Refiners/Upgraders can also increase recycle pressure, and thus reactor pressure, to increase hydrogen partial pressure to improve catalyst performance. A booster compressor is typically added to the recycle circuit. A comparison between increasing hydrogen partial pressure via increased reactor pressure and increasing hydrogen partial pressure via increased hydrogen purity is an important analysis in determining which route, if any, to take to improve VGO hydrotreater performance. Table 7.3, on page 202, shows the results from increasing hydrogen purity (from Table 7.2) to 99% and if the recycle pressure is increased by 15%[3]. The increased recycle pressure creates an increase in catalyst activity, resulting in an average increase of crude flow in the range of 0.7 kBPD to 1.7 kBPD.

Table 7.3 – Compare Increasing Recycle Pressure versus Increasing H_2 Purity

Plant	Existing Reactor		Model - 99% H2		Model - P up 15%	
	Pressure PSIG	P_{H2} PSIG	P_{H2} PSIG	Avg Crude Increase KBPD	P_{H2} PSIG	Avg Crude Increase KBPD
A	675.0	560.3	668.3	2.5	644.3	1.2
B	1065.0	820.1	1054.4	3.2	943.1	1.7
C	970.0	737.2	960.3	2.2	847.8	1.2
D	1550.0	1364.0	1534.5	2.5	1568.6	1.1
E	460.0	395.6	455.4	1.5	454.9	0.7
F	475.0	432.3	470.3	3.6	497.1	1.6

The increase in crude flow from increased recycle pressure is 43-54% of the increase in crude flow from increased hydrogen purity. The impact of increased hydrogen purity in the developed model translates into a more effective way of mitigating catalyst deactivation versus simply increasing the reactor pressure[20].

7.4 Decision Making/Training Tool

Another benefit of the model was highlighted in nearly all the plants analyzed in chapter six. The model can be used:

a) as a decision making tool base on process variable changes

b) as a training and learning tool to gain operating experience

c) as a troubleshooting tool to identify faulty measurements

thus aiding operators in operating the hydrotreater more effectively. Often, operator decisions contributed to increased catalyst deactivation as noted in Figures 6.9 (plant E), Figure 6.11 (plant F) and Figure 6.15 (plant B), and thus reduced the reactor run length. Figure 6.15 shows that the temperature was re-adjusted upward by operations rather quickly to prevent/minimize “off-spec”

sulfur. These examples (March 30th and July 5th) for plant B illustrate the value of the model as a tool to set the appropriate operating conditions due to changes in the feed composition. The model would limit sulfur specification excursions, along with increasing catalyst life but not exposing the catalyst to such sudden swings in temperature and stresses caused by sub-optimal operator decisions.

The model can be used to identify measurements that are off and also provide confidence to operators to make changes based on the model output when certain measurements (ex. Lab analysis for sulfur product) are not available. For plant C, the sulfur outlet lab analysis was providing faulty readings and the operators were essentially operating “blind”. The model can be used to predict the product composition, thus provide input into operational process variable settings.

Finally, plant A provides an example (Figure 6.15) where operations made an incorrect temperature adjustment when the feed sulfur increased. The sulfur “spiked” and operations lowered the WABT, when it should have been raised to increase catalyst activity to mitigate the added sulfur. Alternatively, the crude flow could have been lowered, and/or hydrogen partial pressure increased, but these were not done, so lowering the WABT was detrimental to the process. Based on the conditions entered into the model, the model WABT increased as would be expected. The model should/could have been used to validate any operational

changes. Note, all the above examples of operator ineffectiveness could have been mitigated by using the model developed in this research project.

7.5 Summary

The developed model, via case studies using actual plant data, can be used to improve the operation and effectiveness (increasing crude flow and/or run length), of a VGO hydrotreater by being a tool for learning and training operations, by being a decision making tool during plant operation to improve variable change decisions and by being a tool to quantifiably and justify the addition of higher purity hydrogen (where applicable) for increased crude production.

Case studies were performed using the validated model to illustrate that the model can be used to modify the hydrogen purity to determine its impact on key hydrotreater operating objectives that include maintaining sulphur product content below specification, increasing crude flow for same run length and increasing run length at a given average crude flow rate. The developed model does provide the refiners/operators with a tool to add millions of dollars of value to their VGO hydrotreaters by increasing the purity of hydrogen in the feed to the reactor.

Chapter 8: Conclusion

8.1 Objectives Achieved

A very key element of this research project entailed gathering a substantial amount of relevant industrial data specific to vacuum gas oil hydrotreaters. The gathered and vetted data is required to validate a theory based, correlation optimized lumped parameter steady state hydrotreater model that is embedded in a dynamic model that is part of a commercially available software package (HYSYS®). The specific objectives of this study can be summarized as follows:

1. Develop a correlative, partially predictive model that simulates the process over the length of an industrial hydrotreater's operation incorporating the effects of catalyst activity specific to "start of run", "middle of run" and "end of run".
2. Apply the model to determine economic ways to improve the operation of a VGO hydrotreater.

A first-of-a-kind dynamically oriented lumped parameter industrial VGO hydrotreater model that incorporates key variables to provide an accurate representation for industrial conditions was developed. The model:

1. uses lumped parameters that match data available from industrial operations,
2. uses a mix of industrial correlations, kinetic theory and academic research findings,
3. factors in changes in operating conditions in response to disturbances in operation,

4. incorporates changing reaction rate, wetting efficiency, catalyst deactivation in the three zones of the hydrotreater run life,
5. uses parameters for all key process variables,
6. is run in dynamic mode to track the key variable product sulfur and the representative value of performance (WABT),
7. incorporates familiar software (Excel® and HYSYS®) for easy translation into existing operations and acceptance by users, and
8. is partially predictive.

By using industrial data for validation purposes, and creating a model that responds to various disturbances during the entire hydrotreater operation, refiners/upgraders will now have the necessary software tool to justify the use, and have confidence to introduce the concept of increased hydrogen (purity and thus partial pressure) to improve hydrotreater operation. Improved operation does translate into increased crude through put capacity either by more crude produced during a given run length or increased run length for a given crude.

8.1.1 Plants Evaluated

Six plants were analyzed illustrating how the model compared to the plant WABT and sulfur outlet composition. Table 6.2, on page 206, reproduced from chapter 6, provides a summary of the statistical comparison of the model predictions to the plant data.

For the product sulphur the model had an R^2 of 0.86-0.88 for two plants (A,F) and over 0.90 for the other four plants. For the WABT, the model had an R^2 in the range of 0.91 to 0.935.

Table 6.3 – Statistical Results for each Plant – Model vs. Plant

	Plant A	Plant B	Plant C	Plant D	Plant E	Plant F
Sulfur R^2	0.86	0.92	0.90	0.93	0.95	0.88
WABT R^2	0.91	0.925	0.925	0.927	0.935	0.916

Overall, the model provides a credible match of the overall plant operation for a lumped parameter model. The major mismatches are typically due to inaccuracies in the plant measurements and the operator choices (on temperature) that are not always optimal for the situation. These anomalies were not matched and of course one would not want to include them in the plant data sets. In addition, since the model is by design lumped, the model will not be able to capture all the cause and effect relationships from the various disturbances. As a result, statistically, the best the model will likely accomplish is in the 0.93-0.95 R^2 range.

Overall, refiners/operators now have a tool that responds to and reflects actual industrial plant operation, hence the model can be used to determine whether changing operational variables to improve VGO hydrotreating operation is economically feasible. Since operators struggle to meet run length targets, a tool to realistically analyze options was needed.

8.1.2 Application of Model

The model developed in this study can be used to improve the operation and effectiveness (increasing crude flow and/or run length), of a VGO hydrotreater by:

1. being a tool for learning and training operations
2. being a decision making tool during operation to improve variable change decisions
3. being a tool to quantifiably justify the addition of even higher purity hydrogen (where applicable) for increased crude production.

Case studies were performed using the validated model to show that the model can be used to modify the hydrogen purity and to determine its impact on the key hydrotreater operating objectives of:

1. Maintain sulfur in the product below specification
2. Increase crude flow for same run length
3. Increase run length at given average crude flow rate

The results would indicate that refiners/operators should be able to add millions of dollars of value to their VGO hydrotreaters by increasing the purity of hydrogen in the feed at a constant hydrogen flow to the reactor. The additional crude that could be processed ranged from an average of 1.5KBPD to 3.6 KBPD with value ranging from $13.5 MM to $45.3MM CAD. These values may not make the top of a refiner's/operator's economic project priority list, but the values are large enough that strong consideration should be made for providing the provision to

increase the hydrogen partial pressure (via increased hydrogen purity) where possible.

8.2 Benefits of the Model

Nearly all literature for HDS dynamic models is based solely on validation with pilot plant data [4,21,32]. This approach to model validation does not transfer well to industrial applications for the following reasons:

1. Previous dynamic models were run only for some forty minutes to three months in length [4,21,32]
2. Multiple variable disturbances and operator responses are not considered[4,12,20]
3. Low conversion occurs since a pilot plant reactor length is 10-20 times shorter[7,12]

All the dynamic models developed are run over such a short time, that the accuracy of any catalyst deactivation factors, if included, cannot be ascertained. In addition, the robustness of these models cannot be verified since the interaction of various variables (crude, temperature and hydrogen changes) is not demonstrated. Finally, non-validated correlations[40-44] have been developed and used to model the incomplete catalyst wetting through contacting effectiveness that creates lower sulfur conversion in pilot plants. As a result, there is little or no confidence in scaling up a pilot plant validated dynamic model to industrial scale conditions.

Any one of these factors are reason enough to create a dynamic VGO hydrotreater model that is valid over an entire run length (at least 1.5 years) of an

industrial plant. The model developed in this study addresses the above shortcomings of the existing research when applied to an industrial setting. Hence, to meet this study's primary objective, detailed industrial data from various sources was needed and was gathered from forty-five refineries/upgraders. For publication purposes, confidentiality agreements with six of the refinery/upgrading operators (all in North America) have been obtained. Catalyst, process and laboratory data, and equipment information was among the necessary data needed and gathered. Access to this information is crucial for this study and can, of course, now be used by other researchers to further the development.

Since a major aim of the study was to develop a model that refiners/operators could readly use it has the following features:

1. Readily available to the operators
2. Uses familiar software tool(s)
3. Relatively inexpensive
4. User friendly

For instance, all the necessary kinetic relationships and correlations, such as outlet sulfur concentration and hydrogen consumption, are Excel® based at each time calculated. HYSYS® is used to simulate the entire unit and run the model in dynamic mode.

In addition to the wetting efficiency impacting the HDS trickle bed reaction rate, the following factors impact reaction rate[7,9,10,12,15,20] and are included in the model:

1. Catalyst deactivation
2. Catalyst type
3. Temperature
4. Pressure
5. Feed
6. % hydrogen
7. Recycle hydrogen flow rate

In summary, the benefits of the developed model are:

1. Actual plant data was used to develop this completely new model
2. No issues with scaling up from a laboratory plant scale data based model
3. Model matches disturbances well, with key performance variables included
4. Provide confidence to refiners/upgraders to justify increasing hydrogen use to improve operations
5. Model is lumped parameter based on readily available plant data so use can be widely applied

8.3 Limitations of the model

The following limitations of the developed model should be appreciated when using the model:

1. Model is dependent on available process and laboratory data
2. Need to modify model's parameters to address each refiner's/upgrader's specific crude and catalyst

3. Model is lumped so can't be used to decipher detailed catalyst performance and interaction between phases

Considering the objectives set out and met in this study, the limitations are minimal.

8.4 Summary

A high fidelity dynamic model for industrial refinery/upgrader hydrotreaters has been developed based on 14 actual operating hydrotreaters (six publishable). The model accurately simulates local disturbances, and performs well over the entire run length of the hydrotreater. This robust model can be applied to demonstrate the tangible economic benefit of increasing hydrogen (purity and flow) use to improve the operation of a hydrotreater by increasing run length and/or improving crude processing. The objectives of the study have been accomplished and have successfully demonstrated the following:

1. Experimentation (gathering and using multiple industrial scale reactor data),
2. Correlation (improved parameters, new applications of relationships)
3. Application (vary key parameter to demonstrate improving VGO hydrotreater operation)

REFERENCES

1. US Federal Register, *Rules and Regulations*,**V55**, #28, 4722-4770 (2000)
2. Golden, S. and Martin, G., *ePTQ*, 64-71 Spring (2005)
3. Remesat, D., *Personal Interviews with Operators* (2000-2006)
4. Mederos, F., Rodriquez, M.,Ancheyta, J. and Arce, E., *Energy & Fuels*, **20**, 936-945 (2006)
5. Robinson, P., *ePTQ*, Spring, 43-49 (2004)
6. Nelson, W.L., *Petroleum Refinery Engineering*, McGraw-Hill, 4th Edition (1969)
7. Katalco, *Hydroprocessing Catalyst Seminar* (1985) CONFIDENTIAL
8. Freeman S. et al, *AICHe*, ISBN 0-8169-0814-1 (2000)
9. Lucien, P., van den Berg, J.,Germaine, G. Hooijdonk, M. Gjers, M. and Thielmans, G. , *Catalytic HydroProcessing of Petroleum and Distillates*, **16**, 291-313 (1993)
10. Satterfield, C., et al, *AICHe Journal*, March 1969, Vol. 15, 226-234
11. HYSYS, *Dynamic Control Concepts*, Chapter 8, 2001
12. Korsten, H., and Hoffmann, U., *AICHe Journal*, May, Vol. 42,No.5, 1352-1360 (1996)
13. Ho, T.,Hydrotreatment and Hydrocracking of Oil Fractions, Elsevier Science B.V., 179-186 (1999)
14. Aris, R., Archive Rational. Mechanical Analysis, 27, 35-39 (1968)
15. Smith, M.J., *Chemical Engineering Kinetics*, Third Edition, McGraw-Hill (1981)

16. Fogler, H.S., Elements of Chemical Reaction Engineering, Second Addition, Prentice Hall (1992)

17. W.L. Nelson, *Oil and Gas Journal*, December,139-145 (1970)

18. D.C. McCulloch and R.A. Roeder, *Hydrocarbon Processing*, February, 46-57 (1976).

19. Thakur,D., and Thomas, Michael, *Applied Catalysis*, **15**, 197-225 (1985)

20. Bartholomew, C.H., *Catalytic HydroProcessing of Petroleum and Distillates*, **16**, 1-32 (1993)

21. Chao, Y., Liaw, H., and Huang, H., *Chemical Engineering Communications*, Volume 104, pp 267-290 (1991)

22. Dumesic, J., Fixed Bed Catalytic Reactors, University of Wisconsin, Nob Hill Publishing (2006)

23. Nelson, W.L., *Oil and Gas Journal*, November, 72.-87(1976)

24. Van Speybroeck, V. and Reyniers, M., Marin, G., Waroquier, M., *CHEMPHYSCHEM*, **3**, 863-870 (2002)

25. Satterfield, C., *AICHe Journal*, **Vol. 21**, No. 2 March, 209-229 (1975)

26. Gianetto, A. and Specchia, V., *Chemical Engineering Science*, Vol. 47, No. 13/14, 3197-3213 (1992)

27. Narasimhan, C., Sau, M. and Verma, R*., Hydrotreatment and Hydrocracking of Oil Fractions*, 297-306 (1999)

28. Oballa, M., Wong, C. and Krzywicki, A*., Catalytic Hydroprocessing of Petroleum and Distillates*, **2**, 33-54 (1993)

29. Koyama, H., Nagai, E., Torii, H., and Kumagai, H*., Catalysts in Petroleum Refining and Petrochemical Industries*, 147-155 (1995)

30. Leglise, J., Finot, L., van Gestel, J., and Duchet, J*., Hydrotreatment and Hydrocracking of Oil Fractions*, 51-65 (1999)

31. Tamm, P., Harnsberger, H., and Bridge, A*., Industrial Engineering Chemical Process Design and Development,* **20**, 262-273 (1981)

32. Kodama, S., Nitta, H., Takatsuka, T., Yokoyama, T*., Journal of the Japanese Petroleum Institute*, **23**, 5, 310-320 (1980)

33. Levenspiel, O., and Szepe., S. *Chemical Engineering Science*, **23**, 881-914 (1968)

34. Kokayeff, P., *Catalytic Hydroprocessing of Petroleum and Distillates*, **14**, 253-278 (1993)

35. Hu, M. et al, *PTQ*, 2001, Spring, Refining, 47-53

36. Haitham, M., Lababidi, H., Al-Radwan, S., Alper, E., Chemical Engineering Technology, 21, 193-200 (1998)

37. Dohler, W., and Rupp, M., *Chemical Engineering Technology*, **10**, 349-352 (1987)

38. Ancheyta-Juarez, J., Aguilar-Rodriquez, E., Salazar-Sotelo, D., Betancourt-Rivera, G., and Quiroz-Sosa, G., *Hydrotreatment and Hydrocracking of Oil Fractions*, 347-350 (1999)

39. Chowdhury, R., Pedernera, E., and Reimert, R., *AICHe Journal*, **Vol 48**, No. 1, 126-135 (2002)

40. Hofman, H., *International Chemical Engineering*, Vol. 17, No. 1, 19-27, January (1977)

41. Satterfield, C., Pelosso, G., and Sherwood, T., *AIChE Journal*, 226-234, March (1969)

42. Iliuta, I., Thyrion, F., and Muntean, O., Transaction *IchemE*, Vol 76, Part A, January (1998)

43. Iliuta, I., Larachi, F., and Grandjean, B., *Chemical Engineering Science*, **54**, 4099-4109 (1999)

44. Al-Dahhan, M., and Dudokovic, M., *Chemical Engineering Science*, **50**, 2377-2389 (1995)

45. Froment, G.F., and K.B. Bischoff, *Chemical Reactor Analysis and Design*, 2nd Edition, John Wiley & Sons, Inc., NY. (1990)

46. Hu, M., Te, M., Briker, J., Ring Z., *ePTQ*, Spring, 85-91 (2002)

47. HYSYS, *Dynamic Simulation*, Chapter 8, (2001)

48. Svrcek, W., Mahoney, D., Young B., *A Real-Time Approach to Process Control*, 1st Edition, John Wiley & Sons, Inc., NY. (2000)

49. Behie, L., *Reactor Design*, ENCH617-University of Calgary Course Notes (2001)

50. Dautzenberg, F., Van Klinken, J., Pronk, M., Sie, S., and Wiffles, J, 5th *International Symposium on Chemical Reaction Engineering*, Houston, March 13-15 (1978)

51. Silbernagel,G.,Riley, K., *Catalyst Deactivation*, Elsevier, Amsterdam, p. 313-321 (1980)

52. Oballa, M., Wong, W., Kryzwicki, A., *AICHe Annual Meeting Presentation*, San Francisco, Nov. 5-10 (1989)

53. Tamm, P., Harnsberfer, H., and Bridge, A*., International Engineering Communications, Process Design Development*, 20 (1981)

54. Hannerup, P., and Jacobsen, A*., American Chemistry Society, Petroleum Chemistry*, **28**, 576 (1983)

55. Jacobsen, A., Hannerup, P., Cooper, B., Bartholdy, J., and Nielsen, A., *AICHe Presentation*, Houston, March (1983)

56. Remesat, D., *Inside-Out Design Approach to Improving Distillation Operation, Hydrocarbon Processing*, August (2006)

57. Kreysig, E., *Advanced Engineering Mathematics*, Sixth Edition, John Wiliey & Sons, (1988)

58. Chevron Research Company, *Desulfurization Equilbrium*, 1993 CONFIDENTIAL

59. Seborg, D.E., Edgar, T.F., and Mellichamp, D.A*., Process Dynamics and Control, John Wiley and Sons*, USA (1989)

60. Kaes, G., *Refinery Process Modeling*, First Edition, The Athens Printing Company, USA (2000)

61. Private Discussion with PDVSa Hydroprocessing Specialist, AIChE Houston, (2007)

62. Private Discussion with AspenTech Hydroprocessing Specialist, AIChE Houston, (2007)

63. Praxair, Inc., *Six Sigma Statistical Training Manual*, (2004)

APPENDIX A

REACTOR INFORMATION

Plant A

ID in Ft. =	*13*	***Revision***	***1***
132.732	**Ft2/Ft Cross. Area**		

Ft3	Catalyst	BED # / Function	Inches
44	KG-50		4
66	KF-542-5R		6
66	KF-542-5.4Q		6
3263	**KF-557R-3Q**	(Regen - from PB)	295.00
		Rx Catalyst	
		Total Ft3 = **4424**	
		% Fresh = **0.0**	
1161	**KF-655R - 1.5E**	(Regen - from PB)	105.00
		Catalyst down to 6" below TL	
25	1/8" Support	These Ft3	
40	¼" Support	Are Approx.	
80	½" Support		
4569	**Ft3 Total**		
4424	**Ft3 Catalyst**		

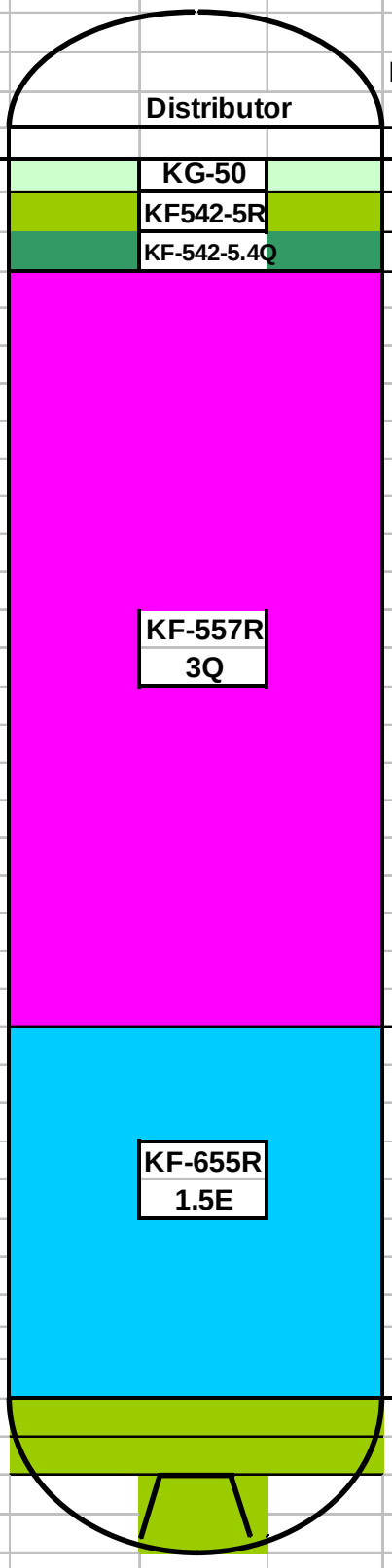

Plant B

ID in Ft. =	*12*	***Revision***			EST.
113.097	**Ft2/Ft Cross. Area**			**Inches**	**Height Feet / In.**
Ft3	**Catalyst**	**BED # / Function**	**Distributor**		12"
38	TK-10 - 5/8"		**TK-10**	4	4"
57	TK-711 - 3/16"		**TK-711**	6	6"
57	TK-551 - 3/16"		**TK-551**	6	6"
226	**KF-843R - 3Q**	(Regen - from PB)	**KF-843R 3Q**	24	**2'0"**
952	**KF-901R - 1.5E**	(Regen - from PB)	**KF-901R 1.5E**	101	**8'5"**
		Rx Catalyst			
		Total Ft3 = **2865**			
		% Fresh = **0.0**			
1687	**KF-843R-1.3Q**	(Regen - from PB)	**KF-843R 1.3Q**	179.00	**14'11"**
		Catalyst down to 6" below TL			
25	1/8" Support	These Ft3			**Btm.**
40	¼" Support	Are Approx.			
80	½" Support				**0**
3010	**Ft3 Total**				**Total**
2865	**Ft3 Catalyst**				

Plant C

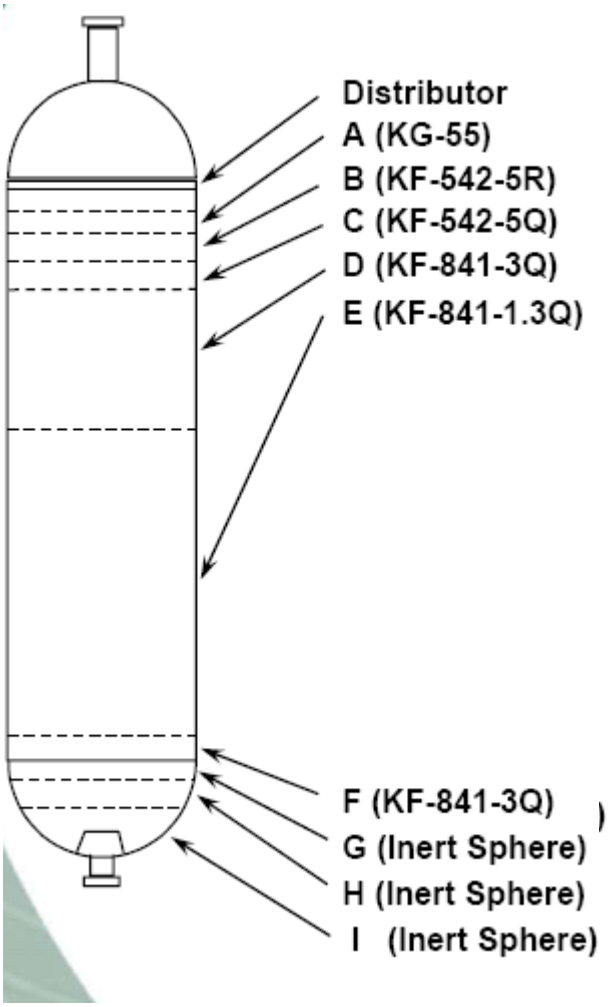

Layer	Depth	Size	Material	Example
A	6" - 1'	5/8"	High Void Inert	KG-55
B	1 - 2'	1/5"	Active Ring	KF-542-5R
C	1 - 2'	1/5"	Active Support	KF-542-5Q
D	20 - 30%	1/10"	NiMo Catalyst	KF-841-3Q
E	70 - 80%	1/20"	NiMo Catalyst	KF-841-1.3Q
F	6" - 1'	1/10"	NiMo Catalyst	KF-841-3Q
G	6" - 1'	1/4"	Inert Sphere	
H	6" - 1'	1/2"	Inert Sphere	
I		1"	Inert Sphere	

A, B, C, D – Top Beds / Grading
Contaminant & Particulate Control

D, E, F – High Activity Catalyst Beds
HDS, HDN, ASAT Reactions

F, G, H, I – Bottom Grading
Stabilize Catalyst Beds

Plant D

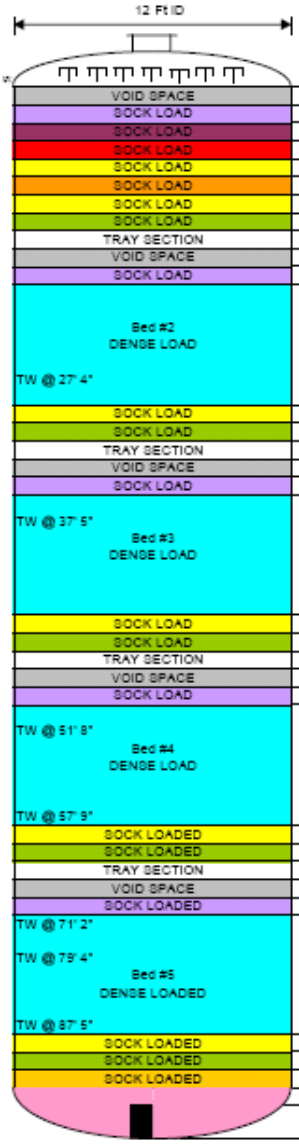

	Outage (Ft)	Outage (in)	Catalyst Type	Vol/Rx (cuft)	Mass/Rx (lbs)	Number of Containers			
	8'	1"							
VOID SPACE	9'	4"	void						
SOCK LOAD	9'	11"	Inert 5/8"	66.00	2970.0	9 X 330 DRUM	38370.0	0.12	1 Magnesium Aluminate Grading Inert
SOCK LOAD	11'	0"	NiMo 3/16"	123.00	3600.0	3 X 1200 BAGS			Grading Catalyst
SOCK LOAD	12'	4"	NiMo 1/8"	151.00	6000	5 X 1200 BAGS			Grading Catalyst
SOCK LOAD	16'	5"	NiMo 1/12"	471.00	18000.0	10 X 1800 BAGS			Silicon trap Catalyst
SOCK LOAD	18'	0"	Ni 1/15"	170.00	6000.0	4 X 1500 BAGS			Arsenic Trap
SOCK LOAD	18'	6"	NiMo 1/12"	57.00	1800.0	1 X 1800 BAG			Silicon trap Catalyst
SOCK LOAD	18'	9"	1/4" BALLS						Inert support
TRAY SECTION	22'	8"	tray						
VOID SPACE	23'	4"	void						
SOCK LOAD	23'	10"	Inert 5/8"	57.00	2970.0	9 X 330 DRUM	28170.0	0.09	2 Magnesium Aluminate Grading Inert
Bed #2 DENSE LOAD			NiMo 1/16"	509.00	23400.0	13 X 1800 BAG			Hydrotreating Catalyst
TW @ 27' 4"									
	28'	4"							
SOCK LOAD	28'	7"	NiMo 1/12"	28.00	1800.0	1 X 1800 BAG			Silicon trap Catalyst
SOCK LOAD	28'	10"	1/4" BALLS	28.00					Inert support
TRAY SECTION	32'	9"	tray						
VOID SPACE	33'	5"	void						
SOCK LOAD	33'	11"	Inert 5/8"	57.00	2970.0	9 X 330 DRUM	49770.0	0.16	3 Magnesium Aluminate Grading Inert
TW @ 37' 5" Bed #3 DENSE LOAD			NiMo 1/16"	980.00	45000.0	25 X 1800 BAG			Hydrotreating Catalyst
	42'	7"							
SOCK LOAD	42'	10"	NiMo 1/12"	28.00	1800.0	1 X 1800 BAG			Silicon trap Catalyst
SOCK LOAD	43'	1"	1/4" BALLS	28.00					Inert support
TRAY SECTION	47'	0"	tray						
VOID SPACE	47'	8"	void						
SOCK LOAD	48'	2"	Inert 5/8"	57.00	2970.0	9 X 330 DRUM	78570.0	0.25	4 Magnesium Aluminate Grading Inert
TW @ 51' 8" Bed #4 DENSE LOAD			NiMo 1/16"	1574.00	73800.0	41 X 1800 BAG			Hydrotreating Catalyst
TW @ 57' 9"	62'	1"							
SOCK LOADED	62'	4"	NiMo 1/12"	28.00	1800.0	1 X 1800 BAG			Silicon trap Catalyst
SOCK LOADED	62'	7"	1/4" BALLS	28.00					Inert support
TRAY SECTION	66'	6"	tray						
VOID SPACE	67'	2"	void						
SOCK LOADED	67'	8"	Inert 5/8"	57.00	2970.0	9 X 330/DRUM	121770.0	0.38	5 Magnesium Aluminate Grading Inert
TW @ 71' 2" TW @ 79' 4" Bed #5 DENSE LOADED			NiMo 1/16"	2347.00	115200.0	64 X 1800 BAG			Hydrotreating Catalyst
TW @ 87' 5"	88'	5"							
SOCK LOADED	88'	11"	NiMo 1/12"	57.00	3600	2 X 1800 BAG			Silicon trap Catalyst
SOCK LOADED	88'	3"	1/4" balls	25.00					Inert support
SOCK LOADED	89'	7"	1/2" balls	25.00					Inert support
	89'	11"							
			3/4" INERTS	70.00					Inert support
	91'	6"			316650.0			1.00	

Plant E

ID in Ft. =	*11*	***Revision***	***0***		EST.
95.033	Ft2/Ft Cross. Area				Height
				Inches	Feet / In.
Ft3	**Catalyst**		Distributor		
		BED # / Function			12"
32	TK-10 - 5/8"		**TK-10**	4	4"
48	TK-711 - 3/16"		**TK-711**	6	6"
48	TK-551 - 3/16"		**TK-551**	6	6"
190	**NM-761**		**NM-761**	24	**2'0"**
863	**NM-504**		**NM-504**	109	**8'5"**
		Rx Catalyst			
		Total Ft3 =	**2415**		
		% Fresh =	**0.0**		
1362	**NM-761**		**NM-761**	172.0	**14'6"**
		Catalyst down to 6" below TL			
25	1/8" Support	These Ft3			**Btm.**
40	¼" Support	Are Approx.			
80	½" Support				**0**
2560	**Ft3 Total**				**Total**
2415	**Ft3 Catalyst**				

Plant F

ID in Ft. =	*14*	***Revision***	***0***
153.938	**Ft2/Ft Cross. Area**		

Ft3	**Catalyst**	**BED # / Function**		**Inches**
154	HVIS			12.0
99	520X			7.7
0				
406	**526m**		8.7332452	31.7
3462	**535**		74.376539	269.8
		Rx Catalyst		
		Total Ft3 =	**453**	
		% Fresh =	**100**	
		Fresh - Purchase		
		Catalyst down		
47	**535**	**to 6" below**	1.0098681	3.7
77	**520X**			6.0
25	1/8" Support	These Ft3		
40	¼" Support	Are Approx.		
80	½" Support			
4333	**Ft3 Total**			
4189	**Ft3 Catalyst**			

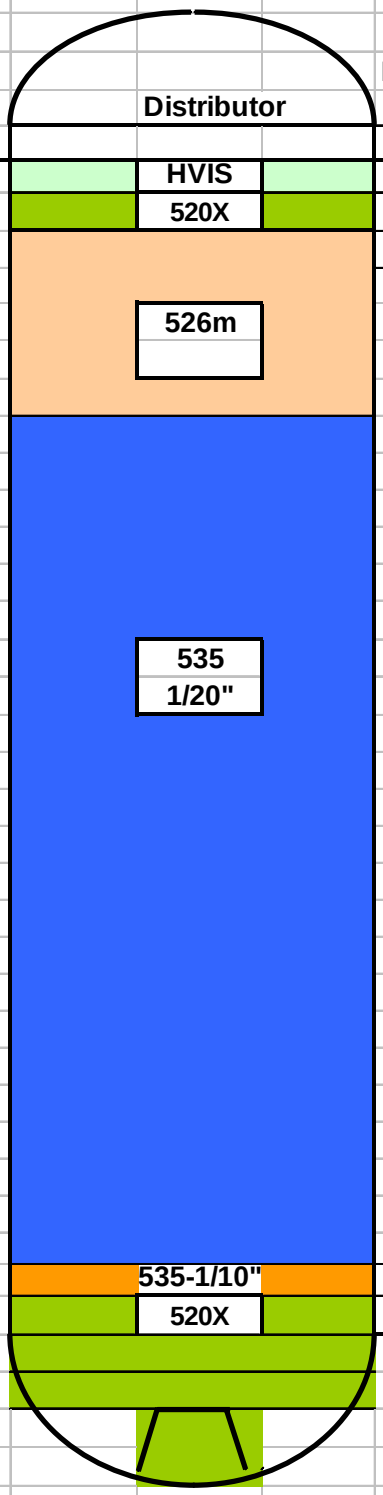

APPENDIX B

PROCESS INFORMATION

Order:

Plant B
Plant F
Plant A
Plant D
Plant C
Plant E

Plant B

			29-Jul-99
Total Feed		MBPD	11.2
LCO Feed		**MBPD**	**1.7**
Charge	API	API	31.7
	Sulfur	wt%	1.046
Product	**API**	**API**	**32.6**
	Sulfur	**wt%**	**0.046**
	Flash Pt.	**Deg. F**	**182.0**
	Cloud Pt.	**Deg. F**	**22.0**
	Pour Pt.	**Deg. F**	**15.0**
	ASTM Color		**1.5**
	End Point	**Deg. F**	**667**
Cetane (old)			**47.48**
Cetane (new)			**48.42**
% Desulfurization		**%HDS**	**95.6**
API Improvement		**API**	**0.97**
H2 Consump. To Diesel		**scf H2/bbl**	**#VALUE!**
Reactor Inlet T		**deg F**	**714.6**
Bed 1 Delta T		deg F	#VALUE!
Bed 1 WABT		deg F	#VALUE!
Bed 1 Radial Delta T		deg F	#VALUE!
Bed 2 Delta T		deg F	#VALUE!
Bed 2 WABT		deg F	704.7
Bed 2 Radial Delta T		deg F	#VALUE!
Reactor Inlet P		psig	325.7
Reactor ΔP		**psi**	**8**
Rctr ΔP, Feed/Recy Corr.		psi	7.2
DP Increase Rate		psi/day	-0.01
Next SHDN, Based on ΔP			note 1
Total H2 Consumption		scf H2/bbl	-42
Treat Ratio		scf H2/bbl	731
H2 Partial Press., Rx In			292
H2 Partial Press., Rx Out			#VALUE!
Wild Naphtha		MBPD	0.21
LHSV		1/hr	0.5
Product	Rate	MBPD	11.3
Unit Balances		LVY%	98.4
		Mass Bal.	#VALUE!
Operating Costs			
Charge Heater Duty		MMBtu/h	
Frac Heater Duty		MMBtu/h	
Fuel Gas Cost		$/Day	
Net Steam Usage		M#/h	

Steam Cost			$/Day	
Hydrogen Consumption				
H2 IN	Pass A	MMSCFD		4.57
H2 IN	Pass B	MMSCFD		4.57
H2 Purity		%		89.57
MMSCFD H2 IN		MMSCFD		**8.19**
Cold sep. off Gas	DFI149.PV	MMSCFD		10.14
Cold sep. off gas H2 purity		%		85.36
Stripper off gas	DFI238.PV	MMSCFD		0.32
Stripper off gas H2 purity		%		NR
MMSCFD H2 OUT		MMSCFD		**#VALUE!**
H2 Consump. To Diesel		SCFB		**#VALUE!**
Total H2 Consumption		SCFB		**-42.00**
Reactor DP Rate Of Increase				
7/8/1999	7/10/1999			
Use slope over a		day period		20.00
Base Feed Rate		MBPD		10.50
Base Recy Rate		MMSCFD		8.50
EOR Rx ΔP		PSI		70.00
		PSI	DIESEL RX PRESS DIFF	7.80
		MBPD	DIESEL TOTAL CHARGE	10.37
		MMSCFD	DIESEL TREAT HYDROGEN	9.80
Rctr ΔP, Feed/Recy Corr.		PSI		7.31
Next SHDN, Based on DP				29-May-74

LAB DATA ARCHIVE

TREAT HYDROGEN		
Gas Gravity		0.14
Net BTU	NBTU	343.84
Nitrogen	mol%	0.05
Hydrogen	mol%	89.57
H2S	mol%	2.40
CS OFF GAS		
Gas Gravity		0.21
Net BTU	NBTU	380.68
Nitrogen	mol%	0.04
H2 out cold separator	% H2	85.36
H2S	mol%	7.36
STRIPPER OFF GAS		
Gas Gravity		NR
Net BTU	NBTU	NR
Nitrogen	mol%	NR
H2 out strip ovhd.	% H2	NR
H2S	mol%	NR
VGO A152 PRODUCT		

IBP	^{O}F	399.10
2 Oil 05% Pt.	^{O}F	449.60
2 Oil 10% Pt.	^{O}F	478.60
2 Oil 30% Pt.	^{O}F	522.30
2 Oil 50% Pt.	^{O}F	551.80
2 Oil 70% Pt.	^{O}F	584.00
2 Oil 90% Pt.	^{O}F	633.30
2 Oil 95% Pt.	^{O}F	661.80
2 Oil End Pt.	^{O}F	666.60
Flash Pt.	^{O}F	182.00
Cloud Point	^{O}F	22.00
Pour Point	^{O}F	15.00
ASTM Color	^{O}F	1.50
Product Sulfur	wt.%	0.05
API Product	API	32.62
DIESEL FEED		
Feed Sulfur	wt.%	1.05
Feed API Gravity		31.65

PI VALUES

DATE 7/29/1999

TAG #	VALUE		UNITS	DESCRIPTION
GAI40A.PV		5.54331017	vol %	CHG HTR O2
DFC101A.PV		4.56570196	MMSCFD	DIESEL TREAT H2 PASS #A
DFC101B.PV		4.57348919	MMSCFD	DIESEL TREAT H2 PASSB
DFC183.PV		11.1696405	MBPD	DIESEL TOTAL CHARGE
10FC228.PV		1.7396673	BPD	HOT LCO PRODUCT TO HDS
DFC163 .PV		2299.26855	MLB/HR	STR STRIPPING STM
GFC631.PV		-67.880966	MLB/HR	S. STM TO FRAC
GFI507.PV		0.24887325	MMSCFD	CHG HTR FUEL GAS
DFI101AB.pv		9.14158154	MMSCFD	DIESEL TREAT HYDROGEN
DFI149.PV		10.1397581	MMSCFD	DIESEL COLD SEP OFF GAS
DFI238.PV		315.308685	MSCFD	DIESEL STRIPPER OFF GAS
GFI629.PV		-7.721E-05	MMSCFD	FRAC HTR FUEL GAS
DFI175.PV		208.953659	BPD	DIESEL WILD NAPTHA
GFI787.PV		4.13542938	MMSCFD	MAKEUP SPILLBACK FLOW
DMOLRAT.PV		730.72467	RATIO	DIESEL H2 TO FEED MOLE/RAT
dpc119.pv		325.660583	PSIG	DIESEL RX PRESSURE CONT
GPC633.PV		27.7160759	PSIG	FRACTIONATOR PRESSURE
dpdi116.pv		7.67250156	PSI	DIESEL RX PRESS DIFF
DTC234.PV		714.566345	DEG F	DIESEL CHG HTR TRANSFER
ISOFRC.PV	No good data for this point for this time: -106		MMBTU/HR	FRACTIONATOR HTR DUTY
DFI248.pv		11.2761869	MBPD	DIESEL PRODUCT

C2FC14.PV	9.30767536	MBPD	#2 OIL TO FIELD

Plant F

		8/26
Charge Rate, BPD		26347.3
LCGO mbpd		4.361772
Virgin mbpd		21.98554
API GRAV		35.1
API GRAV		35.3986
	10%	483
	30%	519
50%		546
70%		574
90%		611
FBP		639
SULFUR (WT%)		0.4716
NITROGEN (PPM)		362.7
Total Recycle		102.157
Makeup		23.9234
		512.8196
REC_H2%		73.19537
rxtr press out		1062.814
rxtr press out		989.237
		613.6047
		651.781
		648.49
		673.1208
		666.2817
		673.8832
bed4 top		666.2817
bed4 btm		673.8832
bed 1-3 A WABT		655.278
bed4 A delta T		-0.54932
bed3bdelta T		-0.54932
		24.62681
		38.17631
		62.2538
total		1.673857
bed 1-3A		2.438478
bed 1-4A LHSV		5.220566
naphtha		2612.959
naphtha		6.22346
FBP		354
IBP		424
#2 FO SUL, ppm		153
#2 FO Product Nitrogen (ppm)		2.41

naphtha / Jet Cutpoint		396
Hydrocracking WABT		674.1579
bed1 top		613.6047
bed1 btm		651.781
bed2 top		648.494
bed2 btm		673.1208
bed3 top		666.2817
bed3 btm		673.8832
bed4 top		0
bed4 btm		0
Rec H2 to 1/2 quench		
Rec H2 to 2/3 quench		
Rec H2 to 3/4 quench		89.6239
B1 in-WABT		0.154302
B1 Out-WABT		0.000207
B2 in-WABT		617.4763
B2 Out-WABT		612.4357
B3 in-WABT		610.9023
B3 Out-WABT		650.5433
B4 in-WABT		648.39
B4 Out-WABT		656.4099
23 LCGO EP		674.0377
19 LVGO EP		672.1918
Nap EP		354
Nap/Jet CP		396
	% UCO in Product	93.78
%UCO in LPS		0.00
% UCO in Feed		0.00
BPD UCO in Feed		0
BPD UCO from R-1		0.00
R1 Conversion Gross		6.22
R-1 Net Conversion		6.22
DeltaP		73.58
DeltaP/MBBL		0.00
	HDN	
FN		363
EP		639
90%		611
50%		546
10%		483
FS		0.5
AN PT		152.3
API		35.10
FK700		18.40
AE		23922
PSIG		989
H2		73.2
NIT		2.4
LHSV, FF		1.674

TEMP		662.45
ACAT		0
-		
nit		2.4
lhsv		1.674
temp		662.4
K700		23.4018
acat		1.2719
fap		152.2565
S		-28.25
BR		185.4203
FUNN		5.013949
FUNP		1.492632
FUNT		1.868094
fun T		2.063641
Adjusted Reactor Temp (Base Feed)		656.7
Target T		676.00
FN at Design outlet N		4.339349
FUNT At Target T		1.483864
Days		105.00
Acat Pred		0.5398
FUNT of HT Beds		2.115013
FUN N at HT Bed Outlet		2.642098
N at HT outlet		25.8
FAPI		35.1
FN,PPM		363
FANPT		152
FEP		639
F90%		611
F50%		546
F10%		483
TOT CONV		6.2235
CUTPT		396
P IN F		0
RO,%FF		0
ROAPI		40
	R1N|RGNH3	25.828
CAT DENS		45
TEMP		670.36
H2%		73.195
PSIG		989.24
SCF/B		2433
LHSV, RC		5.221
ACAT		0

temp			670.4
lhsv			5.221
acat			1.9206
1/T, R			0.000885
	ACAT/Tfun		2.0144
fsg			0.8493
fap			152.2565
cor conv			6.22346
funcx			0.22676
funcm			0.004439
funHSF			0.110699
		effect fn	362.7
nh3pp			1.20459
funNH3PP			0.293483
r2sg			0.84934
nr2			25.8285
funR1NIT			1.101322
funH2pp			0.429027
funfeed			1.986068
funfeed			1.986068
funt			1.04889
tfun			1.04889
Design Tfun			0.723093
wabt			670.4
HDC Temp Req'd at Design Cond			659.5
HDC TREQ 9/1/97+			
Tfun'			1209.846
Acat'			0.001587
Design Tfun'			874.8319
Temp Req'd			698.2
			0.700346
ACAT"			0.5637
Time From SOR			105
HDC WABT			670.3571
HDN TREQ			656.7
HDC TREQ			659.5
API Gravity			35.1
D-86 Distillation			
IBP			320
10			483
30			519
50			546
70			574
90			611

95	625
EP	639
Total Sulfur (wt%)	0.4716
Total Nitrogen (wppm)	363
Total Silicon (wppm)	
Product Sulfur (wt%)	0.015259
Reactor ABT (degF)	662.4498
LHSV (1/hr)	1.7
Rx Pressure (psig)	989
RG H2 (mol%)	73.2
RG H2S (mol%)	0.001
RG rate (scf/bbl)	2433
H2 Con (scf/bbl)	512.8196
Catalyst	HC-K
Catalyst activity (1 for Fresh HC-K, HC-D, N-100, N-30; 1.1 for N-108)	1
Catalyst loading density (g/ml)	0.769231
Target Product Sulfur (wt%)	0.01
Cycle Length (years)	2
End of Run Temperature (degF)	760
LHSV (1/hr)	1.7
Rx Pressure (psig)	989.237
RG H2 (mol%)	73.19537
RG H2S (mol%)	0.001
RG rate (scf/bbl)	2433.141
H2 Con (scf/bbl)	512.8196
Catalyst	#REF!
Catalyst Activity (1 for Fresh HC-K, HC-D, N-100, N-30; 1.1 for N-108)	1
Catalyst Loading Density (g/ml)	0.769231
Kfeed(pilot plant)	14.67576
Kfeed(predict)	40.74488
Ratio of Kfeed(pilot plant)/Kfeed(predict)	0.360187
Ratio of Kfeed(meas.)/Kfeed(pred.) from similar pilot plant study	0.360187
Kfeed(use for proposal calculation)	9.190788
Required SOR Temp @ given target conditions (degF)	671.6952
Estimated TIR from Deactivation Model (degF/day)	0.016605
Maximum TIR based on Calc. SOR and target EOR Temp. (degF/day)	0.120965
Estimated Catalyst Life Based on Deactivation Model (years)	14.56958
Feed specific gravity (g/ml)	0.84934
Feed VABP (deg F)	546.6
Feed MeABP (deg F)	539.1648
Feed MW (lbs/lbsmole)	220.2147
BR (boiling range factor)	185.4203

Vol% above 600 degF	15.94595
Calculated H2 pp @ Rx Outlet (psia)	533.3692
Calculated H2S pp @ Rx Outlet (psia)	6.795355
Target %HDS calculated from target product S	96.76436

Plant A

Descriptor	Units	VALUE Oct 19 2005	Descriptor	Units	Value
F-1A Excess O2	% O2	10.01128292	C-2B Bed 1 EIT	DEGC	0.0012818
F-1A Excess O2	% O2	6.526412487	C-2A Bed 1 Top	DEGC	0.0012818
F-1B Excess O2	% O2	9.993423462	C-2B Bed 1 Top	DEGC	0.0012818
F-1B Excess O2	% O2	6.526412487	C-2A Bed 1 Top	DEGC	0.0012818
F-2A Excess O2	% O2	10.0074873	C-2B Bed 1 Top	DEGC	0.0012818
F-2A Excess O2	% O2	6.526412487	C-2A Bed 1 Top	DEGC	0.0012818
F-2B Excess O2	% O2	10.01406574	C-2B Bed 1 Top	DEGC	0.0012818
F-2B Excess O2	% O2	6.526412487	C-2A Bed 1 Bottom	DEGC	0.0012818
F-1A Flue gas combustible	PPM	59.6725502	C-2B Bed 1 Bottom	DEGC	0.0012818
F-1B Flue gas combustible	PPM	41.34143829	C-2A Bed 1 Bottom	DEGC	0.0012818
F-2A Flue gas combustible	PPM	0.244200259	C-2B Bed 1 Bottom	DEGC	0.0012818
C-13 Naphtha to C-14	KBPD	0.001971237	C-2A Bed 1 Bottom	DEGC	0.0012818
K-1 Optimization	% OPEN	50	C-2B Bed 1 Bottom	DEGC	0.0012818
Total treat gas to E-6s	MSCFD	Bad	C-2A Bed 1 Bottom	DEGC	0.0012818
2nd stage LGO feed	KBPD	0.014924123	C-2B Bed 1 Bottom	DEGC	0.0012818
F-1A Fuel gas	MSCFD	0.000675845	C-2A Bed 1 Bottom	DEGC	0.0012818
F-1B Fuel gas	MSCFD	0.00045054	C-2B Bed 1 Bottom	DEGC	0.0012818
C-9A Emergency quench	MSCFD	0	C-2A Bed 1 Bottom	DEGC	0.0012818
C-9B Emergency quench	MSCFD	0	C-2B Bed 1 Bottom	DEGC	0.0012818
C-2A Emergency quench	MSCFD	3.411587715	C-5 temp	DEGC	8.52466202
C-2B Emergency quench	MSCFD	0	C-2A Bed 1 Bottom	DEGC	0.0012818
S/U oil	KBPD	0	C-2B Bed 1 Bottom	DEGC	0.0012818
15-1/2 LGO feed	KBPD	0	C-2A Bed 1 Bottom	DEGC	0.0012818
F-1A Air	MSCFD	4.471101284	C-2B Bed 1 Bottom	DEGC	0.0012818
F-1B Air	MSCFD	6.287082195	C-2A Bed 1 Bottom	DEGC	0.0012818
1st stage product to stora	KBPD	0	C-2B Bed 1 Bottom	DEGC	0.0012818
Total treat gas to E-2s	MSCFD	0.011745151	C-2A Bed 1 Bottom	DEGC	0.0012818
C-2A Bed 2 Quench	MSCFD	0.086356156	C-2B Bed 1 Bottom	DEGC	0.0012818
C-2B Bed 2 Quench	MSCFD	0.140957311	C-2A Bed 1 Bottom	DEGC	0.0012818
C-2A Bed 3 Quench	MSCFD	0.014688156	C-2B Bed 1 Bottom	DEGC	0.0012818
C-2B Bed 3 Quench	MSCFD	0.16951552	C-2A Bed 1 Bottom	DEGC	0.0012818
1st stage LGO feed	KBPD	0.022413611	C-2B Bed 1 Bottom	DEGC	0.0012818
Wash water to E-3A/B	USGPM	0	C-2A Bed 1 Bottom	DEGC	0.0012818
C-5 LGO to C-6	KBPD	0	C-2B Bed 1 Bottom	DEGC	0.0012818
Wash water to E-4	USGPM	0	C-2A Bed 1 Bottom	DEGC	0.0012818

Stripping steam to C-6	KPPH	0.000980137	C-2B Bed 1 Bottom	DEGC	0.0012818
C-6 Stripper Reflux	KBPD	0.000515142	E-7G air inlet temp	DEGC	0.0012818
1st stage Naphtha to C-14	KBPD	0.000344082	E-7G air inlet temp	DEGC	0.0012818
HP BFW to Y-3	USGPM	0.001128137	E-7H air inlet temp	DEGC	0.0012818
Lean DEA to C-19	USGPM	0	E-7H air inlet temp	DEGC	0.0012818
1st stage purge to 27-1	MSCFD	0	E-7E air inlet temp	DEGC	0.0012818
Make-up H2 from Plt 9/27	MSCFD	0	E-7E air inlet temp	DEGC	0.0012818
E-6A/E LGO	KBPD	0.002612275	E-7F air inlet temp	DEGC	0.0012818
E-6B/F LGO	KBPD	0.007847995	E-7F air inlet temp	DEGC	0.0012818
E-6C/G LGO	KBPD	0	C-3 temp	DEGC	64.3797455
E-6D/H LGO	KBPD	0.015629457	C-9A/B EIT	DEGC	151.241028
F-2A Fuel gas	MSCFD	0.000202918	C-9A Bed 1 Top	DEGC	0.0012818
F-2B Fuel gas	MSCFD	0	C-9A Bed 1 EIT	DEGC	0.0012818
F-2A Air	MSCFD	8.068032265	C-9B Bed 1 Top	DEGC	0.0012818
F-2B Air	MSCFD	7.196857929	C-9B Bed 1 EIT	DEGC	0.0012818
C-9A Bed 2 Quench	MSCFD	-0.097186804	C-9A Bed 1 Top	DEGC	0.0012818
C-9B Bed 2 Quench	MSCFD	-0.002809451	C-9B Bed 1 Top	DEGC	0.0012818
C-9A Bed 3 Quench	MSCFD	0	C-9A Bed 1 Top	DEGC	0.0012818
C-9B Bed 3 Quench	MSCFD	0.150765717	C-9B Bed 1 Top	DEGC	0.0012818
Treat gas to E-2A/E/J	MSCFD	Bad	C-9A Bed 1 Top	DEGC	0.0012818
Treat gas to E-2B/F/K	MSCFD	Bad	C-9B Bed 1 Top	DEGC	0.0012818
Treat gas to E-2C/G/L	MSCFD	Bad	C-9A Bed 1 Middle	DEGC	0.0012818
Treat gas to E-2D/H/M	MSCFD	Bad	C-9B Bed 1 Middle	DEGC	0.0012818
Wash water to E-7A~H	USGPM	0.041058511	C-9A Bed 1 Middle	DEGC	0.0012818
Wash water to E-8	USGPM	0	C-9B Bed 1 Middle	DEGC	0.0012818
C-12 LGO to C-14	KBPD	0	C-9A Bed 1 Middle	DEGC	0.0012818
Stripping steam to C-14	KPPH	-0.007489546	C-9B Bed 1 Middle	DEGC	0.0012818
C-15 Reflux to C-14	KBPD	0	C-9A Bed 1 Middle	DEGC	0.0012818
Product Naphtha to Plt 13	KBPD	0	C-9B Bed 1 Middle	DEGC	0.0012818
2nd stage LGO to storage	KBPD	0	C-9A Bed 1 Middle	DEGC	0.0012818
2nd stage LGO recycle to C	KBPD	0	C-9B Bed 1 Middle	DEGC	0.0012818
E-2A/E/J UTLGO	KBPD	0.002084201	C-9A Bed 1 Middle	DEGC	0.0012818
E-2B/F/K UTLGO	KBPD	0.012213972	C-9B Bed 1 Middle	DEGC	0.0012818
E-2C/G/L UTLGO	KBPD	9.20534E-05	C-6 Tray 35	DEGC	11.7041054
E-2D/H/M UTLGO	KBPD	9.20534E-05	C-2A Bed 2 Top	DEGC	0.0012818
Sour gas to 8-1/2C-8	MSCFD	5	C-2A Bed 2 EIT	DEGC	0.0012818
1st Stage untreated LGO fe	KBPD	0.014865518	C-2B Bed 2 Top	DEGC	0.0012818
2nd Stage LGO feed	KBPD	0	C-2B Bed 2 EIT	DEGC	0.0012818
E-3A/B WW to feed ratio	USGPM / KBPD	0	C-2A Bed 2 Top	DEGC	0.0012818
E-4 WW to feed ratio	USGPM / KBPD	0	C-2B Bed 2 Top	DEGC	0.0012818
E-7A~H WW to feed ratio	USGPM / KBPD	5	C-2A Bed 2 Top	DEGC	0.0012818
E-8 WW to feed ratio	USGPM / KBPD	0	C-2B Bed 2 Top	DEGC	0.0012818
Stripper steam to feed rat	KPPH / KBPD	0	C-2A Bed 2 Top	DEGC	0.0012818

Stabilizer steam to feed r	KPPH / KBPD	0.150000006	C-2B Bed 2 Top	DEGC	0.0012818
LGO feed from storage	KBPD	0	C-2A Bed 2 Top	DEGC	0.0012818
C-7 Sour gas to Plt 8	MSCFD	-0.001279669	C-2B Bed 2 Top	DEGC	0.0012818
E-5 Steam	KPPH	0.016522408	C-2A Bed 2 Top	DEGC	0.0012818
C-15 Sour gas to Plt 8 LER	MSCFD	1.45751E-05	C-2B Bed 2 Top	DEGC	0.0012818
C-13 Sour gas to 27-1	MSCFD	0.000945469	C-2A Bed 2 Top	DEGC	0.0012818
E-12 Steam	KPPH	0.00160861	C-2B Bed 2 Top	DEGC	0.0012818
Sour water to D-55	USGPM	0.165533289	C-2A Bed 2 Top	DEGC	0.0012818
E-5/12 Combined steam	KPPH	0.053252891	C-2B Bed 2 Top	DEGC	0.0012818
E-2A/E/J UTLGO trip	KBPD	0.007619048	C-2A Bed 2 Top	DEGC	0.0012818
E-2B/F/K UTLGO trip	KBPD	0	C-2B Bed 2 Top	DEGC	0.0012818
E-2C/G/L UTLGO trip	KBPD	0	C-2A Bed 2 Top	DEGC	0.0012818
E-2D/H/M UTLGO trip	KBPD	0	C-2B Bed 2 Top	DEGC	0.0012818
E-5 BFW	KPPH	0	C-2A Bed 2 Upper	DEGC	0.0012818
Sour gas to 8-1/2C-8	MSCFD	0.000945469	C-2B Bed 2 Upper	DEGC	0.0012818
C-15 sour gas to H-2	MSCFD	0.000640899	C-2A Bed 2 Upper	DEGC	0.0012818
E-12 BFW	KPPH	0	C-2B Bed 2 Upper	DEGC	0.0012818
LP NG import	MSCFD	6.37293E-05	C-2A Bed 2 Upper	DEGC	0.0012818
HP NG import	MSCFD	1.39138329	C-2B Bed 2 Upper	DEGC	0.0012818
HP N2 import	MSCFD	0	C-2A Bed 2 Upper	DEGC	0.0012818
LP N2 import	MSCFD	0	C-2B Bed 2 Upper	DEGC	0.0012818
HP flare	MSCFD	0.536910415	C-2A Bed 2 Upper	DEGC	0.0012818
LP flare	MSCFD	0.013337438	C-2B Bed 2 Upper	DEGC	0.0012818
Wash water to E-7A	USGPM	0.00976575	C-2A Bed 2 Upper	DEGC	0.0012818
Wash water to E-7B	USGPM	0.001933873	C-2B Bed 2 Upper	DEGC	0.0012818
Wash water to E-7C	USGPM	0	C-2A Bed 2 Lower	DEGC	0.0012818
Wash water to E-7D	USGPM	0	C-2B Bed 2 Lower	DEGC	0.0012818
Wash water to E-7E	USGPM	0.003942645	C-2A Bed 2 Lower	DEGC	0.0012818
Wash water to E-7F	USGPM	0	C-2B Bed 2 Lower	DEGC	0.0012818
Wash water to E-7G	USGPM	0	C-2A Bed 2 Lower	DEGC	0.0012818
Wash water to E-7H	USGPM	0	C-2B Bed 2 Lower	DEGC	0.0012818
Wash water to E-3A	USGPM	0.008008075	C-2A Bed 2 Lower	DEGC	0.0012818
Wash water to E-3B	USGPM	0.008008075	C-2B Bed 2 Lower	DEGC	0.0012818
Filter backwash to slops	KBPD	0	C-2A Bed 2 Lower	DEGC	0.0012818
1st/2nd stage recycle to E	KBPD	0.007548094	C-2B Bed 2 Lower	DEGC	0.0012818
F-1A Air	MACFD	10.23394966	C-2A Bed 2 Lower	DEGC	0.0012818
F-1B Air	MACFD	11.45755672	C-2B Bed 2 Lower	DEGC	0.0012818
F-2A Air	MACFD	14.56216717	C-14 O/H temp	DEGC	0.0012818
F-2B Air	MACFD	14.81600761	C-14 Tray 43	DEGC	6.89371014
G-5A Seal Gas Flow	SCFH	0	C-9A Bed 1 Bottom	DEGC	0.0012818
C-6 Stripper Reflux	KBPD	0.001281798	C-9B Bed 1 Bottom	DEGC	0.0012818
G-1 Seal Gas Flow	SCFH	0.480652422	C-9A Bed 1 Bottom	DEGC	0.0012818
G-3A Seal Gas Flow	SCFH	5.006408215	C-9B Bed 1 Bottom	DEGC	0.0012818
G-3B Seal Gas Flow	SCFH	0.43356657	C-9A Bed 1 Bottom	DEGC	0.0012818
G-5B Seal Gas Flow	SCFH	0	C-9B Bed 1 Bottom	DEGC	0.0012818
G-6A Seal Gas Flow	SCFH	1.843473434	C-9A Bed 1 Bottom	DEGC	0.0012818
G-6B Seal Gas Flow	SCFH	3.818211555	C-9B Bed 1 Bottom	DEGC	0.0012818
15-1 LGO Feed	KBPD	0.001281798	C-9A Bed 1 Bottom	DEGC	0.0012818
15-2 LGO Feed	KBPD	0.001281798	C-9B Bed 1 Bottom	DEGC	0.0012818
G-1 Seal Gas Flow	SCFH	4.597208977	C-9A Bed 1 Bottom	DEGC	0.0012818

G-3A Seal Gas Flow	SCFH	2.065928221	C-9B Bed 1 Bottom	DEGC	0.0012818
G-3B Seal Gas Flow	SCFH	3.758810282	C-9A Bed 1 Bottom	DEGC	0.0012818
G-5A Seal Gas Flow	SCFH	0	C-9B Bed 1 Bottom	DEGC	0.0012818
G-5B Seal Gas Flow	SCFH	0	C-9A Bed 1 Bottom	DEGC	0.0012818
G-6A Seal Gas Flow	SCFH	0	C-9B Bed 1 Bottom	DEGC	0.0012818
G-6B Seal Gas Flow	SCFH	1.0351336	C-9A Bed 1 Bottom	DEGC	0.0012818
Recycle gas flow	MSCFD	107.6434708	C-9B Bed 1 Bottom	DEGC	0.0012818
Treat gas to E-6A/E trip	MSCFD	23.70020866	C-9A Bed 1 Bottom	DEGC	0.0012818
Treat gas to E-6B/F trip	MSCFD	23.70679665	C-9B Bed 1 Bottom	DEGC	0.0012818
Treat gas to E-6C/G trip	MSCFD	23.78913116	C-9A Bed 1 Bottom	DEGC	0.0012818
Treat gas to E-6D/H trip	MSCFD	23.78913116	C-9B Bed 1 Bottom	DEGC	0.0012818
E-6A/E LGO trip	KBPD	0	C-9A Bed 1 Bottom	DEGC	0.0012818
E-6B/F LGO trip	KBPD	0	C-9B Bed 1 Bottom	DEGC	0.0012818
E-6C/G LGO trip	KBPD	0	C-9A Bed 1 Bottom	DEGC	0.0012818
E-6D/H LGO trip	KBPD	0	C-9B Bed 1 Bottom	DEGC	0.0012818
Wash water from Plt 16	USGPM	0.07696718	C-9A Bed 1 Bottom	DEGC	0.0012818
Treat gas to E-2A/E/J trip	MSCFD	23.69203949	C-9B Bed 1 Bottom	DEGC	0.0012818
Treat gas to E-2B/F/K trip	MSCFD	23.69371796	C-14 LGO inlet temp	DEGC	10.605938
Treat gas to E-2C/G/L trip	MSCFD	23.822052	C-14 Tray 40	DEGC	7.87945557
Treat gas to E-2D/H/M trip	MSCFD	23.68545341	C-2A Bed 2 Bottom	DEGC	0.0012818
C-13 Sour gas to 27-1	MSCFD	0.003340423	C-2B Bed 2 Bottom	DEGC	0.0012818
Sour gas to 8-1/2C-8	MSCFD	-0.000656016	C-2A Bed 2 Bottom	DEGC	0.0012818
C-13 Naphtha to C-14	% OPEN	-5	C-2B Bed 2 Bottom	DEGC	0.0012818
K-1 Optimizer	%	0	C-2A Bed 2 Bottom	DEGC	0.0012818
F-1A Fuel gas	% OPEN	28.70000076	C-2B Bed 2 Bottom	DEGC	0.0012818
F-1B Fuel gas	% OPEN	29	C-2A Bed 2 Bottom	DEGC	0.0012818
C-9A Emergency quench	% OPEN	-6	C-2B Bed 2 Bottom	DEGC	0.0012818
C-9B Emergency quench	% OPEN	-6	C-2A Bed 2 Bottom	DEGC	0.0012818
C-2A Emergency quench	% OPEN	-6	C-2B Bed 2 Bottom	DEGC	0.0012818
C-2B Emergency quench	% OPEN	0	C-2A Bed 2 Bottom	DEGC	0.0012818
S/U oil	% OPEN	0	C-2B Bed 2 Bottom	DEGC	0.0012818
15-1/2 LGO feed	% OPEN	6.900000095	C-2A Bed 2 Bottom	DEGC	0.0012818
F-1A Air	% OPEN	29.35614586	C-2B Bed 2 Bottom	DEGC	0.0012818
F-1B Air	% OPEN	20.54411888	C-2A Bed 2 Bottom	DEGC	0.0012818
1st stage product to stora	% OPEN	0	C-2B Bed 2 Bottom	DEGC	0.0012818
C-2A Bed 2 Quench	% OPEN	-5	C-2A Bed 2 Bottom	DEGC	0.0012818
C-2B Bed 2 Quench	% OPEN	-5	C-2B Bed 2 Bottom	DEGC	0.0012818
C-2A Bed 3 Quench	% OPEN	-5	C-2A Bed 2 Bottom	DEGC	0.0012818
C-2B Bed 3 Quench	% OPEN	-5	C-2B Bed 2 Bottom	DEGC	0.0012818
Wash water to E-3A/B	% OPEN	-5	C-2A Bed 2 Bottom	DEGC	0.0012818
LGO to C-6	% OPEN	-5	C-2B Bed 2 Bottom	DEGC	0.0012818
Wash water to E-4	% OPEN	0	C-2A Bed 2 Bottom	DEGC	0.0012818
C-6 Stripping Steam Flow	% OPEN	-3	C-2B Bed 2 Bottom	DEGC	0.0012818
C-6 Stripper Reflux	% OPEN	-5	C-2A Bed 2 Bottom	DEGC	0.0012818
1st stage Naphtha to C-14	% OPEN	50	C-2B Bed 2 Bottom	DEGC	0.0012818
HP BFW to Y-3	% OPEN	0	C-2A Bed 2 Bottom	DEGC	0.0012818
Lean DEA to C-19	% OPEN	6.900000095	C-2B Bed 2 Bottom	DEGC	0.0012818
1st stage purge to 27-1	% OPEN	98.10868073	C-2A Bed 2 Bottom	DEGC	0.0012818

Make-up H2 from Plt 9/27	% OPEN	-5	C-2B Bed 2 Bottom	DEGC	0.0012818
Treat gas to E-6A/E	% OPEN	45	C-2A Bed 2 Bottom	DEGC	0.0012818
Treat gas to E-6B/F	% OPEN	45	C-2B Bed 2 Bottom	DEGC	0.0012818
Treat gas to E-6C/G	% OPEN	45	C-2A Bed 2 Bottom	DEGC	0.0012818
Treat gas to E-6D/H	% OPEN	45	C-2B Bed 2 Bottom	DEGC	0.0012818
E-6A/E LGO	% OPEN	0	C-2A Bed 2 Bottom	DEGC	0.0012818
E-6B/F LGO	% OPEN	0	C-2B Bed 2 Bottom	DEGC	0.0012818
E-6C/G LGO	% OPEN	0	C-9A Bed 2 top	DEGC	0.0012818
E-6D/H LGO	% OPEN	0	C-9A Bed 2 EIT	DEGC	0.0012818
F-2A Fuel gas	% OPEN	22.85446358	C-9B Bed 2 top	DEGC	0.0012818
F-2B Fuel gas	% OPEN	24.85446358	C-9B Bed 2 EIT	DEGC	0.0012818
F-2A Air	% OPEN	35	C-9A Bed 2 top	DEGC	0.0012818
F-2B Air	% OPEN	35	C-9B Bed 2 top	DEGC	0.0012818
C-9A Bed 2 Quench	% OPEN	-5	C-9A Bed 2 top	DEGC	0.0012818
C-9B Bed 2 Quench	% OPEN	-5	C-9B Bed 2 top	DEGC	0.0012818
C-9A Bed 3 Quench	% OPEN	-5	C-9A Bed 2 top	DEGC	0.0012818
C-9B Bed 3 Quench	% OPEN	-5	C-9B Bed 2 top	DEGC	0.0012818
Treat gas to E-2A/E/J	% OPEN	50	C-9A Bed 2 top	DEGC	0.0012818
Treat gas to E-2B/F/K	% OPEN	50	C-9B Bed 2 top	DEGC	0.0012818
Treat gas to E-2C/G/L	% OPEN	50	C-9A Bed 2 top	DEGC	0.0012818
Treat gas to E-2D/H/M	% OPEN	50	C-9B Bed 2 top	DEGC	0.0012818
Wash water to E-7A~H	% OPEN	-5	C-9A Bed 2 top	DEGC	0.0012818
Wash water to E-8	% OPEN	25	C-9B Bed 2 top	DEGC	0.0012818
C-12 LGO to C-14	% OPEN	-5	C-9A Bed 2 top	DEGC	0.0012818
C-14 stripping steam	% OPEN	-5	C-9B Bed 2 top	DEGC	0.0012818
C-15 Reflux to C-14	% OPEN	105	C-9A Bed 2 top	DEGC	0.0012818
Product Naphtha to Plt 13	% OPEN	105	C-9B Bed 2 top	DEGC	0.0012818
2nd stage LGO to storage	% OPEN	105	C-9A Bed 2 top	DEGC	0.0012818
2nd stage LGO recycle to C	% OPEN	0	C-9B Bed 2 top	DEGC	0.0012818
E-2A/E/J UTLGO	% OPEN	0.326510757	C-14 Bottom outlet temp	DEGC	17.8851051
E-2B/F/K UTLGO	% OPEN	0.614730716	C-9A Bed 2 upper	DEGC	0.0012818
E-2C/G/L UTLGO	% OPEN	0.000990406	C-9B Bed 2 upper	DEGC	0.0012818
E-2D/H/M UTLGO	% OPEN	-0.011936586	C-9A Bed 2 upper	DEGC	0.0012818
K-1 Anti-surge Valve Posit	%	99.70696259	C-9B Bed 2 upper	DEGC	0.0012818
K-1 Anti-surge	% OPEN	0.001281798	C-9A Bed 2 upper	DEGC	0.0012818
E-1 product bypass	%	0.001281798	C-9B Bed 2 upper	DEGC	0.0012818
E-5 Bypass	%	0.001281798	C-9A Bed 2 upper	DEGC	0.0012818
K-1 Perf. Controller Manua	%	16	C-9B Bed 2 upper	DEGC	0.0012818
High rate unit depressure		CLOSED	C-9A Bed 2 upper	DEGC	0.0012818
Low rate unit depressure		CLOSED	C-9B Bed 2 upper	DEGC	0.0012818
FV-88 Bypass	% OPEN	100	C-9A Bed 2 upper	DEGC	0.0012818
LV-2 Bypass	% OPEN	0	C-9B Bed 2 upper	DEGC	0.0012818
Recycle to E-1	% OPEN	0	C-9A Bed 2 lower	DEGC	0.0012818
2nd stage recycle to E-1	% OPEN	0	C-9B Bed 2 lower	DEGC	0.0012818
LGO feed from storage	% OPEN	0	C-9A Bed 2 lower	DEGC	0.0012818
E-1 product bypass	% OPEN	105	C-9B Bed 2 lower	DEGC	0.0012818
E-1 product forced flow	% OPEN	105	C-9A Bed 2 lower	DEGC	0.0012818
C-19 Bypass	% OPEN	105	C-9B Bed 2 lower	DEGC	0.0012818
E-5 Bypass	% OPEN	0	C-9A Bed 2 lower	DEGC	0.0012818

E-5 Forced flow	% OPEN	100	C-9B Bed 2 lower	DEGC	0.0012818
High rate unit depressure	% OPEN	0.001281798	C-9A Bed 2 lower	DEGC	0.0012818
Low rate unit depressure	% OPEN	0.001281798	C-9B Bed 2 lower	DEGC	0.0012818
K-1 Motor amps	Amps	148.9597168	C-9A Bed 2 lower	DEGC	0.0012818
K-1 status	-	RUNNING	C-9B Bed 2 lower	DEGC	0.0012818
K-2 status	-	RUNNING	C-2A Bed 3 Top	DEGC	0.0012818
K-3 status	-	RUNNING	C-2A Bed 3 EIT	DEGC	0.0012818
K-4 status	-	RUNNING	C-2B Bed 3 Top	DEGC	0.0012818
K-5 status	-	RUNNING	C-2B Bed 3 EIT	DEGC	0.0012818
C-1 Level to FIC-173	%	68.36061096	C-2A Bed 3 Top	DEGC	0.0012818
C-4 Oil/water interface	%	-0.356204808	C-2B Bed 3 Top	DEGC	0.0012818
C-30 Filter backwash level	%	0.37998566	C-2A Bed 3 Top	DEGC	0.0012818
C-4 Oil level	%	-0.299961865	C-2B Bed 3 Top	DEGC	0.0012818
C-5 Level	%	0.149980187	C-2A Bed 3 Top	DEGC	0.0012818
C-1 Level	%	68.40622711	C-2B Bed 3 Top	DEGC	0.0012818
C-6 Level	%	1.245170474	C-2A Bed 3 Top	DEGC	0.0012818
C-7 Oil/water interface	%	0.563432157	C-2B Bed 3 Top	DEGC	0.0012818
C-7 Nap Level	%	0.292902917	C-2A Bed 3 Top	DEGC	0.0012818
E-5 BFW level	%	-0.769767284	C-2B Bed 3 Top	DEGC	0.0012818
C-24 Oil/water interface	%	0.056242943	C-2A Bed 3 Top	DEGC	0.0012818
C-28 Steam KO level	%	25.5783596	C-2B Bed 3 Top	DEGC	0.0012818
C-17 Lean DEA level	%	48.79189682	C-2A Bed 3 Top	DEGC	0.0012818
C-19 Level	%	0.435991824	C-2B Bed 3 Top	DEGC	0.0012818
C-21 Level	%	0.084102154	C-2A Bed 3 Top	DEGC	0.0012818
C-8 Water boot interface	%	0.323940456	C-2B Bed 3 Top	DEGC	0.0012818
C-8 Level	%	-0.178369299	C-2A Bed 3 Top	DEGC	0.0012818
C-10 Level	%	-0.261003256	C-2B Bed 3 Top	DEGC	0.0012818
C-11 Oil/water interface	%	-0.276988745	F-1 Convection section tem	DEGC	187.303925
C-11 Oil level	%	0.765327513	C-2A Bed 3 Upper	DEGC	0.0012818
C-12 Level	%	-0.010946049	C-2B Bed 3 Upper	DEGC	0.0012818
C-13 Oil/water interface	%	0.334335923	C-2A Bed 3 Upper	DEGC	0.0012818
C-13 Naphtha level	%	1.459374905	C-2B Bed 3 Upper	DEGC	0.0012818
C-14 Level	%	-0.135546923	C-2A Bed 3 Upper	DEGC	0.0012818
C-15 Oil/water interface	%	-0.367584825	C-2B Bed 3 Upper	DEGC	0.0012818
C-15 Naphtha level	%	-0.321256965	C-2A Bed 3 Upper	DEGC	0.0012818
E-12 BFW level	%	-0.329017639	C-2B Bed 3 Upper	DEGC	0.0012818
C-16 Water boot level	%	0.617363036	C-2A Bed 3 Upper	DEGC	0.0012818
C-22 Oil/water interface	%	42.7434082	C-2B Bed 3 Upper	DEGC	0.0012818
C-29 CHD level	%	0.52043581	C-2A Bed 3 Upper	DEGC	0.0012818

C-3 Level	%	0.10404896	C-2B Bed 3 Upper	DEGC	0.0012818
C-29 Oil/water interface	%	Bad	C-2A Bed 3 Lower	DEGC	0.0012818
D-28 Level	%	0.001281798	C-2B Bed 3 Lower	DEGC	0.0012818
C-3 Level	%	0	C-2A Bed 3 Lower	DEGC	0.0012818
G-10B Lube Oil System	%	64.81074524	C-2B Bed 3 Lower	DEGC	0.0012818
G-1 Lube Oil System	%	100	C-2A Bed 3 Lower	DEGC	0.0012818
G-3A Lube Oil System	%	100	C-2B Bed 3 Lower	DEGC	0.0012818
G-3B Lube Oil System	%	0	C-2A Bed 3 Lower	DEGC	0.0012818
G-5A Lube Oil System	%	100	C-2B Bed 3 Lower	DEGC	0.0012818
G-5B Lube Oil System	%	0	E-5 LGO outlet temp	DEGC	41.012558
G-6A Lube Oil System	%	100	C-2A Bed 3 Lower	DEGC	0.0012818
G-6B Lube Oil System	%	100	C-2B Bed 3 Lower	DEGC	0.0012818
C-4 Oil/water interface	%	0	C-2A Bed 3 Lower	DEGC	0.0012818
C-4 Oil level	%	0	C-2B Bed 3 Lower	DEGC	0.0012818
C-1 Level	%	0.001281798	F-1 Pass 1 inlet temp	DEGC	127.252983
C-5 level	%	0	C-9A Bed 2 bottom	DEGC	0.0012818
E-5 BFW level	%	3.500336409	C-9B Bed 2 bottom	DEGC	0.0012818
E-12 BFW level	%	-0.361969322	C-9A Bed 2 bottom	DEGC	0.0012818
C-24 Oil/water interface	%	0	C-9B Bed 2 bottom	DEGC	0.0012818
C-24 level	%	-0.179383144	C-9A Bed 2 bottom	DEGC	0.0012818
C-7 Naphtha level	%	0	C-9B Bed 2 bottom	DEGC	0.0012818
C-17 Lean DEA level	%	48.96215057	C-9A Bed 2 bottom	DEGC	0.0012818
C-19 Level	%	0	C-9B Bed 2 bottom	DEGC	0.0012818
C-18 Level	%	0.435372561	C-9A Bed 2 bottom	DEGC	0.0012818
C-21 Level	%	0.024420027	C-9B Bed 2 bottom	DEGC	0.0012818
C-20 Level	%	3.394383669	C-9A Bed 2 bottom	DEGC	0.0012818
C-1 Water boot interface	%	3.57642293	C-9B Bed 2 bottom	DEGC	0.0012818
C-8 Level	%	0	C-9A Bed 2 bottom	DEGC	0.0012818
C-10 Level	%	0.537240565	C-9B Bed 2 bottom	DEGC	0.0012818
C-1 Level	%	68.91330719	C-9A Bed 2 bottom	DEGC	0.0012818
C-11 Oil/water interface	%	1.098901153	C-9B Bed 2 bottom	DEGC	0.0012818
C-11 Oil level	%	0	C-9A Bed 2 bottom	DEGC	0.0012818
C-15 Naphtha level	%	0	C-9B Bed 2 bottom	DEGC	0.0012818
C-22 Oil/water interface	%	37.55799866	C-9A Bed 2 bottom	DEGC	0.0012818
C-22 Level	%	37.99678802	C-9B Bed 2 bottom	DEGC	0.0012818
C-6 Level	%	0.195360214	F-1 Pass 2 inlet temp	DEGC	127.147331
C-28 Steam KO level	%	28.99243164	C-9A Bed 2 bottom	DEGC	0.0012818
C-14 Level	%	0	C-9B Bed 2 bottom	DEGC	0.0012818
C-26 FGKO level	%	17.46275902	C-9A Bed 2 bottom	DEGC	0.0012818
C-29 level	%	0.927960992	C-9B Bed 2 bottom	DEGC	0.0012818
C-4 Oil/water interface	% OPEN	-5	C-9A Bed 2 bottom	DEGC	0.0012818
C-4 Oil/water interface	% OPEN	-5	C-9B Bed 2 bottom	DEGC	0.0012818
C-30 Filter backwash level	% OPEN	-5	C-9A Bed 2 bottom	DEGC	0.0012818
C-4 Oil level	% OPEN	-5	C-9B Bed 2 bottom	DEGC	0.0012818
C-4 Oil level	% OPEN	-5	C-9A Bed 2 bottom	DEGC	0.0012818
C-1 Level from tankage/rec	% OPEN	0.001281798	C-9B Bed 2 bottom	DEGC	0.0012818
C-6 Level to LV-2	% OPEN	0	C-9A Bed 2 bottom	DEGC	0.0012818
C-7 Oil/water interface	% OPEN	-5	C-9B Bed 2 bottom	DEGC	0.0012818
E-5 BFW level	% OPEN	0	C-9A Bed 2 bottom	DEGC	0.0012818

C-6 Level to FIC-88	% OPEN	0.001281798	C-9B Bed 2 bottom	DEGC	0.0012818
C-6 Level to FIC-2	% OPEN	0.001281798	C-9A Bed 2 bottom	DEGC	0.0012818
C-6 Level to LY-1A	% OPEN	0.001281798	C-9B Bed 2 bottom	DEGC	0.0012818
C-24 Oil/water interface	% OPEN	-5	F-1 Pass 3 inlet temp	DEGC	126.66832
C-28 Steam KO level	% OPEN	8.210716248	F-1 Pass 4 inlet temp	DEGC	125.34848
C-17 Lean DEA level	%	10	F-1B Firebox top temp	DEGC	390.186249
C-19 Level	% OPEN	-5	F-1 Xover Pass 3	DEGC	41.9618454
C-19 Level	% OPEN	-5	C-2A Bed 3 Bottom	DEGC	0.0012818
C-21 Level	% OPEN	100	C-2B Bed 3 Bottom	DEGC	0.0012818
C-8 Water boot interface	% OPEN	-5	C-2A Bed 3 Bottom	DEGC	0.0012818
C-10 Level	% OPEN	-5	C-2B Bed 3 Bottom	DEGC	0.0012818
C-10 Level	% OPEN	-5	C-2A Bed 3 Bottom	DEGC	0.0012818
C-11 Oil/water interface	% OPEN	-5	C-2B Bed 3 Bottom	DEGC	0.0012818
C-11 Oil/water interface	% OPEN	-5	C-2A Bed 3 Bottom	DEGC	0.0012818
C-11 Oil level	% OPEN	-5	C-2B Bed 3 Bottom	DEGC	0.0012818
C-11 Oil level	% OPEN	-5	C-2A Bed 3 Bottom	DEGC	0.0012818
C-13 Oil/water interface	% OPEN	-5	C-2B Bed 3 Bottom	DEGC	0.0012818
C-14 Level to FIC-88	% OPEN	0.001281798	C-2A Bed 3 Bottom	DEGC	0.0012818
C-14 Level to FIC-89	%	0.001281798	C-2B Bed 3 Bottom	DEGC	0.0012818
C-14 Level to LY-1A	%	0.001281798	C-2A Bed 3 Bottom	DEGC	0.0012818
C-15 Oil/water interface	% OPEN	-5	C-2B Bed 3 Bottom	DEGC	0.0012818
E-12 BFW level	% OPEN	-5	C-2A Bed 3 Bottom	DEGC	0.0012818
C-16 Water boot level	% OPEN	105	C-2B Bed 3 Bottom	DEGC	0.0012818
C-22 Oil/water interface (	% OPEN	-5	C-2A Bed 3 Bottom	DEGC	0.0012818
C-22 Level (BFW make-up)	% OPEN	-5	C-2B Bed 3 Bottom	DEGC	0.0012818
C-22 Level (WW to C-24)	% OPEN	-5	C-2A Bed 3 Bottom	DEGC	0.0012818
C-29 CHD level	% OPEN	0	C-2B Bed 3 Bottom	DEGC	0.0012818
C-3 Level	% OPEN	-5	F-1 Xover Pass 4	DEGC	28.8899384
C-3 Level	% OPEN	-5	C-2A Bed 3 Bottom	DEGC	0.0012818
C-19 Outlet pressure	PSIG	1060.529297	C-2B Bed 3 Bottom	DEGC	0.0012818
F-1A Pilot gas pressure	PSIG	10.00251389	C-2A Bed 3 Bottom	DEGC	0.0012818
F-1B Pilot gas pressure	PSIG	10.06303883	C-2B Bed 3 Bottom	DEGC	0.0012818
C-30 pressure (NG blanket	PSIG	14.31857109	C-2A Bed 3 Bottom	DEGC	0.0012818
C-30 pressure (NG blanket	PSIG	14.31209373	C-2B Bed 3 Bottom	DEGC	0.0012818
C-24 Pressure (to flare)	PSIG	8.966732025	C-2A Bed 3 Bottom	DEGC	0.0012818
C-4 Pressure	PSIG	1059.958862	C-2B Bed 3 Bottom	DEGC	0.0012818
C-7 Pressure	PSIG	154.7346649	C-2A Bed 3 Bottom	DEGC	0.0012818
C-24 Pressure (to H-2)	PSIG	8.964744568	C-2B Bed 3 Bottom	DEGC	0.0012818
C-17 Pressure (NG blanket	PSIG	105.1166687	C-2A Bed 3 Bottom	DEGC	0.0012818
C-17 Pressure (NG blanket	PSIG	105.1194611	C-2B Bed 3 Bottom	DEGC	0.0012818
C-21 Pressure	PSIG	6.888640881	C-2A Bed 3 Bottom	DEGC	0.0012818
C-8 Pressure (NG blanket o	PSIG	14.52484417	C-2B Bed 3 Bottom	DEGC	0.0012818
C-8 Pressure (NG blanket i	PSIG	14.54091549	C-2A Bed 3 Bottom	DEGC	0.0012818
C-1 Pressure (NG blanket o	PSIG	49.95307922	C-2B Bed 3 Bottom	DEGC	0.0012818
C-1 Pressure (NG blanket i	PSIG	49.80207443	F-1B Firebox bottom temp	DEGC	341.218109
F-2 Fire box pressure	INH2O	-0.161721513	F-1 Xover Pass 2	DEGC	44.8372955

F-2A Pilot gas pressure	PSIG	10.02167892	C-9A Bed 3 top	DEGC	0.0012818
F-2B Pilot gas pressure	PSIG	9.947300911	C-9A Bed 3 EIT	DEGC	0.0012818
C-13 Pressure	PSIG	13.51927567	C-9B Bed 3 top	DEGC	0.0012818
C-15 Pressure	PSIG	17.4975338	C-9B Bed 3 EIT	DEGC	0.0012818
C-22 Pressure	PSIG	20.82194328	C-9A Bed 3 top	DEGC	0.0012818
E-5/12 Combined steam pres	PSIG	149.3437958	C-9B Bed 3 top	DEGC	0.0012818
K-2 Discharge pressure	INH2O	3.856868029	C-9A Bed 3 top	DEGC	0.0012818
K-4 Discharge pressure	INH2O	3.599595785	C-9B Bed 3 top	DEGC	0.0012818
F-1 Firebox pressure	INH2O	-0.161942616	C-9A Bed 3 top	DEGC	0.0012818
Normalized PD61A	PSID	10.40683746	C-9B Bed 3 top	DEGC	0.0012818
Normalized PD61B	PSID	25.04226112	C-9A Bed 3 top	DEGC	0.0012818
Normalized PD62A	PSID	21.00436592	C-9B Bed 3 top	DEGC	0.0012818
Normalized PD62B	PSID	35.32761383	C-9A Bed 3 top	DEGC	0.0012818
Normalized PD63A	PSID	42.39459229	C-9B Bed 3 top	DEGC	0.0012818
Normalized PD63B	PSID	Bad	C-9A Bed 3 top	DEGC	0.0012818
Normalized PD64A	PSID	Bad	C-9B Bed 3 top	DEGC	0.0012818
Normalized PD64B	PSID	Bad	C-9A Bed 3 top	DEGC	0.0012818
Normalized PD89A	PSID	Bad	C-9B Bed 3 top	DEGC	0.0012818
Normalized PD89B	PSID	Bad	C-9A Bed 3 top	DEGC	0.0012818
C-2A circuit DP	PSID	Bad	C-9B Bed 3 top	DEGC	0.0012818
C-2A DP normalization fact	-	94.43933868	C-9A Bed 3 top	DEGC	0.0012818
C-2B circuit DP	PSID	Bad	C-9B Bed 3 top	DEGC	0.0012818
C-2B DP normalization fact	-	110	F-1 Xover Pass 1	DEGC	26.7788124
C-9A circuit DP	PSID	Bad	C-9A Bed 3 upper	DEGC	0.0012818
C-9A DP normalization fact	-	110	C-9B Bed 3 upper	DEGC	0.0012818
C-9B circuit DP	PSID	Bad	C-9A Bed 3 upper	DEGC	0.0012818
C-9B DP normalization fact	-	110	C-9B Bed 3 upper	DEGC	0.0012818
Normalized PD90A	PSID	13.42391777	C-9A Bed 3 upper	DEGC	0.0012818
Normalized PD90B	PSID	46.30249786	C-9B Bed 3 upper	DEGC	0.0012818
Normalized PD91A	PSID	39.81251526	C-9A Bed 3 upper	DEGC	0.0012818
Normalized PD91B	PSID	0	C-9B Bed 3 upper	DEGC	0.0012818
Normalized PD92A	PSID	4.101708412	C-9A Bed 3 upper	DEGC	0.0012818
Normalized PD92B	PSID	Bad	C-9B Bed 3 upper	DEGC	0.0012818
Instrument air filter DP	PSID	0.001281798	C-9A Bed 3 upper	DEGC	0.0012818
Feed filter DP	PSID	2.421720266	C-9B Bed 3 upper	DEGC	0.0012818
E-21 Flue gas DP	INH2O	2.600954771	C-9A Bed 3 middle	DEGC	0.0012818
E-22 Flue gas DP	INH2O	4.290657043	C-9B Bed 3 middle	DEGC	0.0012818
E-5/12 steam to LGO DP	PSID	0	C-9A Bed 3 middle	DEGC	0.0012818
K-1 DP	PSID	181.6849823	C-9B Bed 3 middle	DEGC	0.0012818
K-1 Seal Gas Inlet/Balanci	PSID	15.8827858	C-9A Bed 3 middle	DEGC	0.0012818
G-10B Lube Oil Filter DP	PSID	6.742857456	C-9B Bed 3 middle	DEGC	0.0012818
G-1 Lube Oil Filter DP	PSID	9.099514008	C-9A Bed 3 middle	DEGC	0.0012818
G-3A Lube Oil Filter DP	PSID	9.17807579	C-9B Bed 3 middle	DEGC	0.0012818
G-3B Lube Oil Filter DP	PSID	18.52014732	F-1A Firebox top temp	DEGC	390.617218
G-5A Lube Oil Filter DP	PSID	27.30158806	C-9A Bed 3 middle	DEGC	0.0012818
G-5B Lube Oil Filter DP	PSID	14.59340668	C-9B Bed 3 middle	DEGC	0.0012818
G-6A Lube Oil Filter DP	PSID	16.32035637	C-9A Bed 3 middle	DEGC	0.0012818
G-6B Lube Oil Filter DP	PSID	20.58119774	C-9B Bed 3 middle	DEGC	0.0012818
Y-12 DP	PSID	0.002685142	C-9A Bed 3 lower	DEGC	0.0012818

C-16 DP	PSID	0	C-9B Bed 3 lower	DEGC	0.0012818
F-1A Pass 1 DP	PSID	4.181627274	C-9A Bed 3 lower	DEGC	0.0012818
F-1A Pass 2 DP	PSID	3.017828465	C-9B Bed 3 lower	DEGC	0.0012818
F-1B Pass 3 DP	PSID	4.07652235	C-9A Bed 3 lower	DEGC	0.0012818
C-9A Bed 1 DP	PSID	0.087507233	C-9B Bed 3 lower	DEGC	0.0012818
C-9B Bed 1 DP	PSID	0.213176638	C-9A Bed 3 lower	DEGC	0.0012818
C-9A Bed 2 DP	PSID	0.176645949	C-9B Bed 3 lower	DEGC	0.0012818
C-9B Bed 2 DP	PSID	0.297871858	C-9A Bed 3 lower	DEGC	0.0012818
C-9A Bed 3 DP	PSID	0.362006128	C-9B Bed 3 lower	DEGC	0.0012818
C-9B Bed 3 DP	PSID	0.547796488	C-9A Bed 3 lower	DEGC	0.0012818
C-9A Overall DP	PSID	0.831139088	C-9B Bed 3 lower	DEGC	0.0012818
C-9B Overall DP	PSID	0.553737819	F-1 Pass 1 COT	DEGC	165.477203
F-1B Pass 4 DP	PSID	4.654711723	150# BFW temp	DEGC	18.5145283
C-19 DP	PSID	0.795236647	E-2A/E/J UTLGO inlet temp	DEGC	51.4706039
C-2A Overall DP	PSID	0.913186669	E-2B/F/K UTLGO inlet temp	DEGC	51.7807693
C-2B Overall DP	PSID	0.537809372	E-2C/G/L UTLGO inlet temp	DEGC	51.5550919
C-2A Bed 1 DP	PSID	0.143917918	E-2D/H/M UTLGO inlet temp	DEGC	51.619606
C-2B Bed 1 DP	PSID	0.203996539	F-1 Pass 3 COT	DEGC	166.659973
C-2A Bed 2 DP	PSID	0.41867128	F-1A Outlet temp	DEGC	165.714294
C-2B Bed 2 DP	PSID	0.016846964	C-9A Bed 3 bottom	DEGC	0.0012818
C-2A Bed 3 DP	PSID	0.048254043	C-9B Bed 3 bottom	DEGC	0.0012818
C-2B Bed 3 DP	PSID	0.405002624	C-9A Bed 3 bottom	DEGC	0.0012818
F-1 Convection section pre	INH2O	-0.189304024	C-9B Bed 3 bottom	DEGC	0.0012818
F-2 Convection section pre	INH2O	-1	C-9A Bed 3 bottom	DEGC	0.0012818
F-1A Air pressure	INH2O	0	C-9B Bed 3 bottom	DEGC	0.0012818
F-1A Air pressure	INH2O	-0.029375546	C-9A Bed 3 bottom	DEGC	0.0012818
E-21 Flue gas outlet press	INH2O	-2.624397755	C-9B Bed 3 bottom	DEGC	0.0012818
E-21 Flue gas inlet pressu	INH2O	-0.039072037	C-9A Bed 3 bottom	DEGC	0.0012818
E-22 Flue gas inlet pressu	INH2O	-8	C-9B Bed 3 bottom	DEGC	0.0012818
F-1A Firebox pressure	INH2O	-0.58777529	C-9A Bed 3 bottom	DEGC	0.0012818
E-22 Flue gas outlet press	INH2O	-3.703904867	C-9B Bed 3 bottom	DEGC	0.0012818
E-12 LGO inlet pressure	PSIG	17.83275414	C-9A Bed 3 bottom	DEGC	0.0012818
E-5 LGO inlet pressure	PSIG	154.9687347	C-9B Bed 3 bottom	DEGC	0.0012818
H-2 discharge pressure to	PSIG	0.001281798	C-9A Bed 3 bottom	DEGC	0.0012818
K-1 Suction pressure	PSIG	1055.677734	C-9B Bed 3 bottom	DEGC	0.0012818
K-1 Discharge pressure	PSIG	1246.47937	C-9A Bed 3 bottom	DEGC	0.0012818
F-1A Pilot gas pressure tr	PSIG	9.91941452	C-9B Bed 3 bottom	DEGC	0.0012818
F-1B Pilot gas pressure tr	PSIG	10.01060581	C-9A Bed 3 bottom	DEGC	0.0012818
K-1 Discharge-End Prinmary	PSIG	3.858364105	C-9B Bed 3 bottom	DEGC	0.0012818
K-1 Suction-End Primary Ve	PSIG	3.858364105	F-1B Outlet temp	DEGC	163.22345
F-1A Fuel gas pressure	PSIG	0.001281798	C-9A Bed 3 bottom	DEGC	0.0012818
F-1B Fuel gas pressure	PSIG	0.001281798	C-9B Bed 3 bottom	DEGC	0.0012818

G-10B Lube Oil Inlet Heade	PSIG	45.78388596	C-9A Bed 3 bottom	DEGC	0.0012818
G-10B Lube Oil Inlet Heade	PSIG	47.44810867	C-9B Bed 3 bottom	DEGC	0.0012818
F-1A Fuel gas pressure tri	PSIG	3.211798906	C-9A Bed 3 bottom	DEGC	0.0012818
F-1B Fuel gas pressure tri	PSIG	5.219521523	C-9B Bed 3 bottom	DEGC	0.0012818
F-1B Outlet pressure	PSIG	0.001281798	C-9A Bed 3 bottom	DEGC	0.0012818
K-1 Lube Oil Pump Discharg	PSIG	0.278765678	C-9B Bed 3 bottom	DEGC	0.0012818
K-1 N2 Seal Header	PSIG	14.52014732	C-9A Bed 3 bottom	DEGC	0.0012818
G-1 Lube Oil Inlet Header	PSIG	31.02014732	C-9B Bed 3 bottom	DEGC	0.0012818
G-1 Lube Oil Inlet Header	PSIG	30.99678421	C-9A Bed 3 bottom	DEGC	0.0012818
G-1 Lube Oil Inlet Header	PSIG	30.87362671	C-9B Bed 3 bottom	DEGC	0.0012818
G-3A Lube Oil Inlet Header	PSIG	28.90110016	C-9A Bed 3 bottom	DEGC	0.0012818
G-3B Lube Oil Inlet Header	PSIG	27.6556778	C-9B Bed 3 bottom	DEGC	0.0012818
G-3A Lube Oil Inlet Header	PSIG	28.86446953	C-9A Bed 3 bottom	DEGC	0.0012818
G-3B Lube Oil Inlet Header	PSIG	27.54578781	C-9B Bed 3 bottom	DEGC	0.0012818
G-3A Lube Oil Inlet Header	PSIG	28.86446953	E-2A Effluent outlet temp	DEGC	0
G-3B Lube Oil Inlet Header	PSIG	27.3992672	E-2B Effluent outlet temp	DEGC	65.4456711
E-21 Air outlet pressure	INH2O	1.5	E-2C Effluent outlet temp	DEGC	65.3235703
G-5A Lube Oil Inlet Header	PSIG	28.16849899	E-2D Effluent outlet temp	DEGC	63.4920654
G-5B Lube Oil Inlet Header	PSIG	28.24175835	Air to F-1A/B	DEGC	110.06778
G-5A Lube Oil Inlet Header	PSIG	28.31501961	E-6A/E Effluent outlet tem	DEGC	72.5274734
G-5B Lube Oil Inlet Header	PSIG	28.53479958	E-6B/F Effluent outlet tem	DEGC	65.7875443
G-5A Lube Oil Inlet Header	PSIG	28.02197838	E-6C/G Effluent outlet tem	DEGC	70.9157486
G-5B Lube Oil Inlet Header	PSIG	29.7857151	E-6D/H Effluent outlet tem	DEGC	68.7179489
G-6A Lube Oil Inlet Header	PSIG	27.94871902	C-2A Outlet temp	DEGC	146.977142
G-6B Lube Oil Inlet Header	PSIG	25.23809624	C-2B Outlet temp	DEGC	145.954559
G-6A Lube Oil Inlet Header	PSIG	28.97435951	C-13 Naphtha to C-14	DEGC	12.5592155
G-6B Lube Oil Inlet Header	PSIG	25.23809624	E-2J UTLGO outlet temp	DEGC	127.381187
G-6A Lube Oil Inlet Header	PSIG	27.80219841	E-2K UTLGO outlet temp	DEGC	127.015884
G-6B Lube Oil Inlet Header	PSIG	25.20146561	E-2L UTLGO outlet temp	DEGC	125.664581
C-26 Pressure	PSIG	58.28265381	E-2M UTLGO outlet temp	DEGC	125.93161
K-1 Discharge pressure	PSIG	0.001281798	Treat Gas Temp	DEGC	51.1543808
2nd Stage feed pump suctio	PSIG	14.83516502	H-2 Discharge temp to 8-1/	DEGC	47.8528099
C-9A Inlet pressure	PSIG	1060.439453	Make-up H2 temp	DEGC	19.1620083
C-9B Inlet pressure	PSIG	1060.794312	E-3A air inlet temp	DEGC	13.1641569
C-6 Stripping steam pressu	PSIG	608.0148926	E-3A air inlet temp	DEGC	11.6557026
C-1 Pressure (NG blanket o	PSIG	0.001281798	E-3B air inlet temp	DEGC	12.8966284
C-1 Pressure (NG blanket i	PSIG	0.001281798	E-3B air inlet temp	DEGC	12.6270065
F-1A Pass 1 inlet pressure	PSIG	0.001281798	E-4 Air inlet temp	DEGC	3.46385169
F-2 Fire box pressure trip	INH2O	-0.153738692	E-4 Air inlet temp	DEGC	4.19281673
F-2A Firebox pressure	INH2O	-0.435646981	E-7A air outlet temp	DEGC	11.2580776

F-1A Pass 2 inlet pressure	PSIG	0.001281798	E-7A air outlet temp	DEGC	8.25025272
F-2A Pilot gas pressure tr	PSIG	9.728939056	E-7B air outlet temp	DEGC	14.1405869
F-2B Pilot gas pressure tr	PSIG	9.91941452	E-7B air outlet temp	DEGC	12.0166626
F-2A Fuel gas pressure	PSIG	0.001281798	E-7C air outlet temp	DEGC	14.5918789
F-2B Fuel gas pressure	PSIG	0.001281798	E-7C air outlet temp	DEGC	13.9994287
F-2A Fuel gas pressure tri	PSIG	7.678543091	E-7D air outlet temp	DEGC	13.2496881
F-2B Fuel gas pressure tri	PSIG	8.485411644	E-7D air outlet temp	DEGC	12.888176
Instrument air pressure to	PSIG	112.7530212	E-8 air inlet temp	DEGC	2.22998357
Instrument air pressure to	PSIG	112.4717026	E-8 air inlet temp	DEGC	4.2149992
Instrument air pressure to	PSIG	112.6963882	E-9A air inlet temp	DEGC	2.27292609
E-22 Air outlet pressure	INH2O	1.5	E-9A air inlet temp	DEGC	2.72557187
F-1B Pass 3 inlet pressure	PSIG	0.001281798	E-9B air inlet temp	DEGC	7.31797886
C-6 O/H Pressure	PSIG	155.028244	E-9B air inlet temp	DEGC	2.62229443
F-1B Pass 4 inlet pressure	PSIG	0.001281798	E-14B air inlet temp	DEGC	6.40266609
F-1A Outlet pressure	PSIG	0.001281798	E-14B air inlet temp	DEGC	5.18049955
K-3 Discharge pressure	INH2O	0.143179938	E-14A air inlet temp	DEGC	5.09780359
F-1B Firebox pressure	INH2O	-0.470321655	E-14A air inlet temp	DEGC	5.45627022
C-9A Outlet pressure	PSIG	1060.775635	E-14D air inlet temp	DEGC	2.88462138
C-9B Outlet pressure	PSIG	1059.596436	E-14D air inlet temp	DEGC	2.75822806
Make-up H2 pressure	PSIG	0.001281798	E-14C air inlet temp	DEGC	3.74837279
C-14 O/H pressure	PSIG	17.5573616	E-14C air inlet temp	DEGC	3.163872
F-2B Firebox pressure	INH2O	-0.470701188	E-21 Air inlet temp	DEGC	10.9646158
C-14 Stripping steam press	PSIG	608.5379028	E-21 Air outlet temp	DEGC	138.928833
C-2A Inlet pressure	PSIG	1063.043945	E-22 Air inlet temp	DEGC	12.9178495
C-2B Inlet pressure	PSIG	1064.609009	E-22 Air outlet temp	DEGC	118.460045
K-5 Discharge pressure	INH2O	0.421025634	C-2A Bed 1 Top	DEGC	163.595139
F-1 Firebox pressure trip	INH2O	-0.13392581	C-2B Bed 1 Top	DEGC	161.683228
C-2A Outlet pressure	PSIG	1064.100342	C-2A Bed 1 Top	DEGC	161.609222
C-2B Outlet pressure	PSIG	1062.977905	C-2B Bed 1 Top	DEGC	161.818176
F-2A Air pressure	INH2O	0.019531136	C-2A Bed 1 Top	DEGC	163.596802
F-2B Air pressure	INH2O	0.115765572	C-2B Bed 1 Top	DEGC	161.546097
C-30 pressure (NG blanket	PSIG	14.36080647	C-2A Bed 1 Top	DEGC	161.900757
C-30 pressure (NG blanket	PSIG	14.27633476	C-2B Bed 1 Top	DEGC	160.139603
H-2 discharge pressure to	PSIG	10.32300568	C-2A Bed 1 Bottom	DEGC	162.25383
F-1A Fuel gas pressure	PSIG	3.072086573	C-2B Bed 1 Bottom	DEGC	161.488281
F-1B Fuel gas pressure	PSIG	4.864146233	C-2A Bed 1 Bottom	DEGC	162.042099
K-1 Discharge pressure	PSIG	1235.033691	C-2B Bed 1 Bottom	DEGC	161.920776
C-17 Pressure (NG blanket	PSIG	105.2232666	C-2A Bed 1 Bottom	DEGC	161.595703
C-17 Pressure (NG blanket	PSIG	105.06987	C-2B Bed 1 Bottom	DEGC	161.625473
C-8 Pressure (NG blanket o	PSIG	14.56390476	C-2A Bed 1 Bottom	DEGC	162.519806
C-8 Pressure (NG blanket i	PSIG	14.47978497	C-2B Bed 1 Bottom	DEGC	160.674683
C-1 Pressure (NG blanket o	PSIG	49.84109116	C-2A Bed 1 Bottom	DEGC	161.857086
C-1 Pressure (NG blanket i	PSIG	49.84706116	C-2B Bed 1 Bottom	DEGC	161.481705
F-2A Fuel gas pressure	PSIG	8.005834579	C-2A Bed 1 Bottom	DEGC	161.972107
F-2B Fuel gas pressure	PSIG	8.453835487	C-2B Bed 1 Bottom	DEGC	161.940262
Make-up H2 pressure	PSIG	1743.649902	C-2A Bed 1 Bottom	DEGC	162.257126

F-1A Pilot gas pressure	% OPEN	3.209705353	C-2B Bed 1 Bottom	DEGC	160.60817
F-1B Pilot gas pressure	% OPEN	1.592534781	C-2A Bed 1 Bottom	DEGC	162.303696
C-30 pressure (NG blanket	% OPEN	-5	C-2B Bed 1 Bottom	DEGC	160.34465
C-30 pressure (NG blanket	% OPEN	-5	C-2A Bed 1 Bottom	DEGC	163.089096
C-24 Pressure (to flare)	% OPEN	100	C-2B Bed 1 Bottom	DEGC	160.855591
C-7 Pressure	% OPEN	-3.937699795	C-2A Bed 1 Bottom	DEGC	163.261703
C-24 Pressure (to H-2)	% OPEN	100	C-2B Bed 1 Bottom	DEGC	161.345306
C-17 Pressure (NG blanket	% OPEN	-5	C-2A Bed 1 Bottom	DEGC	162.910919
C-17 Pressure (NG blanket	% OPEN	-5	C-2B Bed 1 Bottom	DEGC	161.60611
C-21 Pressure	% OPEN	-5	C-2A Bed 1 Bottom	DEGC	162.928894
C-8 Pressure (NG blanket o	% OPEN	-5	C-2B Bed 1 Bottom	DEGC	160.753693
C-8 Pressure (NG blanket i	% OPEN	-4.94763279	C-2A Bed 1 Bottom	DEGC	162.033081
C-1 Pressure (NG blanket o	% OPEN	1.050642371	C-2B Bed 1 Bottom	DEGC	160.788895
C-1 Pressure (NG blanket i	% OPEN	-5	C-2A Bed 1 Bottom	DEGC	163.2202
F-2 Fire box pressure	% OPEN	22	C-2B Bed 1 Bottom	DEGC	160.721054
F-2 Fire box pressure (dam	% OPEN	0	E-7G air inlet temp	DEGC	16.0369167
F-2A Pilot gas pressure	% OPEN	9.544822693	E-7G air inlet temp	DEGC	16.0369167
F-2B Pilot gas pressure	% OPEN	3.156511068	E-7H air inlet temp	DEGC	16.2192898
C-13 Pressure	% OPEN	-5	E-7H air inlet temp	DEGC	14.9382668
C-15 Pressure	% OPEN	-5	E-7E air inlet temp	DEGC	14.1034374
C-22 Pressure	% OPEN	-5	E-7E air inlet temp	DEGC	10.8904657
E-5/12 Combined steam pres	% OPEN	50	E-7F air inlet temp	DEGC	14.8554125
K-2 Discharge pressure	% OPEN	28.29249573	E-7F air inlet temp	DEGC	14.7405882
K-4 Discharge pressure	% OPEN	31	C-9A Bed 1 Top	DEGC	157.254852
F-1 Firebox pressure	% OPEN	10.2814455	C-9B Bed 1 Top	DEGC	153.924332
F-1 Firebox pressure (damp	% OPEN	-5	C-9A Bed 1 Top	DEGC	157.424622
K-1 Perf. Controller O/P	PSIG	794.8718262	C-9B Bed 1 Top	DEGC	152.641663
C-30 pressure (NG blanket	% OPEN	Bad	C-9A Bed 1 Top	DEGC	156.581375
C-17 Pressure (NG blanket	% OPEN	-0.216421485	C-9B Bed 1 Top	DEGC	154.458572
C-8 Pressure (NG blanket o	% OPEN	41.7841301	C-9A Bed 1 Top	DEGC	155.896912
C-1 Pressure (NG blanket o	% OPEN	1.531075954	C-9B Bed 1 Top	DEGC	153.848785
K-1 Super Imposed Speed	-	118.6813202	C-9A Bed 1 Middle	DEGC	156.739349
K-1 Speed	RPM	10245.82422	C-9B Bed 1 Middle	DEGC	153.193359
K-1 Speed	KRPM	0.001281798	C-9A Bed 1 Middle	DEGC	156.292892
K-1 Output Speed	RPM	49.18193054	C-9B Bed 1 Middle	DEGC	153.618591
K-1 Output Speed	RPM	49.18193054	C-9A Bed 1 Middle	DEGC	156.317123
C-28 steam temp	DEGC	257.6503906	C-9B Bed 1 Middle	DEGC	153.128403
E-14 LGO outlet temp	DEGC	49.02451706	C-9A Bed 1 Middle	DEGC	155.20639
E-6A Effluent outlet temp	DEGC	74.4182663	C-9B Bed 1 Middle	DEGC	152.442856
E-6B Effluent outlet temp	DEGC	67.73103333	C-9A Bed 1 Middle	DEGC	155.274963
E-6C Effluent outlet temp	DEGC	70.90003967	C-9B Bed 1 Middle	DEGC	153.968826
E-6D Effluent outlet temp	DEGC	70.1142807	C-9A Bed 1 Middle	DEGC	156.745178
K-4 inlet temp	DEGC	25.14175606	C-9B Bed 1 Middle	DEGC	154.214447

C-6 O/H temp	DEGC	10.18018341	C-2A Bed 2 Top	DEGC	159.320358
E-16 Vapour outlet	DEGC	0.001281798	C-2B Bed 2 Top	DEGC	159.019379
F-2A Outlet temp	DEGC	161.7839661	C-2A Bed 2 Top	DEGC	160.808807
F-2A Outlet temp	DEGC	157.9441223	C-2B Bed 2 Top	DEGC	160.105667
E-16 outlet temp	DEGC	25.73928642	C-2A Bed 2 Top	DEGC	160.122162
E-3's Fan Motor Control	%	-5	C-2B Bed 2 Top	DEGC	155.196655
Stripper O/H Acc. Temp	DEGC	8.451743126	C-2A Bed 2 Top	DEGC	157.281952
E-4's Fan Motor Control	%	69.66156769	C-2B Bed 2 Top	DEGC	158.268509
C-11 Inlet temp	DEGC	50.20044708	C-2A Bed 2 Top	DEGC	159.257034
E-7's Fan Motor Control	%	0	C-2B Bed 2 Top	DEGC	158.358749
E-8 process outlet temp	DEGC	7.159174919	C-2A Bed 2 Top	DEGC	160.410889
E-8's Fan Motor Control	%	0	C-2B Bed 2 Top	DEGC	157.425903
C-15 temp	DEGC	7.439739704	C-2A Bed 2 Top	DEGC	159.964737
E-9's Fan Motor Control	%	0	C-2B Bed 2 Top	DEGC	158.20993
C-27 Condensate blowdown t	DEGC	13.40150261	C-2A Bed 2 Top	DEGC	160.476288
K-2 inlet temp	DEGC	10.48980331	C-2B Bed 2 Top	DEGC	159.44046
E-21 Flue gas outlet temp	DEGC	75.21339417	C-2A Bed 2 Top	DEGC	160.389847
E-22 Flue gas outlet temp	DEGC	72.08912659	C-2B Bed 2 Top	DEGC	158.242386
2nd stage LGO temp	DEGC	39.06752396	C-2A Bed 2 Top	DEGC	159.615036
E-29 Lean DEA outlet temp	DEGC	15.80372238	C-2B Bed 2 Top	DEGC	158.902786
C-2A Bed 2 Avg Inlet	DEGC	159.8902893	C-2A Bed 2 Upper	DEGC	159.52594
C-2B Bed 2 Avg Inlet	DEGC	158.3341064	C-2B Bed 2 Upper	DEGC	158.65184
C-14 O/H temp	DEGC	7.5204072	C-2A Bed 2 Upper	DEGC	159.619003
C-9A Bed 2 Avg Inlet	DEGC	152.7293854	C-2B Bed 2 Upper	DEGC	158.245117
C-9B Bed 2 Avg Inlet	DEGC	151.9982147	C-2A Bed 2 Upper	DEGC	159.332153
C-2A Bed 3 Avg Inlet	DEGC	154.6762543	C-2B Bed 2 Upper	DEGC	157.239746
C-2B Bed 3 Avg Inlet	DEGC	153.0225372	C-2A Bed 2 Upper	DEGC	159.04776
E-2A/E/J effluent outlet t	DEGC	65.9797821	C-2B Bed 2 Upper	DEGC	158.221909
E-2B/F/K effluent outlet t	DEGC	67.22138214	C-2A Bed 2 Upper	DEGC	158.034729
E-2C/G/L effluent outlet t	DEGC	66.59993744	C-2B Bed 2 Upper	DEGC	157.902771
E-2D/H/M effluent outlet t	DEGC	64.77757263	C-2A Bed 2 Upper	DEGC	160.050049
C-9A Bed 3 Avg Inlet	DEGC	149.8513031	C-2B Bed 2 Upper	DEGC	156.879486
C-9B Bed 3 Avg Inlet	DEGC	150.4467316	C-2A Bed 2 Lower	DEGC	158.991257
F-1A Outlet temp	DEGC	166.6330566	C-2B Bed 2 Lower	DEGC	156.602646
F-1B Outlet temp	DEGC	166.076355	C-2A Bed 2 Lower	DEGC	158.738724
C-2A/B EIT	DEGC	0.001281798	C-2B Bed 2 Lower	DEGC	156.426544
C-2A Bed 1 2/3 EIT	DEGC	162.1923523	C-2A Bed 2 Lower	DEGC	159.269775
C-2B Bed 1 2/3 EIT	DEGC	161.0956268	C-2B Bed 2 Lower	DEGC	155.218201
C-9A Bed 1 2/3 EIT	DEGC	154.9939575	C-2A Bed 2 Lower	DEGC	156.69693
C-9B Bed 1 2/3 EIT	DEGC	152.4161835	C-2B Bed 2 Lower	DEGC	157.559525
C-2A Bed 2 2/3 EIT	DEGC	157.827652	C-2A Bed 2 Lower	DEGC	158.748367
C-2B Bed 2 2/3 EIT	DEGC	155.9834137	C-2B Bed 2 Lower	DEGC	156.879974
C-9A Bed 2 2/3 EIT	DEGC	151.6834259	C-2A Bed 2 Lower	DEGC	159.218369
C-9B Bed 2 2/3 EIT	DEGC	151.3846283	C-2B Bed 2 Lower	DEGC	157.165131
C-2A Bed 3 2/3 EIT	DEGC	150.7835693	C-9A Bed 1 Bottom	DEGC	152.209122
C-2B Bed 3 2/3 EIT	DEGC	149.7583008	C-9B Bed 1 Bottom	DEGC	153.429733
E-2A/E/J UTLGO forced flow	% OPEN	105	C-9A Bed 1 Bottom	DEGC	154.734604
E-2A/E/J UTLGO B/P	% OPEN	-5	C-9B Bed 1 Bottom	DEGC	151.919968

E-2B/F/K UTLGO forced flow	% OPEN	105	C-9A Bed 1 Bottom	DEGC	153.919983
E-2B/F/K UTLGO B/P	% OPEN	-4.987654209	C-9B Bed 1 Bottom	DEGC	152.082916
E-2C/G/L UTLGO forced flow	% OPEN	105	C-9A Bed 1 Bottom	DEGC	154.480789
E-2C/G/L UTLGO B/P	% OPEN	-5	C-9B Bed 1 Bottom	DEGC	151.317734
E-2D/H/M UTLGO forced flow	% OPEN	105	C-9A Bed 1 Bottom	DEGC	153.912033
E-2D/H/M UTLGO B/P	% OPEN	-5	C-9B Bed 1 Bottom	DEGC	150.506195
C-9A Bed 3 2/3 EIT	DEGC	148.2123108	C-9A Bed 1 Bottom	DEGC	153.990341
C-9B Bed 3 2/3 EIT	DEGC	148.6815948	C-9B Bed 1 Bottom	DEGC	151.180328
Reactor C-2A WABT	DEGC	156.374176	C-9A Bed 1 Bottom	DEGC	153.437012
Reactor C-2B WABT	DEGC	154.6163788	C-9B Bed 1 Bottom	DEGC	152.555496
Reactor C-9A WABT	DEGC	151.4501953	C-9A Bed 1 Bottom	DEGC	154.794373
Reactor C-9B WABT	DEGC	150.9514008	C-9B Bed 1 Bottom	DEGC	152.50882
C-2A Bed 1 average temp	DEGC	162.5240021	C-9A Bed 1 Bottom	DEGC	154.284531
C-2B Bed 1 average temp	DEGC	161.0104675	C-9B Bed 1 Bottom	DEGC	152.410034
C-2A Bed 1 inlet average t	DEGC	162.5498199	C-9A Bed 1 Bottom	DEGC	154.122162
C-2B Bed 1 inlet average t	DEGC	160.9738464	C-9B Bed 1 Bottom	DEGC	152.132813
C-2A Bed 1 outlet average	DEGC	162.1550598	C-9A Bed 1 Bottom	DEGC	154.807632
C-2B Bed 1 outlet average	DEGC	160.9868164	C-9B Bed 1 Bottom	DEGC	152.549667
C-2A Bed 1 outlet spread t	DEGC	0.868557334	C-9A Bed 1 Bottom	DEGC	154.860321
C-2B Bed 1 outlet spread t	DEGC	0.63159889	C-9B Bed 1 Bottom	DEGC	151.544769
C-2A Bed 2 average temp	DEGC	158.1875	C-9A Bed 1 Bottom	DEGC	154.064819
C-2B Bed 2 average temp	DEGC	156.3614044	C-9B Bed 1 Bottom	DEGC	152.131821
C-2A Bed 2 inlet average t	DEGC	159.7862854	C-9A Bed 1 Bottom	DEGC	155.808792
C-2B Bed 2 inlet average t	DEGC	158.4343567	C-9B Bed 1 Bottom	DEGC	152.531036
C-2A Bed 2 outlet average	DEGC	157.2202911	C-2A Bed 2 Bottom	DEGC	157.226578
C-2B Bed 2 outlet average	DEGC	155.0097504	C-2B Bed 2 Bottom	DEGC	155.497787
C-2A Bed 2 inlet spread te	DEGC	0.888058424	C-2A Bed 2 Bottom	DEGC	156.738037
C-2B Bed 2 inlet spread te	DEGC	1.759442568	C-2B Bed 2 Bottom	DEGC	155.684937
C-2A Bed 2 outlet spread t	DEGC	1.903775454	C-2A Bed 2 Bottom	DEGC	157.569489
C-2B Bed 2 outlet spread t	DEGC	1.105167031	C-2B Bed 2 Bottom	DEGC	154.936844
C-2A Bed 3 average temp	DEGC	151.6808929	C-2A Bed 2 Bottom	DEGC	157.180603
C-2B Bed 3 average temp	DEGC	149.7183533	C-2B Bed 2 Bottom	DEGC	155.608704
C-2A Bed 3 inlet average t	DEGC	154.5403748	C-2A Bed 2 Bottom	DEGC	157.006302
C-2B Bed 3 inlet average t	DEGC	152.8177948	C-2B Bed 2 Bottom	DEGC	155.308319
C-2A Bed 3 outlet average	DEGC	149.3596954	C-2A Bed 2 Bottom	DEGC	156.229919
C-2B Bed 3 outlet average	DEGC	148.0543213	C-2B Bed 2 Bottom	DEGC	154.757874
C-2A Bed 3 inlet spread te	DEGC	1.391807795	C-2A Bed 2 Bottom	DEGC	156.398468
C-2B Bed 3 inlet spread te	DEGC	1.094186306	C-2B Bed 2 Bottom	DEGC	154.837494
C-9A Bed 1 average temp	DEGC	154.7237701	C-2A Bed 2 Bottom	DEGC	158.401718
C-9B Bed 1 average temp	DEGC	152.4580688	C-2B Bed 2 Bottom	DEGC	155.355408
C-9A Bed 1 inlet average t	DEGC	156.5750122	C-2A Bed 2 Bottom	DEGC	159.296265
C-9B Bed 1 inlet average t	DEGC	153.6392212	C-2B Bed 2 Bottom	DEGC	155.645599
C-9A Bed 1 outlet average	DEGC	154.2081604	C-2A Bed 2 Bottom	DEGC	157.54393
C-9B Bed 1 outlet average	DEGC	152.3969879	C-2B Bed 2 Bottom	DEGC	155.673569
C-9A Bed 1 outlet spread t	DEGC	1.658494592	C-2A Bed 2 Bottom	DEGC	156.552704
C-9B Bed 1 outlet spread t	DEGC	0.966546655	C-2B Bed 2 Bottom	DEGC	153.740891
C-9A Bed 2 average temp	DEGC	151.7853088	C-2A Bed 2 Bottom	DEGC	157.068329

C-9B Bed 2 average temp	DEGC	151.1401062	C-2B Bed 2 Bottom	DEGC	155.088867
C-9A Bed 2 inlet average t	DEGC	152.8771362	C-2A Bed 2 Bottom	DEGC	156.709518
C-9B Bed 2 inlet average t	DEGC	151.6990051	C-2B Bed 2 Bottom	DEGC	156.503799
C-9A Bed 2 outlet average	DEGC	150.9818726	C-2A Bed 2 Bottom	DEGC	157.903854
C-9B Bed 2 outlet average	DEGC	151.2227173	C-2B Bed 2 Bottom	DEGC	155.583923
C-9A Bed 2 inlet spread te	DEGC	50	C-2A Bed 2 Bottom	DEGC	158.213745
C-9B Bed 2 inlet spread te	DEGC	50	C-2B Bed 2 Bottom	DEGC	155.648453
C-9A Bed 2 outlet spread t	DEGC	50	C-2A Bed 2 Bottom	DEGC	156.669662
C-9B Bed 2 outlet spread t	DEGC	50	C-2B Bed 2 Bottom	DEGC	155.985214
C-9A Bed 3 average temp	DEGC	148.1099548	C-2A Bed 2 Bottom	DEGC	157.275787
C-9B Bed 3 average temp	DEGC	148.6453094	C-2B Bed 2 Bottom	DEGC	155.577927
C-9A Bed 3 inlet average t	DEGC	149.8498535	C-2A Bed 2 Bottom	DEGC	158.158005
C-9B Bed 3 inlet average t	DEGC	150.4473572	C-2B Bed 2 Bottom	DEGC	155.400299
C-9A Bed 3 outlet average	DEGC	147.5078735	C-9A Bed 2 top	DEGC	154.249207
C-9B Bed 3 outlet average	DEGC	148.0843964	C-9B Bed 2 top	DEGC	151.915085
C-9A Bed 3 inlet spread te	DEGC	0.678610623	C-9A Bed 2 top	DEGC	153.185211
C-9B Bed 3 inlet spread te	DEGC	0.866812587	C-9B Bed 2 top	DEGC	151.879669
E-1 UTLGO inlet temp	DEGC	24.86976242	C-9A Bed 2 top	DEGC	149.98233
15-1 LGO feed temp	DEGC	0.001281798	C-9B Bed 2 top	DEGC	152.092209
G-1 Lube Oil System	DEGC	35.24523926	C-9A Bed 2 top	DEGC	152.521683
G-1 Thrust Bearing Temp	DEGC	36.47130585	C-9B Bed 2 top	DEGC	150.343399
G-1 Thrust Bearing Temp	DEGC	36.98827744	C-9A Bed 2 top	DEGC	153.498749
G-1 Thrust Bearing Temp	DEGC	35.45702362	C-9B Bed 2 top	DEGC	152.2173
G-1 Thrust Bearing Temp	DEGC	34.72742844	C-9A Bed 2 top	DEGC	152.322571
G-1 NDE J. Bearing Temp	DEGC	32.74725342	C-9B Bed 2 top	DEGC	152.743729
G-1 Skin Temp	DEGC	21.17907333	C-9A Bed 2 top	DEGC	152.783569
15-2 LGO feed temp	DEGC	0.001281798	C-9B Bed 2 top	DEGC	152.666962
G-1 Skin Temp	DEGC	20.65934181	C-9A Bed 2 top	DEGC	152.894257
G-1 DE J. Bearing Temp	DEGC	30.73260117	C-9B Bed 2 top	DEGC	152.324875
G-3A Lube Oil System	DEGC	35.9007225	C-9A Bed 2 top	DEGC	152.031525
G-3B Lube Oil System	DEGC	42.63492203	C-9B Bed 2 top	DEGC	151.932358
G-3A Thrust Bearing Temp	DEGC	35.40496445	C-9A Bed 2 top	DEGC	153.115463
G-3B Thrust Bearing Temp	DEGC	42.1978035	C-9B Bed 2 top	DEGC	151.34108
G-3A Thrust Bearing Temp	DEGC	37.43589783	C-9A Bed 2 upper	DEGC	153.098282
G-3B Thrust Bearing Temp	DEGC	43.58974457	C-9B Bed 2 upper	DEGC	151.27536
G-3A Thrust Bearing Temp	DEGC	34.4715271	C-9A Bed 2 upper	DEGC	152.813583
G-3B Thrust Bearing Temp	DEGC	40.47619247	C-9B Bed 2 upper	DEGC	151.105164
G-3A Thrust Bearing Temp	DEGC	36.54622269	C-9A Bed 2 upper	DEGC	151.332993
G-3B Thrust Bearing Temp	DEGC	43.55311584	C-9B Bed 2 upper	DEGC	152.085785
G-3A NDE J. Bearing Temp	DEGC	16.66666603	C-9A Bed 2 upper	DEGC	152.732681
G-3B NDE J. Bearing Temp	DEGC	40.1098938	C-9B Bed 2 upper	DEGC	151.004028
G-3A Skin Temp	DEGC	45.89704132	C-9A Bed 2 upper	DEGC	152.164108
G-3B Skin Temp	DEGC	36.63003922	C-9B Bed 2 upper	DEGC	148.239166
G-3A Skin Temp	DEGC	38.31634903	C-9A Bed 2 upper	DEGC	152.143143
G-3B Skin Temp	DEGC	31.40415192	C-9B Bed 2 upper	DEGC	151.684708
G-3A DE J. Bearing Temp	DEGC	30.99833488	C-9A Bed 2 lower	DEGC	152.002258
G-3B DE J. Bearing Temp	DEGC	37.80220032	C-9B Bed 2 lower	DEGC	151.283661
G-5A Lube Oil System	DEGC	38.42857361	C-9A Bed 2 lower	DEGC	151.699738
G-5B Lube Oil System	DEGC	37.61904907	C-9B Bed 2 lower	DEGC	151.722443

G-5A Thrust Bearing Temp	DEGC	40.87912369	C-9A Bed 2 lower	DEGC	148.926956
G-5B Thrust Bearing Temp	DEGC	40.43956375	C-9B Bed 2 lower	DEGC	151.240952
G-5A Thrust Bearing Temp	DEGC	41.0256424	C-9A Bed 2 lower	DEGC	151.171509
G-5B Thrust Bearing Temp	DEGC	39.41392136	C-9B Bed 2 lower	DEGC	149.535233
G-5A Thrust Bearing Temp	DEGC	39.48718262	C-9A Bed 2 lower	DEGC	152.125809
G-5B Thrust Bearing Temp	DEGC	39.67033005	C-9B Bed 2 lower	DEGC	151.353592
G-5A Thrust Bearing Temp	DEGC	40.91575241	C-9A Bed 2 lower	DEGC	151.294342
G-5B Thrust Bearing Temp	DEGC	40.98901367	C-9B Bed 2 lower	DEGC	151.108521
G-5A NDE J. Bearing Temp	DEGC	39.96337128	C-2A Bed 3 Top	DEGC	153.245651
G-5B NDE J. Bearing Temp	DEGC	39.41392136	C-2B Bed 3 Top	DEGC	153.335266
G-5A Skin Temp	DEGC	63.14175034	C-2A Bed 3 Top	DEGC	154.916092
G-5B Skin Temp	DEGC	64.8711853	C-2B Bed 3 Top	DEGC	152.83493
G-5A Skin Temp	DEGC	49.20814514	C-2A Bed 3 Top	DEGC	156.186935
G-5B Skin Temp	DEGC	53.73129654	C-2B Bed 3 Top	DEGC	152.32901
G-5A DE J. Bearing Temp	DEGC	35.56776428	C-2A Bed 3 Top	DEGC	153.621384
G-5B DE J. Bearing Temp	DEGC	37.98535156	C-2B Bed 3 Top	DEGC	152.912399
G-6A Lube Oil System	DEGC	37.69557953	C-2A Bed 3 Top	DEGC	154.491104
G-6B Lube Oil System	DEGC	37.46031952	C-2B Bed 3 Top	DEGC	153.06987
G-6A Thrust Bearing Temp	DEGC	36.81318665	C-2A Bed 3 Top	DEGC	155.193817
G-6B Thrust Bearing Temp	DEGC	36.227108	C-2B Bed 3 Top	DEGC	153.105759
G-6A Thrust Bearing Temp	DEGC	36.44688797	C-2A Bed 3 Top	DEGC	155.490402
G-6B Thrust Bearing Temp	DEGC	37.50915909	C-2B Bed 3 Top	DEGC	152.817886
G-6A Thrust Bearing Temp	DEGC	36.44688797	C-2A Bed 3 Top	DEGC	155.080673
G-6B Thrust Bearing Temp	DEGC	36.00732422	C-2B Bed 3 Top	DEGC	153.052094
G-6A Thrust Bearing Temp	DEGC	36.44688797	C-2A Bed 3 Top	DEGC	155.264465
G-6B Thrust Bearing Temp	DEGC	36.48351669	C-2B Bed 3 Top	DEGC	153.390015
G-6A NDE J. Bearing Temp	DEGC	34.24908447	C-2A Bed 3 Top	DEGC	154.265045
G-6B NDE J. Bearing Temp	DEGC	34.46886444	C-2B Bed 3 Top	DEGC	154.338562
G-6A Skin Temp	DEGC	50.15873337	C-2A Bed 3 Upper	DEGC	153.570618
G-6B Skin Temp	DEGC	48.74237061	C-2B Bed 3 Upper	DEGC	151.421661
E-12 LGO outlet temp	DEGC	25.80714607	C-2A Bed 3 Upper	DEGC	152.553711
G-6A Skin Temp	DEGC	40.39742661	C-2B Bed 3 Upper	DEGC	152.430878
G-6B Skin Temp	DEGC	47.96092987	C-2A Bed 3 Upper	DEGC	153.495712
G-6A DE J. Bearing Temp	DEGC	32.67399216	C-2B Bed 3 Upper	DEGC	150.699478
G-6B DE J. Bearing Temp	DEGC	33.69963455	C-2A Bed 3 Upper	DEGC	151.626083
E-29 backwash outlet temp	DEGC	32.62498856	C-2B Bed 3 Upper	DEGC	150.922668
C-2A inlet nozzle skin	DEGC	100.186821	C-2A Bed 3 Upper	DEGC	152.202881
C-2B inlet nozzle skin	DEGC	95.27835846	C-2B Bed 3 Upper	DEGC	151.642242
C-2A inlet nozzle skin	DEGC	79.90427399	C-2A Bed 3 Upper	DEGC	153.91777
C-2B inlet nozzle skin	DEGC	93.11257172	C-2B Bed 3 Upper	DEGC	151.603287
C-2A top shell skin	DEGC	132.4894714	C-2A Bed 3 Lower	DEGC	150.882156
C-2B top shell skin	DEGC	120.6150055	C-2B Bed 3 Lower	DEGC	149.962479
C-2A top shell skin	DEGC	124.7185593	C-2A Bed 3 Lower	DEGC	151.350327
C-2B top shell skin	DEGC	121.5274048	C-2B Bed 3 Lower	DEGC	149.887466
C-2A Bed 1 skin bottom	DEGC	111.9464874	C-2A Bed 3 Lower	DEGC	152.156906
C-2B Bed 1 skin bottom	DEGC	111.4931717	C-2B Bed 3 Lower	DEGC	150.95401
C-2A Bed 1 skin bottom	DEGC	107.8822861	C-2A Bed 3 Lower	DEGC	150.623047

C-2B Bed 1 skin bottom	DEGC	111.6034317	C-2B Bed 3 Lower	DEGC	150.050705
C-2A Bed 1 skin bottom	DEGC	112.765358	C-2A Bed 3 Lower	DEGC	151.225418
C-2B Bed 1 skin bottom	DEGC	112.6261063	C-2B Bed 3 Lower	DEGC	149.485596
C-2A Bed 1 skin bottom	DEGC	112.5974121	C-2A Bed 3 Lower	DEGC	151.82428
C-2B Bed 1 skin bottom	DEGC	108.8853912	C-2B Bed 3 Lower	DEGC	148.692108
C-2A Bed 2 skin middle	DEGC	117.1146088	C-9A Bed 2 bottom	DEGC	150.240662
C-2B Bed 2 skin middle	DEGC	111.2696304	C-9B Bed 2 bottom	DEGC	151.688705
C-2A Bed 2 skin middle	DEGC	117.6391983	C-9A Bed 2 bottom	DEGC	150.292038
C-2B Bed 2 skin middle	DEGC	107.8220139	C-9B Bed 2 bottom	DEGC	149.7957
C-2A Bed 2 skin middle	DEGC	111.2433395	C-9A Bed 2 bottom	DEGC	150.787842
C-2B Bed 2 skin middle	DEGC	107.37043	C-9B Bed 2 bottom	DEGC	150.516754
C-2A Bed 2 skin middle	DEGC	110.5552597	C-9A Bed 2 bottom	DEGC	149.88147
C-2B Bed 2 skin middle	DEGC	108.0381699	C-9B Bed 2 bottom	DEGC	151.892838
C-2A Bed 2 skin bottom	DEGC	115.8178558	C-9A Bed 2 bottom	DEGC	152.060944
C-2B Bed 2 skin bottom	DEGC	107.9060593	C-9B Bed 2 bottom	DEGC	151.881363
C-2A Bed 2 skin bottom	DEGC	109.718483	C-9A Bed 2 bottom	DEGC	152.204697
C-2B Bed 2 skin bottom	DEGC	104.5197525	C-9B Bed 2 bottom	DEGC	149.8414
C-2A Bed 2 skin bottom	DEGC	106.1081696	C-9A Bed 2 bottom	DEGC	151.538803
C-2B Bed 2 skin bottom	DEGC	114.5255356	C-9B Bed 2 bottom	DEGC	152.607269
C-2A Bed 2 skin bottom	DEGC	110.8429031	C-9A Bed 2 bottom	DEGC	150.676575
C-2B Bed 2 skin bottom	DEGC	105.166008	C-9B Bed 2 bottom	DEGC	152.74678
C-2A Bed 3 skin top	DEGC	106.7370148	C-9A Bed 2 bottom	DEGC	151.252197
C-2B Bed 3 skin top	DEGC	111.222702	C-9B Bed 2 bottom	DEGC	151.93808
C-2A Bed 3 skin top	DEGC	103.9140015	C-9A Bed 2 bottom	DEGC	151.625732
C-2B Bed 3 skin top	DEGC	108.2025223	C-9B Bed 2 bottom	DEGC	151.164459
C-2A Bed 3 skin top	DEGC	107.3528748	C-9A Bed 2 bottom	DEGC	150.539398
C-2B Bed 3 skin top	DEGC	110.4853516	C-9B Bed 2 bottom	DEGC	150.919357
C-2A Bed 3 skin top	DEGC	107.0136795	C-9A Bed 2 bottom	DEGC	151.287003
C-2B Bed 3 skin top	DEGC	111.6623917	C-9B Bed 2 bottom	DEGC	151.755203
C-2A Bed 3 skin middle	DEGC	108.0096588	C-9A Bed 2 bottom	DEGC	152.147202
C-2B Bed 3 skin middle	DEGC	117.2881393	C-9B Bed 2 bottom	DEGC	149.869095
C-2A Bed 3 skin middle	DEGC	108.5577774	C-9A Bed 2 bottom	DEGC	151.0755
C-2B Bed 3 skin middle	DEGC	111.7890854	C-9B Bed 2 bottom	DEGC	150.39946
C-2A Bed 3 skin middle	DEGC	120.3792419	C-9A Bed 2 bottom	DEGC	149.650513
C-2B Bed 3 skin middle	DEGC	111.3401794	C-9B Bed 2 bottom	DEGC	149.67897
C-2A Bed 3 skin middle	DEGC	114.6536407	C-9A Bed 2 bottom	DEGC	150.393448
C-2B Bed 3 skin middle	DEGC	109.5753555	C-9B Bed 2 bottom	DEGC	150.562576
C-2A Bed 3 skin bottom	DEGC	104.8345871	C-9A Bed 2 bottom	DEGC	149.441483
C-2B Bed 3 skin bottom	DEGC	102.8813095	C-9B Bed 2 bottom	DEGC	150.641525
C-2A Bed 3 skin bottom	DEGC	98.564888	C-9A Bed 2 bottom	DEGC	151.124542
C-2B Bed 3 skin bottom	DEGC	101.8590088	C-9B Bed 2 bottom	DEGC	151.51741
C-2A Bed 3 skin bottom	DEGC	105.1044083	C-2A Bed 3 Bottom	DEGC	149.389725
C-2B Bed 3 skin bottom	DEGC	103.9845352	C-2B Bed 3 Bottom	DEGC	146.609009
C-2A Bed 3 skin bottom	DEGC	104.5326309	C-2A Bed 3 Bottom	DEGC	149.919998
C-2B Bed 3 skin bottom	DEGC	105.3538895	C-2B Bed 3 Bottom	DEGC	147.795792
C-2A Bottom shell skin	DEGC	108.3968735	C-2A Bed 3 Bottom	DEGC	148.511093
C-2B Bottom shell skin	DEGC	115.2655411	C-2B Bed 3 Bottom	DEGC	147.606308
C-2A Bottom shell skin	DEGC	109.9805222	C-2A Bed 3 Bottom	DEGC	147.246078
C-2B Bottom shell skin	DEGC	112.681015	C-2B Bed 3 Bottom	DEGC	147.480637
C-9A inlet nozzle skin	DEGC	99.49519348	C-2A Bed 3 Bottom	DEGC	147.912048

C-9B inlet nozzle skin	DEGC	85.53178406	C-2B Bed 3 Bottom	DEGC	147.350235
C-9A inlet nozzle skin	DEGC	81.47157288	C-2A Bed 3 Bottom	DEGC	148.322784
C-9B inlet nozzle skin	DEGC	88.38459015	C-2B Bed 3 Bottom	DEGC	148.605484
C-9A top shell skin	DEGC	116.0774689	C-2A Bed 3 Bottom	DEGC	148.877609
C-9B top shell skin	DEGC	127.1777649	C-2B Bed 3 Bottom	DEGC	147.288193
C-9A top shell skin	DEGC	129.2779236	C-2A Bed 3 Bottom	DEGC	149.46489
C-9B top shell skin	DEGC	110.6983261	C-2B Bed 3 Bottom	DEGC	148.067352
C-9A Bed 1 skin bottom	DEGC	109.3676758	C-2A Bed 3 Bottom	DEGC	149.27446
C-9B Bed 1 skin bottom	DEGC	109.8187103	C-2B Bed 3 Bottom	DEGC	148.425354
C-9A Bed 1 skin bottom	DEGC	101.1927948	C-2A Bed 3 Bottom	DEGC	149.586609
C-9B Bed 1 skin bottom	DEGC	101.108345	C-2B Bed 3 Bottom	DEGC	148.977203
C-9A Bed 1 skin bottom	DEGC	105.963913	C-2A Bed 3 Bottom	DEGC	150.838928
C-9B Bed 1 skin bottom	DEGC	96.92684937	C-2B Bed 3 Bottom	DEGC	148.818634
C-9A Bed 1 skin bottom	DEGC	104.415657	C-2A Bed 3 Bottom	DEGC	150.74855
C-9B Bed 1 skin bottom	DEGC	107.7874451	C-2B Bed 3 Bottom	DEGC	148.576324
C-9A Bed 2 skin middle	DEGC	105.8484573	C-2A Bed 3 Bottom	DEGC	149.311539
C-9B Bed 2 skin middle	DEGC	109.1974945	C-2B Bed 3 Bottom	DEGC	147.961441
C-9A Bed 2 skin middle	DEGC	112.2852325	C-2A Bed 3 Bottom	DEGC	147.874786
C-9B Bed 2 skin middle	DEGC	109.1962585	C-2B Bed 3 Bottom	DEGC	148.440918
C-9A Bed 2 skin middle	DEGC	107.8941803	C-2A Bed 3 Bottom	DEGC	148.887482
C-9B Bed 2 skin middle	DEGC	101.8390656	C-2B Bed 3 Bottom	DEGC	149.025391
C-9A Bed 2 skin middle	DEGC	106.7545013	C-2A Bed 3 Bottom	DEGC	149.309692
C-9B Bed 2 skin middle	DEGC	112.1923599	C-2B Bed 3 Bottom	DEGC	147.881714
C-9A Bed 2 skin bottom	DEGC	110.8191757	C-2A Bed 3 Bottom	DEGC	149.549988
C-9B Bed 2 skin bottom	DEGC	115.1775589	C-2B Bed 3 Bottom	DEGC	147.626205
C-9A Bed 2 skin bottom	DEGC	114.8978806	C-2A Bed 3 Bottom	DEGC	149.432312
C-9B Bed 2 skin bottom	DEGC	109.4525833	C-2B Bed 3 Bottom	DEGC	148.88855
C-9A Bed 2 skin bottom	DEGC	112.3410797	C-9A Bed 3 top	DEGC	150.278931
C-9B Bed 2 skin bottom	DEGC	113.1885147	C-9B Bed 3 top	DEGC	150.687515
C-9A Bed 2 skin bottom	DEGC	111.6434097	C-9A Bed 3 top	DEGC	149.329315
C-9B Bed 2 skin bottom	DEGC	107.3290024	C-9B Bed 3 top	DEGC	149.85437
C-9A Bed 3 skin upper	DEGC	115.3068542	C-9A Bed 3 top	DEGC	148.7332
C-9B Bed 3 skin upper	DEGC	113.9431992	C-9B Bed 3 top	DEGC	151.099457
C-9A Bed 3 skin upper	DEGC	109.4097214	C-9A Bed 3 top	DEGC	149.431381
C-9B Bed 3 skin upper	DEGC	113.9980545	C-9B Bed 3 top	DEGC	150.045502
C-9A Bed 3 skin upper	DEGC	98.28042603	C-9A Bed 3 top	DEGC	149.226746
C-9B Bed 3 skin upper	DEGC	109.8882294	C-9B Bed 3 top	DEGC	150.411499
C-9A Bed 3 skin upper	DEGC	112.7806015	C-9A Bed 3 top	DEGC	149.405212
C-9B Bed 3 skin upper	DEGC	112.0890884	C-9B Bed 3 top	DEGC	151.341248
C-9A Bed 3 skin lower	DEGC	107.6080551	C-9A Bed 3 top	DEGC	149.610657
C-9B Bed 3 skin lower	DEGC	109.8641891	C-9B Bed 3 top	DEGC	151.004852
C-9A Bed 3 skin lower	DEGC	109.1627579	C-9A Bed 3 top	DEGC	150.295807
C-9B Bed 3 skin lower	DEGC	107.843277	C-9B Bed 3 top	DEGC	150.297089
C-9A Bed 3 skin lower	DEGC	107.5667038	C-9A Bed 3 top	DEGC	150.282669
C-9B Bed 3 skin lower	DEGC	106.7735138	C-9B Bed 3 top	DEGC	149.459732
C-9A Bed 3 skin lower	DEGC	101.8514557	C-9A Bed 3 top	DEGC	150.399551
C-9B Bed 3 skin lower	DEGC	110.0500336	C-9B Bed 3 top	DEGC	149.814972
C-9A Bed 3 skin bottom	DEGC	100.5817337	C-9A Bed 3 upper	DEGC	149.577759
C-9B Bed 3 skin bottom	DEGC	98.67750549	C-9B Bed 3 upper	DEGC	149.241913
C-9A Bed 3 skin bottom	DEGC	99.36336517	C-9A Bed 3 upper	DEGC	148.026733

C-9B Bed 3 skin bottom	DEGC	103.534111	C-9B Bed 3 upper	DEGC	148.514236
C-9A Bed 3 skin bottom	DEGC	98.98666382	C-9A Bed 3 upper	DEGC	147.82103
C-9B Bed 3 skin bottom	DEGC	96.36307526	C-9B Bed 3 upper	DEGC	149.273422
C-9A Bed 3 skin bottom	DEGC	100.9735184	C-9A Bed 3 upper	DEGC	148.052246
C-9B Bed 3 skin bottom	DEGC	95.40420532	C-9B Bed 3 upper	DEGC	147.001999
C-9A Bottom shell skin	DEGC	112.7812958	C-9A Bed 3 upper	DEGC	148.915024
C-9B Bottom shell skin	DEGC	114.8819275	C-9B Bed 3 upper	DEGC	149.548065
C-9A Bottom shell skin	DEGC	118.8012619	C-9A Bed 3 upper	DEGC	148.479309
C-9B Bottom shell skin	DEGC	111.8762665	C-9B Bed 3 upper	DEGC	148.563828
C-8 LGO temp	DEGC	16.43288803	C-9A Bed 3 middle	DEGC	147.564896
E-30 recycle LGO outlet te	DEGC	23.05804062	C-9B Bed 3 middle	DEGC	149.33609
Treat gas temp	DEGC	0.001281798	C-9A Bed 3 middle	DEGC	148.603577
Treat Gas Temp	DEGC	49.96337128	C-9B Bed 3 middle	DEGC	148.730484
Treat gas temp	DEGC	0.001281798	C-9A Bed 3 middle	DEGC	146.405975
C-2B inlet piping skin	DEGC	142.0705719	C-9B Bed 3 middle	DEGC	148.065735
C-2B inlet piping skin	DEGC	141.4137878	C-9A Bed 3 middle	DEGC	148.647537
C-2B inlet piping skin	DEGC	147.8241882	C-9B Bed 3 middle	DEGC	148.48558
C-2B inlet	DEGC	165.014679	C-9A Bed 3 middle	DEGC	148.724548
C-2B inlet piping skin	DEGC	146.2033386	C-9B Bed 3 middle	DEGC	148.330124
C-2B inlet piping skin	DEGC	151.4281464	C-9A Bed 3 middle	DEGC	148.521225
C-2B inlet piping skin	DEGC	144.0896301	C-9B Bed 3 middle	DEGC	149.80072
C-2B inlet piping skin	DEGC	143.890564	C-9A Bed 3 lower	DEGC	148.252747
C-2B inlet piping skin	DEGC	113.6006699	C-9B Bed 3 lower	DEGC	148.093048
C-2B inlet piping skin	DEGC	128.7464752	C-9A Bed 3 lower	DEGC	148.315109
C-10 O/H temp	DEGC	69.28761292	C-9B Bed 3 lower	DEGC	148.283585
C-2B inlet piping skin	DEGC	139.5944672	C-9A Bed 3 lower	DEGC	146.769424
C-2A inlet piping skin	DEGC	125.5404892	C-9B Bed 3 lower	DEGC	148.456131
C-2A inlet piping skin	DEGC	119.9329453	C-9A Bed 3 lower	DEGC	148.523483
C-2A inlet piping skin	DEGC	137.6908875	C-9B Bed 3 lower	DEGC	147.921051
C-2A inlet	DEGC	166.2535706	C-9A Bed 3 lower	DEGC	147.84848
C-2A inlet piping skin	DEGC	133.3540192	C-9B Bed 3 lower	DEGC	148.307617
C-2A inlet piping skin	DEGC	135.8860931	C-9A Bed 3 lower	DEGC	147.390427
C-2A inlet piping skin	DEGC	151.7655029	C-9B Bed 3 lower	DEGC	149.351395
C-2A inlet piping skin	DEGC	145.4289856	C-9A Bed 3 bottom	DEGC	147.105743
C-2A inlet piping skin	DEGC	145.2429352	C-9B Bed 3 bottom	DEGC	147.900818
C-2A inlet piping skin	DEGC	152.9826813	C-9A Bed 3 bottom	DEGC	147.441086
C-2A inlet piping skin	DEGC	145.5728149	C-9B Bed 3 bottom	DEGC	148.142258
C-9B inlet piping skin	DEGC	152.9561005	C-9A Bed 3 bottom	DEGC	145.672119
C-9B inlet piping skin	DEGC	154.6399841	C-9B Bed 3 bottom	DEGC	147.073257
C-9B inlet piping skin	DEGC	145.9276123	C-9A Bed 3 bottom	DEGC	146.660065
C-9B inlet	DEGC	157.189209	C-9B Bed 3 bottom	DEGC	147.843552
C-9B inlet piping skin	DEGC	139.7787628	C-9A Bed 3 bottom	DEGC	147.425705
C-9B inlet piping skin	DEGC	146.994278	C-9B Bed 3 bottom	DEGC	145.53215
C-9B inlet piping skin	DEGC	139.4646301	C-9A Bed 3 bottom	DEGC	147.281677
C-9B inlet piping skin	DEGC	136.9935303	C-9B Bed 3 bottom	DEGC	146.367081
Sour gas to C-19 temp	DEGC	24.60076523	C-9A Bed 3 bottom	DEGC	147.386459
C-9B inlet piping skin	DEGC	145.3836823	C-9B Bed 3 bottom	DEGC	148.572662
C-9B inlet piping skin	DEGC	146.7714233	C-9A Bed 3 bottom	DEGC	147.25737
C-9B inlet piping skin	DEGC	148.3866577	C-9B Bed 3 bottom	DEGC	148.005798
C-9A inlet piping skin	DEGC	151.3381348	C-9A Bed 3 bottom	DEGC	147.396271

C-9A inlet piping skin	DEGC	158.7800903	C-9B Bed 3 bottom	DEGC	149.182419
C-9A inlet piping skin	DEGC	138.1131439	C-9A Bed 3 bottom	DEGC	148.147263
C-9A inlet	DEGC	161.0352478	C-9B Bed 3 bottom	DEGC	148.691299
C-9A inlet piping skin	DEGC	140.4598999	C-9A Bed 3 bottom	DEGC	147.319916
C-9A inlet piping skin	DEGC	150.8311615	C-9B Bed 3 bottom	DEGC	148.451553
C-9A inlet piping skin	DEGC	151.1208801	C-9A Bed 3 bottom	DEGC	148.522095
Lean DEA to C-19 temp	DEGC	6.464193344	C-9B Bed 3 bottom	DEGC	149.035797
C-9A inlet piping skin	DEGC	143.5971527	C-9A Bed 3 bottom	DEGC	148.253494
C-9A inlet piping skin	DEGC	141.8687897	C-9B Bed 3 bottom	DEGC	148.450745
C-9A inlet piping skin	DEGC	152.7300873	C-9A Bed 3 bottom	DEGC	147.71814
C-9A inlet piping skin	DEGC	144.3984528	C-9B Bed 3 bottom	DEGC	148.409424
C-2A Bed 2 distributor ski	DEGC	109.796936	C-9A Bed 3 bottom	DEGC	148.727386
C-2B Bed 2 distributor ski	DEGC	112.5213547	C-9B Bed 3 bottom	DEGC	149.026886
C-2A Bed 2 quench nozzle s	DEGC	86.49252319	C-9A Bed 3 bottom	DEGC	148.304733
C-2B Bed 2 quench nozzle s	DEGC	78.28874969	C-9B Bed 3 bottom	DEGC	148.92778
C-2A Bed 3 distributor ski	DEGC	114.9708328	C-9A Bed 3 bottom	DEGC	147.672134
C-2B Bed 3 distributor ski	DEGC	114.1567917	C-9B Bed 3 bottom	DEGC	147.055847
C-2A Bed 3 quench nozzle s	DEGC	105.0319672	C-9A Bed 3 bottom	DEGC	148.119232
C-2B Bed 3 quench nozzle s	DEGC	102.0167313	C-9B Bed 3 bottom	DEGC	147.647659
H-2 Discharge temp to 8-1/	DEGC	0.001281798	E-6A/B feed forced flow	% OPEN	0.0012818
Make-up H2 temp	DEGC	0.001281798	E-6A/E feed B/P	% OPEN	0.0012818
K-1 Suction temp	DEGC	34.3398819	E-6B/F feed forced flow	% OPEN	0.0012818
K-1 Discharge temp	DEGC	51.35531235	E-6B/F feed B/P	% OPEN	0.0012818
E-5/12 steam temp	DEGC	188.0420074	E-6C/G feed forced flow	% OPEN	0.0012818
C-9A Outlet	DEGC	147.0466309	E-6C/G feed B/P	% OPEN	0.0012818
C-9B Outlet	DEGC	146.8631439	E-6D/H feed forced flow	% OPEN	0.0012818
C-9A Bed 2 distributor ski	DEGC	105.2393875	E-6D/H feed B/P	% OPEN	0.0012818
C-9B Bed 2 distributor ski	DEGC	107.8920822	K-4 inlet temp	% OPEN	-5
C-9A Bed 2 quench nozzle s	DEGC	71.24113464	K-2 inlet temp	% OPEN	-3.9796665
C-9B Bed 2 quench nozzle s	DEGC	70.66191864	E-21 Flue gas outlet temp	% OPEN	105
C-9A Bed 3 distributor ski	DEGC	110.1068878	E-22 Flue gas outlet temp	% OPEN	105
C-9B Bed 3 distributor ski	DEGC	107.352684	E-29 Lean DEA outlet temp	% OPEN	0
C-9A Bed 3 quench nozzle s	DEGC	88.16387939	E-2A/E/J UTLGO forced flow	% OPEN	0.0012818
C-9B Bed 3 quench nozzle s	DEGC	79.57790375	E-2A/E/J UTLGO B/P	% OPEN	0.0012818
E-3A/B Vapour outlet temp	DEGC	59.7737236	E-2B/F/K UTLGO forced flow	% OPEN	0.0012818
C-6 LGO inlet temp	DEGC	13.67423153	E-2B/F/K UTLGO B/P	% OPEN	0.0012818
E-6E UTLGO outlet temp	DEGC	126.6740875	E-2C/G/L UTLGO forced flow	% OPEN	0.0012818
E-6F UTLGO outlet temp	DEGC	119.0672607	E-2C/G/L UTLGO B/P	% OPEN	0.0012818
E-6G UTLGO outlet temp	DEGC	123.7789993	E-2D/H/M UTLGO forced flow	% OPEN	0.0012818
E-6H UTLGO outlet temp	DEGC	121.6832123	E-2D/H/M UTLGO B/P	% OPEN	0.0012818

C-6 Bottom outlet temp	DEGC	17.29542732	K-1 Perf. Controller S/P	%	0
E-6A inlet temp	DEGC	52.28404617	K-1 Surge Counter	-	0
E-6B inlet temp	DEGC	51.6999054	E-4 FAN MOTOR 1 VIBE	IN/S	0.00192439
E-6C inlet temp	DEGC	52.02352524	E-4 FAN MOTOR 2 VIBE	IN/S	0.0019536
E-6D inlet temp	DEGC	51.72266769	E-7A FAN MOTOR 1 VIBE	IN/S	0.00174137
E-1 UTLGO outlet temp	DEGC	30.67960739	E-7A FAN MOTOR 2 VIBE	IN/S	0.00620574
F-1A Firebox bottom temp	DEGC	336.230957	E-7B FAN MOTOR 1 VIBE	IN/S	0.00468864
E-6E to F-2A inlet	DEGC	125.5063171	E-3A FAN MOTOR 1 VIBE	IN/S	0.001221
E-6F to F-2A inlet	DEGC	118.1884613	E-7B FAN MOTOR 2 VIBE	IN/S	0.00354963
E-6G to F-2B inlet	DEGC	122.9329529	E-9B FAN MOTOR 1 VIBE	IN/S	0.00432845
E-6H to F-2B inlet	DEGC	122.3136597	E-9B FAN MOTOR 2 VIBE	IN/S	0.00586081
F-2B Firebox top temp	DEGC	341.8697815	E-9A FAN MOTOR 1 VIBE	IN/S	0.00534799
F-2 Xover Pass 3	DEGC	30.00789452	E-9A FAN MOTOR 2 VIBE	IN/S	0.00241758
F-2 Xover Pass 4	DEGC	19.94293976	E-8A FAN MOTOR 1 VIBE	IN/S	0.0039072
F-2B Firebox bottom temp	DEGC	231.7359619	E-8A FAN MOTOR 2 VIBE	IN/S	0.00586214
F-2 Pass 4 COT	DEGC	162.3456421	E-7C FAN MOTOR 1 VIBE	IN/S	0.0014652
F-2 Convection section tem	DEGC	182.1916656	E-3A FAN MOTOR 2 VIBE	IN/S	0.0019536
F-2 Xover Pass 2	DEGC	40.25621796	E-7C FAN MOTOR 2 VIBE	IN/S	0.00250305
F-2 Xover Pass 1	DEGC	27.56820297	E-7D FAN MOTOR 1 VIBE	IN/S	0.00537241
F-2A Firebox top temp	DEGC	338.6482239	E-7D FAN MOTOR 2 VIBE	IN/S	0.0034188
C-6 Tray 30	DEGC	15.31014442	E-7E FAN MOTOR 1 VIBE	IN/S	0.0026862
F-2 Pass 1 COT	DEGC	170.8775787	E-7E FAN MOTOR 2 VIBE	IN/S	0.0043956
F-2 Pass 2 COT	DEGC	157.1633453	E-7F FAN MOTOR 1 VIBE	IN/S	0.0031746
F-2 Pass 3 COT	DEGC	158.0540009	E-7F FAN MOTOR 2 VIBE	IN/S	0.00364425
F-2A Firebox bottom temp	DEGC	272.8252563	E-14A FAN MOTOR 1 VIBE	IN/S	0.00367565
F-2A Outlet temp	DEGC	161.758255	E-14A FAN MOTOR 2 VIBE	IN/S	0.0031826
F-2B Outlet temp	DEGC	159.1208801	E-14B FAN MOTOR 1 VIBE	IN/S	0.00298857
Air to F-2A/B	DEGC	114.937439	E-14B FAN MOTOR 2 VIBE	IN/S	0.00684676
F-1B Pass 3 radiant TMT	DEGC	176.8356934	E-14C FAN MOTOR 1 VIBE	IN/S	0.00229149
F-1B Pass 3 radiant TMT	DEGC	175.6209259	E-3B FAN MOTOR 1	IN/S	0.0029304

			VIBE		
			E-14C FAN MOTOR 2		
F-1B Pass 3 radiant TMT	DEGC	177.2355499	VIBE	IN/S	0.0017094
			E-14D FAN MOTOR 1		
F-1B Pass 3 radiant TMT	DEGC	176.4732666	VIBE	IN/S	0.003663
			E-14D FAN MOTOR 2		
F-1B Pass 4 radiant TMT	DEGC	173.6316528	VIBE	IN/S	0.00530403
			E-7G FAN MOTOR 1		
F-1B Pass 4 radiant TMT	DEGC	174.59198	VIBE	IN/S	0.0043956
			E-7G FAN MOTOR 2		
F-1B Pass 4 radiant TMT	DEGC	178.2125092	VIBE	IN/S	0.00440226
			E-7H FAN MOTOR 1		
F-1B Pass 4 radiant TMT	DEGC	178.4017029	VIBE	IN/S	0.00433019
			E-7H FAN MOTOR 2		
F-1A Pass 2 radiant TMT	DEGC	175.5024109	VIBE	IN/S	0.00318126
			E-3B FAN MOTOR 2		
F-1A Pass 2 radiant TMT	DEGC	176.1673584	VIBE	IN/S	0.0026862
			ACCELEROMETER		
F-1A Pass 2 radiant TMT	DEGC	179.2435913	HOUSING OUTP	IN/S	0.34822956
			ACCELEROMETER		
C-6 Tray 15	DEGC	15.14134979	HOUSING INPU	IN/S	0.20182016
			VORECON RADIAL		
F-1A Pass 2 radiant TMT	DEGC	177.9934387	SHAFT VIBRA	MILS	0.66422468
			VORECON RADIAL		
F-1A Pass 1 radiant TMT	DEGC	174.7746429	SHAFT VIBRA	MILS	3.62266183
			VORECON RADIAL		
F-1A Pass 1 radiant TMT	DEGC	175.5332642	SHAFT VIBRA	MILS	0.83516484
			ELECTRIC MOTOR		
F-1A Pass 1 radiant TMT	DEGC	176.043808	RADIAL	MILS	1.18974364
			ELECTRIC MOTOR		
F-1A Pass 1 radiant TMT	DEGC	178.1459503	RADIAL	MILS	1.11876273
			COMPRESSOR RADIAL		
E-3A air inlet temp	DEGC	0.001281798	BEARING	MILS	0.27838829
			COMPRESSOR RADIAL		
E-3A air inlet temp	DEGC	0.001281798	BEARING	MILS	0.52258855
			G-1 1ST STG GAS OIL		
E-3B air inlet temp	DEGC	0.001281798	FEED P	MILS	0.05128205
			G-1 1ST STG GAS OIL		
E-3B air inlet temp	DEGC	0.001281798	FEED P	MILS	0
			G-1 1ST STG GAS OIL		
E-4 Air inlet temp	DEGC	0.001281798	FEED P	MILS	0
			G-1 1ST STG GAS OIL		
E-4 Air inlet temp	DEGC	0.001281798	FEED P	MILS	0.0012818
			G-3A 2ND STG GAS OIL		
F-2B Pass 3 radiant TMT	DEGC	161.8190002	FEED	MILS	No Data
			G-3B 2ND STG GAS OIL		
F-2B Pass 3 radiant TMT	DEGC	162.8083191	FEED	MILS	No Data
			G-3A 2ND STG GAS OIL		
F-2B Pass 3 radiant TMT	DEGC	163.9388428	FEED	MILS	0.05128205
			G-3B 2ND STG GAS OIL		
F-2B Pass 3 radiant TMT	DEGC	165.9482117	FEED	MILS	0.08547009
			G-3A 2ND STG GAS OIL		
F-2A Pass 2 radiant TMT	DEGC	161.0145721	FEED	MILS	0.07326008
			G-3B 2ND STG GAS OIL		
F-2A Pass 2 radiant TMT	DEGC	162.8995514	FEED	MILS	0.11355312
F-2A Pass 2 radiant TMT	DEGC	165.1132965	G-3A 2ND STG GAS OIL	MILS	0

			FEED		
F-2A Pass 2 radiant TMT	DEGC	166.4467926	G-3B 2ND STG GAS OIL FEED	MILS	0.12087914
F-2A Pass 1 radiant TMT	DEGC	176.1999512	G-5A LEAN AMINE PUMP BEARI	MILS	0.1001221
F-2A Pass 1 radiant TMT	DEGC	175.0213623	G-5B LEAN AMINE PUMP BEARI	MILS	0.08547009
F-2A Pass 1 radiant TMT	DEGC	176.4211884	G-5A LEAN AMINE PUMP BEARI	MILS	0.06593407
F-2A Pass 1 radiant TMT	DEGC	175.8553467	G-5B LEAN AMINE PUMP BEARI	MILS	0.09279609
F-2B Pass 4 radiant TMT	DEGC	167.7750397	G-5A LEAN AMINE PUMP EL.MO	MILS	0.07326008
F-2B Pass 4 radiant TMT	DEGC	170.9078217	G-5B LEAN AMINE PUMP EL.MO	MILS	0.07326008
F-2B Pass 4 radiant TMT	DEGC	176.6685638	G-5A LEAN AMINE PUMP EL.MO	MILS	0.07326008
F-2B Pass 4 radiant TMT	DEGC	177.9660797	G-5B LEAN AMINE PUMP EL.MO	MILS	0.0879121
E-7A air outlet temp	DEGC	0.001281798	G-6A HP WASH WATER PUMP BE	MILS	0.05128205
E-7A air outlet temp	DEGC	0.001281798	G-6B HP WASH WATER PUMP BE	MILS	0.05128205
E-7B air outlet temp	DEGC	0.001281798	G-6A WASH WATER PUMP BEARI	MILS	0.05128205
E-7B air outlet temp	DEGC	0.001281798	G-6B WASH WATER PUMP BEARI	MILS	0.05860806
E-7C air outlet temp	DEGC	0.001281798	G-6A HP WASH WATER PUMP EL	MILS	0
E-7C air outlet temp	DEGC	0.001281798	G-6B HP WASH WATER PUMP EL	MILS	0
E-7D air outlet temp	DEGC	0.001281798	G-6A HP WASH WATER PUMP EL	MILS	0
E-7D air outlet temp	DEGC	0.001281798	G-6B HP WASH WATER PUMP EL	MILS	0
E-8 air inlet temp	DEGC	0.001281798	G-1 1ST STG GAS OIL FEED P	MILS	No Data
E-8 air inlet temp	DEGC	0.001281798	G-6A HP WASH WATER PUMP EL	MILS	0.0012818
E-8 process outlet temp	DEGC	0.001281798	G-6B HP WASH WATER PUMP EL	MILS	0.0012818
E-9A air inlet temp	DEGC	0.001281798	VORECON RADIAL SHAFT VIBRA	MILS	0.73748475
E-9A air inlet temp	DEGC	0.001281798	VORECON RADIAL SHAFT VIBRA	MILS	3.48571444
E-9B air inlet temp	DEGC	0.001281798	VORECON RADIAL SHAFT VIBRA	MILS	0.92796093
E-9B air inlet temp	DEGC	0.001281798	ELECTRIC MOTOR RADIAL	MILS	0.75115997
E-14B air inlet temp	DEGC	0.001281798	ELECTRIC MOTOR RADIAL	MILS	0.81719685
E-14B air inlet temp	DEGC	0.001281798	COMPRESSOR RADIAL BEARING	MILS	0.47863248
E-14A air inlet temp	DEGC	0.001281798	COMPRESSOR RADIAL BEARING	MILS	0.51282054
E-14A air inlet temp	DEGC	0.001281798	G-1 1ST STG GAS OIL	MILS	0.04884005

			FEED P		
			G-1 1ST STG GAS OIL		
E-14D air inlet temp	DEGC	0.001281798	FEED P	MILS	0
			G-1 1ST STG GAS OIL		
E-14D air inlet temp	DEGC	0.001281798	FEED P	MILS	0
			G-1 1ST STG GAS OIL		
E-14C air inlet temp	DEGC	0.001281798	FEED P	MILS	0.0012818
			G-3A 2ND STG GAS OIL		
E-14C air inlet temp	DEGC	0.001281798	FEED	MILS	No Data
			G-3B 2ND STG GAS OIL		
1st stage LGO temp	DEGC	23.66016197	FEED	MILS	No Data
			G-3A 2ND STG GAS OIL		
E-21 Air inlet temp	DEGC	0.001281798	FEED	MILS	0.07570208
			G-3B 2ND STG GAS OIL		
E-21 Flue gas inlet temp	DEGC	166.3837738	FEED	MILS	0.09279609
			G-3A 2ND STG GAS OIL		
E-21 Air outlet temp	DEGC	0.001281798	FEED	MILS	0.07326008
			G-3B 2ND STG GAS OIL		
F-1 Stack temp	DEGC	72.96703339	FEED	MILS	0.10622711
			G-3A 2ND STG GAS OIL		
E-22 Air inlet temp	DEGC	0.001281798	FEED	MILS	0
			G-3B 2ND STG GAS OIL		
E-22 Flue gas inlet temp	DEGC	161.7015991	FEED	MILS	0.12087914
			G-5A LEAN AMINE		
E-22 Air outlet temp	DEGC	0.001281798	PUMP BEARI	MILS	0.10989011
			G-5B LEAN AMINE		
F-2 Stack temp	DEGC	66.37362671	PUMP BEARI	MILS	0.08302809
			G-5A LEAN AMINE		
F-1 Pass 2 COT	DEGC	168.085907	PUMP BEARI	MILS	0.10500611
			G-5B LEAN AMINE		
F-1 Pass 4 COT	DEGC	166.1418762	PUMP BEARI	MILS	0.06349207
			G-5A LEAN AMINE		
G-1 suction temp	DEGC	49.10633469	PUMP EL.MO	MILS	0.07326008
			G-5B LEAN AMINE		
C-29 temp	DEGC	7.810737133	PUMP EL.MO	MILS	0.0952381
			G-5A LEAN AMINE		
E-29 slop outlet temp	DEGC	6.681133747	PUMP EL.MO	MILS	0.0879121
			G-5B LEAN AMINE		
E-21 Flue gas outlet temp	DEGC	76.04396057	PUMP EL.MO	MILS	0.07326008
			G-6A HP WASH WATER		
E-22 Flue gas outlet temp	DEGC	71.50183105	PUMP BE	MILS	0.05372405
K-1 Lube Oil Temp After			G-6B HP WASH WATER		
Co	DEGC	47.66788864	PUMP BE	MILS	0.05128205
K-1 Lube Oil Temp After			G-6A WASH WATER		
Co	DEGC	49.18193054	PUMP BEARI	MILS	0.05616606
			G-6B WASH WATER		
K-1 Gear Lube Oil Return	DEGC	47.69230652	PUMP BEARI	MILS	0.05860806
			G-6A HP WASH WATER		
K-1 Bearing #1	DEGC	66.7399292	PUMP EL	MILS	0
			G-6B HP WASH WATER		
K-1 Bearing #2	DEGC	68.75457764	PUMP EL	MILS	0
			G-6A HP WASH WATER		
K-1 Bearing #3	DEGC	68.38827515	PUMP EL	MILS	0
			G-6B HP WASH WATER		
K-1 Bearing #4	DEGC	50.98901367	PUMP EL	MILS	0
K-1 Bearing #6	DEGC	52.8571434	G-1 1ST STG GAS OIL	MILS	No Data

			FEED P		
			G-6A HP WASH WATER		
K-1 Bearing #11	DEGC	64.17582703	PUMP EL	MILS	0.0012818
			G-6B HP WASH WATER		
K-1 Gear Lube Oil Return	DEGC	55.78754807	PUMP EL	MILS	0.0012818
			AXIAL DISPLACEMENT		
G-10B Lube Oil System	DEGC	56.99633789	PROBE	MILS	8.54701233
			COMPRESSOR AXIAL		
K-1 Thrust Bearing Active	DEGC	63.51648331	DISPLACEM	MILS	6.30036926
K-1 Thrust Bearing Non			COMPRESSOR AXIAL		
Act	DEGC	65.78754425	DISPLACEM	MILS	6.16361618
K-1 Journal Bearing Drive	DEGC	82.06397247	K-1 Guide vane	%	15.7264967
			G-1 ST STG OIL FEED		
K-1 Journal Bearing Drive	DEGC	70.80586243	PUMP A	MILS	0
K-1 Journal Bearing Non			G-1 ST STG OIL FEED		
Dr	DEGC	72.38095093	PUMP A	MILS	0
K-1 Journal Bearing Non			G-3A 2ND STG OIL		
Dr	DEGC	73.9751358	FEED PUMP	MILS	0
			G-3B 2ND STG OIL		
K-1 Thrust Bearing Active	DEGC	62.67399216	FEED PUMP	MILS	0
K-1 Thrust Bearing Non			G-3A 2ND STG OIL		
Act	DEGC	66.08058929	FEED PUMP	MILS	0
			G-3B 2ND STG OIL		
C-2A/B EIT	DEGC	155.5512085	FEED PUMP	MILS	0
			G-5A LEAN AMINE		
C-2A Bed 1 Top	DEGC	0.001281798	PUMP AXIAL	MILS	0.45909882
			G-5B LEAN AMINE		
C-2A Bed 1 EIT	DEGC	0.001281798	PUMP AXIAL	MILS	0
			G-5A LEAN AMINE		
C-2B Bed 1 Top	DEGC	0.001281798	PUMP AXIAL	MILS	0
			G-5B LEAN AMINE		
C-2B Bed 1 EIT	DEGC	0.001281798	PUMP AXIAL	MILS	0
			G-6A HP WASH WATER		
C-2A Bed 1 Top	DEGC	0.001281798	PUMP AX	MILS	0
			G-6B HP WASH WATER		
C-2B Bed 1 Top	DEGC	0.001281798	PUMP AX	MILS	1.14286041
			G-6A HP WASH WATER		
C-2A Bed 1 Top	DEGC	0.001281798	PUMP AX	MILS	0
			G-6B HP WASH WATER		
C-2B Bed 1 Top	DEGC	0.001281798	PUMP AX	MILS	0.42002869

Plant D

Process Data from Plant D Excerpt from Data base

	Date	11-Jul-2006	12-Jul-2006
Feed to Exchanger A, BPD	29-FI-005A	15196.61	15251.10
Feed to Exchanger B, BPD	29-FI-063A	15196.00	15247.38
Feed Temperature to Exchanger A, °F	29-TJI-002	318.59	324.21
Reactor 1 Bed 1 inlet Temperature, °F	29-TIC-003	616.00	616.00
Reactor 1 Bed 1 inlet Temperature, °F	29-TJI-008	610.48	610.51
Reactor 1 Bed 1 bottom temperature, °F	29-TJI-009A	662.57	660.39
Reactor 1 Bed 1 bottom temperature, °F	29-TJI-009B	661.15	659.10

Reactor 1 Bed 1 bottom temperature, °F	29-TJI-009B	661.15	659.10
Reactor 1 Bed 1 bottom temperature, °F	29-TJI-010A	655.99	653.89
Reactor 1 Bed 1 bottom temperature, °F	29-TJI-010B	665.25	663.29
Reactor 1 Bed 1 bottom temperature, °F	29-TJI-011A	663.24	661.04
Reactor 1 Bed 1 bottom temperature, °F	29-TJI-011B	656.87	654.87
Reactor 1 Bed 2 inlet Temperature, °F	29-TIC-012	671.13	668.88
Reactor 1 Bed 2 inlet Temperature, °F	29-TJI-013	669.12	666.73
Reactor 1 Bed 2 inlet Temperature, °F	29-TJI-014	657.94	655.89
Reactor 1 Bed 2 bottom temperature, °F	29-TJI-015A	688.51	685.46
Reactor 1 Bed 2 bottom temperature, °F	29-TJI-015B	687.44	684.53
Reactor 1 Bed 2 bottom temperature, °F	29-TJI-016A	685.08	681.91
Reactor 1 Bed 2 bottom temperature, °F	29-TJI-016B	690.61	687.72
Reactor 1 Bed 2 bottom temperature, °F	29-TJI-017A	687.81	684.85
Reactor 1 Bed 2 bottom temperature, °F	29-TJI-017B	696.81	693.71
Reactor 1 Bed 3 inlet Temperature, °F	29-TIC-018	688.42	688.67
Reactor 1 Bed 3 inlet Temperature, °F	29-TJI-019	682.66	682.81
Reactor 1 Bed 3 inlet Temperature, °F	29-TJI-020	682.54	682.38
Reactor 1 Bed 3 bottom temperature, °F	29-TJI-021A	712.79	714.35
Reactor 1 Bed 3 bottom temperature, °F	29-TJI-021B	702.48	706.88
Reactor 1 Bed 3 bottom temperature, °F	29-TJI-022A	712.19	713.25
Reactor 1 Bed 3 bottom temperature, °F	29-TJI-022B	705.86	709.96
Reactor 1 Bed 3 bottom temperature, °F	29-TJI-023A	706.51	709.72
Reactor 1 Bed 3 bottom temperature, °F	29-TJI-023B	716.13	717.70
Reactor 1 Bed 4 inlet Temperature, °F	29-TIC-024	692.07	694.04
Reactor 1 Bed 4 inlet Temperature, °F	29-TJI-025	690.98	692.95
Reactor 1 Bed 4 inlet Temperature, °F	29-TJI-026	689.59	691.38
Reactor 1 Bed 4 middle temperature, °F	29-TJI-027	696.22	699.14
Reactor 1 Bed 4 middle temperature, °F	29-TJI-028	686.78	689.60
Reactor 1 Bed 4 middle temperature, °F	29-TJI-029	694.37	696.75
Reactor 1 Bed 4 bottom temperature, °F	29-TJI-030A	710.42	712.82
Reactor 1 Bed 4 bottom temperature, °F	29-TJI-030B	313.98	507.13
Reactor 1 Bed 4 bottom temperature, °F	29-TJI-031A	709.80	712.43
Reactor 1 Bed 4 bottom temperature, °F	29-TJI-031B	701.13	703.81
Reactor 1 Bed 4 bottom temperature, °F	29-TJI-032A	700.48	702.89
Reactor 1 Bed 4 bottom temperature, °F	29-TJI-032B	720.52	723.06
Reactor 1 Bed 5 inlet Temperature, °F	29-TIC-033	706.87	709.97
Reactor 1 Bed 5 inlet Temperature, °F	29-TJI-034	699.86	703.04
Reactor 1 Bed 5 inlet Temperature, °F	29-TJI-035	699.41	702.60
Reactor 1 Bed 5 middle temperature, °F	29-TJI-036	699.47	703.17
Reactor 1 Bed 5 middle temperature, °F	29-TJI-037	706.95	710.41
Reactor 1 Bed 5 middle temperature, °F	29-TJI-038	699.41	703.25
Reactor 1 Bed 5 bottom temperature, °F	29-TJI-039	712.66	716.54
Reactor 1 Bed 5 bottom temperature, °F	29-TJI-040	705.48	709.00
Reactor 1 Bed 5 bottom temperature, °F	29-TJI-041	717.14	720.90
Reactor 1 Outlet temperature, °F	29-TJI-042	714.74	719.12
Reactor 1 Bed 1 Inlet pressure, Psig	29-PI-055	1606.38	1605.92
Reactor 1 Bed 2 Inlet pressure, Psig	29-PI-056	1601.96	1601.47
Reactor 1 Bed 3 Inlet pressure, Psig	29-PI-057	1597.65	1596.99
Reactor 1 Bed 4 Inlet pressure, Psig	29-PI-058	1593.87	1593.39

Reactor 1 Bed 5 Inlet pressure, Psig	29-PI-059	1581.57	1581.34
Reactor 1 Outlet pressure, Psig	29-PI-060	1558.18	1558.36
H2 Make Up flow, mmscfd	29-FI-017	41.72	41.43
H2 flow to exchanger A, mmscfd	29-FIC-008	60.19	60.99
H2 flow to exchanger B, mmscfd	29-FIC-062	60.17	60.99
Reactor 1 Bed 2 Quench Flow, mmscfd	29-FIC-009	-0.01	-0.01
Reactor 1 Bed 3 Quench Flow, mmscfd	29-FIC-010	15.82	12.02
Reactor 1 Bed 4 Quench Flow, mmscfd	29-FIC-011	27.35	28.01
Reactor 1 Bed 5 Quench Flow, mmscfd	29-FIC-012	8.92	7.53
LPCFD Off gas flow, mmscfd	29-FI-013	1.91	1.57
LPCFD Off gas temperature, °F	29-TJI-107	135.05	133.51
LPCFD Off gas pressure, Psig	29-PIC-010	374.98	375.00
Purge gas flow, mmscfd	29-FIC-056	4.77	4.45
Purge gas temperature, °F	29-TI-250A	136.53	134.88
Purge gas pressure, Psig	29-PI-048	1466.17	1466.31
Make Up Hydrogen flow, mmscfd	29-FI-017	41.72	41.43
Make Up Hydrogen temperature, °F	21-TJI-742	196.35	192.45
Make Up Hydrogen pressure, Psig	21-PIC-751	1723.47	1723.52
Unstabilized Naphtha Product flow, BPD	29-FIC-022	734.15	750.24
Unstabilized Naphtha Product temperature, °F	29-TJI-119	96.16	95.46
Stripper Sour Off Gas flow, mmscfd	29-FI-025	0.93	0.94
Stripper Sour Off Gas temperature, °F	29-TJI-120	91.65	91.53
Stripper Sour Off Gas pressure, Psig	29-PIC-020	115.00	115.00
Heavy Naphtha Product flow, BPD	29-FIC-042	652.24	644.12
Heavy Naphtha Product temperature, °F	29-TJI-141	88.65	86.71
Distillate Product flow, BPD	29-FIC-049	13344.11	14439.44
Distillate Product temperature, °F	29-TJI-147	129.08	123.92
Diesel Product flow, BPD	29-FIC-052	6149.81	5137.87
Diesel Product temperature, °F	29-TJI-149	133.95	126.43
Frac Bottoms Product flow, BPD	29-FIC-045	8939.93	10624.92
Frac Bottoms Product temperature, °F	29-TJI-143	186.05	185.57
Recycle Gas + Makeup Hydrogen flow to exchanger A, mmscfd	29-FI-008A	60.19	61.00
Recycle Gas + Makeup Hydrogen flow to exchanger B, mmscfd	29-FI-062A	60.17	61.00
Reactor 2 Bed 1 inlet Temperature, °F	29-TIC-352	695.50	697.00
Reactor 2 Bed 1 inlet Temperature, °F	29-TJI-353	691.72	693.28
Reactor2 Bed 1 top temperature, °F	29-TJI-301	692.16	693.93
Reactor2 Bed 1 top temperature, °F	29-TJI-302	692.43	694.14
Reactor2 Bed 1 top temperature, °F	29-TJI-303	692.24	693.99
Reactor 2 Bed 1 Middle temperature, °F	29-TJI-304	702.49	704.42
Reactor 2 Bed 1 Middle temperature, °F	29-TJI-305	707.46	709.29
Reactor 2 Bed 1 Middle temperature, °F	29-TJI-306	702.50	704.39
Reactor 2 Bed 1 bottom temperature, °F	29-TJI-307	715.94	717.70
Reactor 2 Bed 1 bottom temperature, °F	29-TJI-308	722.05	723.39
Reactor 2 Bed 1 bottom temperature, °F	29-TJI-309	715.85	717.43
Reactor 2 Bed 2 inlet Temperature, °F	29-TIC-354	710.87	712.01
Reactor 2 Bed 2 middle temperature, °F	29-TJI-313	716.94	718.02

Reactor 2 Bed 2 middle temperature, °F		29-TJI-314	717.61	718.60
Reactor 2 Bed 2 middle temperature, °F		29-TJI-315	715.08	716.24
Reactor 2 Bed 2 bottom temperature, °F		29-TJI-316	721.36	722.14
Reactor 2 Bed 2 bottom temperature, °F		29-TJI-317	726.48	727.06
Reactor 2 Bed 2 bottom temperature, °F		29-TJI-318	722.69	723.45
Reactor Bed 2 outlet temperature, °F		29-TJI-351	724.46	725.11
Reactor 2 Bed 1 inlet pressure, Psig		29-PI-303	1550.65	1550.72
Reactor 2 Bed 2 inlet pressure, Psig		29-PI-302	1533.40	1533.62
Reactor 2 Bed 2 outlet pressure, Psig		29-PI-304	1516.51	1516.64
Reactor 2 Bed 1 Quench Flow, mmscfd		29-FI-304	12.02	13.87
Reactor 2 Bed 2 Quench Flow, mmscfd		29-FI-303	3.55	3.87
HDS Combined Feed		29-AP-100		
API Gravity	API	29-1API-100	22.4	22.3
Nitrogen -ppm	mg/kg	29-1N2A-100	1153	1182
Pour Point - Auto	Deg F.	29-1POURA-100		
FBP D86 Correlation	Deg F.	29-1SCEP-100	884	882
IBP D86 Correlation	Deg F.	29-1SCIP-100	386	386
5% D86 Correlation	Deg F.	29-1SC05-100	424	425
10% D86 Correlation	Deg F.	29-1SC10-100	461	463
20% D86 Correlation	Deg F.	29-1SC20-100	508	510
30% D86 Correlation	Deg F.	29-1SC30-100	549	551
50% D86 Correlation	Deg F.	29-1SC50-100	631	632
70% D86 Correlation	Deg F.	29-1SC70-100	718	718
80% D86 Correlation	Deg F.	29-1SC80-100	767	767
90% D86 Correlation	Deg F.	29-1SC90-100	821	821
95% D86 Correlation	Deg F.	29-1SC95-100	853	852
			2.537	2.041
Unstabilized Naphtha		29-AP-106		
API Gravity	API	29-1API-106	54.2	56.8
C4 minus	mass %	29-1M4L-106		
C5 total	mass %	29-1M5S-106		
C6 total	mass %	29-1M6S-106		
C7 plus	mass %	29-1M7P-106		
FBP D86 Correlation	Deg F.	29-1SCEP-106	371	370
IBP D86 Correlation	Deg F.	29-1SCIP-106	106	119
5% D86 Correlation	Deg F.	29-1SC05-106	142	150
10% D86 Correlation	Deg F.	29-1SC10-106	175	178
20% D86 Correlation	Deg F.	29-1SC20-106	204	207
30% D86 Correlation	Deg F.	29-1SC30-106	225	229
50% D86 Correlation	Deg F.	29-1SC50-106	258	263
70% D86 Correlation	Deg F.	29-1SC70-106	292	294
80% D86 Correlation	Deg F.	29-1SC80-106	309	311
90% D86 Correlation	Deg F.	29-1SC90-106	326	327
95% D86 Correlation	Deg F.	29-1SC95-106	347	347
SULH	mass %	29-1SULH-106	0.363	0.469

Frac OH Heavy Nap		29-AP-108		
API Gravity	API	29-1API-108	46.9	45.4
End Point Recovery Point	Deg F.	29-1DEPR-108	386.4	380.8
5% Recovery Point	Deg F.	29-1D05R-108	267.3	278.4
10% Recovery Point	Deg F.	29-1D10R-108	271.2	281.8
20% Recovery Point	Deg F.	29-1D20R-108	276.1	287.1
30% Recovery Point	Deg F.	29-1D30R-108	282.4	292.8
40% Recovery Point	Deg F.	29-1D40R-108	288.5	298
50% Recovery Point	Deg F.	29-1D50R-108	295	304
60% Recovery Point	Deg F.	29-1D60R-108	301.5	309.9
70% Recovery Point	Deg F.	29-1D70R-108	308.7	316.9
80% Recovery Point	Deg F.	29-1D80R-108	317.8	325.2
90% Recovery Point	Deg F.	29-1D90R-108	331.3	337.3
95% Recovery Point	Deg F.	29-1D95R-108	346.1	349
IBP-Recovery	Deg F.	29-1IBPR-108	251.1	255.4
Nitrogen -ppm	mg/kg	29-1N2A-108		
% Recovered	Vol %	29-1RECR-108	97.3	98.5
Sulfur -antek	mg/kg	29-1SULA-108	4	4
Fractionator Bottoms		29-AP-110		
API Gravity	API	29-1API-110	25.9	27.3
Nitrogen-ppm	mg/kg	29-1N2A-110	9	
FBP D86 Correlation	Deg F.	29-1SCEP-110	886	898
IBP D86 Correlation	Deg F.	29-1SCIP-110	536	570
5% D86 Correlation	Deg F.	29-1SC05-110	578	614
10% D86 Correlation	Deg F.	29-1SC10-110	616	653
20% D86 Correlation	Deg F.	29-1SC20-110	654	689
30% D86 Correlation	Deg F.	29-1SC30-110	680	712
50% D86 Correlation	Deg F.	29-1SC50-110	724	747
70% D86 Correlation	Deg F.	29-1SC70-110	769	788
80% D86 Correlation	Deg F.	29-1SC80-110	796	814
90% D86 Correlation	Deg F.	29-1SC90-110	836	853
95% D86 Correlation	Deg F.	29-1SC95-110	862	877
Sulfur by Horiba	mass %	29-1SULH-110		0.006
Distillate Product		29-AP-111		
API Gravity	API	29-1API-111	34.1	34
Cloud Point - Auto	Deg F.	29-1CLDA-111	-31.4	-31
End Point Recovery Point	Deg F.	29-1DEPR-111	606.7	612.5
5% Recovery Point	Deg F.	29-1D05R-111	419	420.4
10% Recovery Point	Deg F.	29-1D10R-111	425.7	426.4
20% Recovery Point	Deg F.	29-1D20R-111	438.6	439.9
30% Recovery Point	Deg F.	29-1D30R-111	452.7	453.4
40% Recovery Point	Deg F.	29-1D40R-111	468.3	467.8
50% Recovery Point	Deg F.	29-1D50R-111	484.2	483.6
60% Recovery Point	Deg F.	29-1D60R-111	501.4	500.9
70% Recovery Point	Deg F.	29-1D70R-111	520.2	520

80% Recovery Point	Deg F.	29-1D80R-111	541.4	541
90% Recovery Point	Deg F.	29-1D90R-111	568.6	568.8
95% Recovery Point	Deg F.	29-1D95R-111	590.7	590.7
Flash Point - Auto	Deg F.	29-1FLA-111	190	184
IBP-Recovery	Deg F.	29-1IBPR-111	402.8	406.4
Pour Point - Auto	Deg F.	29-1POURA-111	-49	-43.6
% Recovered	Vol %	29-1RECR-111	97.9	98.4
Sulfur -antek	mg/kg	29-1SULA-111	1.7	2
Nitrogen -ppm	mg/kg	29-1N2A-111		
Cetane Number		29-1CETA-111	42	
Distillate Product		29-AP-112		
API Gravity	API	29-1API-112	28.7	28.6
Cloud Point - Auto	Deg F.	29-1CLDA-112	25.2	24.8
Flash Point - Auto	Deg F.	29-1FLA-112	310	315
Pour Point - Auto	Deg F.	29-1POURA-112	15.8	15.8
FBP D86 Correlation	Deg F.	29-1SCEP-112	679	681
IBP D86 Correlation	Deg F.	29-1SCIP-112	537	543
5% D86 Correlation	Deg F.	29-1SC05-112	560	567
10% D86 Correlation	Deg F.	29-1SC10-112	581	589
20% D86 Correlation	Deg F.	29-1SC20-112	602	611
30% D86 Correlation	Deg F.	29-1SC30-112	615	623
50% D86 Correlation	Deg F.	29-1SC50-112	637	644
70% D86 Correlation	Deg F.	29-1SC70-112	649	656
80% D86 Correlation	Deg F.	29-1SC80-112	658	663
90% D86 Correlation	Deg F.	29-1SC90-112	666	670
95% D86 Correlation	Deg F.	29-1SC95-112	672	676
			10	30
Sulfur	Simulation		10.54	31.62
Sulfur by Horiba	mass %	29-1SULH-112		0.003
Cetane Number		29-1CETA-112	47.7	
HDS Combined Feed		29-AP-100		
FBP D2887	Deg F.	29-1SDEP-100	995	992
IBP D2887	Deg F.	29-1SDIP-100	271	268
5% D2887	Deg F.	29-1SD05-100	381	383
10% D2887	Deg F.	29-1SD10-100	420	422
20% D2887	Deg F.	29-1SD20-100	481	483
30% D2887	Deg F.	29-1SD30-100	535	537
50% D2887	Deg F.	29-1SD50-100	641	643
70% D2887	Deg F.	29-1SD70-100	743	743
90% D2887	Deg F.	29-1SD90-100	865	865
95% D2887	Deg F.	29-1SD95-100	913	912
Fractionator Bottoms		29-AP-110		
FBP D2887	Deg F.	29-1SDEP-110	997	1010
IBP D2887	Deg F.	29-1SDIP-110	428	460
5% D2887	Deg F.	29-1SD05-110	542	579
10% D2887	Deg F.	29-1SD10-110	584	623

20% D2887	Deg F.	29-1SD20-110	636	674
30% D2887	Deg F.	29-1SD30-110	675	708
50% D2887	Deg F.	29-1SD50-110	737	761
70% D2887	Deg F.	29-1SD70-110	798	817
90% D2887	Deg F.	29-1SD90-110	884	903
95% D2887	Deg F.	29-1SD95-110	924	941
Diesel Product		29-AP-112		
FBP D2887	Deg F.	29-1SDEP-112	746	749
IBP D2887	Deg F.	29-1SDIP-112	480	483
5% D2887	Deg F.	29-1SD05-112	531	539
10% D2887	Deg F.	29-1SD10-112	555	563
20% D2887	Deg F.	29-1SD20-112	586	594
30% D2887	Deg F.	29-1SD30-112	609	618
50% D2887	Deg F.	29-1SD50-112	647	655
70% D2887	Deg F.	29-1SD70-112	678	685
90% D2887	Deg F.	29-1SD90-112	712	717
95% D2887	Deg F.	29-1SD95-112	723	727
Sour Recycle Gas		29-AP-113		
Hydrogen / Methane ratio		29-1CA1-113	82.3	98.8
SCF per barrel	scf/bbls	29-1CA2-113	3826	4605.4
BTU per SCF	btu/scf	29-1CA3-113	491.9	337.9
Carbon Monoxide	Vol %	29-1VCO-113	0	0
Carbon Dioxide	Vol %	29-1VCO2-113	0.02	0
Hydrogen -v	Vol %	29-1VH2-113	74.03	98.07
Hydrogen Sulphide -v	Vol %	29-1VH2S-113	0.77	0.64
Specific Gravity -c		29-1VLSG-113	0.1732	0.087
molecular weight -b	g/mole	29-1VMW-113	6.02	2.52
Nitrogren -v	Vol %	29-1VN2-113	1.14	0.16
Oxygen -v	Vol%	29-1VO2-113	0	0.03
Olefins - total -v	Vol%	29-1VTO-113	0	0
Methane -v	Vol %	29-1V1-113	23.63	0.78
Ethylene	Vol %	29-1V21-113	0	0
Ethane	Vol %	29-1V22-113	0.36	0.11
Acetylene	Vol %	29-1V23-113	0	0
C3 plus	Vol %	29-1V3P-113	0.05	0.21
Propane -v	Vol%	29-1V31-113	0.01	0.12
Propylene -v	Vol %	29-1V32-113	0	0
Propadiene	Vol%	29-1V33-113	0	0
isobutane -v	Vol %	29-1V41-113	0	0.02
n-butane -v	Vol %	29-1V42-113	0.01	0.05
isobutene	Vol %	29-1V43-113	0	0
trans-2-butene	Vol%	29-1V44-113	0	0
cis-2-butene	Vol%	29-1V45-113	0	0
1-butene	Vol%	29-1V46-113	0	0
isopentane -v	Vol%	29-1V51-113	0	0.01

n-pentane -v	Vol%	29-1V52-113	0	0.01
neopentane -v	Vol%	29-1V54-113	0	0
C6 plus	Vol%	29-1V6P-113	0.03	0
LPCS Flash Gas		29-AP-102		
Hydrogen / Methane ratio		29-1CA1-102	2.2	7.7
SCF per barrel	scf/bbls	29-1CA2-102	3643.6	4091.6
BTU per SCF	btu/scf	29-1CA3-102	516.9	431.5
Carbon Monoxide	Vol %	29-1VCO-102	0	0
Carbon Dioxide	Vol %	29-1VCO2-102	0.15	0
Hydrogen -v	Vol %	29-1VH2-102	64.03	81.9
Hydrogen Sulphide -v	Vol %	29-1VH2S-102	1.24	5.54
Specific Gravity -c		29-1VLSG-102	0.222	0.1824
molecular weight -b	g/mole	29-1VMW-102	8.1	5.92
Nitrogren -v	Vol %	29-1VN2-102	5.33	0.95
Oxygen -v	Vol%	29-1VO2-102	0.06	0
Olefins - total	Vol%	29-1VTO-102	0	0
Methane -v	Vol %	29-1V1-102	28.53	10.69
Ethylene	Vol %	29-1V21-102	0	0
Ethane	Vol %	29-1V22-102	0.58	0.39
Acetylene	Vol %	29-1V23-102	0	0
C3 plus	Vol %	29-1V3P-102	0.08	0.53
Propane -v	Vol%	29-1V31-102	0.03	0.27
Propylene -v	Vol %	29-1V32-102	0	0
Propadiene	Vol%	29-1V33-102	0	0
isobutane -v	Vol %	29-1V41-102	0	0.1
n-butane -v	Vol %	29-1V42-102	0.01	0.1
isobutene	Vol %	29-1V43-102	0	0
trans-2-butene	Vol%	29-1V44-102	0	0
cis-2-butene	Vol%	29-1V45-102	0	0
1-butene	Vol%	29-1V46-102	0	0
isopentane -v	Vol%	29-1V51-102	0	0.03
n-pentane -v	Vol%	29-1V52-102	0	0.01
neopentane -v	Vol%	29-1V54-102	0	0
C6 plus	Vol%	29-1V6P-102	0.04	0.02
Stripper OH off Gas		29-AP-107		
Hydrogen / Methane ratio		29-1CA1-107	1.1	2.3
SCF per barrel	scf/bbls	29-1CA2-107	3265.7	3220.8
BTU per SCF	btu/scf	29-1CA3-107	640.1	696.3
Carbon Monoxide	Vol %	29-1VCO-107	0	0
Carbon Dioxide	Vol %	29-1VCO2-107	0	0
Hydrogen -v	Vol %	29-1VH2-107	49.57	50.12
Hydrogen Sulphide -v	Vol %	29-1VH2S-107	0	20.12
Specific Gravity -c		29-1VLSG-107	0.2422	0.3622
molecular weight -b	g/mole	29-1VMW-107	9.85	14.93
Nitrogren -v	Vol %	29-1VN2-107	4.14	0.82
Oxygen -v	Vol%	29-1VO2-107	0.12	0.22
Olefins - total	Vol%	29-1VTO-107	0	0

Methane -v	Vol %	29-1V1-107	44.83	21.77
Ethylene	Vol %	29-1V21-107	0	0
Ethane	Vol %	29-1V22-107	1.18	1.98
Acetylene	Vol %	29-1V23-107	0	0
C3 plus	Vol %	29-1V3P-107	0.16	4.97
Propane -v	Vol%	29-1V31-107	0.07	2.21
Propylene -v	Vol %	29-1V32-107	0	0
Propadiene	Vol%	29-1V33-107	0	0
isobutane -v	Vol %	29-1V41-107	0	0.82
n-butane -v	Vol %	29-1V42-107	0.02	1.32
isobutene	Vol %	29-1V43-107	0	0
trans-2-butene	Vol%	29-1V44-107	0	0
cis-2-butene	Vol%	29-1V45-107	0	0
1-butene	Vol%	29-1V46-107	0	0
isopentane -v	Vol%	29-1V51-107	0	0.34
n-pentane -v	Vol%	29-1V52-107	0	0.21
neopentane -v	Vol%	29-1V54-107	0	0
C6 plus	Vol%	29-1V6P-107	0.07	0.07
Rich DGA		29-AP-103		
H2S Titration	Grains	29-1H2SL-103	2514	3240
Hydrogen Sulphide	ppm	29-1H2SP-103	42989.4	55404

PLANT C

			9/30/2004
HDS feed		**BPD**	14,009.2
		API	29.78
		Wt%S	0.41%
hds product		**BPD**	14,396.9
		API	31.28
		Wt%S	0.000%
H2 Mup		**mmscfd**	4.03
Purge gas		**mmscfd**	0.04
LP OG		**mmscfd**	0.14
LE part of napththa		**mmscfd**	0.07
Strip OG		**mmscfd**	0.39
Net Gas Bleeds		**mmscfd**	0.64
Unit Delta		**mmscfd**	3.39
H2 Mup		**% H2**	86.9%
Purge gas		**% H2**	82.7%
LP OG		**% H2**	57.0%
LE part of napththa		**% H2**	0.0%
Strip OG		**% H2**	5.7%
Treat Gas Ratio		**SCF/BBl**	**654**
Recycle after make-up		MSCFH	382.0
HPFD Temp	F		98.6

HPFD Press	psig	608.5
LPFD Temp	F	101.3
LPFD Press	psig	125.0
Strp OH Drum Temp	F	120.3
Strp OH Drum Press	psig	90.0
Recycle Comp Suct Press	psig	608.5
Recycle Comp Disch Press	psig	765.2
Make Up Comp Suct Press	psig	219.6

		bpd/*mscfh*	API/*MW*	lb/h	T (F)	P (psig)
HDS charge from charge pumps	FIC17105	14009.2	29.8	179659.0		
Hydrogen from reformer	FI17115	*168.1*	*7.5*	2499.8	99.3	219.6
Purge gas from HP separator to amine contactor	FIC17109	*1.5*	*5.0*	19.4	98.6	608.5
Offgas from LP flash drum to amine contactor	FI17146	*5.9*	*10.6*	164.9	101.3	125.0
Fuel gas separator offgas to amine contactor	FI17121	*16.4*	*32.0*	1386.0	120.3	90.0
Wild naphtha to crude preflash tower	FI17122	620.4	79.5	6081.8		
Treated diesel less hot oil makeup	FI17114	14396.9	31.3	182921.9		
Recycle gas to Rx	FI1706	*382.0*	*6.0*	6029.7	145.7	765.2
Desulfurizer sep offgas to HDS fuel contactor	FI24019	*161.4*	*4.9*	2078.0	120.3	90.0
Sweet gas to fuel	FIC17130	*185.5*	*7.75*	3795.0	120.3	90.0

Oil fraction - Sum products

% vol	TBP	ASTM D86
0.0	130.0	231.2
1.0	162.6	251.3
2.0	204.7	279.9
3.5	278.1	334.9
5.0	318.5	366.8
7.5	358.5	398.8
10.0	389.3	423.3
12.5	409.1	439.0
15.0	422.3	449.2
17.5	433.3	457.8
20.0	444.3	466.1
25.0	472.2	487.0
30.0	486.3	497.2
35.0	497.6	504.8
40.0	513.1	515.2
45.0	528.3	525.4
50.0	542.3	535.0
55.0	555.8	544.4
60.0	569.0	553.9
65.0	582.4	563.8
70.0	596.7	574.8
75.0	613.6	588.5
80.0	629.6	601.9
85.0	644.3	614.6
90.0	664.4	632.4
92.5	676.6	643.4
95.0	690.2	655.8
96.5	698.6	663.5
98.0	707.1	671.3
99.0	712.6	676.4
100.0	718.0	681.4

Flowrate 14967.96 bpd

	929.83	lbmole/h
API	30.96	

	Hydrogen from reformer		
	Avg	offgas from LP flsash	
H2	85.1%	H2	0.5700142
C1	4.5%	C1	0.2910375
C2	3.5%	C2	0.0676044
c2=	0.0%	c2=	0
C3	3.1%	C3	0.0206128
c3=	0.0%	c3=	0
IC4	0.8%	IC4	0.0030951
NC4	0.9%	NC4	0.0021544
B-1	0.0%	B-1	0
ib=	0.0%	ib=	0
T-2	0.0%	T-2	0
C-2	0.0%	C-2	0
IC5	0.4%	IC5	0
NC5	0.2%	NC5	0
c5=	0.0%	c5=	0
1,3BD	0.0%	1,3BD	0
C6+	1.4%	C6+	0
N2	0.0%	N2	0
CO	0.0%	CO	0
CO2	0.0%	CO2	0
O2	0.0%	O2	0
H2O	0.0%	H2O	0
H2S	0.0%	H2S	0.0454816
	100.0%		1

Purge gas from HP separator		Recycle gas to HDS	
H2	82.7%	H2	0.8402666
C1	13.9%	C1	0.095829
C2	2.1%	C2	0.0257923
c2=	0.0%	c2=	0
C3	0.6%	C3	0.0169527
c3=	0.0%	c3=	0
IC4	0.1%	IC4	0.0040648
NC4	0.0%	NC4	0.0050754
B-1	0.0%	B-1	0
ib=	0.0%	ib=	0
T-2	0.0%	T-2	0
C-2	0.0%	C-2	0
IC5	0.0%	IC5	0.0021148
NC5	0.0%	NC5	0.0020023
c5=	0.0%	c5=	0
1,3BD	0.0%	1,3BD	0
C6+	0.0%	C6+	0.0024995

N2	0.0%	N2	0
CO	0.0%	CO	0
CO2	0.0%	CO2	0
O2	0.0%	O2	0
H2O	0.0%	H2O	0
H2S	0.6%	H2S	0.0054026
	100.0%		1

	MMSFD						
	H2	**C1**	**C2**	**C3**	**C4**	**H2S**	**Total**
H2 Mup	3.505	0.183	0.144	0.129	0.072	0.000	4.03
Purge gas	0.029	0.005	0.001	0.000	0.000	0.000	0.04
LP OG	0.081	0.041	0.010	0.003	0.001	0.006	0.14
LE part of r	0.000	0.000	0.000	0.025	0.049	0.000	0.07
Strip OG	0.023	0.073	0.085	0.061	0.024	0.128	0.39
Net Gas Bl	0.132	0.119	0.095	0.090	0.074	0.135	0.64
Unit Delta	3.373	0.064	0.049	0.040	-0.002	-0.135	3.39
						Total C1+ Prodn	
	240.740	**4.563**	**3.525**	**2.832**	**-0.167**	**-9.610**	**10.8**

	MASS BAL		LAB %						
	H2		H2	C1	C2	C3	C4+	H2S	Sum
Hydrogen from reformer	86.9%		0.87	0.05	0.04	0.03	0.02	0.00	1.00
Purge gas from HP separator to amine contactor	82.73%		0.827	0.139	0.021	0.006	0.001	0.006	1.00
Offgas from LP flash drum to amine contactor	57.0%		0.57	0.29	0.07	0.02	0.01	0.05	1.00
Naphtha LE	0.0%		0.00	0.00	0.00	0.34	0.66	0.00	1.00
Fuel gas separator offgas to amine contactor	5.7%		0.06	0.19	0.21	0.16	0.06	0.32	1.00
Recycle gas to reactor	84.6%		0.846	0.096	0.026	0.0171	0.0092	0.005	1.00
	MMSCFD		**H2**	**C1**	**C2**	**C3**	**C4**		
Recycle Gas(after bleed)	5.13		4.25	0.72	0.11	0.03	0.01	0.03	5.13
Recy to Rx(purity calc from MB)			0.846	0.098	0.027	0.0175	0.0084	0.0033	1.00
Recy to Rx(from MB)			7.75	0.90	0.25	0.16	0.08	0.03	9.17

	M/U H2 to Reacto	Recy H2 Purge	LPFD OG	Naphtha LE	Stripp OG	Recycle H2 to Rx	Recycle H2 (afte	Reactor gas out	
	MMSCFD	MMSCFD	MMSCFD	MMSCFD	MMSCFD	MMSCFD	MMSCFD	MMSCFD	lbmol/h
H2	3.50	0.03	0.08	0.00	0.02	7.75	4.25	4.4	480.9
C1	0.18	0.00	0.04	0.00	0.07	0.90	0.72	0.8	91.7
C2	0.14	0.00	0.01	0.00	0.08	0.25	0.11	0.2	22.0
C3	0.13	0.00	0.00	0.03	0.06	0.16	0.03	0.1	13.2
C4	0.07	0.00	0.00	0.05	0.02	0.08	0.01	0.1	8.7
H2S	0.00	0.00	0.01	0.00	0.13	0.03	0.03	0.2	18.1
Total	**4.0**	**0.04**	**0.1**	**0.07**	**0.4**	**9.2**	**5.13**	5.8	634.6
Total (lbmol/h)	442.83	3.85	15.51	8.15	43.29	1006.61	563.78	634.56	

Plant E

SAMPLE POINT	**LAB TEST**	**UNITS**	**DESCRIPTION**	
726TRTR:	GRVCSP:		Gas Gravity	0.14366
726TRTR:	NBTU:	NBTU	Net BTU	343.842
726TRTR:	#N2:	mol%	Nitrogen	0.05002
726TRTR:	#H2:	mol%	Hydrogen	89.5733
726TRTR:	#H2S:	mol%	H2S	2.40158
726CSOGS:	GRVCSP:		Gas Gravity	0.21271
726CSOGS:	NBTU:	NBTU	Net BTU	380.683
726CSOGS:	#N2:	mol%	Nitrogen	0.03835
726CSOGS:	#H2:	% H2	H2 out cold separator	85.3614
726CSOGS:	#H2S:	mol%	H2S	7.364
726STOGS:	GRVCSP:		Gas Gravity	NR
726STOGS:	NBTU:	NBTU	Net BTU	NR

726STOGS:	#N2:	mol%	Nitrogen	NR
726STOGS:	#H2:	% H2	H2 out strip ovhd.	NR
726STOGS:	#H2S:	mol%	H2S	NR
726DSL:	DSEN00:	^{O}F	IBP	399.1
726DSL:	DSEN05:	^{O}F	2 Oil 05% Pt.	449.6
726DSL:	DSEN10:	^{O}F	2 Oil 10% Pt.	478.6
726DSL:	DSEN30:	^{O}F	2 Oil 30% Pt.	522.3
726DSL:	DSEN50:	^{O}F	2 Oil 50% Pt.	551.8
726DSL:	DSEN70:	^{O}F	2 Oil 70% Pt.	584
726DSL:	DSEN90:	^{O}F	2 Oil 90% Pt.	633.3
726DSL:	DSEN95:	^{O}F	2 Oil 95% Pt.	661.8
726DSL:	DSENMX:	^{O}F	2 Oil End Pt.	666.6
726DSL:	FLAPMC:	^{O}F	Flash Pt.	182
726DSL:	CLOUPT:	degF	Cloud Point	22
726DSL:	POURPT:	degF	Pour Point	15
726DSL:	COLAST:	degF	ASTM Color	1.5
726DSL:	ES%XRY:	wt.%	Product Sulfur	0.05
726DSL:	GRVAPI:	API	API Product	32.62
726DSL:	VK100F:	Cp	Viscosity @ 100 F	3.74
726DFEED:	ES%XRY:	wt.%	Feed Sulfur	1.05
726DFEED:	GRVAPI:		Feed API Gravity	31.65
726STWAT:	WTPH:	pH	pH	
726STWAT:	NH3BA:	ppm	Ammonia	
726STWAT:	EWTPS=:	ppm	Sulfides	
726STWAT:	@BZ:	ppm	Benzene	
726STWAT:	EFE-AA:	ppm	Iron	
STRM@S42:	GRVAPI:	API	API Gravity	
STRM@S42:	DSEN00:	OF	IBP	
STRM@S42:	DSEN05:	OF	2 Oil 05% Pt.	
STRM@S42:	DSEN10:	OF	2 Oil 10% Pt.	
STRM@S42:	DSEN50:	OF	2 Oil 50% Pt.	
STRM@S42:	DSEN90:	OF	2 Oil 90% Pt.	
STRM@S42:	DSENMX:	OF	2 Oil End Pt.	
STRM@S42:	POURPT:	degF	Pour Point	
STRM@S42:	COLAST:	degF	ASTM Color	
STRM@S42:	CLOUPT:	degF	Cloud Point	
STRM@S42:	HAZE:		Haze	
STRM@S42:	VK100F:	CST	Viscosity @ 100 deg F	
				5-Mar-97
Total Feed			MBPD	9.3
LCO Feed			**MBPD**	**1.8**
Charge	API		API	28.8
	Sulfur		wt%	0.356
Product	**API**		**API**	**30.2**
	Sulfur		**wt%**	**0.024**
	Flash Pt.		**Deg. F**	**176.00**

Cloud Pt.	**Deg. F**		**18.00**
Pour Pt.	**Deg. F**		**10.00**

	ASTM Color		**1.00**
	End Point	**Deg. F**	**653.00**
Cetane (old)			**44.21**
Cetane (new)			**43.30**
% Desulfurization		**%HDS**	**93.26**
API Improvement		**API**	**1.40**
H2 Consump. To Diesel		**scf H2/bbl**	**160.6**
Reactor Inlet T		**deg F**	**630.2**
Bed 1 Delta T		deg F	23.7
Bed 1 WABT		deg F	646.6
Bed 1 Radial Delta T		deg F	8.9
Bed 2 Delta T		deg F	1.9
Bed 2 WABT		deg F	655.2
Bed 2 Radial Delta T		deg F	3.4
Reactor Inlet P		psig	340
Reactor DP		**psi**	**37**
Rctr DP, Feed/Recy Corr.		psi	36.2
DP Increase Rate		psi/day	-2.47
Next SHDN, Based on DP			note 1
Total H2 Consumption		scf H2/bbl	173.4
Treat Ratio		scf H2/bbl	950
H2 Partial Press., Rx In			278
H2 Partial Press., Rx Out			238
Wild Naphtha		MBPD	0.16
LHSV		1/hr	0.4
Product	Rate	MBPD	9.7
Unit Balances		LVY%	97.3
		Mass Bal.	100.0
Operating Costs			
Charge Heater Duty		MMBtu/h	
Frac Heater Duty		MMBtu/h	
Fuel Gas Cost		$/Day	
Net Steam Usage		M#/h	
Steam Cost		$/Day	
Hydrogen Consumption			
H2 IN	Pass A	MMSCFD	5.00
H2 IN	Pass B	MMSCFD	5.00
H2 Purity		%	81.84
MMSCFD H2 IN		MMSCFD	8.19
Cold sep. off Gas	DFI149.PV	MMSCFD	8.56
Cold sep. off gas H2 purity		%	76.72
Stripper off gas	DFI238.PV	MMSCFD	0.45
Stripper off gas H2 purity		%	26.26
MMSCFD H2 OUT		MMSCFD	6.69
H2 Consump. To Diesel		SCFB	160.63
Total H2 Consumption		SCFB	173.39

Reactor DP Rate Of Increase			
12/18/1996 12/20/1996			
Use slope over a	day period		20.00
Base Feed Rate	MBPD		10.50
Base Recy Rate	MMSCFD		8.50
EOR Rx DP	PSI		70.00
	PSI	DIESEL RX PRESS DIFF	4.91
	MBPD	DIESEL TOTAL CHARGE	0.18
	MMSCFD	DIESEL TREAT HYDROGEN	1.66
Rctr DP, Feed/Recy Corr.	PSI		85.54
Next SHDN, Based on DP			35480.30

LAB DATA ARCHIVE

TREAT HYDROGEN		
Gas Gravity		0.23
Net BTU	NBTU	488.71
Nitrogen	mol%	0.02
Hydrogen	mol%	81.84
H2S	mol%	0.01
CS OFF GAS		
Gas Gravity		0.27
Net BTU	NBTU	536.00
Nitrogen	mol%	0.03
H2 out cold separator	% H2	76.72
H2S	mol%	1.74
STRIPPER OFF GAS		
Gas Gravity		1.15
Net BTU	NBTU	1737.37
Nitrogen	mol%	0.01
H2 out strip ovhd.	% H2	26.26
H2S	mol%	5.01
DIESEL PRODUCT		
IBP	OF	359.00
1 Oil 05% Pt.	OF	455.00
2 Oil 10% Pt.	OF	479.00
3 Oil 30% Pt.	OF	528.00
2 Oil 50% Pt.	OF	557.00
3 Oil 70% Pt.	OF	585.00
2 Oil 90% Pt.	OF	622.00
3 Oil 95% Pt.	OF	640.00
2 Oil End Pt.	OF	653.00
Flash Pt.	OF	176.00
Cloud Point	OF	18.00
Pour Point	OF	10.00

ASTM Color	OF	1.00
Product Sulfur	wt.%	0.02
API Product	API	30.20
DIESEL PRODUCT		
Feed Sulfur	wt.%	0.36
Feed API Gravity		28.80
STRIPPER WATER		
pH	pH	
Ammonia	ppm	
Sulfides	ppm	
Benzene	ppm	
Iron	ppm	
DIESEL AT TANK 42		
API Gravity	API	30.80
IBP	OF	365.00
2 Oil 05% Pt.	OF	438.00
2 Oil 10% Pt.	OF	463.00
2 Oil 50% Pt.	OF	543.00
2 Oil 90% Pt.	OF	605.00
2 Oil End Pt.	OF	634.00
Pour Point	OF	0.00
ASTM Color	OF	1.00
Cloud Point	OF	12.00
Haze		1.00
Viscosity @ 100 deg F	CST	3.50

APPENDIX C

PROCESS INFORMATION

KOCH-GLITSCH CANADA COMPANY

CALCULATIONS AND SKETCHES

BY A. Clement DATE SHEET 1 OF 1

SUBJECT 1.5 Order Version of Sulfur product Equation 5.15 to Equation 5.16 JOB NO.

(1) $\frac{\exp\left(a-\frac{b}{T_1}\right)}{\exp\left(a-\frac{b}{T_2}\right)} = \frac{LHSV_1}{LHSV_2}\cdot\frac{f(S_{F_1},S_{P_1})}{f(S_{F_2},S_{P_2})}$, Equation 5.15 (2) $= \frac{LHSV_1}{LHSV_2}\cdot\frac{\frac{1}{\sqrt{S_{P_1}}}-\frac{1}{\sqrt{S_{F_1}}}}{\frac{1}{\sqrt{S_{P_2}}}-\frac{1}{\sqrt{S_{F_2}}}}$

a) Substitute in relation for 1.5 reaction order

(3) $\exp\left(a-\frac{b}{T_1}-\left(a-\frac{b}{T_2}\right)\right) = \frac{LHSV_1}{LHSV_2}\cdot\left(\frac{\sqrt{S_{F_2}}-\sqrt{S_{P_1}}}{\sqrt{S_{F_1}}\cdot\sqrt{S_{P_1}}}\right)\Big/\left(\frac{\sqrt{S_{F_2}}-\sqrt{S_{P_2}}}{\sqrt{S_{P_2}}\cdot\sqrt{S_{F_2}}}\right)$ b) simplify

(4) $\exp\left(\frac{b}{T_2}-\frac{b}{T_1}\right) = \frac{LHSV_1}{LHSV_2}\cdot\frac{\sqrt{S_{P_2}}\cdot\sqrt{S_{F_2}}}{\sqrt{S_{F_1}}\cdot\sqrt{S_{P_1}}}\cdot\left(\frac{\sqrt{S_{F_1}}-\sqrt{S_{P_1}}}{\sqrt{S_{F_2}}-\sqrt{S_{P_2}}}\right)$

c) multiply through by $(\sqrt{S_{F_2}}-\sqrt{S_{P_2}})$ + expand

(5) $\exp\left(\frac{b}{T_2}-\frac{b}{T_1}\right)\cdot\sqrt{S_{F_2}} - \exp\left(\frac{b}{T_2}-\frac{b}{T_1}\right)\cdot\sqrt{S_{P_2}} = \frac{LHSV_1}{LHSV_2}\cdot\frac{\sqrt{S_{P_2}}\cdot\sqrt{S_{F_2}}\cdot\sqrt{S_{F_1}}}{\sqrt{S_{F_1}}\cdot\sqrt{S_{P_1}}} - \frac{LHSV_1}{LHSV_2}\cdot\frac{\sqrt{S_{P_2}}\cdot\sqrt{S_{F_2}}\cdot\sqrt{S_{P_2}}}{\sqrt{S_{F_1}}\cdot\sqrt{S_{P_1}}}$ d) consolidate $\sqrt{S_{P_2}}$ terms

(6) $\exp\left(\frac{b}{T_2}-\frac{b}{T_1}\right)\cdot\sqrt{S_{F_2}} = \sqrt{S_{P_2}}\cdot\left[\exp\left(\frac{b}{T_2}-\frac{b}{T_1}\right)+\frac{LHSV_1}{LHSV_2}\cdot\frac{\sqrt{S_{F_2}}}{\sqrt{S_{P_1}}} - \frac{LHSV_1}{LHSV_2}\cdot\sqrt{S_{F_2}}/\sqrt{S_{F_1}}\right]$ e) Isolate for $\sqrt{S_{P_2}}$

(7) $\sqrt{S_{P_2}} = \frac{\sqrt{S_{F_2}}\cdot\exp\left(\frac{b}{T_2}-\frac{b}{T_1}\right)}{\exp\left(\frac{b}{T_2}-\frac{b}{T_1}\right)+\frac{LHSV_1}{LHSV_2}\cdot\left(\frac{\sqrt{S_{F_2}}}{\sqrt{S_{P_1}}}-\frac{\sqrt{S_{F_2}}}{\sqrt{S_{F_1}}}\right)}$ f) ÷ RHS by $\sqrt{S_{F_2}}\cdot\exp\left(\frac{b}{T_2}-\frac{b}{T_1}\right)$ in numerator & denominator

+ Note: $\left(\frac{\sqrt{S_{F_2}}}{\sqrt{S_{P_1}}}-\frac{\sqrt{S_{F_2}}}{\sqrt{S_{F_1}}}\right) = \sqrt{S_{F_2}}\cdot\left(\frac{1}{\sqrt{S_{P_1}}}-\frac{1}{\sqrt{S_{F_1}}}\right)$

(8) $\sqrt{S_{P_2}} = \frac{1}{\frac{1}{\sqrt{S_{F_2}}}+\frac{LHSV_1}{LHSV_2}\cdot\exp\left(-\left(\frac{b}{T_2}-\frac{b}{T_1}\right)\frac{\sqrt{S_{F_2}}}{\sqrt{S_{F_2}}}\left(\frac{1}{\sqrt{S_{P_1}}}-\frac{1}{\sqrt{S_{F_1}}}\right)\right)}$ g) Simplify and use $(\,)^{-1}$ form

(9) $\sqrt{S_{P_2}} = \left(\frac{LHSV_1}{LHSV_2}\cdot\exp\left(\frac{b}{T_1}-\frac{b}{T_2}\right)\cdot\left(\frac{1}{\sqrt{S_{P_1}}}-\frac{1}{\sqrt{S_{F_1}}}\right)+\frac{1}{\sqrt{S_{F_2}}}\right)^{-1}$ h) Multiply both sides by $(\,)^2$

(10) $S_{P_2} = \left\{\left[\left(\frac{1}{\sqrt{S_{P_1}}}-\frac{1}{\sqrt{S_{F_1}}}\right)\cdot e^{\left(\frac{b}{T_1}-\frac{b}{T_2}\right)}\cdot\frac{LHSV_1}{LHSV_2}+\frac{1}{\sqrt{S_{F_2}}}\right]^{-1}\right\}^2$ i) let subscript 2 ≡ current timestep i; let subscript 1 = previous timestep $i-1$

(11) $S_{P_i} = \left\{\left[\left(\frac{1}{\sqrt{S_{P_{i-1}}}}-\frac{1}{\sqrt{S_{F_{i-1}}}}\right)\cdot\frac{LHSV_{i-1}}{LHSV_i}\cdot e^{\left(\frac{b}{T_{i-1}}-\frac{b}{T_i}\right)}+\frac{1}{\sqrt{S_{F_i}}}\right]^{-1}\right\}^2$ j) note $k_{HOS_{i-1}} \approx LHSV_{i-1}\left(\frac{1}{\sqrt{S_{P_{i-1}}}}-\frac{1}{\sqrt{S_{F_{i-1}}}}\right)$ Substitute $k_{HOS\,i-1}$ into relation

(12) $S_{P_i} = \left\{\left[k_{HOS_{i-1}}\cdot\frac{(LHSV_{i-1})^2}{(LHSV_i)}\cdot e^{\left(\frac{b}{T_{i-1}}-\frac{b}{T_i}\right)}\cdot\frac{1}{\sqrt{S_{F_i}}}\right]^{-1}\right\}^2$

(11a) $S_{P_i} = \left\{\left[\left(\frac{1}{\sqrt{S_{P_{i-1}}}}-\frac{1}{\sqrt{S_{F_{i-1}}}}\right)\frac{LHSV_{i-1}}{LHSV_i}\cdot e^{\left(\frac{b}{T_{i-1}}-\frac{b}{T_i}\right)}\cdot\left(\frac{P_{i-1}}{P_i}\right)^p\cdot\left(\frac{G_{i-1}}{G_i}\right)^q+\frac{1}{\sqrt{S_{F_i}}}\right]^{-1}\right\}^2$ = Equation 5.16

k: Apply parameters P + q into relation: Use ratio format as original derivation step in (1) like ideal gas law $\left(\frac{P_{i-1}}{P_i}\right)^p + \left(\frac{G_{i-1}}{G_i}\right)^q$ In steady state: form: $\frac{(P_i)^p}{(G_i)^q}$

(12b) $S_{P_i} = \left\{\left[k_{HOS_{i-1}}\cdot\frac{(LHSV_{i-1})^2}{(LHSV_i)}\cdot\left(\frac{P_{i-1}}{P_i}\right)^p\cdot\left(\frac{G_{i-1}}{G_i}\right)^q\cdot e^{\left(\frac{b}{T_{i-1}}-\frac{b}{T_i}\right)}+\frac{1}{\sqrt{S_{F_i}}}\right]^{-1}\right\}^2$ = Equation 5.17

6/98Q PS-1524

KOCH-GLITSCH CANADA COMPANY

CALCULATIONS AND SKETCHES

BY D. Romerah DATE SHEET 1 OF 1

SUBJECT Fractional Reaction Order between 1.5 - 2.0 JOB NO.

Equation derivation, for 5.24a, b

a) Start from Step (7) in 1.5 Order Version of Equation, and substitute $\left(\frac{1}{\sqrt{S_P}} - \frac{1}{\sqrt{S_F}}\right)$ for $\left(\frac{1}{(S_P)^{n-1}} - \frac{1}{(S_F)^{n-1}}\right)$ where $1.0 < n \leq 2$ & n is the Reaction order.

(8) $$(S_{P_2})^{n-1} = \frac{(S_{F_2})^{n-1} \cdot \exp\left(\frac{b}{T_2} - \frac{b}{T_1}\right)}{\exp\left(\frac{b}{T_2} - \frac{b}{T_1}\right) + \frac{LHSV_1}{LHSV_2} \cdot \left(\frac{(S_{F_2})^{n-1}}{(S_{P_1})^{n-1}} - \frac{(S_{F_2})^{n-1}}{(S_{F_1})^{n-1}}\right)}$$

b) ÷ RHS by $(S_{F_2})^{n-1} \cdot \exp\left(\frac{b}{T_2} - \frac{b}{T_1}\right)$ in numerator & denominator + simplify $\bar{w}\ (S_{F_2})^{n-1}\left(\frac{1}{(S_{P_1})^{n-1}} - \frac{1}{(S_{F_1})^{n-1}}\right)$

(9) $$(S_{P_2})^{n-1} = \frac{1}{\frac{1}{(S_{F_2})^{n-1}} + \frac{LHSV_1}{LHSV_2} \cdot \exp\left(\frac{b}{T_1} \frac{b}{T_2}\right) \cdot \left(\frac{1}{(S_{P_1})^{n-1}} - \frac{1}{(S_{F_1})^{n-1}}\right)}$$

c) use $(\ )^{-1}$ form

(10) $$(S_{P_2})^{n-1} = \left(\frac{LHSV_1}{LHSV_2} \cdot \left(\frac{1}{(S_{P_1})^{n-1}} - \frac{1}{(S_{F_1})^{n-1}}\right) \cdot \exp\left(\frac{b}{T_1} - \frac{b}{T_2}\right) + \frac{1}{(S_{F_2})^{n-1}}\right)^{-1}$$

d) Multiply exponent $(n-1)$ by $\frac{1}{n-1}$ to get S_{P_2}

note! $-\left(\frac{1}{n-1}\right) = \frac{1}{1-n}$

(11) $$\therefore S_{P_2} = \left(\left(\frac{1}{(S_{P_1})^{n-1}} - \frac{1}{(S_{F_1})^{n-1}}\right) \cdot \frac{LHSV_1}{LHSV_2} \cdot \exp\left(\frac{b}{T_1} - \frac{b}{T_2}\right) + \frac{1}{(S_{F_2})^{n-1}}\right)^{\frac{1}{1-n}}$$

(12) $$\therefore S_{P_i} = \left(\left(\frac{1}{(S_{P_{i-1}})^{n-1}} - \frac{1}{(S_{F_{i-1}})^{n-1}}\right) \cdot \frac{LHSV_{i-1}}{LHSV_i} \cdot \exp\left(\frac{b}{T_{i-1}} - \frac{b}{T_i}\right) + \frac{1}{(S_{F_i})^{n-1}}\right)^{\frac{1}{1-n_i}}$$

e) let subscript 2 = current time step i
let subscript 1 = previous time step $i-1$
add in $\left(\frac{P_{i-1}}{P_i}\right)^p + \left(\frac{\sigma_{i-1}}{\sigma_i}\right)^q$ same as for Equation 1.5 Reaction order.

(13) $$S_{P_i} = \left(\left(\frac{1}{(S_{P_{i-1}})^{n_{ei}-1}} - \frac{1}{S_{F_{i-1}}^{2n_{ei}-1}}\right) \cdot \frac{LHSV_{i-1}}{LHSV_i} \cdot \exp\left(\frac{b}{T_{i-1}} - \frac{b}{T_i}\right) + \frac{1}{S_{F_i}^{(2n_e-1)}}\right)^{\frac{1}{1-2n_{ei}}}$$

Equation 5.24a.

f) Add in WETTING EFFICIENCY to get appropriate reaction order
$\therefore n_i = 2n_{ei}$
where n_{ei} = Wetting efficiency
$0.5 \leq n_{ei} \leq 1.0$

(14) $$S_{P_i} = \left(k_{HOS_{i-1}} \cdot \frac{(LHSV_{i-1})^2}{LHSV_i} \cdot \exp\left(\frac{b}{T_{i-1}} - \frac{b}{T_i}\right) + \frac{1}{S_{F_i}^{(2n_e-1)}}\right)^{\frac{1}{1-2n_{ei}}}$$

Equation 5.24b

g) Substitute $k_{HOS_{i-1}}$ in

Note!
$$k_{HOS_{i-1}} \cong LHSV_{i-1} \cdot \left(\frac{1}{S_{P_{i-1}}^{n-1}} - \frac{1}{S_{F_{i-1}}^{n-1}}\right)$$

KOCH-GLITSCH CANADA COMPANY

CALCULATIONS AND SKETCHES

BY _____ DATE _____ SHEET 1 OF 1

SUBJECT 2nd Order Version of Equation - Sulfur product JOB NO. _____

Equation (5.15)

a) Substitute in relation for 2nd order reaction

b) Simplify

c) Multiply through by $S_{F_2} - S_{P_2}$

d) Consolidate S_{P_2} terms

e) Isolate for S_{P_2} + convert $\left(\frac{S_{F_2}}{S_{P_1}} - \frac{S_{F_2}}{S_{F_1}}\right) \Rightarrow S_{F_2}\left(\frac{1}{S_{P_1}} - \frac{1}{S_{F_1}}\right)$

f) ÷ RHS numerator + denominator by $S_{F_2} \cdot \exp\left(\frac{b}{T_2} - \frac{b}{T_1}\right)$

g) Simplify + use form $(x)^{-1}$ for $\frac{1}{(x)}$

h) let subscript 2 represent current time step i
let subscript 1 " previous time step i-1

Note: $k_{HOS_{i-1}} = LHSV_{i-1} \cdot \left(\frac{1}{S_{P_{i-1}}} - \frac{1}{S_{F_{i-1}}}\right)$

i) Similar to 1.5 order equation, input $\left(\frac{P_{i-1}}{P_i}\right)^p + \left(\frac{G_{i-1}}{G_i}\right)^g$ as multiplier to $k_{HOS_{i-1}}$ term → those variables included to impact Reaction rate term -

APPENDIX D

RESULTS SUPPORT INFORMATION

Figure 6.3 - Statistical review - Version 3, Plant D, WABT

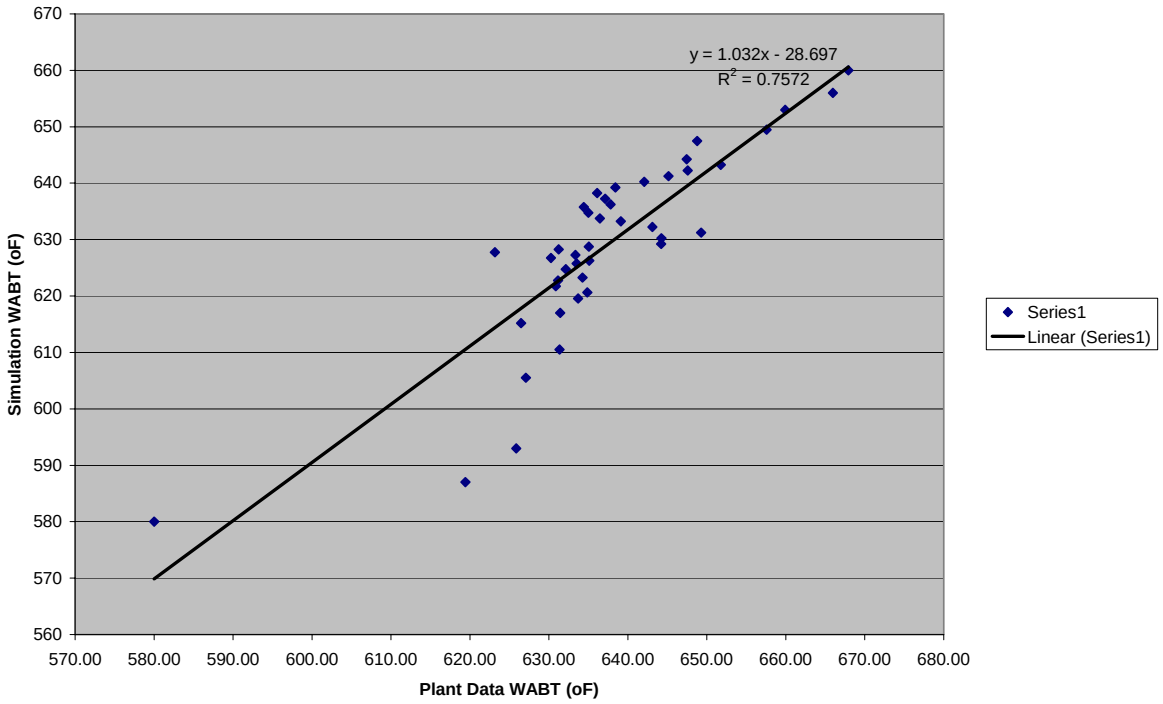

Figure 6.3 -Statistical validation - version 8 wabt plant d

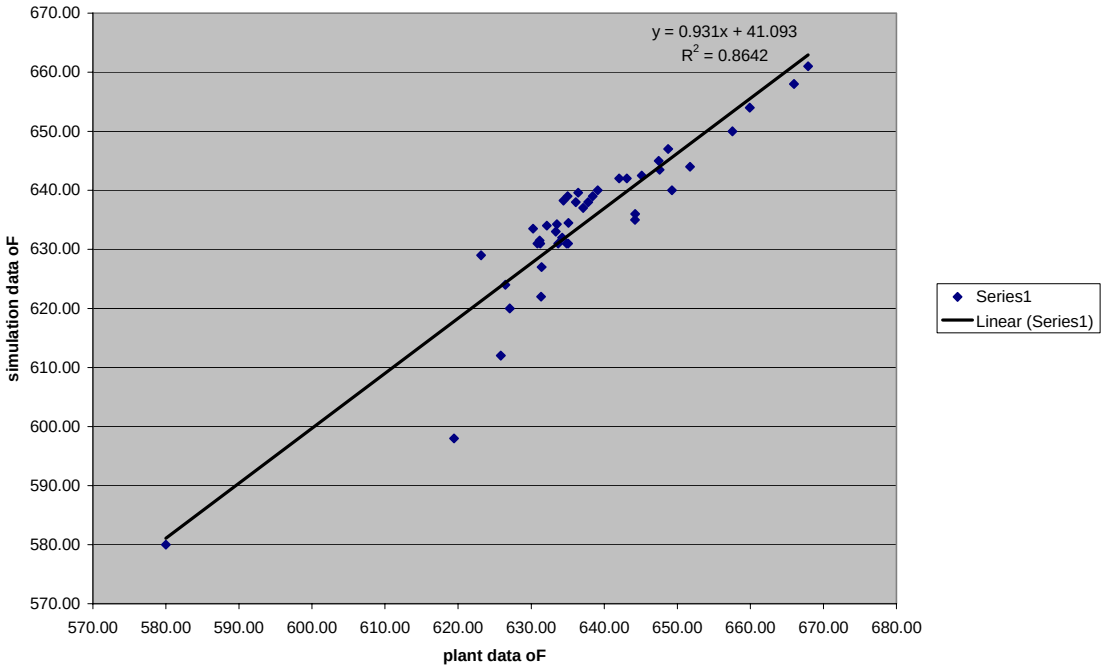

Figure 6.4 - Disturbance 1 - R2 for Sulfur product, Plant D

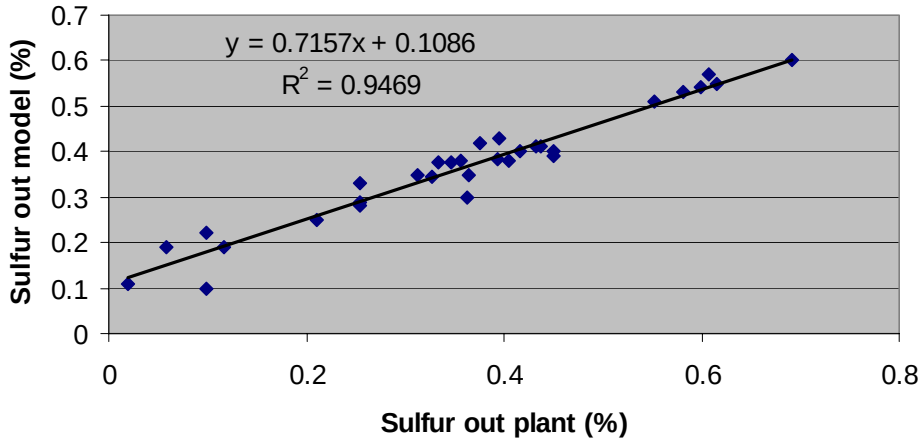

Figure 6.4 - Plant D, disturbance 1, R2 for WABT

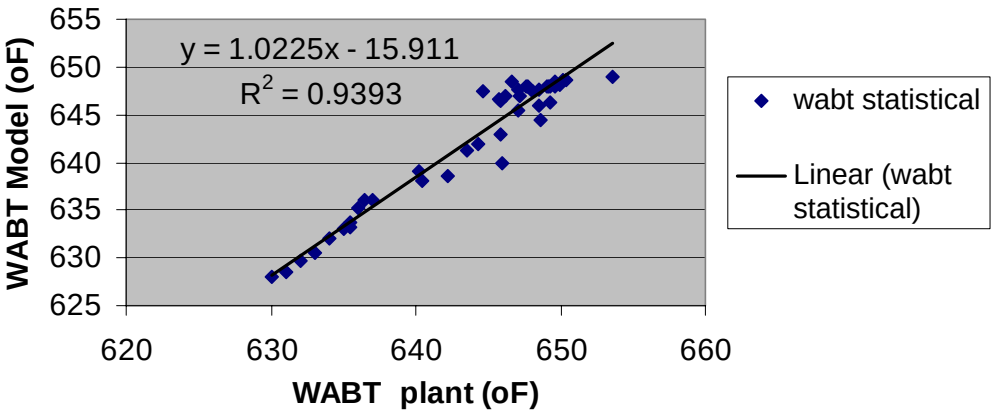

Figure 6.5 - Disturbance 3- Plant D R2 of WABT

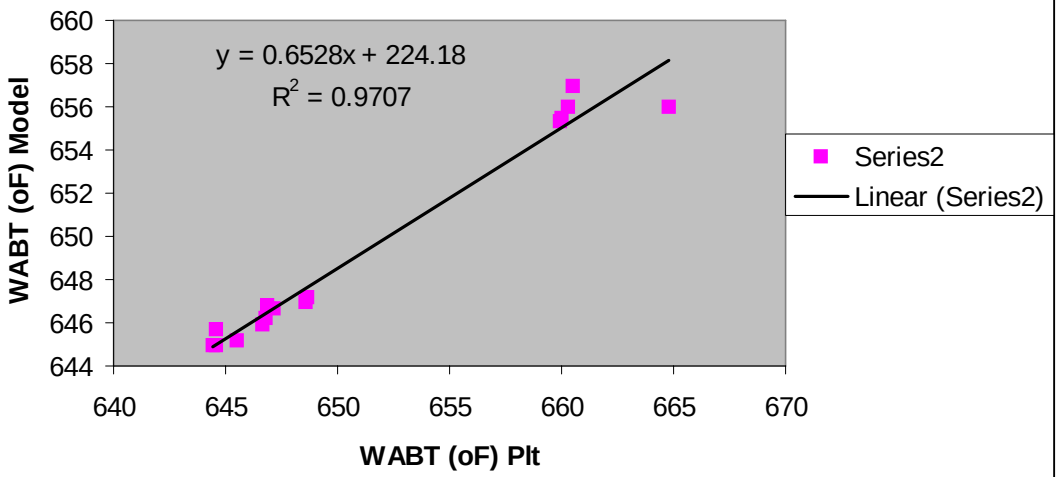

Figure 6.5- Disturbance 3 - Plant D, WABT of Sout

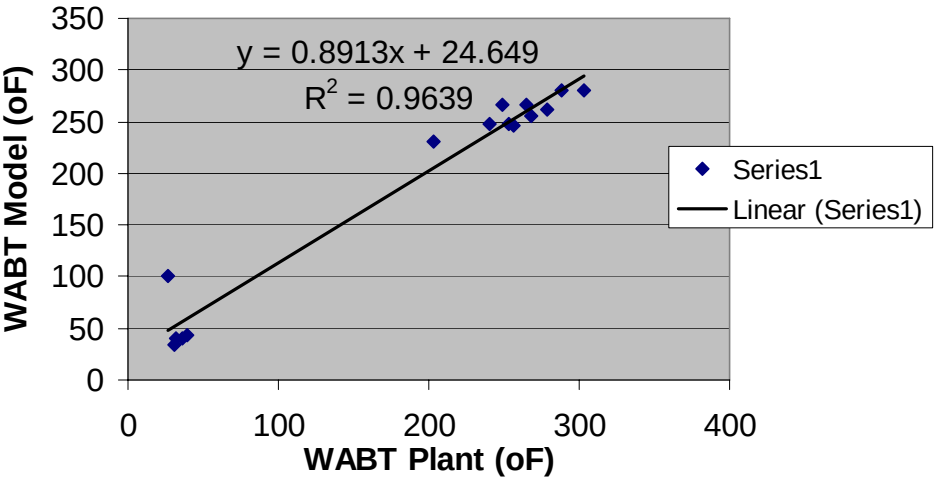

Figure 6.7 Plant D- Entire Run - Version 9, Statistical WABT

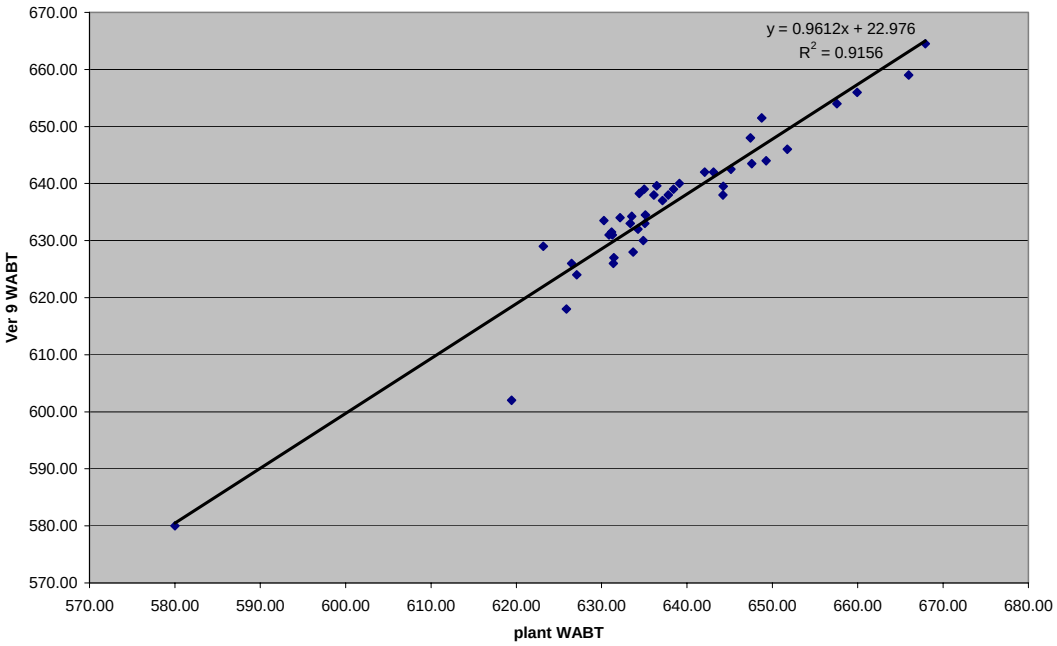

Figure 6.6 PLANT D- Entire run - Statistical

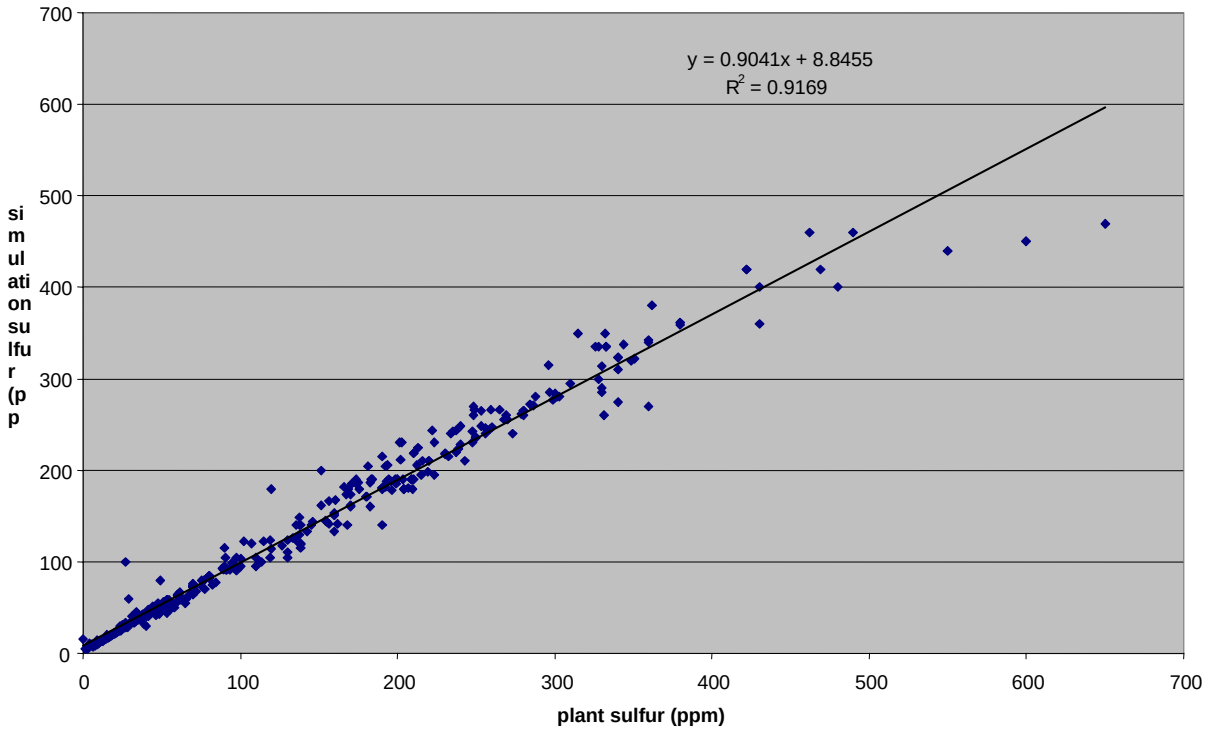

Figure 6.8 - Plant E, Stat Sulfur, Ver 9

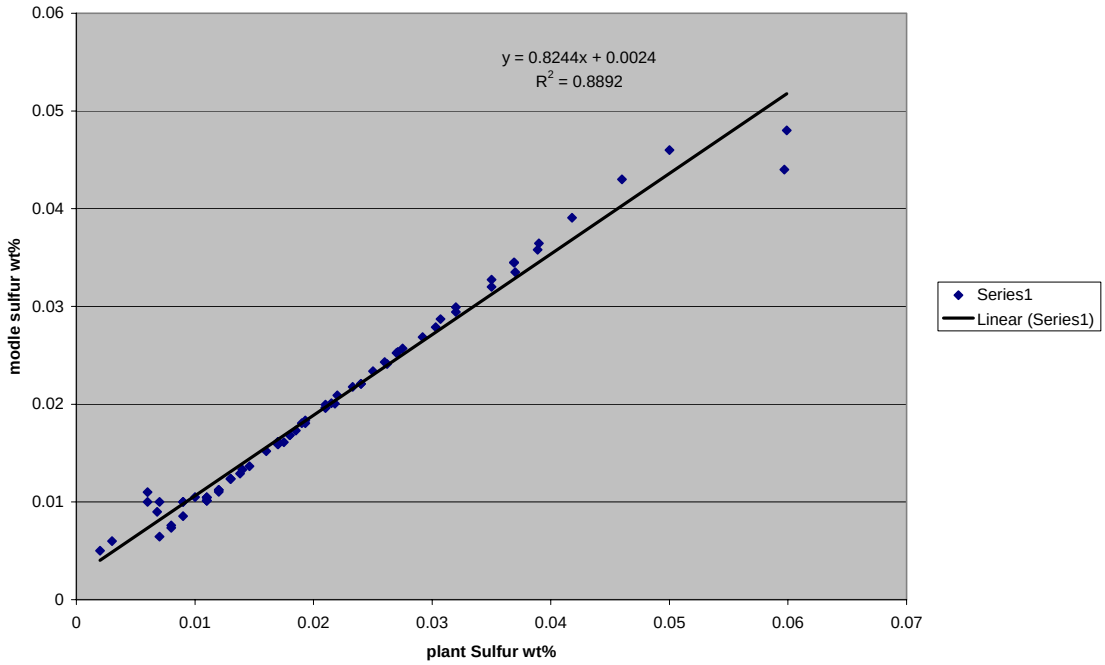

Figure 6.9,Plant E - Statistical WABT V9 Entire Run

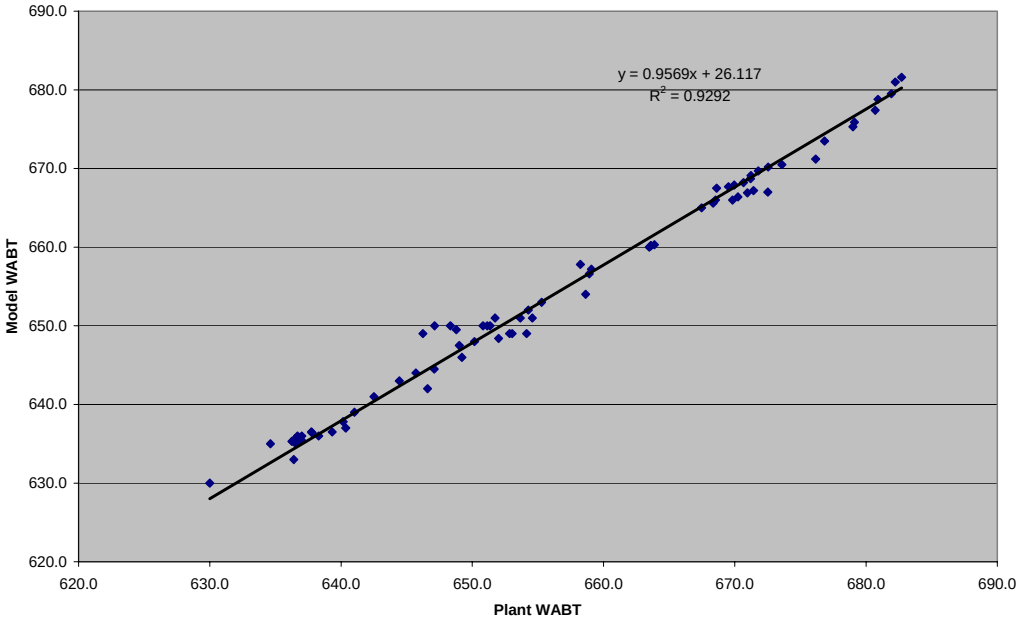

Figure 6.11 Plant f - Entire Run Stat WABT V9

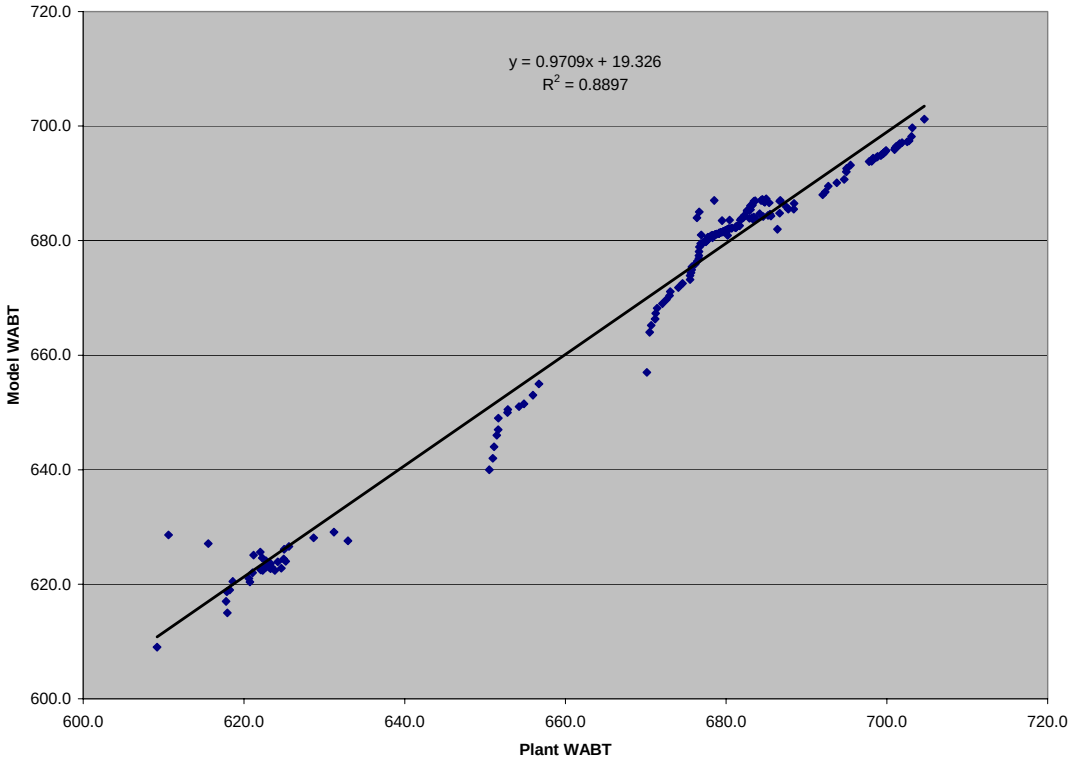

Figure 6.10 - Plant F Sulf out Stat V9

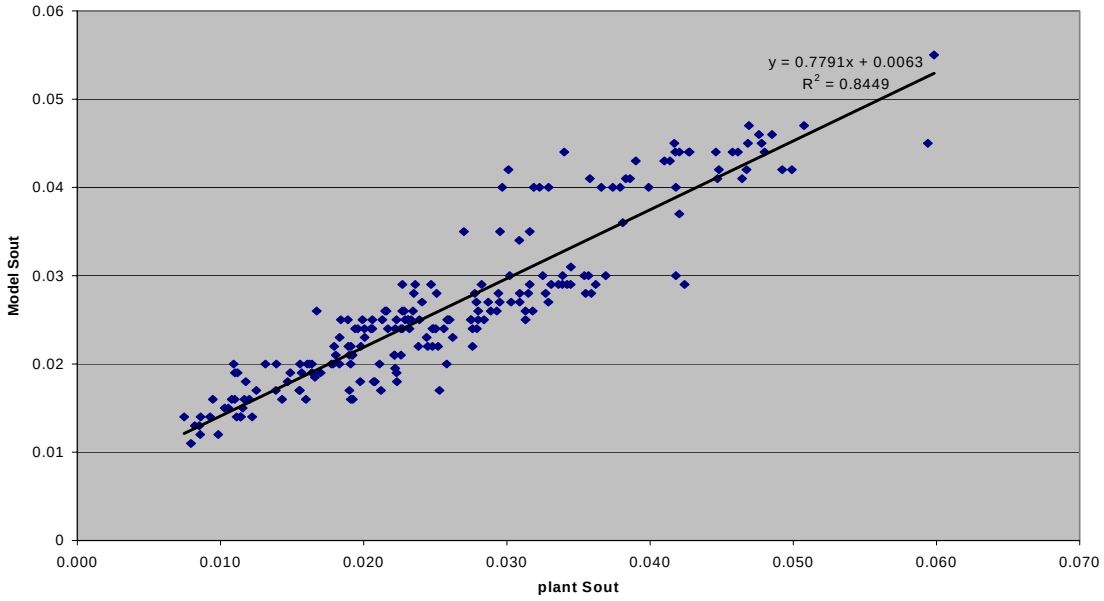

Figure 6.15 Plt b, WABT Full run, V9 Stats

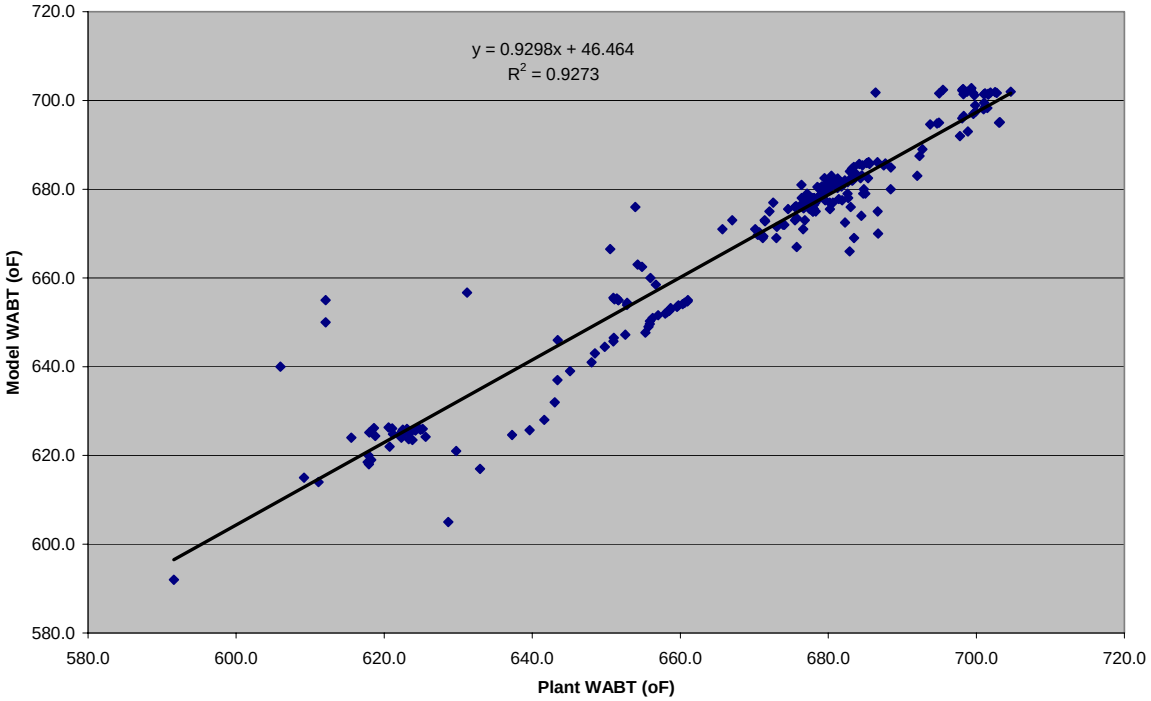

Fig 6.14 -Plt B Sulf out V9 stat

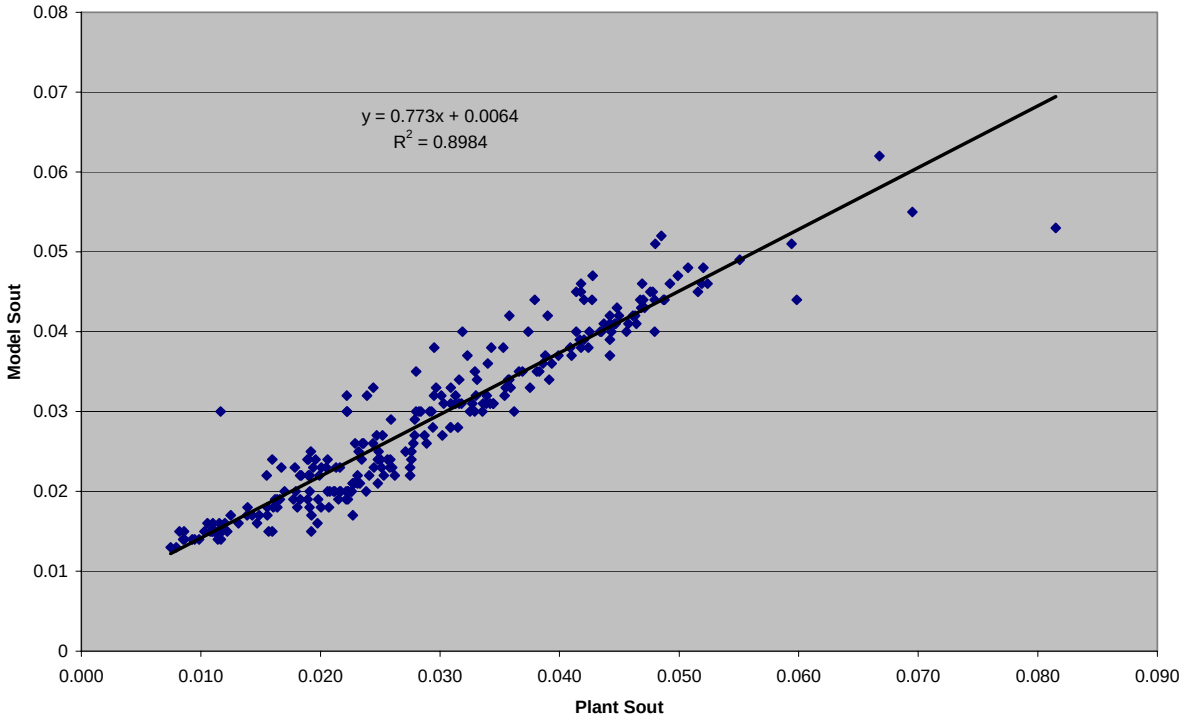

Figure 6.14 - Plant A, Sout V9 Stat

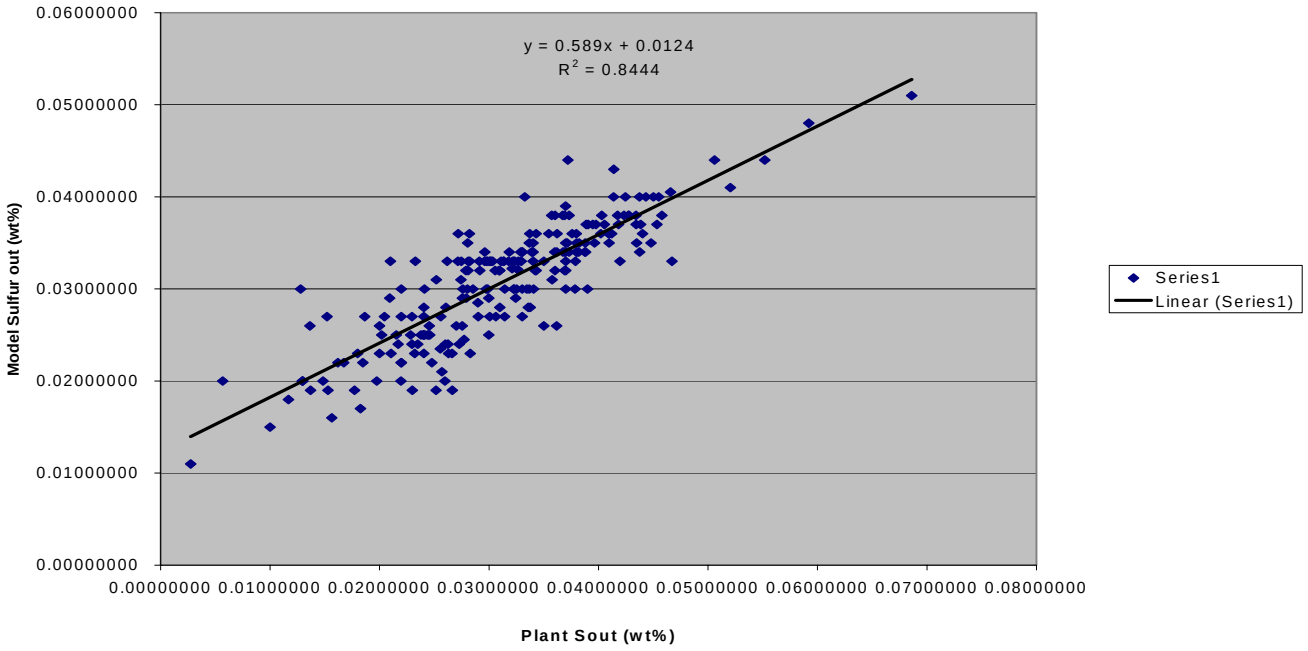

Figure 6.13 - Plant A, Entire run, WABT V9 stat

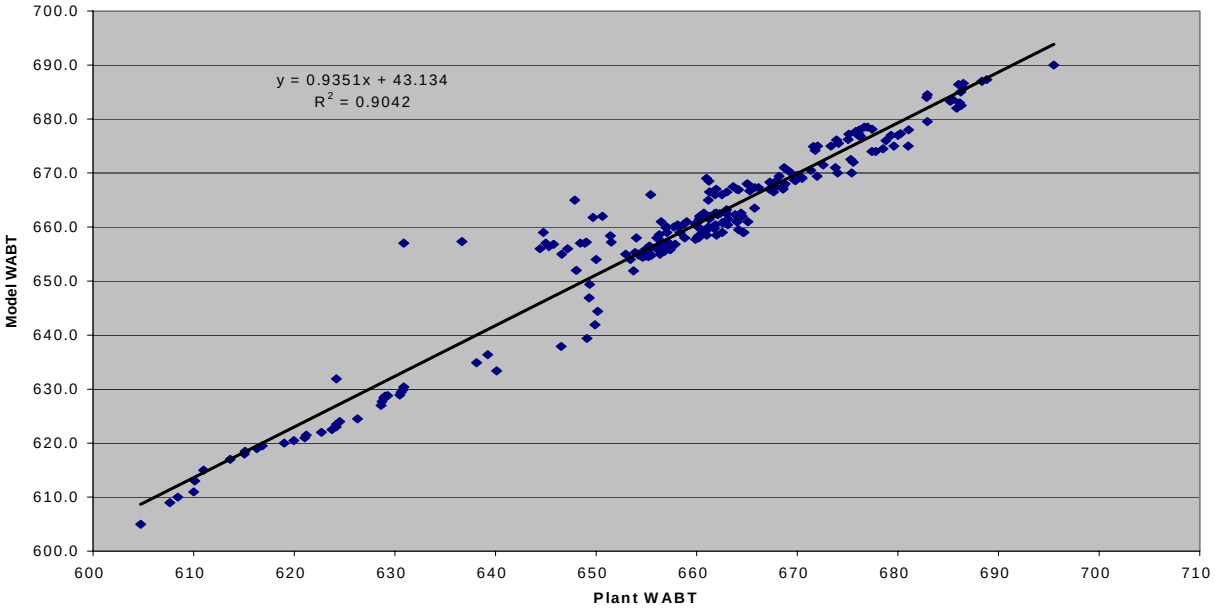

Figure 6.17 - Plant C -WABT V9 Stat

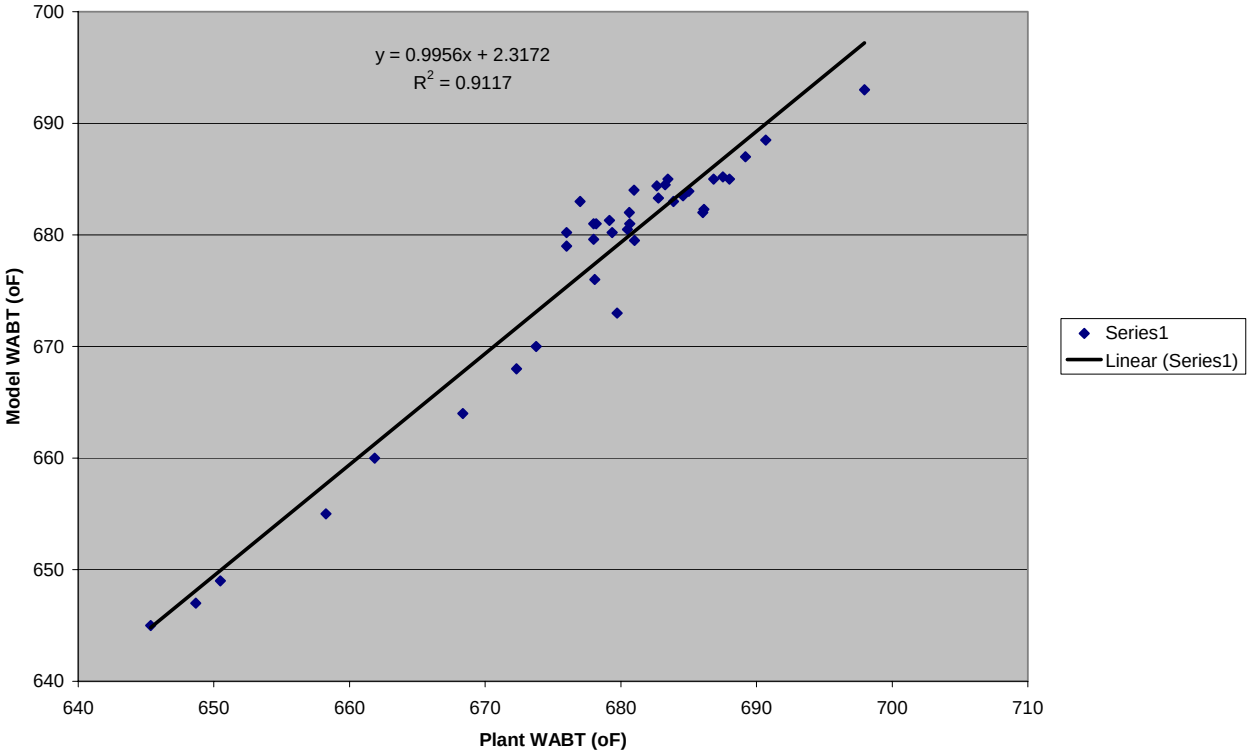

Figure 6.16- Plant C, Sulfur out V9 stat

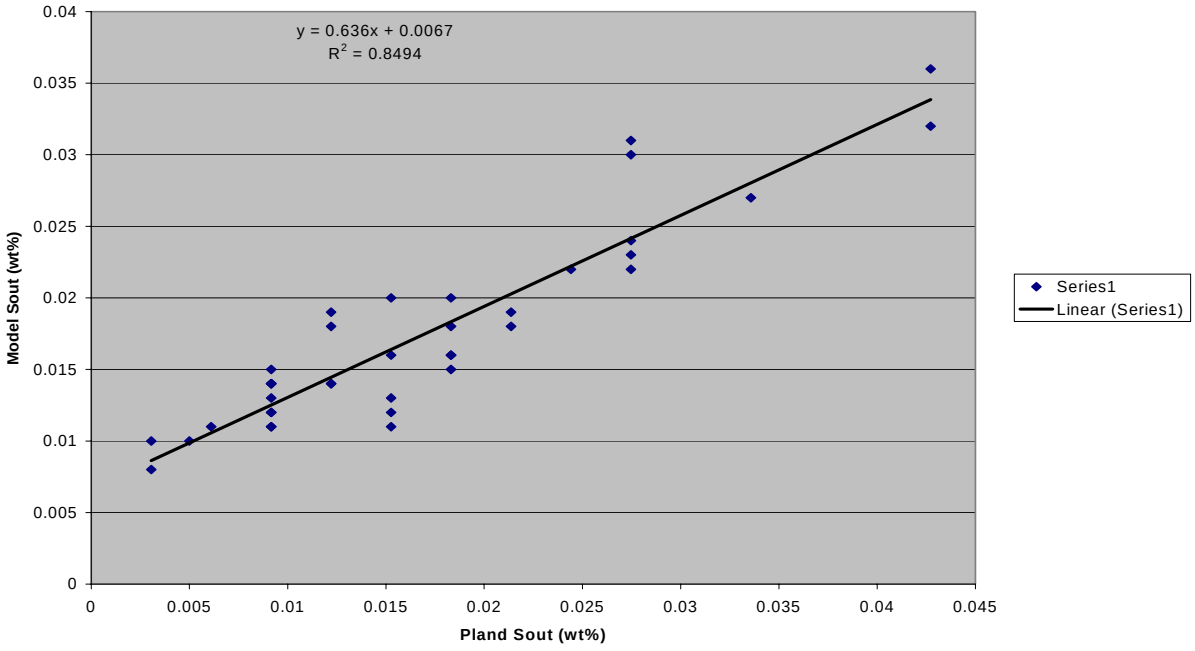

Figure 6.21-

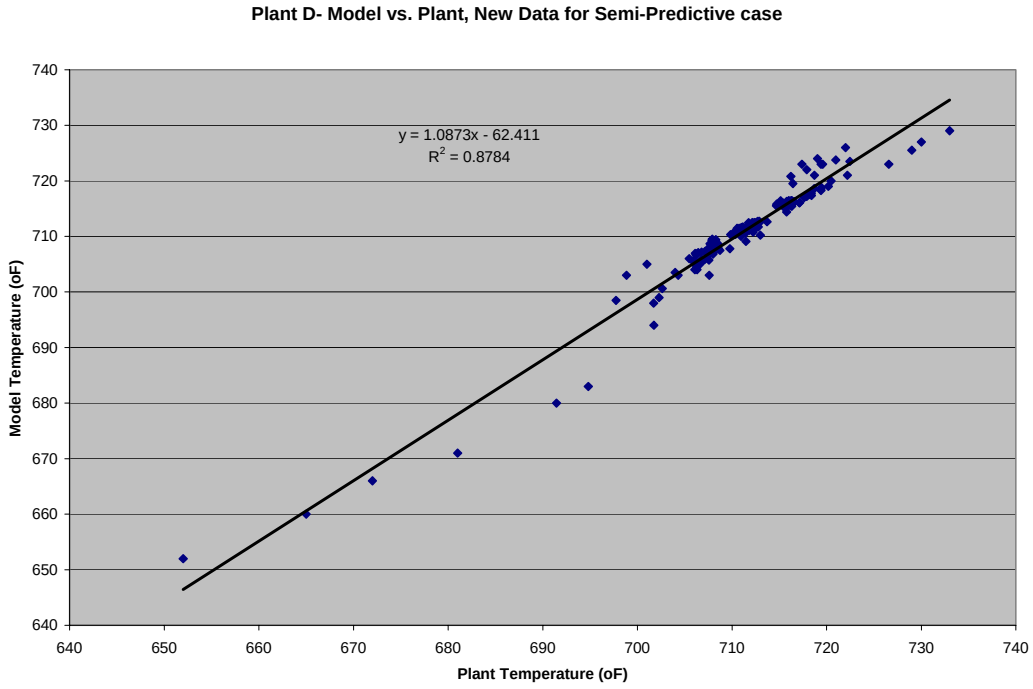

Figure 6.19 - plant d - total run, version agg, stat WABT

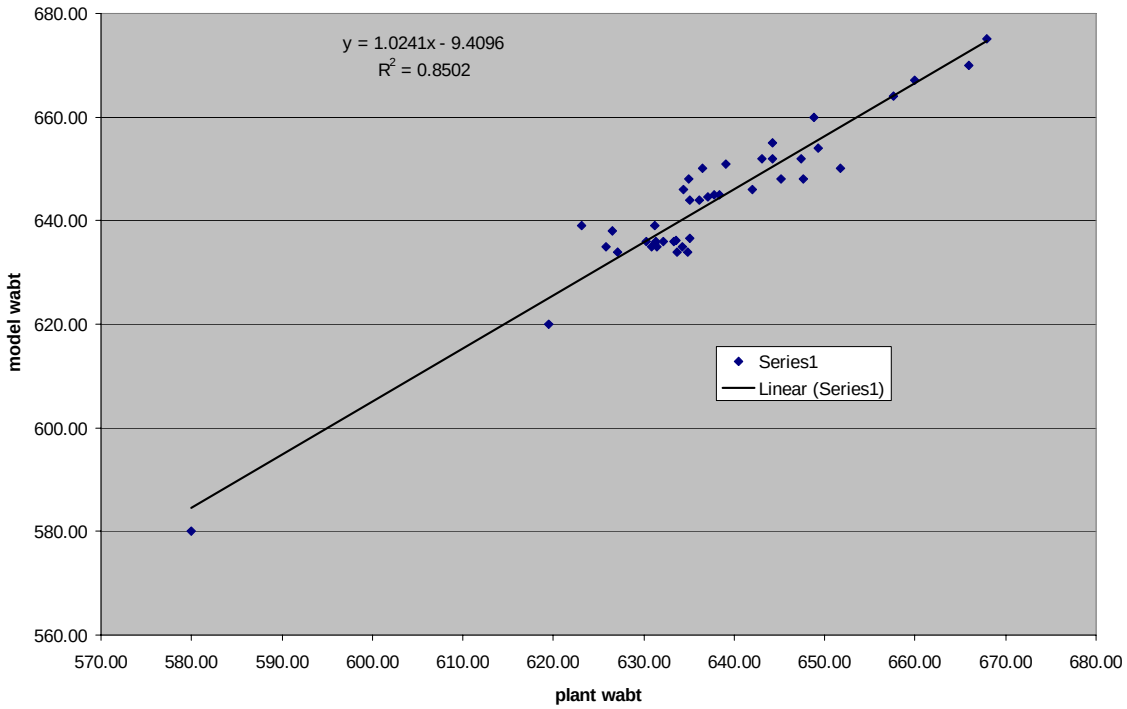

Figure 6.20